PACIFIC EARTHQUAKE ENGINEERING RESEARCH CENTER

Performance and Reliability of Exposed Column Base Plate Connections for Steel Moment-Resisting Frames

Ady Aviram
Bozidar Stojadinovic
Armen Der Kiureghian

University of California, Berkeley

PEER 2010/107
AUGUST 2010

Performance and Reliability of Exposed Column Base Plate Connections for Steel Moment-Resisting Frames

Ady Aviram

Bozidar Stojadinovic

Armen Der Kiureghian

Department of Civil and Environmental Engineering
University of California, Berkeley

PEER Report 2010/107
Pacific Earthquake Engineering Research Center
College of Engineering
University of California, Berkeley

August 2010

ABSTRACT

Many steel buildings, especially those with special moment-resisting frames (SMRFs), suffered failures at their column base connections during the 1995 Kobe, Japan, and the 1994 Northridge, and 1989 Loma Prieta, California, earthquakes. These failures prompted a need to investigate the reliability of current column base designs.

A parametric study was carried out on a typical low-rise building in Berkeley, California, featuring a SMRF with column base rotational stiffness varying from pinned to fixed. Pushover and nonlinear time history analyses carried out on the SMRFs indicate that the seismic demand in SMRFs with stiff column base connections approaches that of SMRFs with fixed column supports. Reduction in the connection’s stiffness resulted in damage concentration that could induce an undesirable first-story soft-story mechanism. System reliability analysis of the base plate connection was carried out to evaluate the system’s safety with respect to its diverse failure modes, as well as the adequacy of the limit-state formulation based on the AISC Design Guide No. 1-2005 procedure.

This study illustrates the importance of an accurate evaluation of the mechanical characteristics, the reliability, and the failure modes of the column base connection, and provides guidance for formulating performance-based design criteria, including important considerations of the economic feasibility of the structure.

Keywords: Semi-Rigid; Pushover; Time-History; Performance-Based; Seismic.

ACKNOWLEDGMENTS

This work was supported in part by the LASPAU-OAS (Organization of American States) fellowship under award 20040536, by the Earthquake Engineering Research Centers Program of the National Science Foundation under award number EEC-9701568 through the Pacific Earthquake Engineering Research Center (PEER); and by PEER's Transportation Systems Research Program funded by the State of California.

Any opinions, findings, and conclusions or recommendations expressed in this material are those of the authors and do not necessarily reflect those of the National Science Foundation.

CONTENTS

LIST OF FIGURES

LIST OF TABLES

LIST OF SYMBOLS

The main symbols and acronyms used in this report are as follows:

a_i	Absolute total acceleration at i_{th} floor
A	Area of base plate
A_1, A_2	Area of the steel base plate and area of the supporting concrete foundation, geometrically similar to the base plate area
A_c	Contact area between base plate and the supporting concrete foundation
A_g	Gross cross section of anchor bolts
b_{ap}, b_{sl}, b_w	Width of steel anchor plate, shear lugs and weld, respectively
b_{eff}	Effective width of the plate resisting bending
b_f	Flange width of W-section steel column
B	Base plate width
c.o.v.	Coefficient of variation
C	Post-earthquake repair cost
C_0, …, C_4	Coefficients from FEMA 356 coefficient method
CP	Collapse Prevention performance level, as per FEMA 356
d_b	Anchor bolt diameter
d_c	Steel column cross-section depth
d_{edge}	Distance between centerline of anchor bolt and edge of base plate
DM	Damage measure
DS	Damage state
DV	Decision variable
e	Eccentricity of axial load in base plate connection
E	Elastic modulus of steel
EDP	Engineering demand parameter
f'_c	Concrete compressive strength
f_p	Concrete bearing stress
F	Fixed column base
F_{EXX}	Electrode strength for welds

FORM	First-order reliability method
F_{yb}, F_{ub}	Anchor bolt design strength and ultimate strength, respectively
$F_{y,col}$, $F_{u,col}$	Steel column tensile and yielding stress, respectively
$F_{y,pl}$, $F_{u,PL}$	Tension-yielding stress and ultimate tensile stress of steel base plate, respectively
g	Acceleration of gravity
$g(x)$	Limit-state function, where x is the vectors of random variables
h	Height of concrete pedestal or foundation
h_{ef}	Embedment length of anchor plates
H	Story height
$H(S_a)$	Seismic hazard
I	Moment of inertia of column
IM	Earthquake intensity measure
IO	Immediate Occupancy performance level, as per FEMA 356
k, k_0	Coefficients defining the power-law hazard curve
k	In reliability analysis: Concrete confinement coefficient
K_{el}	Elastic rotational stiffness
K_{norm}	Rotational stiffness normalized with respect to the column stiffness
l	Largest cantilever of the base plate
l_{ap}, l_{sl}	Length of steel anchor plate and shear lugs, respectively
L	Height of steel column
LRFD	Load and Resistance Factor Design
LS	Life Safety performance level, as per FEMA 356
M_b	Overturning moment
M_{el}, M_{inel}	Elastic and inelastic bending moment, respectively
M_{max}	Maximum bending moment at column base
M_p	Plastic bending moment. In reliability analysis: Bending moment at the column base occurring at same time step as P_{max}
$M_{p,col}$, $M_{p,g}$	Plastic moment of column and girder, respectively
M_v	Bending moment in the column base occurring at the same time step as V_{max}
M_w	Earthquake moment magnitude
n_b	Total number of anchor bolts specified for the connection
N	Base plate length

N_p	Axial capacity of steel column
P	Pinned column base
PBEE	Performance-Based Earthquake Engineering
PE	Probability of exceedance
P_{f1}	Failure probability using FORM approximation
PG	Performance group
P_m	Axial force in compression in the column base occurring at the same time step as M_{max}
P_{max}	Maximum axial load in compression in the column base
POA	Pushover analysis
P_v	Axial force in compression in the column base occurring at the same time step as V_{max}
R	Return period
RV	Random variable
s	Spacing between anchor bolt centerline
S	Section modulus of base plate
S_a	Pseudo-spectral acceleration, respectively
SAP	SAP2000 Nonlinear structural analysis program
$S_{d,el}$, $S_{d,inel}$	Elastic and inelastic spectral displacement, respectively
SMRF	Special moment-resisting frame
SORM	Second-order reliability method
SR	Semi-rigid
t_g	Grout thickness
t_{PL}, t_{sl}	Thickness of base plate and shear lugs, respectively
T	Natural period. In reliability analysis: Tension force in the anchor bolts
T_n	n^{th}-mode period. In reliability analysis: Anchor bolt tension capacity
T_s	Period defined by FEMA 350 as the transition point between the constant acceleration and the constant velocity ranges in a response spectrum
UX	Participating mass for the main translational degree of freedom
V_b	Base shear
V_g	Shear due to gravity loads
V_m	Shear force in the column base occurring at the same time step as M_{max}

V_{max}	Maximum shear force at column base
V_n	Shear capacity of base plate connection
V_p	Shear capacity. In reliability analysis: shear force at column base occurring at the same time step as P_{max}
Y	Bearing length in the concrete supporting the base plate connection
Z_{col}	Plastic modulus of steel column
β	Slope of fragility curve in PBEE. In reliability analysis: reliability index.
δ_1, δ_{roof}	Displacement of the 1st story and of the roof level
δ_{max}, Δ_{max}	Maximum inelastic displacement and drift ratio at the roof level of the SMRF, respectively
Δu_i	Interstory drift at ith story
ε	Error or difference
Γ_n	Modal contribution factor corresponding to the nth-mode
μ	Mean or median value of EDP, as specified. In reliability analysis: Friction coefficient between the concrete surface and the steel plate
σ	Standard deviation
θ_{el}, θ_{inel}	Elastic and inelastic rotation, respectively
θ_p	Plastic rotation
ζ	Viscous damping coefficient

1 Introduction

1.1 BEHAVIOR OF STEEL MOMENT-RESISTING FRAMES

Steel special moment-resisting frames (SMRFs) are one of the most commonly used lateral load-resisting structural systems. They are considered to be most effective for this function due to their high ductility and high energy-dissipation capacity due, in turn, to plastic hinge formation in the beams and the column bases, and joint panel zone shear deformation. The ability of SMRFs to resist lateral load is provided by frame action: the development of bending moments, and shear forces in the frame members and joints. Due to their high ductility, U.S. building codes assign the largest force reduction factors to SMRFs, thus obtaining the lowest lateral design forces for an equivalent static analysis. From an architectural standpoint, SMRF systems permit a very effective use of space and maximum flexibility for openings layout, due to the absence of bracing elements or structural walls.

However, the effectiveness of a typical low-rise moment-resisting frame depends on the rotational stiffness of the column base connection, a property that differs greatly with the configuration of the base plate connection. For example, if the base plate is thin and its footing area is close to the size of the column, the base plate will present almost no impedance to rotation of the column and will behave as a pinned connection. On the other hand, if the plate is thick or sufficiently stiff, the arrangement and size of the anchor bolts are adequate, and the footing area is large, the base plate will greatly resist rotation of the column, and the column base will approach the behavior of a fixed support. In between these two extremes are partially restrained or semi-rigid connections, which can be approximated by rotational springs of varying stiffness values.

In order for the frame to achieve sufficient lateral stiffness and comply with code provisions for drift control, the dimensions of the frame elements can become significant. Reduction in the column base stiffness and strength due to inadequate detailing, poor workmanship, deterioration of foundation concrete, long-term deformations, or cumulative damage from previous earthquakes also can lead to an important increase in the displacement demand of the frame. Larger drifts of the frame will cause higher structural and nonstructural damage, resulting in high repair costs after a significant earthquake. Large drifts can also lead to a soft-story mechanism and buckling instability hazard due to P-Delta effects.

Observations after the 1994 Northridge and 1989 Loma Prieta, California, earthquakes suggest that the rotational stiffness of base plate assemblages significantly affected the damage suffered by structures not only directly to the base plate but also to other parts of the frame (Bertero, Anderson, and Krawinkler 1994; Youssef, Bonowitz, and Gross 1995). Investigation of this effect is one of the main goals of this report.

1.2 THEORETICAL BEHAVIOR OF BASE PLATE CONNECTION

A typical column base connection between the column of a steel moment-resisting frame and its concrete foundation, commonly used in U.S. steel construction today, consists of an exposed steel base plate supported on unreinforced grout and secured to the concrete foundation using steel anchor bolts. This moment-resisting connection is generally subjected to a combination of high bending moments, and axial and shear forces. A number of steel buildings, particularly low-rise moment-resisting frame systems, developed failure at the column base plate connection during the 1995 Kobe, Japan, and the 1994 Northridge and 1989 Loma Prieta, California, earthquakes due to such severe load combination. It was found (Bertero et al. 1994; Youssef et al. 1995) that the rotational stiffness and strength of the base plate assemblages affected the damage these structures suffered not only directly in the column bases, but also in other parts of their lateral load-resisting frames. The theoretical behavior of an exposed base plate connection can be explained as follows.

In a base plate connection, column axial forces are transmitted to the base plate through the gross cross-section area of the column, where both flanges and web are effective. Depending on the base plate flexural stiffness, the bearing stress on the supporting concrete foundation can vary from uniform throughout the entire base plate for thick plates, to irregular with stress concentrations under the column flanges and web for thin plates, where only part of the plate area is effective in transmitting compression to the concrete foundation.

As lateral load due to wind pressure or earthquake ground motion increases, the compression stress bulb on the supporting concrete foundation shifts from the center of the column toward the edges of the base plate in the direction of the applied load. For thick or stiff plates, a behavior similar to rigid body rotation occurs with respect to the base plate centroid, producing maximum strain and stresses at the edges of the plate. Due to plate bending in the case of thin base plates, the bearing stress concentration is located under the column flanges in compression. As concrete fibers reach their ultimate capacity, the resulting stress distribution in both cases flattens and becomes more uniform. In most design methods the stress distribution is approximated for simplicity as an equivalent rectangular distribution, similar to the Whitney compression block used in reinforced concrete load resistant factor design (LRFD) (ACI 318, 2002). On the other side of the column, the tension in the column flange induces tensile forces in the anchor bolts, necessary to maintain vertical force and moment equilibrium in the case of moderate to large eccentricities.

The column bending moment is resisted by coupled tension-compression force, with a lever arm equal to the distance between the resultant of the concrete bearing stresses on the compression side of the base plate and the centerline of the anchor bolts on the tension side. The maximum bending demand in the base plate is the greater of the effects of cantilever bending on the tension side of the plate caused by tensile forces in the column flange and in anchor bolts, or cantilever bending due to bearing stress distribution on the compression side (Drake, Elkin 1999). In the center of the plate, in the transition zone between tension and compression, the plate is subjected to high shear stresses.

The shear resistance and horizontal force equilibrium of the column base connection is provided by a combination of three mechanisms: (1) friction along the contact area between the concrete surface and the steel base plate, which can be taken as the effective bearing area resisting compressive loads; (2) bending and shear in the anchor bolts; and (3) bearing of shear lugs installed underneath the base plate (or the side of the base plate if it is embedded) against the adjacent concrete or grout.

1.3 PREVIOUS RESEARCH ON COLUMN BASE BEHAVIOR AND SPECIAL MOMENT-RESISTING FRAME RESPONSE

An extensive literature review was carried out related to base plate connections and special moment-resisting frame (SMRF) design and response under seismic loading.

A number of methodologies for the design of column base plate connections under various load conditions are found in the literature. Among them are the Drake and Elkin method (Drake and Elkin 1999), the AISC Design Guide No.1-1990 (DeWolf and Bicker 1990), the AISC Design Guide No.1-2005 (Fisher and Kloiber 2005), the Astaneh, Bergsma and Shen method (Astaneh 1992), and the Wald component method (Wald 2000). These methods are based on different assumptions for Allowable Stress Design or Load and Resistance Factor Design approaches, and on bearing stress distribution, effective bearing area due to plate bending, and interaction between the components of the connection. A comparative study of these design methods (Aviram and Stojadinovic 2006) found significant differences in the resulting dimensions of the connection, under conditions of small, moderate, and large eccentricities. These variations included the base plate thickness, the concrete bearing length and location of the stress resultant, the governing failure mode of the base plate (between the compression or tension side) and the diameter of the anchor bolts. The most recent method presented in the AISC Design Guide No. 1-2005 (Fisher and Kloiber 2005) is already widely implemented in current U.S. engineering practice.

Reliability analysis of a column base connection in a moment-resisting frame, based on the AISC Design Guide No. 1-2005 procedure, has not been carried out to date. Yet, such reliability analysis is needed to assess the safety of this important structural component with respect to its diverse failure modes and to evaluate the adequacy of the design method and limit-state formulation. A sensitivity analysis of the different components of the column base connection is needed to identify the critical parameters in the design process. A model uncertainty analysis using actual test data, carried out by comparing the observed and expected behavior of the connection, will assist in evaluating and adjusting the design procedure for base plate connections.

Recent experimental, analytical, and parametric studies of exposed base plate connections (Lee, Goel, and Stojadinovic 2003; Fahmy, Stojadinovic, Goel and Sokol 1999; Fahmy, Goel, and Stojadinovic 1999; Burda and Itani 1999; Li, Sakai, and Matsi 2000; Wald 2000; Cabrero and Bayo 2005, etc.) provide some insights on the concrete bearing stress distribution, the anchor bolt behavior, the shear resistance mechanisms, the base plate yielding line patterns, the force flow throughout the assembly, the evaluation of the connection's semi-rigidity degree, the component interaction and relative stiffness, the biaxial bending, as well as the desired overall ductility and actual strength of the connection including steel strain-hardening properties. The above-mentioned column base design procedures available in practice do not readily incorporate such considerations.

The unexpected failures of base plate connections in recent earthquakes (Bertero, Anderson, and Krawinkler 1994; Youssef, Bonowitz, and 1995), detailed according to the available design procedures, as well as the significant variations in the resulting dimensions of the connection components following each methodology, prompts an urgent need to continue investigating with greater accuracy the connection characteristics and the different unresolved issues mentioned above, partially addressed in recent studies.

A parametric study aimed at evaluating the effects of using semi-rigid models for moment-resisting column bases was conducted by Stojadinovic et al. (1998). Two typical three-story steel moment-resisting frame buildings designed according to U.S. codes were modeled in SNAP-2D and FEAP. The column bases were modeled as rotational springs with a varying degree of stiffness and strength to simulate a range of semi-rigid behavior, from fixed to pinned. A pushover analysis was carried out for the buildings, examining the resulting force-deformation relationship for the frame and the sequence in the plastic hinge formation. A time history analysis was performed as well to verify some of the results. Additional parameters and effects related to the frame response, such as mode shapes, rotational demand on plastic hinges, moment-rotation relationship of the column bases, joint equilibrium and strong column–weak girder provision, distribution of damage throughout the building, and post-earthquake repair costs, were not examined in this parametric study.

A practical implementation of the PEER Center performance-based earthquake engineering (PBEE) methodology was developed (Yang 2005, 2006) to evaluate the earthquake damage to structural framing systems and the repair costs associated with restoring the buildings to their original conditions. This evaluation procedure includes a fully consistent, probabilistic analysis of the seismic hazard and structural response of the building system. As a part of the ATC-58 project for the development of next-generation performance-based seismic design procedures for new and existing buildings, the PEER methodology was used to evaluate three different lateral force-resisting systems: a special moment-resisting frame (SMRF) with a fixed base, a special concentrically braced frame, and a special eccentrically braced frame (Yang et al. 2006). A series of time history analyses of the building using a suite of ground motions that represent the hazard at the building site is performed and several engineering demand parameters (EDPs) of interest are recorded. The EDPs selected for this project consist of interstory drifts and floor accelerations. A lognormal distribution is used to fit the data obtained from the nonlinear dynamic analyses. Monte-Carlo simulation is used to generate additional EDPs based on the fitted distributions, from which distributions of damage measures (DM) and decision variables (DV), such as repair costs of the buildings with different lateral force-resisting systems, are generated to assist in the selection of a structural system among several competing systems for a building. The same PBEE methodology can be readily applied to evaluate the effect of foundation details, specifically the rotational stiffness of column bases in SMRFs, on the post-earthquake repair cost of buildings with SMRF lateral force-resisting systems.

1.4 PROJECT GOALS AND OBJECTIVES

This research report focuses on the evaluation of the strength, the failure modes, and the reliability of a typical steel column base plate connection detailed according to the latest design provisions, and the effect of its rotational stiffness on the structural response and repair costs of a low-rise special moment-resisting frame subjected to seismic loading. The final objective of the project is the assessment of the desired behavior of the column base connection in terms of its strength and rotational stiffness. Considerations of the structural stability, predictable ductile response, as well as the economy of the moment-resisting frame analyzed, are the main aspects of such assessment. These main research goals were achieved through coordinated work divided into the subsequent four phases:

Phase 1: Pushover Analysis of SMRF

The nonlinear static (pushover) analysis of a typical low-rise SMRF carried out to evaluate different aspects of its structural response for varying column base rotational stiffness was performed with the following intermediate objectives to:

- Determine the seismic demand on the frame in terms of the maximum inelastic displacement obtained from a uniform-hazard response spectrum for a Collapse Prevention structural performance level.
- Determine the force pattern of the pushover based on the first-mode shape of the frame for different values of column base rotational stiffness.
- Analyze the resulting deformed shape of the frame in terms of story displacements and interstory drifts.
- Determine the hierarchy in the formation of plastic hinges in the frame and the effectiveness of the final collapse mechanism obtained.
- Capture the pushover response curves and evaluate the strength and ductility characteristics of the frame for varying column base stiffness.
- Analyze the seismic demand on the frame in terms of base joint reactions, base shear, and overturning moment of the frame.
- Evaluate the seismic demand on the base plate connections through moment-rotation curves of the column bases for varying rotational stiffness values.
- Evaluate the stable and predictable behavior and distribution of damage in the frame in terms of the rotational demand on plastic hinges and the column-girder moment ratio obtained through joint equilibrium.

Phase 2: Time History Analysis of SMRF

Several key aspects of the structural response of a typical low-rise SMRF with varying column base rotational stiffness subjected to earthquake ground motions were evaluated through nonlinear dynamic analysis. A validation of the pushover analysis results of Chapter 2 was carried out by comparison to the results obtained using a different structural analysis program. The seismic response of the frame was evaluated through the following intermediate stages:

- Determination of the seismic demand on the frame in terms of an acceleration time history by selection and scaling of ground motion records applicable for the building site, for the Collapse Prevention structural performance level.
- Analysis of the resulting deformed shape of the frame in terms of story displacements and interstory drifts obtained from displacement response histories.
- Analysis of the seismic response of the frame in terms of base joint reactions and total base shear obtained from the time history analysis of the frame.

- Comparison of the base shear results obtained from a nonlinear static (pushover) and nonlinear dynamic (time history) analyses.

Phase 3: Performance-Based Earthquake Engineering: Repair Cost Evaluation of SMRF

The evaluation of the effect of column base rotational stiffness on the post-earthquake repair cost of a typical low-rise special moment-resisting frame was carried out using the PEER Center Performance-Based Earthquake Engineering (PBEE) methodology. The evaluation of several frame column base models including the fixed, semi-rigid, and pinned column base is carried out for different seismic hazard levels. This repair costs assessment is performed through the following intermediate stages:

- Determination of the seismic demand in terms of the pseudo-spectral acceleration of the first-mode period of each frame obtained from uniform-hazard curves specified for the building site.
- Selection and scaling of ground motion records corresponding to each hazard level considered for the analysis.
- Determination of the interstory drifts and floor accelerations computed for each moment-resisting frame for varying column base rotational stiffness and different hazard levels using nonlinear time history analysis.
- Determination of performance groups and repair costs fragility curves applicable for the structural system and building type.
- Determination of the total repair costs and their disaggregation by performance groups for each frame with varying column base rotational stiffness using the PBEE methodology.

Phase 4: Reliability and Sensitivity Analysis of a Base Plate Connection in a SMRF

The implementation of the system reliability analysis of an exposed base plate connection in a typical SMRF presented the following intermediate objectives:

- Design an exposed base plate connection for the column base of the SMRF analyzed in phases 1–3, following the most recent design criteria. The demand values used for the design correspond to the critical combination of joint reactions obtained from phases 1 and 2.

- Identify the random variables in each failure mode of the base plate connection and their corresponding mean values, standard deviations, coefficients of variation or tolerances, and distributions.
- Identify the different failure modes in the base plate connection and formulate a limit-state function for each mode, based on the unbiased LRFD design procedures without load amplification and capacity reduction factors. The formulation includes model correction factors (as random variables) to account for deviations from the analytical model.
- Perform a component reliability analysis of each failure mode of the base plate connection to compute the normal unit vector parameters and reliability indices.
- Perform a system reliability analysis of the connection considering the multiple failure modes.
- Evaluate the dominating failure modes and the reliability of unfavorable brittle and favorable ductile modes.
- Implement a sensitivity analysis to identify the individual contribution of limit-state parameters or distribution parameters to the system reliability.

1.5 REPORT LAYOUT

The following four chapters of this report cover the four research phases presented above. Additional details of the analyses conducted in each phase are presented in the Appendices. A summary of the findings and recommendations for future work are presented in the last two chapters of the report.

2 Pushover Analysis

2.1 GENERAL PURPOSE

A pushover analysis was carried out for a typical low-rise special moment-resisting frame, selected for the ATC-58 project, to evaluate the effect of the column base rotational stiffness on different aspects of the structural response of the frame. Five SMRFs were analyzed: each has a different column base rotational stiffness varying from fixed to pinned, determined to equally span the range between the first-mode periods of the two extreme case models. The displacement demand used in the pushover analysis of each frame was determined from the response spectra developed for the Seismic Guidelines for UC Berkeley Campus, corresponding to the assumed ATC-58 building site.

2.2 METHODOLOGY

The parametric study of the effect of the column base connection on the seismic demand and behavior of a typical low-rise moment-resisting frame was carried out using a three-story, three-bay frame in the building designed for the ATC-58 PEER project located on the Berkeley campus. The geometry and dimensions of the building are shown in Figure 2.1.

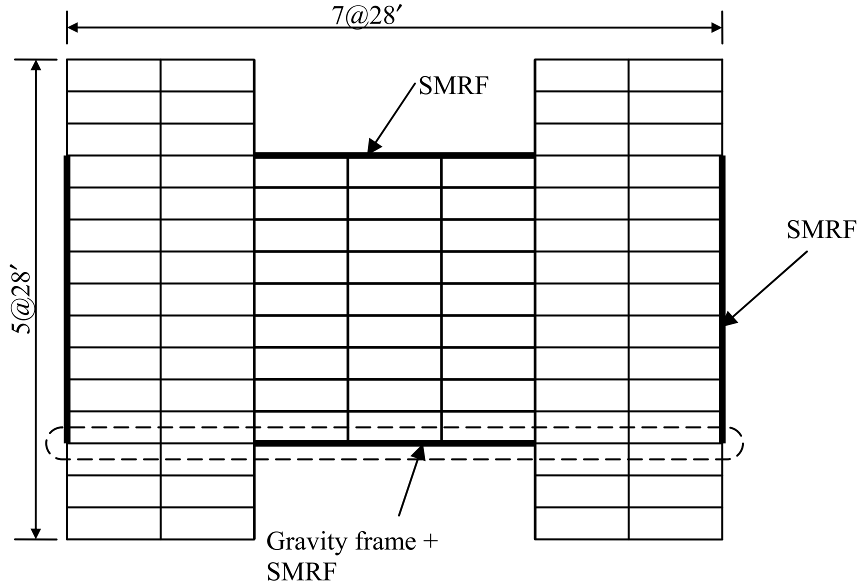

Fig. 2.1 Floor plan of ATC-58 project building.

In each principal direction of the building there are two moment-resisting frames, consisting of three continuous bays (eight columns in total), designed to achieve maximum rigid-frame action. The moment-resisting frames were positioned around the perimeter with a symmetrical distribution in order to increase the resistance of the building to overall torsion due to accidental or intended eccentricities between the building's center of mass and rigidity or asymmetric lateral loading.

The software used for the nonlinear static (pushover) analysis of the building was SAP2000 Nonlinear. The 2D model of the moment-resisting frame included the adjacent gravity frames. Those frames were modeled with shear or pinned beam-column connections, with the purpose of isolating the seismic demand to the lateral load-resisting system. Accounting for the relatively small contribution of the gravity frames to the lateral stiffness of the building is required in order to determine the actual behavior of the moment-resisting frame with greater accuracy required in this column base rotational stiffness study. The geometrical configuration and modeling assumptions of the analyzed frame are shown in Figure 2.2.

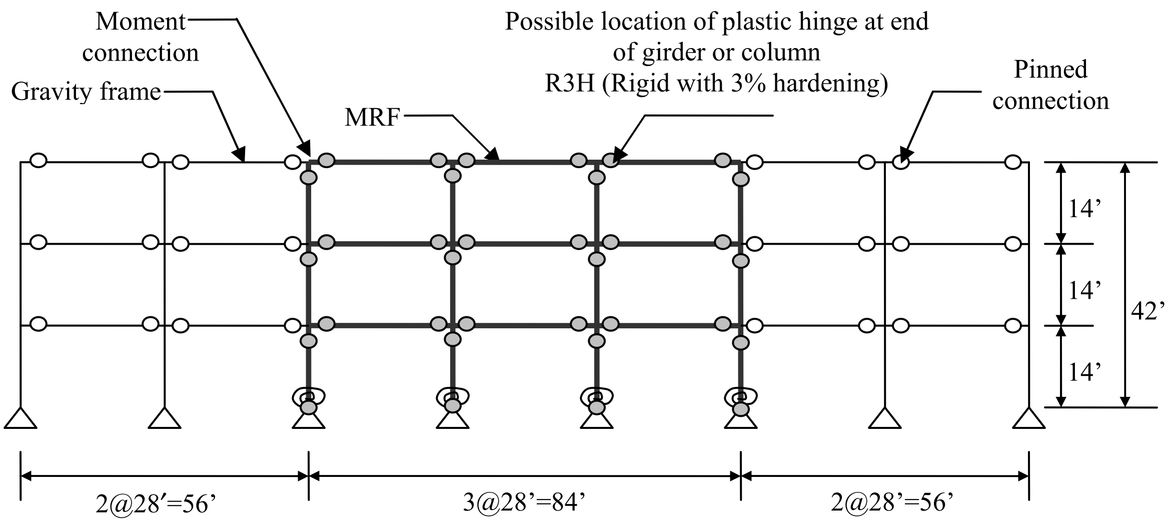

Fig. 2.2 Dimensions and modeling assumptions of the frame.

The beam-column length ratio is 1:2 (14′:28′) which is an efficient aspect ratio commonly used for gravity- and lateral-load resisting frames. Even though the columns and girders in the SMRF have distributed inelasticity, they were modeled as one-component elements in SAP2000 Nonlinear due to their dominant double-curvature bending. Therefore, the model included elastic elements for the beams and columns with possible plastic hinges forming at the ends. The inelastic behavior of the hinges was determined as rigid with a post-yield hardening slope of 3% of the elastic stiffness, as shown in Figure 2.3.

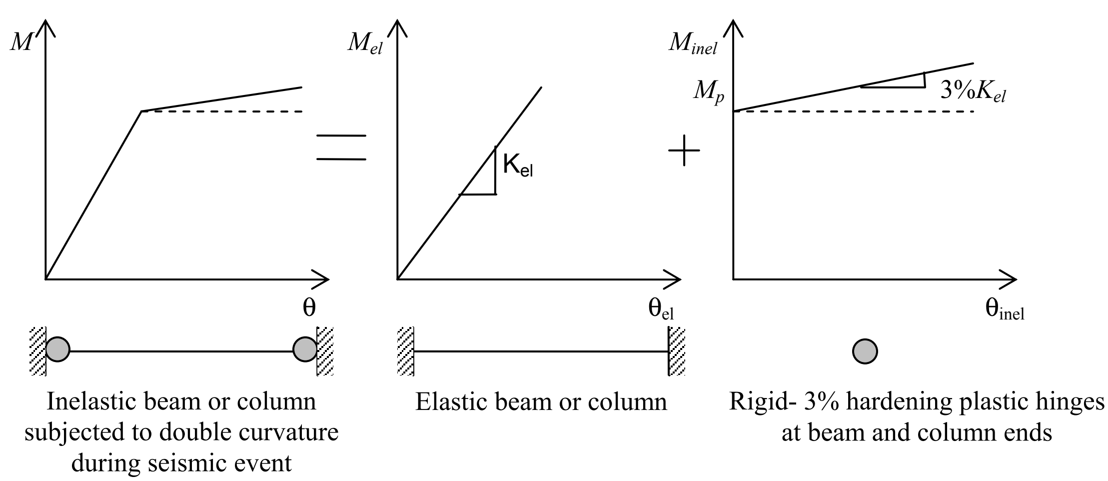

Fig. 2.3 Plastic hinge model (one-component model in SAP2000 Nonlinear).

The design process conforming to the AISC Seismic Provisions 2002, considering steel Grade 50, resulted in sections for the beams and columns of the moment-resisting frame, as well as those of the gravity frames, illustrated in Figure 2.4.

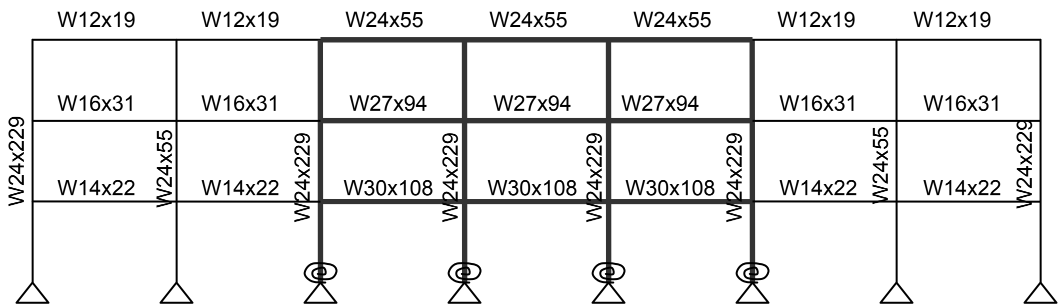

Fig 2.4 Frame element section sizes.

The column bases were modeled with displacement constraints and rotational springs with stiffness varying from 0 (pinned, P) to 2.0e6 or infinity (fixed, F). The stiffness for each model was selected based on the structure fundamental vibration period, spanning from 1.16 sec for the pinned to 0.81 sec for the fixed case. In addition to the SMRF with pinned and fixed column bases, five SMRFs with partially restrained column bases (SR1–SR5) were modeled. A typical measure for the degree of semi-rigidity of a column base connection is the normalized stiffness K_{norm} (normalized with respect to the column rotational stiffness EI/L_{col}). The normalized stiffness K_{norm} with a value between $0.5EI/L_{col}$ and $18EI/L_{col}$ represent a realistic semi-rigid or partially restrained connection (Astaneh 1992). The parameters E, I, and L represent the elastic modulus, the moment of inertia, and the height, respectively, of the steel column connecting to the concrete foundation.

The values of the lumped mass and lateral constraints used for the modal analysis to determine the modal shapes (eigenvectors) and periods (obtained from the eigenvalues) for all frames are illustrated in Figure 2.5.

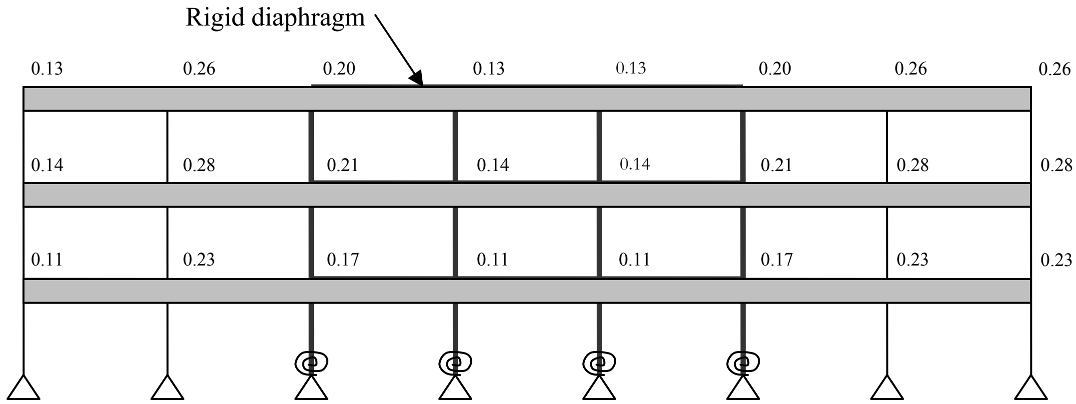

Fig. 2.5 Mass and constraints of the frame.

The pushover analysis was carried out following the modal analysis, thus obtaining a lateral force distribution along the height of the building proportional to the first modal shape of each frame. The displacement demand at the roof level, which is the limit for the pushover analysis, was determined for each frame based on a design spectra developed for the site location on the UC Berkeley campus. The earthquake hazard level used for the pushover analysis was the 2% in 50 years PE (PE), which corresponds to the Collapse Prevention performance level.

Since the frame was pushed up to 5% of the story height, P-Delta effects were included in the nonlinear analysis of the frame model. Thus, in addition to the lateral pushover forces applied to the structure, gravity loads were also considered, proportional to the tributary dead and live loads, and applied as point loads at the beam-column joints.

The pushover analyses compared the strength and stiffness of different frame models, analyzing in detail the effect of varying column base rotational stiffness on the fundamental period and mode shapes, base shear and overturning moment, joint reactions, frame pushover curve, moment-curvature relation of the column base connection, formation sequence of beam and column plastic hinges and rotational demand, story displacement, deformation mechanisms, and interstory drift.

2.3 DEMAND ANALYSIS

The procedure for determining the seismic demand used for the displacement-controlled pushover analysis of the five different SMRFs is presented in this section. The elastic displacement demand on each frame was determined from a response spectra curve for the building site for a hazard level corresponding to the Collapse Prevention performance level. The coefficient method from FEMA 356 was used to determine the inelastic displacement demand of the frames. The force pattern for the pushover analysis selected was the first-mode shape of each frame, obtained through modal analysis.

2.3.1 Response Spectra

Each SMRF model has a different first-mode period T_1 and a corresponding different spectral acceleration S_a and spectral displacement S_d. The pseudo acceleration response spectra S_a vs. T_1 used for the pushover analysis was the uniform-hazard acceleration design spectra with normal fault-rupture directivity effects as defined in the Seismic Guidelines for UC Berkeley Campus for a collapse level earthquake, defined to be a 2% in 50 years event (see Fig. 2.6).

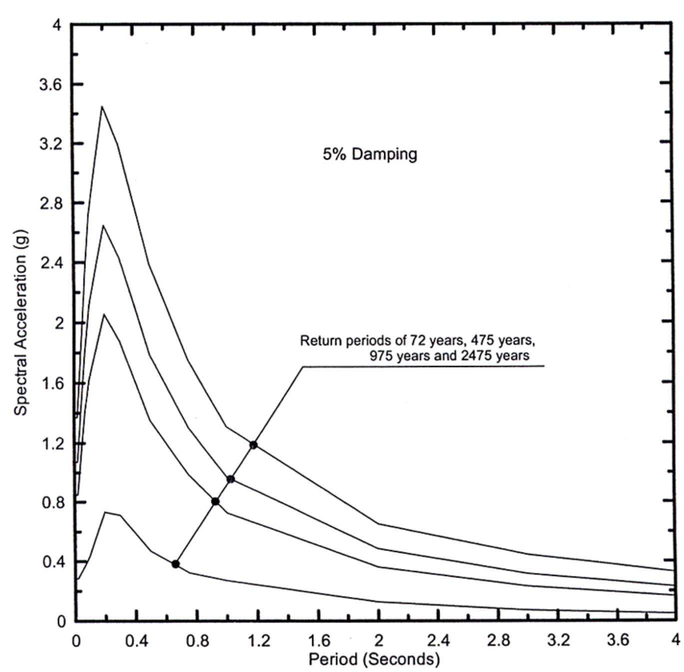

Fig. 2.6 Uniform-hazard pseudo-acceleration response spectra with normal fault-rupture directivity effects (Source: Seismic Guidelines for UC Berkeley Campus).

The displacement spectra was also generated from the pseudo-spectral acceleration using Newmark and Hall's procedure to determine the displacement demand or maximum roof displacement for the Collapse Prevention performance level. The values of the periods, spectral pseudo-acceleration, and spectral displacements for the Collapse Prevention performance level are summarized in Table 2.1.

Table 2.1 Spectral accelerations and displacements for models F–P.

Model	T (sec)	S_a/g	S_d (in)
F- Fixed	0.81	1.62	10.37
SR5	0.84	1.56	10.77
SR4	0.88	1.49	11.25
SR3	0.95	1.38	12.13
SR2	1.02	1.29	13.04
SR1	1.09	1.21	13.91
P- Pinned	1.15	1.14	14.72

2.3.2 Mode Shapes

Although the mass is distributed throughout the building, it was idealized as a concentrated mass at the nodes or beam-column intersection. The effect of the horizontal rigid diaphragm of the floor system constrains the axial deformation of the girders, thus obtaining one lumped mass at each level and eliminating joint rotations. For a three-story frame (low-rise building), the axial deformations of the columns can be neglected and only the horizontal translational degree of freedom was considered, resulting in three modes for the entire building. The variation with base fixity of the first mode (eigenvector), normalized with respect to the roof degree of freedom, can be seen in Figure 2.7. Appendix A presents similar plots of the second- and third-mode shapes.

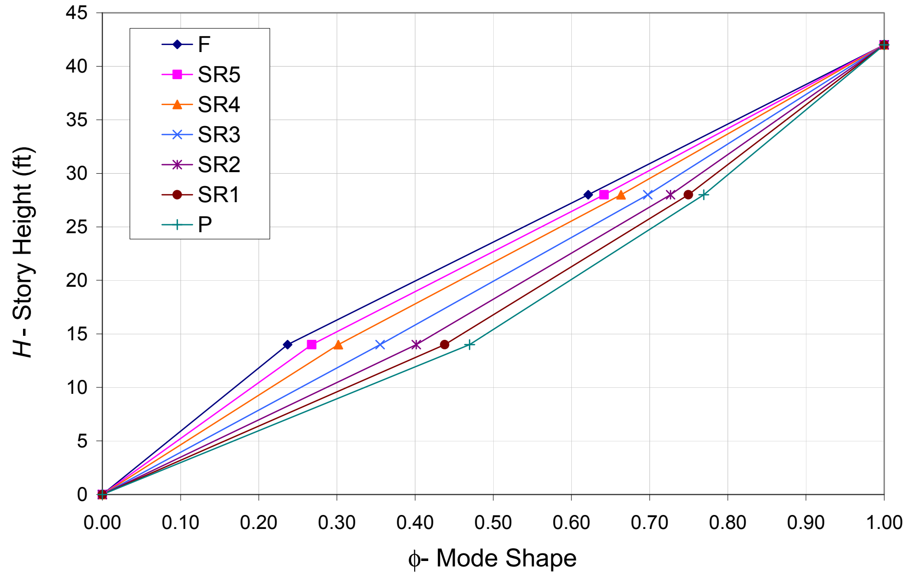

Fig. 2.7 Variation of first-mode shape with base fixity.

The first mode of the frame is close to linear; concentration of deformation in the first story increases with decreasing base fixity. The slope of the mode shapes for the cases of models P and SR1 indicate the tendency for a first soft-story mechanism. For the fixed case F, SR5, and SR4, the deformation of the frame is concentrated in the second and third levels, while for cases SR2 and SR3 the constant slope of the mode shape indicates a uniform deformation demand throughout the height of the building. While the shape of the first modes does not vary significantly among the frames, the small variations at each horizontal degree of freedom or story can induce significant changes in the demand on and performance of the building, as will be demonstrated in the present study.

2.3.3 Modal Participating Mass Ratios

The results of the modal analysis for each frame, including the fundamental periods and mode shapes, are presented in Table 2.2.

Table 2.2 Modal participating mass ratios *UX* and mode shapes.

Case	Mode	Period	UX	SumUX	Mode Shape ϕ		
		Sec	(%)	(%)	N3	N2	N1
	1	**0.8**	**81.3**	**81.3**	**1.0**	**0.6**	**0.2**
F	2	0.2	14.5	95.7	1.0	-1.1	-1.1
	3	0.1	4.3	100.0	1.0	-2.9	4.6
	1	**0.8**	**83.2**	**83.2**	**1.0**	**0.6**	**0.3**
SR5	2	0.2	13.4	96.6	1.0	-1.0	-1.2
	3	0.1	3.4	100.0	1.0	-2.9	4.1
	1	**0.9**	**85.2**	**85.2**	**1.0**	**0.7**	**0.3**
SR4	2	0.3	12.1	97.4	1.0	-1.0	-1.2
	3	0.1	2.7	100.0	1.0	-2.8	3.7
	1	**0.9**	**88.0**	**88.0**	**1.0**	**0.7**	**0.4**
SR3	2	0.3	10.1	98.1	1.0	-0.8	-1.2
	3	0.1	1.9	100.0	1.0	-2.7	3.3
	1	**1.0**	**90.1**	**90.1**	**1.0**	**0.7**	**0.4**
SR2	2	0.3	8.4	98.5	1.0	-0.7	-1.1
	3	0.1	1.5	100.0	1.0	-2.7	3.1
	1	**1.1**	**91.6**	**91.6**	**1.0**	**0.7**	**0.4**
SR1	2	0.3	7.2	98.8	1.0	-0.7	-1.1
	3	0.1	1.2	100.0	1.0	-2.7	3.0
	1	**1.2**	**92.8**	**92.8**	**1.0**	**0.8**	**0.5**
P	2	0.3	6.2	99.0	1.0	-0.6	-1.1
	3	0.1	1.0	100.0	1.0	-2.6	2.9

The contribution of the first mode becomes more pronounced with decreasing base fixity, as shown in Figure 2.8. For models SR2, SR1, and P only the first mode is required for a static analysis, as the modal participating mass is over 90%, which is the minimum established by UBC 1997. In contrast, the contribution of the other two modes becomes more significant with increasing base fixity, and for cases SR3, SR4, SR5, and F the first and second modes are required to obtain a minimum of 90% participating mass for a static analysis of the frame.

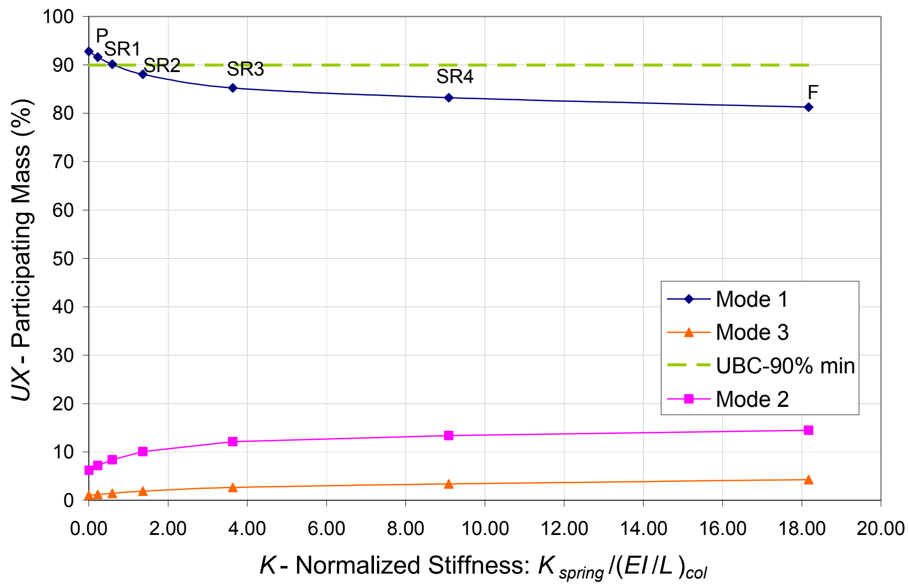

Fig. 2.8 Variation of participating mass ratio with base fixity.

The frame exhibits a dominant first-mode behavior with a mass contribution of over 80% in all cases of base fixity, and therefore the pushover analysis was carried out proportional to the first mode. Based on this analysis, the third mode can be omitted from the analysis for regular SMRFs with similar characteristics.

2.3.4 Modal Periods

The first-mode period was determined carrying out modal analysis of 12 frame models with varying column base stiffness from 0 to infinity. The results are presented in Table 2.3. The first-mode period is decreasing exponentially with increasing base fixity (see Fig. 2.9), with an asymptote of T_1=0.81 sec for the fixed case or for infinite rotational stiffness of the column base connection. This variation indicates a general tendency for increase in the lateral stiffness of the frame while the mass is maintained constant for all models. The stiffness parameters of the 5 semi-rigid models (SR1–SR5) were defined to span the period range between the pinned and fixed support behaviors. The semi-rigid models represent more realistic column base plate assemblies. For models with normalized rotational stiffness K_{norm}> 4.0EI/L_{col}, there is a linear and less sensitive variation of the period. An exponential regression was carried out for the period of the frame in terms of the relative or normalized rotational stiffness of the column base plate connection (see Fig. 2.9).

Table 2.3 Variations of first-mode period with base fixity.

Model	K (K-ft/rad)	K_{norm}	T_1 (sec) (sec)
F	2.0E+06	18.17	0.81
SR5	1.0E+06	9.09	0.84
	7.5E+05	6.82	0.85
	5.0E+05	4.54	0.87
SR4	4.0E+05	3.63	0.88
	3.0E+05	2.73	0.90
	2.0E+05	1.82	0.92
SR3	1.5E+05	1.36	0.95
SR2	6.5E+04	0.59	1.02
	5.0E+04	0.45	1.04
SR1	2.5E+04	0.23	1.09
P	0.0E+00	0.00	1.16

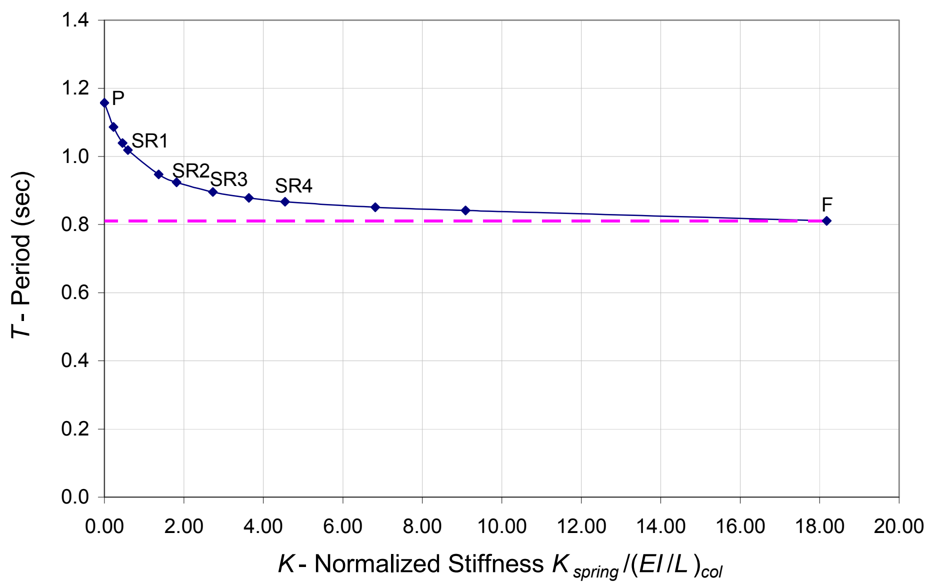

Fig. 2.9 Variation of first-mode period with base fixity.

2.3.5 Displacement Demand

Based on the first-mode period T_1 for each model, the corresponding design elastic displacement $S_{d,el}$ is determined from the design response spectra. The spectra was developed based on a 2% in 50 years PE (2475-yrs return period) corresponding to the Collapse Prevention performance level.

The displacement demand on the structure was determined using the first-mode shape ϕ_1. These values were modified based on the modal contribution factor Γ_1 and coefficients C_0–C_4

from the FEMA 356 coefficient method, accounting for inelasticity, hysteretic loop shape, P-Δ effects, and structural quality. Thus, the maximum inelastic displacement $S_{d,inel}$ expected at the roof level, used in the pushover analysis, is different for each model and exhibits an increasing tendency with decreasing stiffness of the column bases, varying from 16.25 in. for the fixed case to 23.07 in. for the pinned case (corresponding to 3.2% and 4.6%, respectively, of the building total height). That is, the displacement demand on the structure increases by 42% when the column base rigidity is reduced from fixed to pinned. The results for the rest of the models are presented in Table 2.4.

Table 2.4 Displacement demand.

Model	δ_{max} (in)	Δ_{max} (%H)
F- Fixed	16.25	3.22
SR5	17.06	3.38
SR4	17.86	3.54
SR3	19.01	3.77
SR2	20.17	4.00
SR1	21.29	4.22
P- Pinned	23.07	4.58

2.4 DISCUSSION OF RESULTS

2.4.1 Story Displacement

Since the displacement demand increases with decreasing base fixity and reduction of the lateral stiffness for each model, the corresponding displacements at each story of the frame are larger for the pinned case, with a linear variation throughout the height proportional to the first mode of deformation (see Fig. 2.7).

The slope of the displaced shapes for the cases of models P and SR1 exhibit a tendency to develop a first soft-story mechanism due to the concentration of deformation in the first story. For the fixed case F, SR5, and SR4, the deformation of the frame is concentrated in the second and third levels, while for cases SR2 and SR3 the slope of the displaced shape is almost linear, indicating a uniform deformation demand throughout the height of the building.

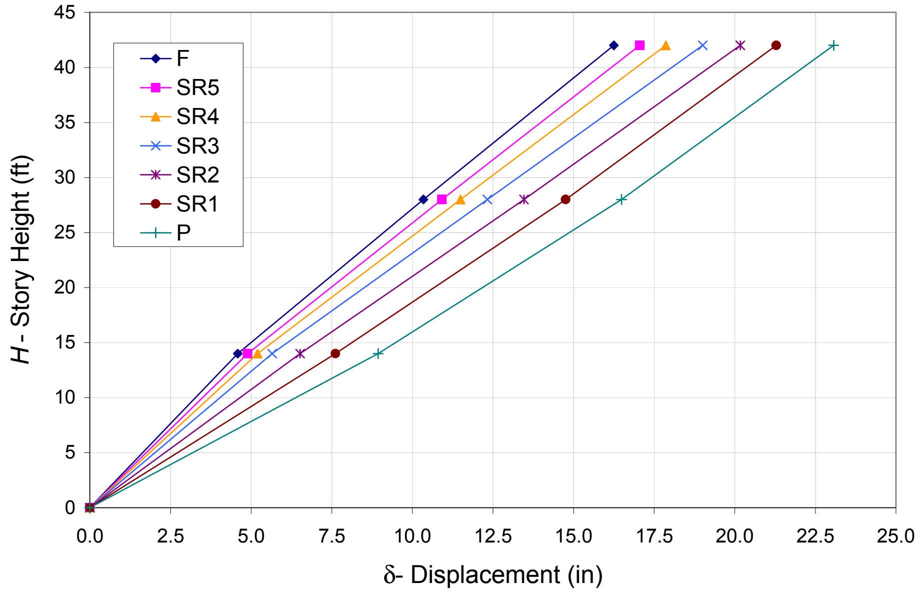

Fig. 2.10 Story displacement for models F–P.

Such behavior of the frame with a semi-rigid column base plate connection is desirable in order to obtain a uniform distribution of the demand on the frame elements in the elastic range or for the Immediate Occupancy (IO) performance level, and to avoid the concentration of damage in the plastic hinges in a certain story for the inelastic range of demand, corresponding to the cases of Life Safety (LS) and Collapse Prevention (CP) performance levels. The results of the story displacements and drifts for each model are summarized in Table 2.5.

Table 2.5 Story displacements and interstory drifts.

Case	Displacement			Δ/H (%)-Drift		
	N3	N2	N1	N3-N2	N2-N1	N1-N0
F	-16.25	-10.34	-4.58	3.52	3.43	2.73
SR5	-17.06	-10.92	-4.89	3.65	3.59	2.91
SR4	17.86	11.49	5.20	3.79	3.74	3.10
SR3	-19.01	-12.32	-5.66	3.98	3.97	3.37
SR2	20.17	13.47	6.52	3.99	4.13	3.88
SR1	21.29	14.76	7.62	3.89	4.25	4.53
P	23.07	16.49	8.94	3.92	4.49	5.32

2.4.2 Interstory Drifts

The interstory drift variation along the height for each model, as well as the established limits in the U.S. design codes for the Immediate Occupancy, Life Safety, and Collapse Prevention performance levels are shown in Figure 2.11.

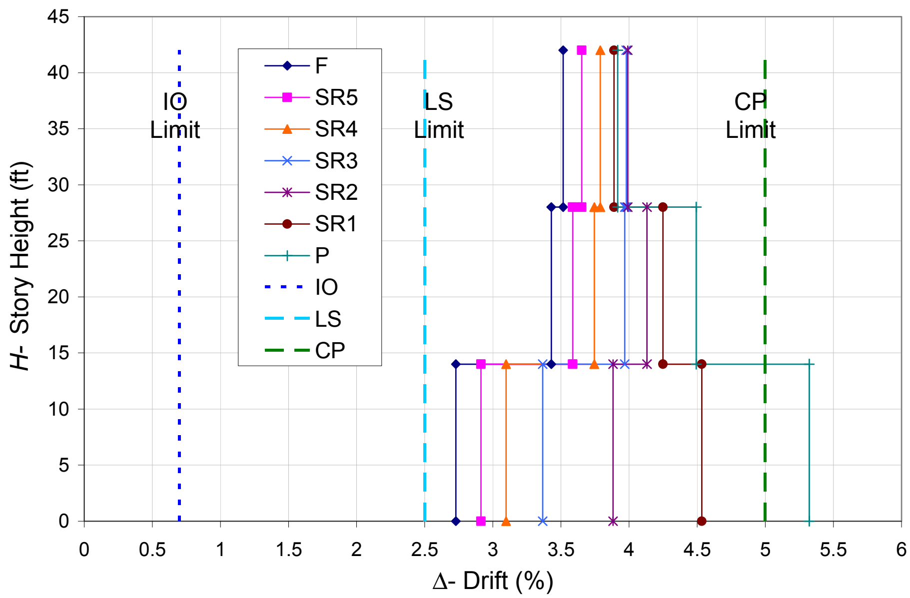

Fig. 2.11 Interstory drifts.

The interstory drift distribution for the cases of the P and SR1 models strongly resembles a behavior caused by a soft-story mechanism, with a drift value of 5.32% and 4.53% for the first story, respectively. Further evidence of this behavior is analyzed with the plastic hinge rotation demands on the lower level (see Section 2.4.3.3). Such mechanism did not form in the frames due to an adequate design and compliance with the strong column–weak girder requirement of the AISC Seismic Provisions for moment frames.

For the pinned case, the drift of 5.32% exceeds the established limit of 5% for the Collapse Prevention performance level in FEMA 356, and therefore does not comply with code requirements. Even though the drift is smaller for the upper floors in those two models (P and SR1), the displacement demand is high and exceeds 4% drift, which could lead to some buckling instability of the moment-resisting frames and connection damage. Exceeding the limit of 5% may also cause irreparable damage to the frame in the pinned case due to dominant P-Delta effects. The Life Safety and Immediate Occupancy performance level limits of 2.5% and 0.7%, respectively, are exceeded for all models, since the displacement demand corresponds to the Collapse Prevention design earthquake with 2% in 50 years PE.

For the other models SR2, SR3, SR4, SR5, and F, the interstory drift is generally smaller than 4% for the first story and almost constant for the upper levels, showing a limited deformation demand on the first level and a more uniform deformation demand in levels 2 and 3, exceeding the recommended 4% limit only in the second story of the SR2 model. Even under such smaller demand levels, considerable structural damage is still expected, including local buckling and partial fracture of the frame elements and pronounced distortion and possibly fracture of moment connections. A permanent interstory drift and deformations will occur, with severe damage to architectural facades and partitions, as well as to mechanical and electrical systems throughout the building. However, if no instability hazard is present (drifts not exceeding 4% drift), the repair and retrofit of the building is technically possible.

2.4.3 Plastic Hinge Formation

2.4.3.1 Hierarchy in the Formation of Plastic Hinges

The desirable strong column–weak girder behavior was engendered in the design process of the moment frame: the plastic hinges form in the girders and also at the bases of the columns in the cases of the SR3, SR4, SR5, and F frames to form a complete collapse mechanism in the pushover analyses. Design code requirements are introduced precisely to avoid a weak-story mechanism at any level and premature collapse of the frame, and they were effective in this case.

Even if the design and detailing of the column base connection is carried out appropriately in accordance with the applicable codes, an unintentional reduction in the column base stiffness can occur. A high degree of base fixity must be guaranteed for the erected column bases and maintained throughout the life span of the structure. It is also recommended to increase the size of first-story columns to reduce the risk of weak-story behavior.

The rotational demand of the plastic hinge is a function of the section capacity and interstory drift, and therefore a concentration of deformation over a certain story will prompt the formation of plastic hinges at the girder of that level.

The girders in the first story (W30x108, Z=346 in.^{3}) are larger than in the second floor (W27x94, Z=278 in.^{3}), since it is expected to obtain higher shears and bending moments at lower levels of a moment frame. However, only in the case of the fixed column base and SR5 model do the first plastic hinges form at the second level. The combination of high flexural strength and small rotational demand on the girders of the first story is beneficial and causes the plastic hinges at that level to occur only later on during the pushover analysis. In all other cases, since base fixity is not fully achieved, a redistribution of the bending moments in the frame to the first-level girders and a concentration of interstory drift in the first story cause the first plastic hinges to form at the lower level. The results of the rotational demand in the plastic hinges formed in the girders and column bases for each frame are presented in Sections 2.4.3.2 and 2.4.3.3.

The hierarchy in the formation of plastic hinges varies for the different models with respect to the different stories; however for a given level, the girder hinges occur initially at the external beam-column connections, where only one beam is connected to the beam-column connection. The sequence in the formation of the plastic hinges for each model is illustrated in Figure 2.12.

After all hinges have formed at the ends of the girders, in models SR3, SR4, SR5, and F, the frame is pushed laterally in the first mode to a sufficient displacement demand, a redistribution of bending moments occurs throughout the frame, and plastic hinges form at the column bases. A complete collapse mechanism is then obtained, reaching a plateau or upper limit for the capacity of the frame to resist additional forces, as can be observed in the pushover curves (Section 2.4.4). The small hardening response of the frame or the slope for maximum base shear of the pushover is due to 3% post-yield strain-hardening of the steel material in the plastic hinges.

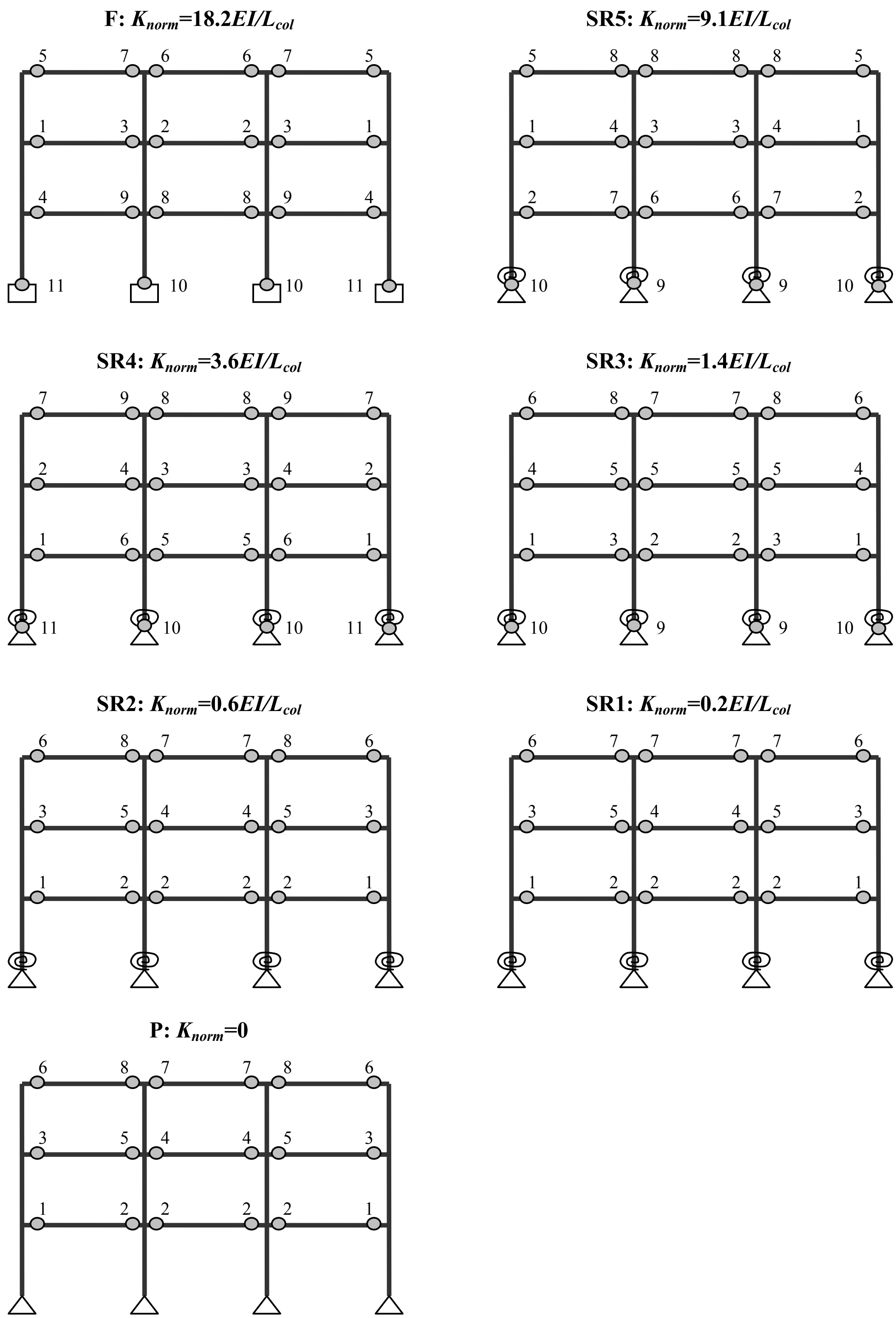

Fig. 2.12 Hierarchy in the formation of plastic hinges.

The column section for both internal and external columns is a W24×229 member; however, at internal columns two beams are connecting to each beam-column intersection thus increasing their stiffness and attracting larger shear forces. Therefore, the formation of plastic hinges at the bases of the columns occurs first at the internal columns for the cases of SR3 to F where the base connection is rigid enough to develop the column plastic capacity, $M_{p,col}$. The cross section of the column is strong enough to avoid the formation of plastic hinges at the top of the columns of the first level and the formation of a weak-story mechanism.

The reduction in the stiffness and strength of column bases leads to an increase of interstory drifts, and rotational demand on the plastic hinges in the girders of the first story and the beam-column connections. This shift in the rotation demand distribution may induce a soft-story mechanism in moment-resisting frames with flexible column bases.

2.4.3.2 Rotational Demand of Girder Plastic Hinges

The hierarchy in the formation of the plastic hinges in the girders is different for different frame models (and different values of column base stiffness) due to different distributions of bending moments and interstory drifts along the height of each frame (see Fig. 2.12). A general increase in the rotational demand on the plastic hinges of the girders in all levels is observed in the pushover analysis with a reduction of column base stiffness and strength (see Fig. 2.13). This increase is exponential for the column base stiffness range between 0 and $2EI/L_{col}$, i.e., for frames with flexible column bases. Small variation in the stiffness results in pronounced variation in the frame response, hierarchy in plastic hinge formation, and rotational demand. Also, for the frames with flexible column bases, the distribution of the rotational demand throughout the different hinges is scattered, resulting in large concentrations of damage in certain beam-column connections.

The variation of the rotational demand in the girder's plastic hinges is linear between the values of 4 and $18EI/L_{col}$ of the base stiffness with almost a horizontal slope or an asymptote for the rotational demand representing a less sensitive design region of the frames. For the semi-rigid base connections, response dispersion is reduced and the rotational demand is almost constant between the different hinges. This behavior is a desirable design goal, distributing the damage to more elements or connections and obtaining a higher degree of redundancy in the moment frame.

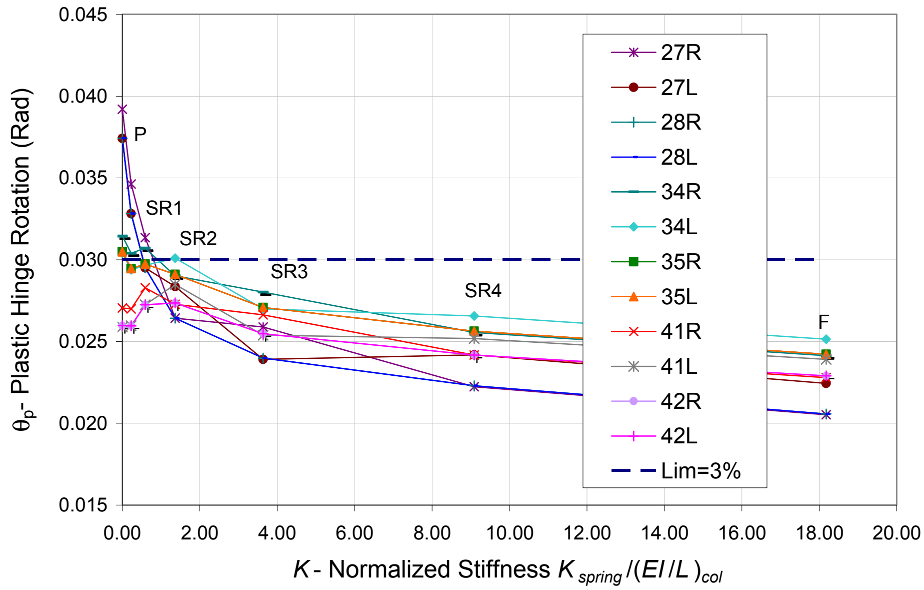

Fig. 2.13 Variation of girder plastic hinge rotation with base fixity.

The current building codes, including the 2002 AISC Seismic Provisions require the use of pre-qualified moment connections that withstand a total rotation of 4% radians without exhibiting premature failure or brittle fracture. Assuming the elastic rotation in the beam-column connection is in the order of 1% radian, we can determine a desirable upper limit for the plastic rotation in the hinges to be of 3% radians. Therefore, as can be seen in Figure 2.13, only the semi-rigid base connections with a normalized rotational stiffness $K_{norm} > 2EI/L_{col}$ will exhibit limited damage in their beam-columns connections and comply with this acceptance criterion.

2.4.3.3 Rotational Demand of Column Base Plastic Hinges

As expected, there is an increase in the rotational demand on the plastic hinges in the column bases with increasing base fixity, as observed in Figure 2.14. In models P, SR1, and SR2 no plastic hinges have formed at the column bases and therefore the plastic rotational demand is zero.

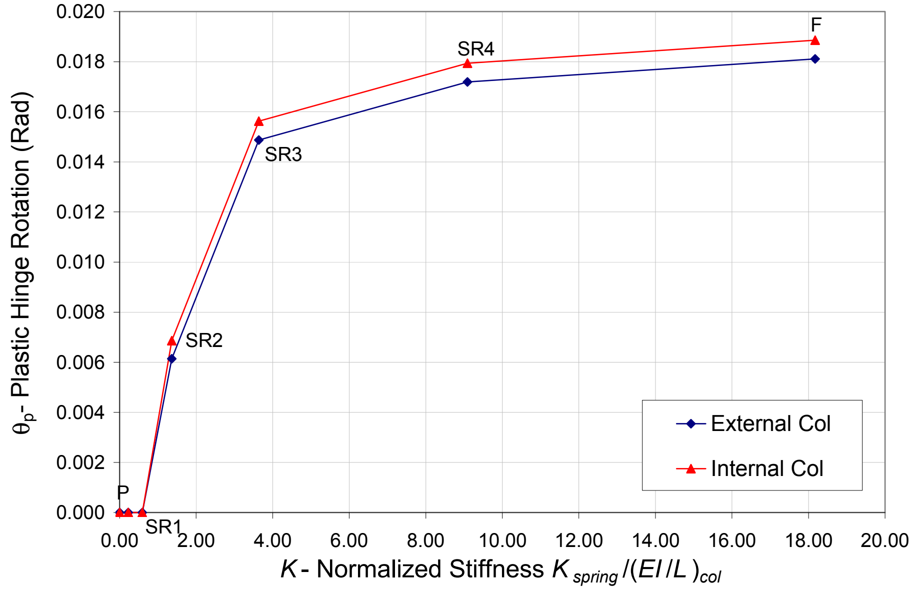

Fig. 2.14 Variation of column base plastic hinge rotation.

For model SR3, the plastic hinges have formed at the last stages of the pushover analysis and therefore the rotational demand is small. Among models SR2, SR3, and SR4 (K_{norm} from 0 to $4EI/L_{col}$), there is a large increase in the rotational demand on the column plastic hinges, which is undesirable because of extreme sensitivity to small variations in the rotational stiffness of the base assembly. Between models SR4 and SR5 there is still an increase in the rotational demand on the plastic hinges; however it is less pronounced than in the previous cases, amounting to only a 15% increase. An asymptote of the rotational demand in the columns can be noticed for a normalized base stiffness K_{norm} greater than $4EI/L_{col}$, representing a less sensitive response region of the frame.

The rotational demand is slightly lower on the plastic hinges of the external columns than that of the interior columns because the formation of plastic hinges in interior columns occurs earlier on during the pushover analysis of the frame.

2.4.4 Pushover Response Curves

Pushover response curves represent the capacity of the frames to sustain lateral loads as they deform to the point of forming a plastic mechanism. The pushover response curves for the analyzed frames are shown in Figure 2.15. The base shear capacity of the frames increases with increasing column base rigidity. The initial slope of the pushover curves also illustrates the increase in the lateral stiffness of the frames with increasing column base fixity. For the more flexible models, the base shear capacity is substantially (as much as 50%) lower.

However, for the cases of the semi-rigid models SR3 through F, a slight increase in the base shear capacity can be observed with decreasing base rigidity. This can be explained by the fact that when all of the plastic hinges have formed in the girders, and the formation of hinges in the base of the column is the next step before a collapse mechanisms forms, it is the rigidity of the base plate, modeled in this study as rotational springs, that is resisting the seismic forces. When the base is fully restrained, the formation of plastic hinges is easier, since the connection cannot rotate to accommodate part of the deformation. At this point, the "fuse" effect is generated, and the structure cannot resist a force increase. In the case of the semi-rigid bases, the connection can accommodate part of the deformation by rotating.

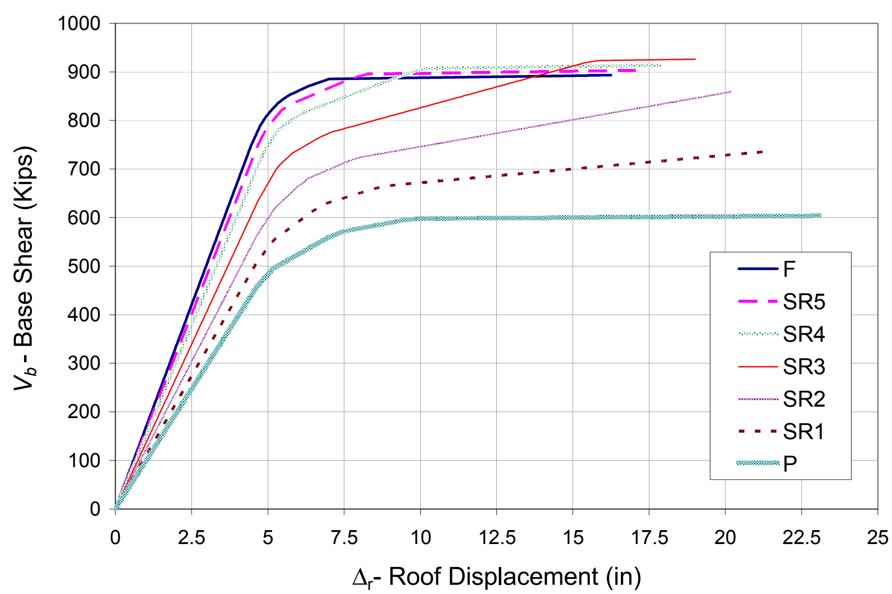

Fig. 2.15 Pushover curves for models F–P.

Evidence of this may be observed in the pushover analysis; as the rotational spring stiffness increases, the slope of the curve between the formation of plastic hinges in the girders and the column also increases. When ultimately, the moment produced by the springs is larger than the moment capacity of the column, a plastic hinge forms at the base, generating the "fuse," and the base shear then tends to a constant value, with a slight positive slope due to the hardening characteristics of the hinge.

The pushover curves are useful in analyzing P-Delta effects in the frame. No stiffness degradation or negative slope in the pushover curves was observed, even though drifts exceeded 5%, as analyzed previously in Section 2.4.2. That is, the deformations in all frame models were small enough and the instability hazard was not yet observed.

In the pinned case, the collapse mechanism was generated immediately after the formation of plastic hinges in the girders, since the column base has no rotational stiffness to resist by itself any force increase. Thus, the base shear for the pinned case attains an almost constant value that is the lowest of the base shear capacitates of the analyzed frames.

In the case of models SR1 and SR2, the roof displacement demanded determined from the design spectra for the assumed location of the structure is not sufficient to generate plastic hinges in the base, yet the partial rigidity of the base plate allows the base shear to increase after the formation of all girder plastic hinges. This can be observed by the positive slope of the pushover curves for these two frame models at very large frame drifts.

2.4.5 Base Joint Reactions

Analysis of the base joint reactions, which define the demand loads for the design of the column base connections, shows the effects of base rigidity on these quantities for external and interior column in the frame (see Fig. 2.16). The results of joint reaction including shear, axial, and moment for external and interior columns, as well as the normalized values with respect to the plastic capacity of the column cross section, are summarized in Appendix A.

The shear demand for both external and interior base plates follows the same tendency observed for the frame pushover curves; the demand for partially rigid connections for which column plastic hinges formed (SR3 to SR5) was slightly larger than for the fixed case, but approaching an asymptote with a constant force value. Comparing the demand on external and interior columns, the loads are larger for interior columns due to the larger stiffness of these subassemblies compared to the external ones.

The maximum axial demand for both external and internal columns is constant, regardless of base plate rigidity. After the formation of all of the plastic hinges in the girders, which occurs for all models, the axial force in the columns is proportional to the plastic moment capacity of the girders and the gravity load ($P=\Sigma M_p/L+V_g$). Comparing the demand on external and interior columns, it is observed that for interior base plates it is close to zero due to cancellation of beam plastic shear, whereas for external base plates, it is large due to the summation of beam shears. Column axial loads due to gravity are relatively small compared to those induced by seismic loads. This observation is consistent with values obtained by a plastic analysis of the frames relating girder plastic moment capacities to column axial force.

The moment demand on both external and internal base plates is constant for those cases where plastic hinging has occurred at the base (SR3 to F), and is equal to the plastic moment capacity of the column. The formation of the column base plastic hinge acts as a fuse that does not allow for a moment increase to occur in the connection. This is corroborated by comparing internal to external base plates; the demand is the same for internal and external columns, since both elements have the same cross section (W24×229) and therefore the same plastic capacity. As expected, the pinned model has no moment demand, since it has no rotational stiffness or strength.

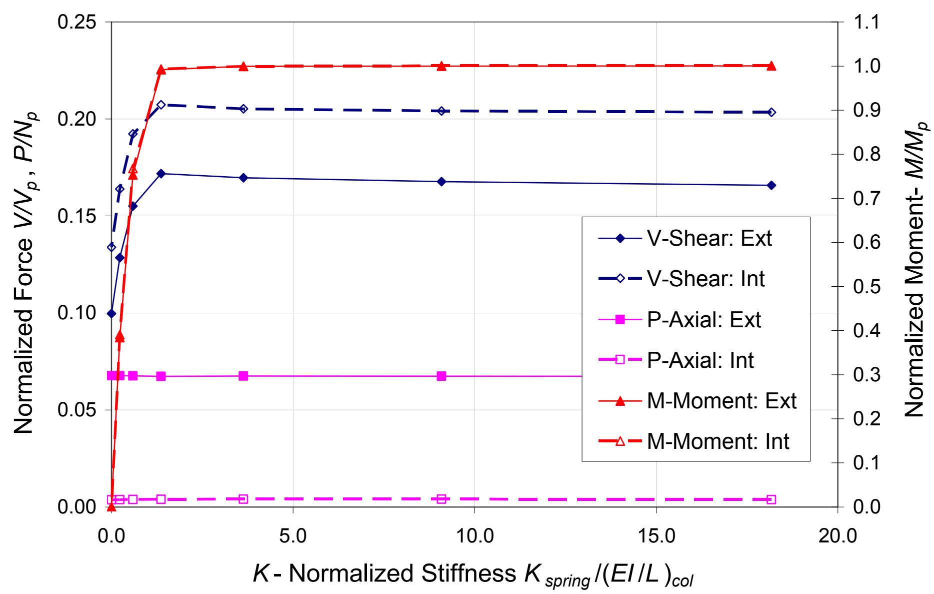

Fig. 2.16 Normalized joint reactions (with respect to plastic capacity).

The plastic capacity of the column is exhausted in bending, a ductile and desirable failure mode. The shear and axial demands remain less than 25% and 10% of the column shear and axial capacities, respectively. The interaction effects were considered low and were not included in this study.

2.4.6 Base Reactions: Base Shear and Overturning Moment

The results for the base shear and overturning moment for each model with varying column base rotational stiffness are presented in Appendix A. The base shear is the sum of the shear reactions in all the columns and therefore it observes the response thoroughly discussed in Sections 2.4.4–2.4.5. The variation of base shear with column base rotational stiffness maintains the same shape as before, with a general increase in base shear with increasing fixity (see Fig. 2.17) and reaching an asymptote for K_{norm} greater than $2.0EI/L_{col}$. The base shear includes the contribution of the gravity frames adjacent to the moment-resisting frame.

The overturning moment is found to be constant for all of the cases where plastic hinges developed in the column bases because the axial forces in the columns are constant for all cases.

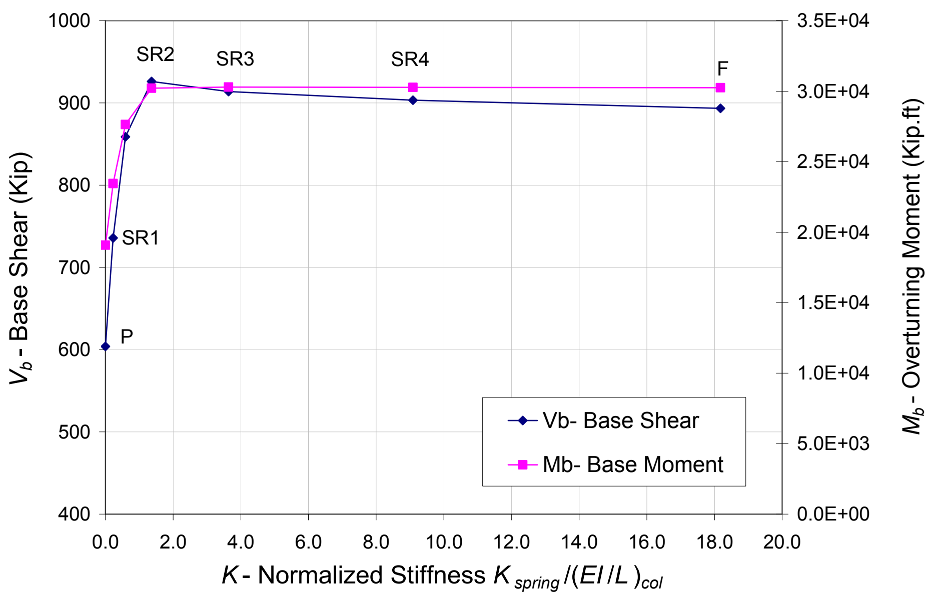

Fig. 2.17 Variation of base shear and overturning moment with base fixity.

2.4.7 Moment-Rotation Relationship

The moment-rotation relationship for the column base connection was determined for the different frames from the results of the modal and pushover analyses, including the base reactions and plastic hinge rotations. The pushover curve yields the roof displacement at which the plastic hinges have formed at the column base. Multiplying that value by the first-story, first-mode value $\phi_{1,N1}$ the displacement at the top of the column is obtained. This displacement divided by the first-story height determines the rotation at which the demand on the base plate reaches the plastic capacity of the column.

The variation in the moment-rotation relation with column base rotational stiffness is represented by the slope of the M-θ curves (see Fig. 2.18). Only models F, SR5, SR4, and SR3 developed plastic hinges at the column base and reached the plastic capacity. The post-yielding 3% hardening slope is shown as well. Models SR2 and SR1 developed only $0.76M_p$ and $0.39M_p$ of the column, respectively. Thus, these frame models did not result in a complete collapse mechanism. Since model P has no rotational stiffness, a horizontal line is obtained for the moment-rotation relation pinned column bases.

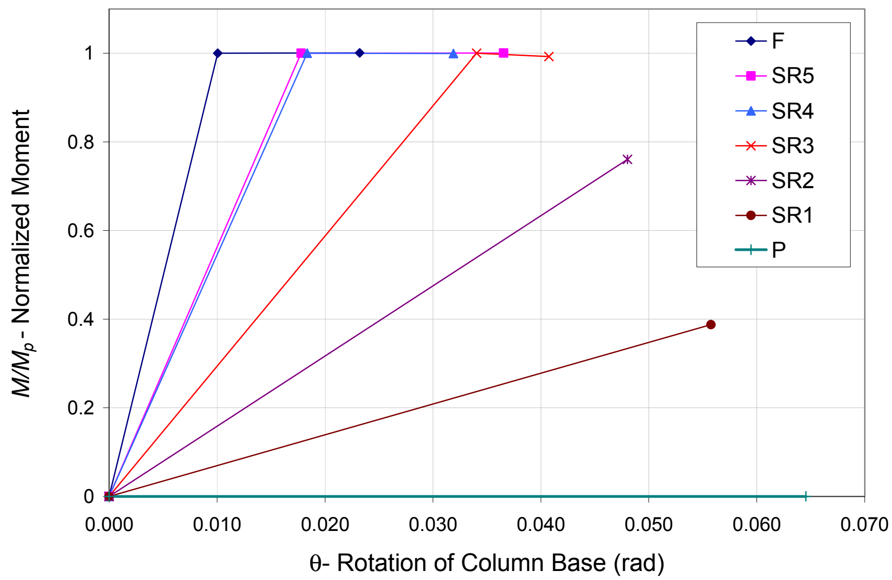

Fig. 2.18 Moment-rotation relation for column base (normalized with respect to column plastic capacity).

2.4.8 Joint Equilibrium

The shape of the bending moment diagram in a moment-resisting frame with semi-rigid column bases is shown in Figure 2.19. The node numbering for beam-column joints in the SAP2000 Nonlinear model is presented as well.

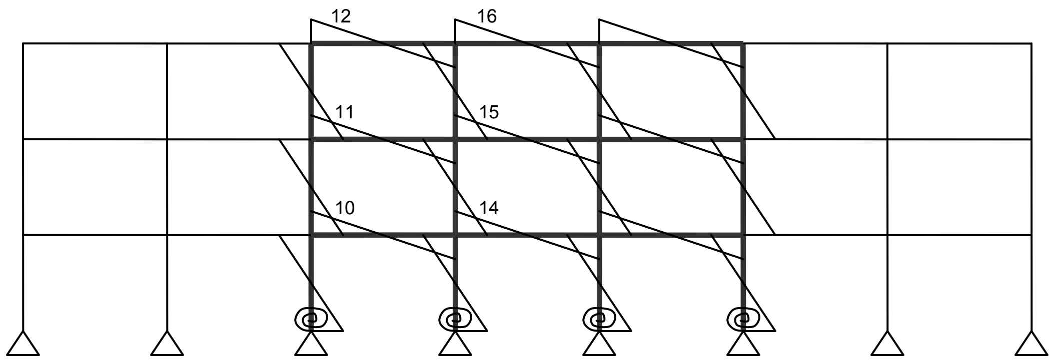

Fig. 2.19 Bending moment diagram in moment-resisting frame.

The design requirement of strong column–weak girder was satisfied in the frame, where plastic hinges form at the girders instead of columns at each joint, preventing the formation of a soft-story mechanism. The AISC design code uses the ratio of the sum of the column moments to the sum of the beam moments meeting at a joint to promote a strong column–weak girder design. Variations of this ratio with base fixity are presented in Table 2.6, where the node numbers are shown in Figure 2.19.

Table 2.6 Joint equilibrium ratio ($\Sigma M_{col}/\Sigma M_{girder}$).

Node	F	SR5	SR4	SR3	SR2	SR1	SR1
10	1.17	1.25	1.33	1.46	1.38	1.17	1.38
11	1.09	1.09	1.13	1.19	1.16	1.17	1.24
12	1.00	1.00	1.00	1.00	1.00	1.00	1.00
14	1.06	1.11	1.16	1.23	1.19	1.08	1.11
15	1.03	1.04	1.06	1.09	1.08	1.04	1.06
16	1.00	1.00	1.00	1.00	1.00	1.00	1.00

As can be observed from Figure 2.20, the variation of the joint equilibrium ratio is sensitive to base fixity for the cases of P, SR1, and SR2, while for models SR3 to F with $K_{norm}>4EI/L_{col}$, the joint equilibrium ratio varies linearly with base fixity, and is nearly constant for some joints. The distribution of the moment demand between the connecting steel elements is therefore more stable for a normalized stiffness of the base plate connection greater than $4EI/L_{col}$, which is a desirable behavior in a lateral force-resisting system. In all cases, a ratio $\Sigma M_{col}/\Sigma M_{girder}$ greater or equal to unity is obtained, which means that the flexural capacity of the columns is larger than that of the beams, as intended by design.

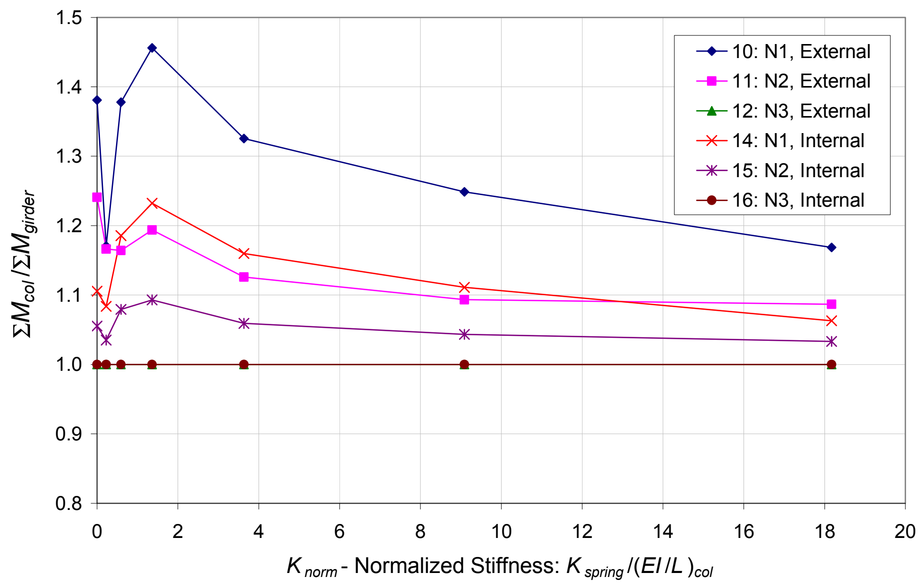

Fig. 2.20 Variations of column-girder moment ratios $\Sigma M_{col}/\Sigma M_{girder}$ with base fixity.

3 Time History Analysis

3.1 GENERAL PURPOSE

A parametric study analyzing the effect of column base rigidity on the seismic demand and behavior of SMRFs was carried out through a series of nonlinear dynamic analyses (time history analyses). The response of the ATC-58 building lateral force-resisting system SMRFs with different column base fixities, presented in Chapter 2, to a set of ground motions selected to represent the typical seismic hazard at the assumed location of the structure (UC Berkeley campus) was computed using two finite element analysis software packages: the OpenSees Navigator package built on the OpenSees nonlinear finite element analysis framework, and the SAP2000 Nonlinear (SAP) package. Nonlinear pushover analyses were carried out first to compare the two software packages. A detailed description of the three-story, three-bay moment frame and the results of the pushover analysis obtained by SAP2000 Nonlinear were presented previously in Chapter 2.

3.2 METHODOLOGY

3.2.1 General Assumptions

The time history analysis was done for SMRF models F (fixed), SR3 (semi-rigid 3), and P (pinned) with column base rotational stiffness K_{norm} of 18.2, 1.4, and 0 EI/L_{col}, respectively. Each model has a different fundamental first period T_1 and a corresponding design spectral acceleration S_a, obtained from a uniform-hazard acceleration design spectra with normal fault rupture directivity effects, defined in the Seismic Guidelines of UC Berkeley Campus, the assumed location of the structure (see Fig. 2.6).

The seismic hazard in the Berkeley area is governed by potential ground motions generated from the Hayward fault which is within 2 miles from the site location of the ATC-58 building. The Hayward fault consists of a strike-slip fault with an expected 7.0 magnitude in the case of a rare earthquake event. The ground motions selected for the design and analysis of the building and utilized in the present study correspond to the fault type, the expected earthquake magnitude, the distance to the fault, and the site conditions (Appendix B).

3.2.2 Modeling Assumptions

The frame model in OpenSees Navigator was defined using a fiber cross-section flexibility-based beam-column finite element with distributed inelasticity and corotational geometric transformation for the beams and columns of the frame, accounting for 3% strain hardening at the material level. The adjacent gravity frames were also included in the model using pinned beam-column connections. Node slaving was defined to account for the horizontal translation of the rigid diaphragm at each level and to disregard modes related to axial deformation of beams and columns. Column base fixity was varied using an elastic rotational spring.

The time history analyses were conducted using the Newmark method integrator. Two damping ratio levels were considered: 5% and 2%. Damping was modeled using Rayleigh damping values that include mass proportional and initial stiffness proportional damping coefficients. The analysis was extended by one half of the duration of the ground motion record beyond its end to observe the structure damping characteristics and decay of motion during free vibration.

The beams and columns of the SMRF SAP2000 Nonlinear model were modeled using elastic beam-column elements and zero length nonlinear link (NLlink) elements with strain-hardening properties corresponding to 3% of the initial stiffness to model the post-yield strain hardening of the plastic hinges. A rigid diaphragm was introduced at each level and only the first three horizontal modes of translation were considered in the analysis. An equivalent 5% viscous damping ratio was considered by default in the fast nonlinear analysis SAP option using the modal superposition method that accounts solely for nonlinearity of the NLlink. The direct integration method that accounts for material and geometric nonlinearities could not be used, since convergence was not achieved due to numerical instability for the previously defined nonlinear behavior of the plastic hinges of the analyzed frames. The time history analysis using modal superposition was carried out for the first 20 sec of each ground motion, which include the strong pulses of each ground motion. Residual displacements were not considered in the SAP analyses.

3.2.3 Pushover Analysis

The load pattern for the pushover analysis was proportional to the first mode of each model with an increasing concentration of deformation in the first story with decreasing base fixity. The displacement demands used for the pushover analysis are presented in Table 3.1.

Table 3.1 Displacement demand for pushover analysis in OpenSees Navigator.

Model	Knorm	T_1-SAP (sec)	T_1-OSN (sec)	ε- Difference (%)	S_a/g 2%-50 yr PE	$S_{d,el}$ (in) 2%-50 yr PE	δ_{roof} (in)
F-Fixed	18.2	0.81	0.75	7.7	1.62	10.37	16.25
SR3	1.4	0.95	0.87	9.0	1.38	12.13	19.01
P-Pinned	0.0	1.15	1.10	4.9	1.14	14.72	23.07

The first-mode period obtained from SAP and OpenSees Navigator differed between 5 and 9% due to differences in the modeling assumptions and the eigenvalue analysis methods. However, the pushover and time history comparison was carried out despite this negligible difference.

3.2.4 Time History Analysis

The time history analyses were conducted using seven ground motions representative of the location of the ATC-58 building in Berkeley, California. The ground motions were scaled to an intensity corresponding to the Collapse Prevention performance level with 2% in 50 years PE, established by FEMA 356. The analyses were carried out using the programs SAP2000 Nonlinear and OpenSees Navigator. The time history analyses were performed to evaluate the actual response of the frames with different column base fixities to severe ground excitation, to compare the time history and the pushover analyses results, and to compare different software packages. According to FEMA 350, both pushover and time history analyses are permitted to be carried out in the Collapse Prevention performance level for regular structures with fundamental first period T_1<$3.5T_s$, which is the case for the analyzed ATC-58 building frames.

The characteristics of the seven ground motions utilized for the nonlinear dynamic analysis (see Appendix B) are presented in Table 3.2.

Table 3.2 Definition of ground motions for time history analysis.

Ground Motion	Earthquake	M_w	Station	Epicentral Distance (km)
LPcorFN	Loma Prieta, USA 10/17/1989	7.0	Corralitos	3.4
LPlgpcFN	Loma Prieta, USA 10/17/1989	7.0	Los Gatos Presentation Center	3.5
LPsrtgFN	Loma Prieta, USA 10/17/1989	7.0	Saratoga Aloha Ave	8.3
LPlex1FN	Loma Prieta, USA 10/17/1989	7.0	Lexington Dam abutment	6.3
KBkobjFN	Kobe, Japan 01/17/1995	6.9	Kobe JMA	0.5
EzerziFN	Erzincan, Turkey 03/13/1992	6.7	Erzincan	1.8
TOhinoFN	Tottori, Japan 10/06/2000	6.6	Hino	1.0

The ground motions with varying durations from 20 to 30 sec and strong pulses from 0.34 to 1.1g were scaled to an equivalent response spectrum (see Fig. 3.1) with respect to the spectral acceleration S_a of each model, corresponding to 2% in 50 years PE hazard level. Other ground motions defined for this site in the Seismic Guidelines of UC Berkeley Campus were disregarded because the required ground motions scale factor greater than 3 was considered to be unrealistic. The scale factors used are provided in Table 3.3.

Table 3.3 Scale factors for ground motions used in time history analysis.

Model	Ground Motions- Scale Factors						
	EZerzi	KBkobj	LPcor	LPlex1	LPlgpc	LPsrtg	TOhino
F-Fixed	2.78	0.63	1.53	1.24	0.80	3.32	0.52
SR3	2.30	0.65	2.34	0.90	1.23	2.83	0.62
P-Pinned	2.21	0.90	2.91	0.85	1.44	2.30	1.02

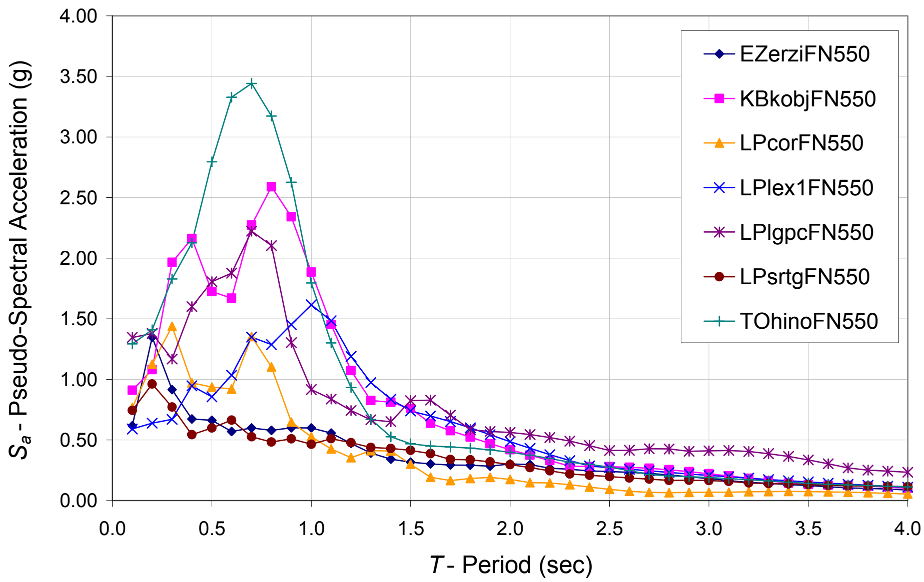

Fig. 3.1 Response spectra for selected ground motions (ζ=5%).

3.3 DISCUSSION OF RESULTS

3.3.1 Displacement Time History

The time history analysis carried out using SAP2000 Nonlinear with the modal superposition method accounts only for the inelastic behavior of the zero length NLlink elements and ignores the frame elements material nonlinearity, as well as the geometric nonlinearity such as P-Delta effects or large deformations. The SMRFs modeled this way exhibit a predominantly symmetric behavior of the frame even after the yielding of the NLlink elements that produces zero residual deformations for all ground motions and the three different frame models, as can be seen in Figures 3.2 and 3.3. These figures also display the time history analysis results obtained using OpenSees Navigator to obtain two different values of Rayleigh damping.

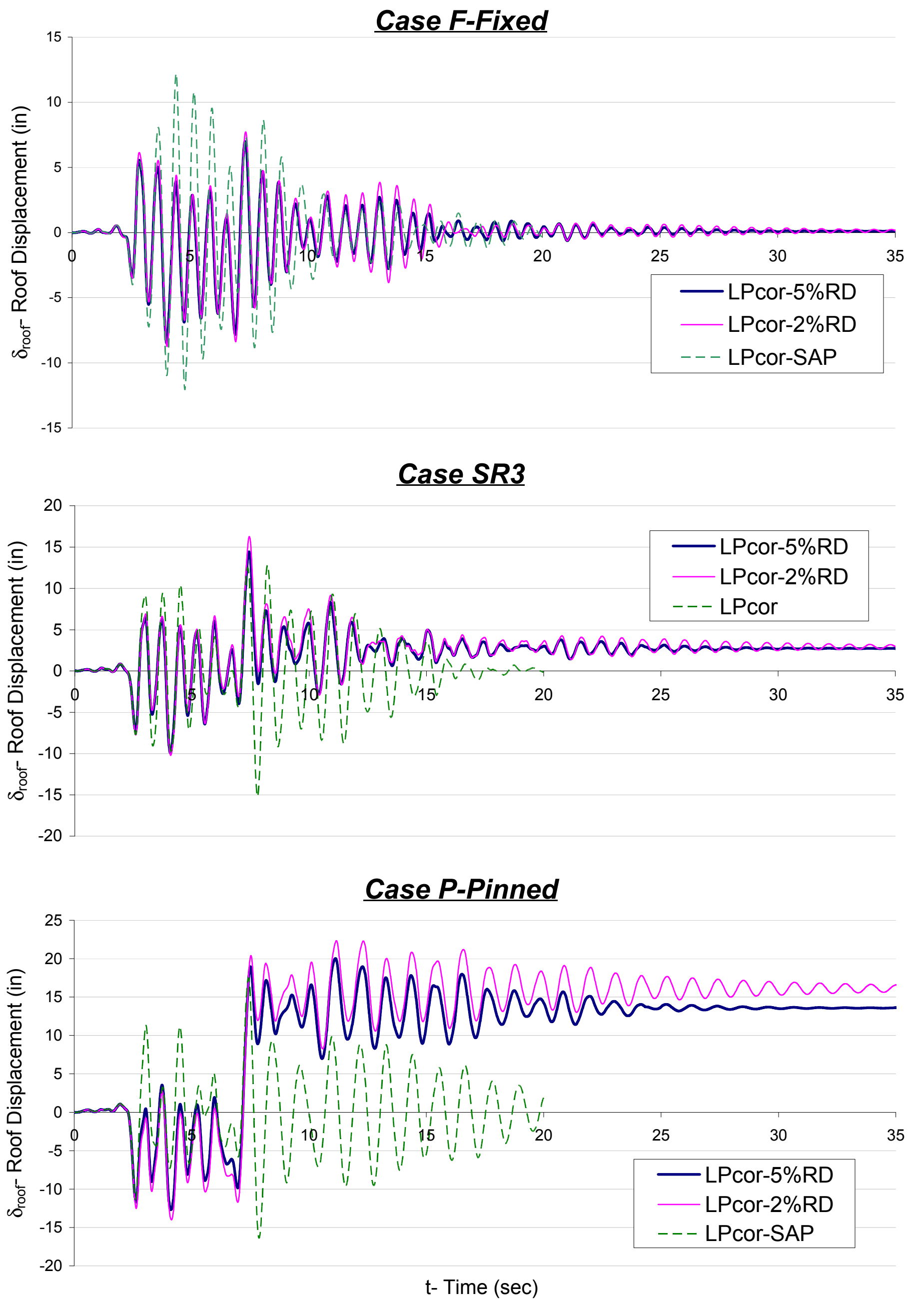

Fig. 3.2 Roof displacement time history (LPcor record) for models F, SR3, and P.

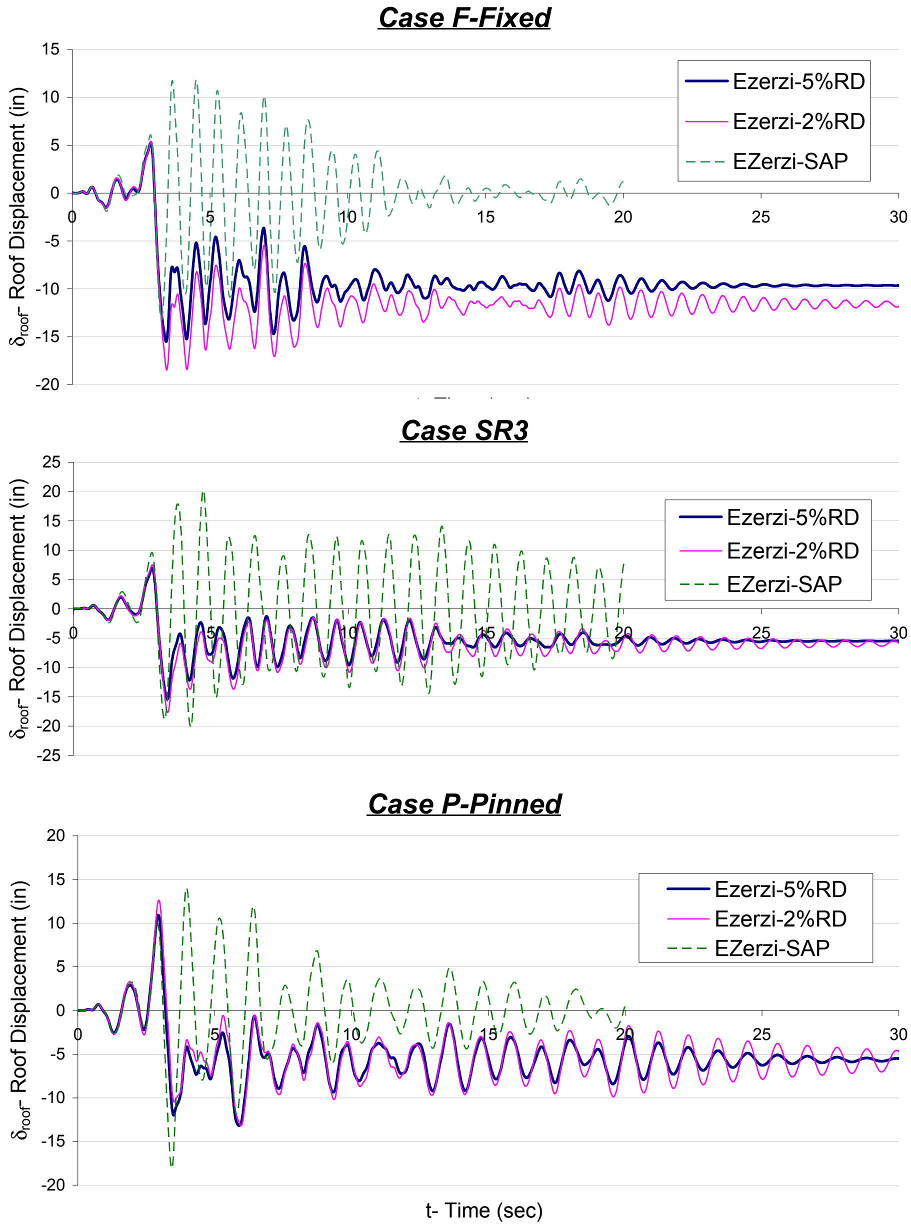

Fig. 3.3 Roof displacement time history (Ezerzi record) for models F, SR3, and P.

The displacement time histories obtained using OpenSees Navigator models exhibit large one-sided inelastic deformations. Such deformations are, in some cases, never recovered and result in significant residual displacements (see Figs. 3.2 and 3.3). This behavior is anticipated for the Collapse Prevention performance level where the intensity of the earthquake is expected to produce significant structural and nonstructural damage. The yielding of the beam-column elements during the strong motions results in permanent deformation in the frame, as well as in permanent rotation of the beam-column and column base connections.

Based on these comparisons, the results obtained from the time history analyses using SAP2000 Nonlinear and the modal superposition method should be considered with significant caution, as they do not seem to be realistic. In a separate project, recommendations for using the direct integration method in SAP2000 Nonlinear to conduct time history analysis of a typical Ordinary Standard Bridge in California were developed (Aviram, Mackie, and Stojadinovic 2007). It may be possible to use these recommendations as a starting point for improved modeling and nonlinear time history analysis of building structures using SAP2000 Nonlinear, but such extension was not made in this project. Henceforth, the time history results discussed in this study will refer to those obtained from the OpenSees Navigator models.

The deformation mechanism and displacement time history of the moment-resisting frame varies with the fundamental first period T_1 of each model. Even though the maximum displacements decrease with base rigidity, the values of the residual displacements do not follow a particular pattern, as can be seen in Figures 3.2 and 3.3. Under certain ground motion excitation, model F has large residual displacements, while model P exhibits no such permanent damage and vice versa. Thus, the comparisons presented below were carried out with respect to the median of the seven time histories, as indicated by FEMA 350, as well as the mean plus or minus one standard deviation values. The EDPs obtained from the time history results were assumed to have a normal distribution, where the mean and median have a similar value (a lognormal distribution has a mean larger than the median, which was not the case for the results in this study).

The effects of two viscous damping ratio values, commonly recommended for the modeling of steel structures, was also analyzed. As can be observed in Figures 3.2 and 3.3, the use of 5% Rayleigh damping ratio (that requires mass and initial stiffness proportional damping coefficients) resulted in smaller displacements and less oscillation during the ground excitation and free vibration phases. Since the values corresponding to 2% Rayleigh damping ratio are more conservative, this value was used for the rest of the analyses.

3.3.2 Maximum Displacements and Drifts

The maximum story displacements and interstory drifts computed during the time-history analysis and pushover analysis are shown in Figures 3.4 and 3.6. The results for the pushover analysis obtained from SAP2000 Nonlinear model differ by less than 1% from those from the OpenSees Navigator model. The pushover forces follow a load pattern proportional to the first mode of each model, which exhibit an increasing tendency of deformation concentration in the first story with reduction in base rigidity. The displacement graphs for both time history and pushover analyses show that the frames responded primarily in their first mode of vibration; however, the actual dynamic response introduces higher-mode effects in the frames, which tend to reduce the maximum displacements and drifts in the structure.

The magnitude of the drifts and displacements varies according to the intensity of the records and the fundamental first period of each frame model. The median and the mean plus one standard deviation (μ+σ) maximum displacement and interstory drift values for the seven time histories of each frame, shown in Figures 3.5 and 3.7, are compared to the pushover analysis results from the same program OpenSees Navigator. The displacement demand obtained using the FEMA356 coefficient method and the displacement spectra corresponding to the Collapse Prevention performance level and first period of each frame should overestimate the displacements obtained through a nonlinear dynamic analysis of the structure. This is confirmed in Figures 3.5 and 3.7, where the maximum values obtained for the pushover analyses (representing the coefficient method deformation targets) are exceeded by 90, 50, and 70% the median of the displacements and drifts from the time history analysis for cases F, SR3, and P, respectively. The pushover analysis deformation values do not exceed by such a large margin the mean plus one standard deviation values of the maximum drifts and displacements obtained from the seven ground motions. As can be observed in Figures 3.5 and 3.7, the results from the two sets of analysis are very similar and differ by only 7, 6, and 11%, in the cases of the F, SR3, and P models, respectively. Thus, the displacement demand coefficient method estimate is adequate, and the results of story displacements and interstory drifts obtained with the pushover analysis are consistent with the time history analysis results for the analyzed frames.

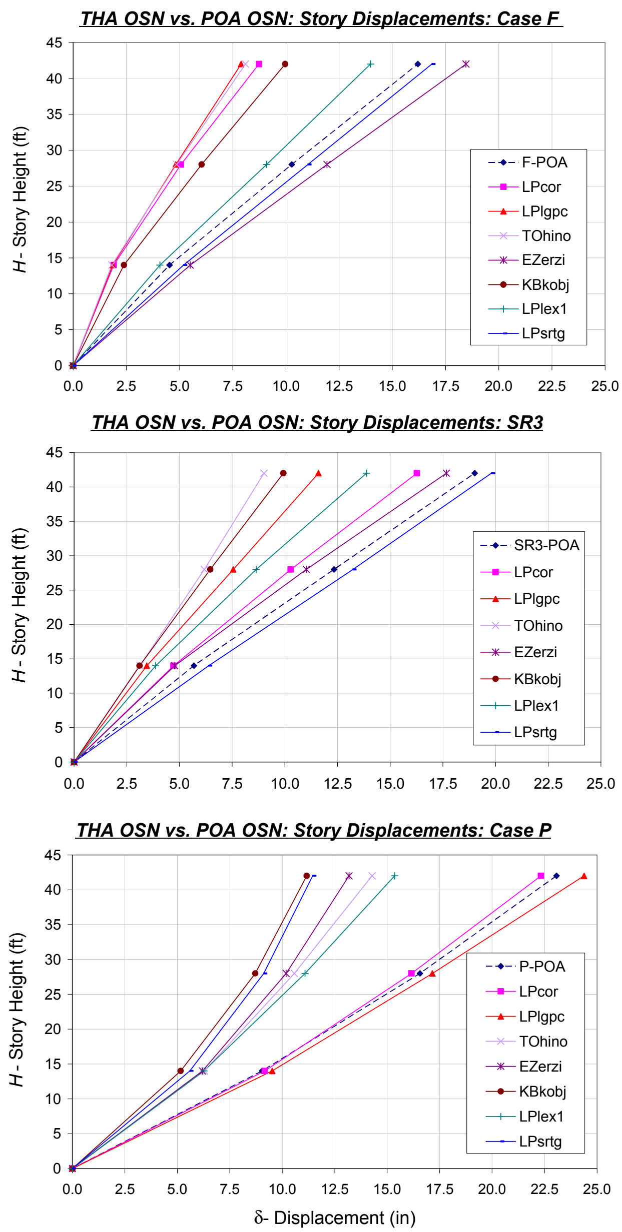

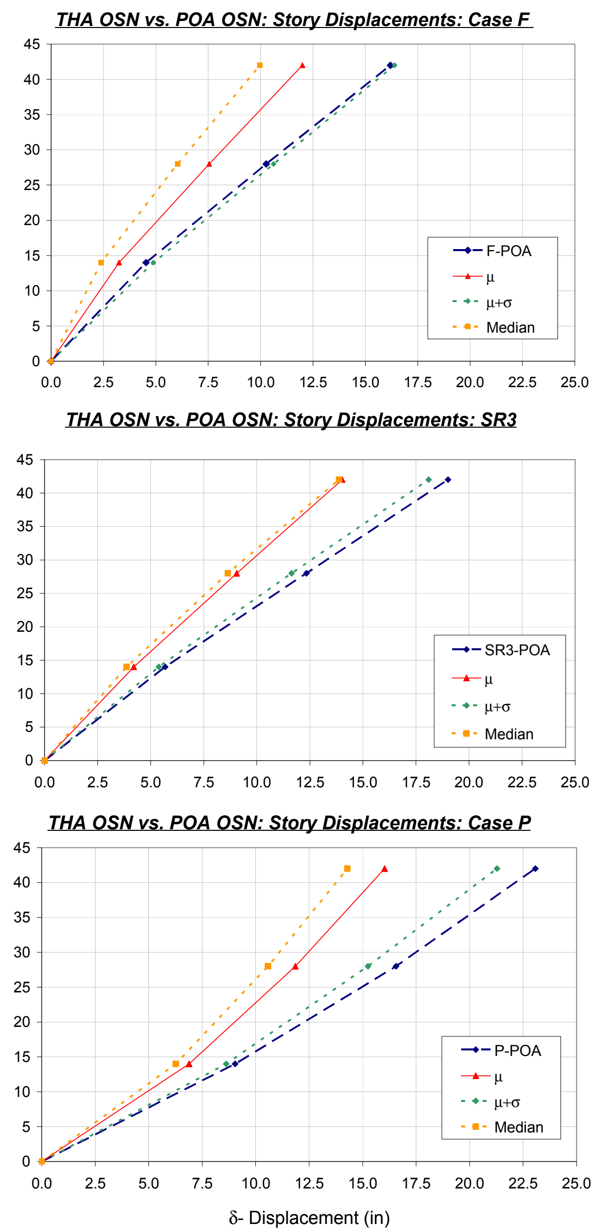

Fig. 3.4 Maximum story displacement for the 7 ground motion records used in time history analysis for models F, SR3, and P.

Fig. 3.5 Comparison between pushover analysis displacements and median, mean and mean plus one standard deviation of the maximum story displacements of the 7 ground motions of time history analysis for models F, SR3, and P.

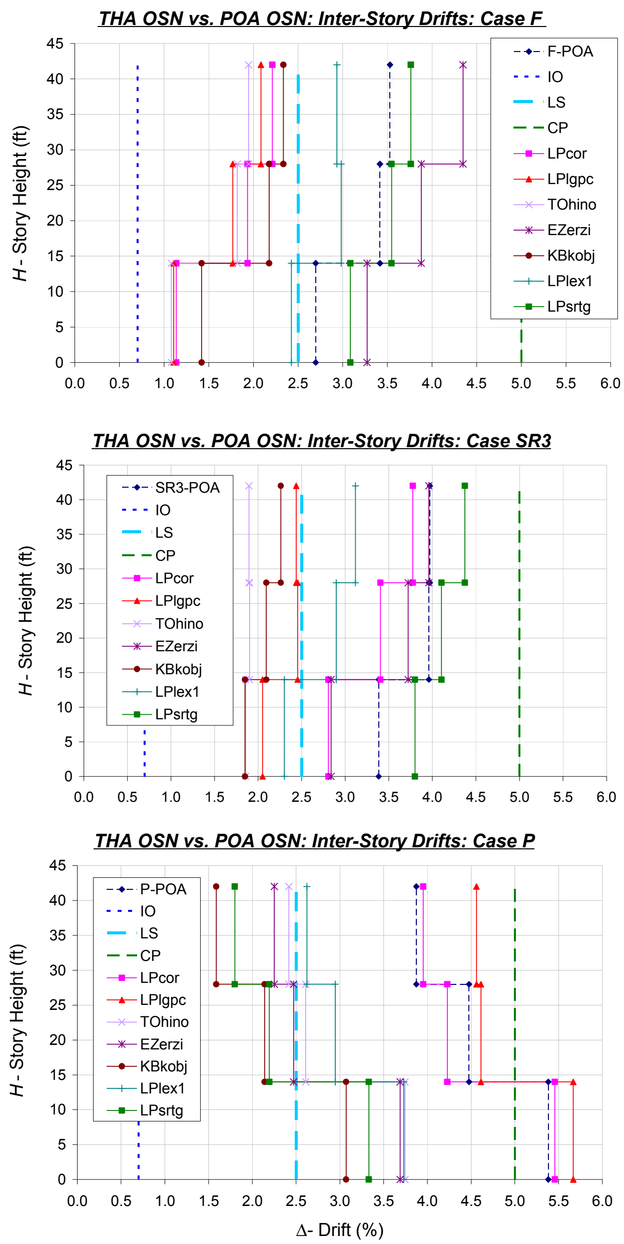

Fig. 3.6 Maximum interstory drifts for the 7 ground motion records used in time history analysis for models F, SR3, and P.

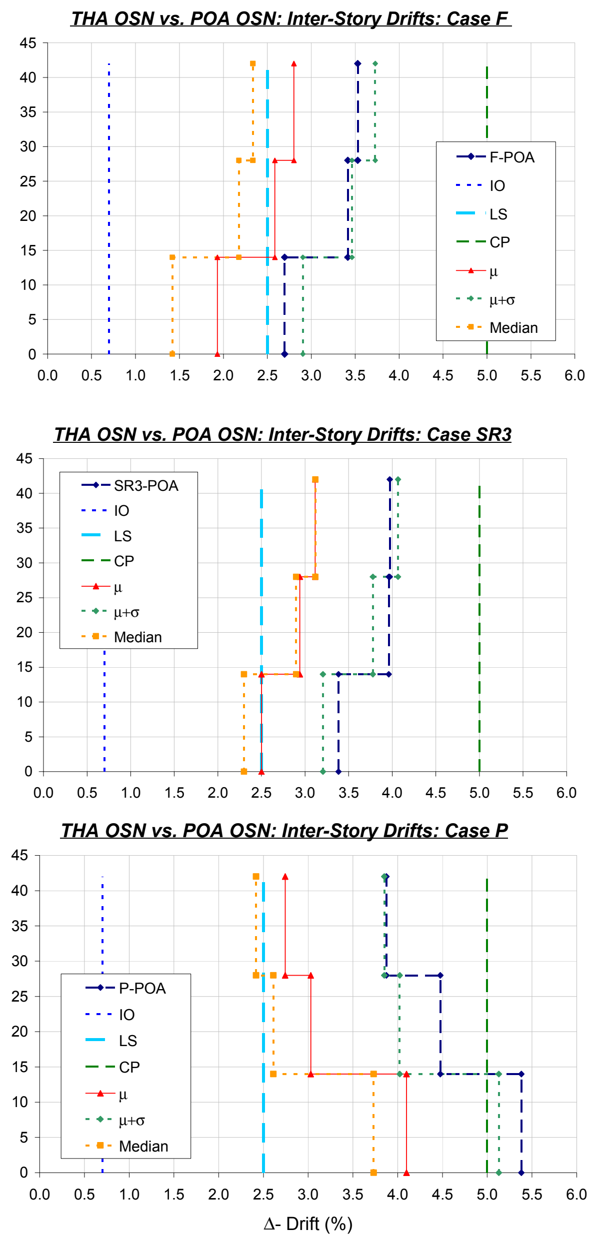

Fig. 3.7 Comparison between pushover analysis drifts and median, mean and mean plus one standard deviation of the maximum interstory drifts of the 7 ground motions of time history analysis for models F, SR3, and P.

3.3.3 Base Shear–Pushover Analysis

The results for the pushover curves obtained from the SAP2000 Nonlinear and OpenSees Navigator analysis programs, shown in Figure 3.8, differ by less than 7% for the three frame types. The initial elastic stiffness of the frames obtained with OpenSees Navigator is slightly higher than that obtained using SAP; nevertheless, the overall shape of the pushover curve and the ultimate base shear are similar for all cases. As expected, the initial stiffness increases with increasing base rigidity. Except for the pinned case, where the base shear capacity is substantially lower, the base shear capacity is almost the same for the semi-rigid and fixed cases.

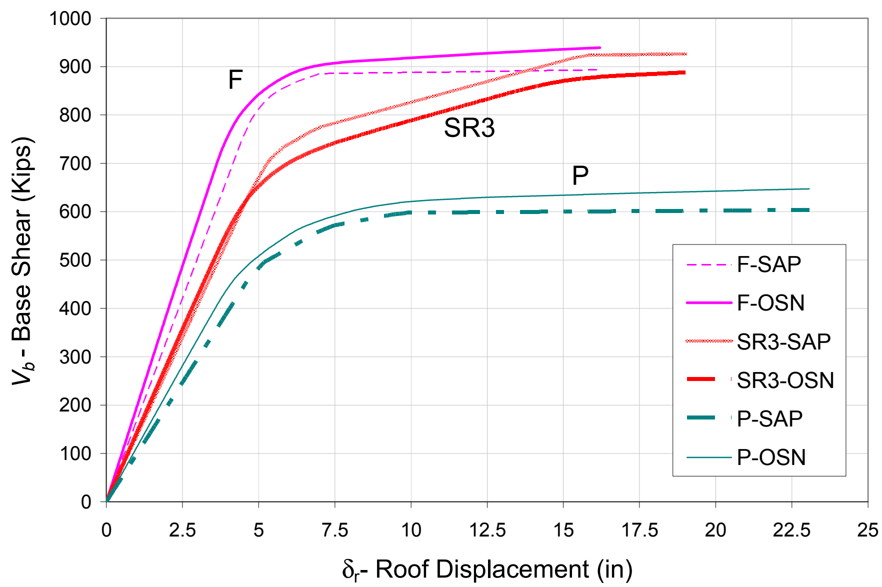

Fig. 3.8 Pushover curves: comparison between SAP and OpenSees Navigator results.

After yielding of the frame beams and columns and the formation of the plastic collapse mechanism, the hardening slope of the pushover response curves for the two programs varies due to differences in modeling assumptions. The SAP models include only a discrete location of the plastic hinges with a bilinear behavior at the ends of beams and columns elements, while OpenSees Navigator models utilize distributed inelasticity of the members. Nevertheless, the differences are small.

3.3.4 Base Shear–Time History Analysis

Material model Steel01, used in OpenSees Navigator to define the behavior of beam-column elements, accounts for isotropic hardening or expansion of the yield surface in all directions, which leads to significant yielding capacity increment after several cycles. The kinematic hardening properties of steel or Bauchinger's effect, which produce the translation of the yield surface, are not included in the OpenSees Navigator model. The model in SAP2000 Nonlinear is bilinear in discrete locations with zero length, and does not account for isotropic or kinematic hardening.

The stress increment in isotropic hardening is dependent on the strain rate and reversal of stress cycles; thus only the time history or nonlinear dynamic analysis of the frame can capture the increase in the yield strength and ultimate capacity, while the pushover analysis, which consists of an incremental monotonic loading does not capture this behavior. Figure 3.9 displays the force-displacement response of the external and the interior first-story columns of the fixed model with significant element shear increase due to strain hardening during dynamic excitation, in this case the LPsrtg ground motion record.

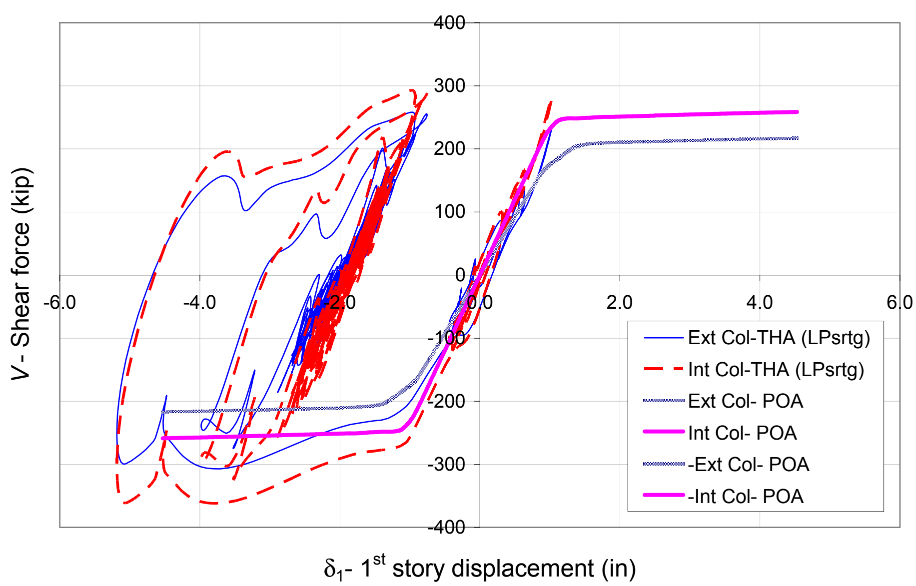

Fig. 3.9 Force-displacement column response for the F model: results of pushover analysis and time history analysis in OpenSees Navigator (LPsrtg record).

The results for the maximum base shear generated during the time history analysis and the ultimate base shear of the pushover analysis for models F, SR3, and P are presented in Figure 3.10. The magnitude of the base shear varies according to the intensity of the records and the fundamental first period of each model. It can be noticed that the maximum base shear values due to the seven ground motions all exceed the results of the pushover analysis in the three frame types due to the significant strain-hardening behavior that can be captured only during the dynamic analysis. The median, as well as the mean minus one standard deviation (μ-σ) of the seven time histories of each frame, seen in Figure 3.11, were compared to the pushover analysis results from the same program OpenSees Navigator. It can also be noticed that the mean and median have a similar value; thus the time history analysis response parameters are likely to have a normal distribution.

The results obtained from the time history analysis are more conservative, since a more realistic estimate of the elements capacity will result in a greater seismic force demand on the frame. Base shear demand will be underestimated using pushover analysis: this may result in local or global failure of the frame for the Collapse Prevention hazard level. The median of the maximum base shear values obtained from the seven ground motions exceed by 15, 21, and 24% the results from the pushover analysis, for cases F, SR3, and P, respectively. However, the difference is reduced to 8, 14, and 18% when comparing the pushover analysis results with the mean minus one standard deviation values of the time history analysis, as can be observed in Figure 3.11. The pushover analysis in OpenSees Navigator and SAP2000 Nonlinear models should be calibrated to account for isotropic hardening or yield strength increment during dynamic loading, which represents a more realistic behavior of the steel beam-column elements and the entire moment-resisting frame.

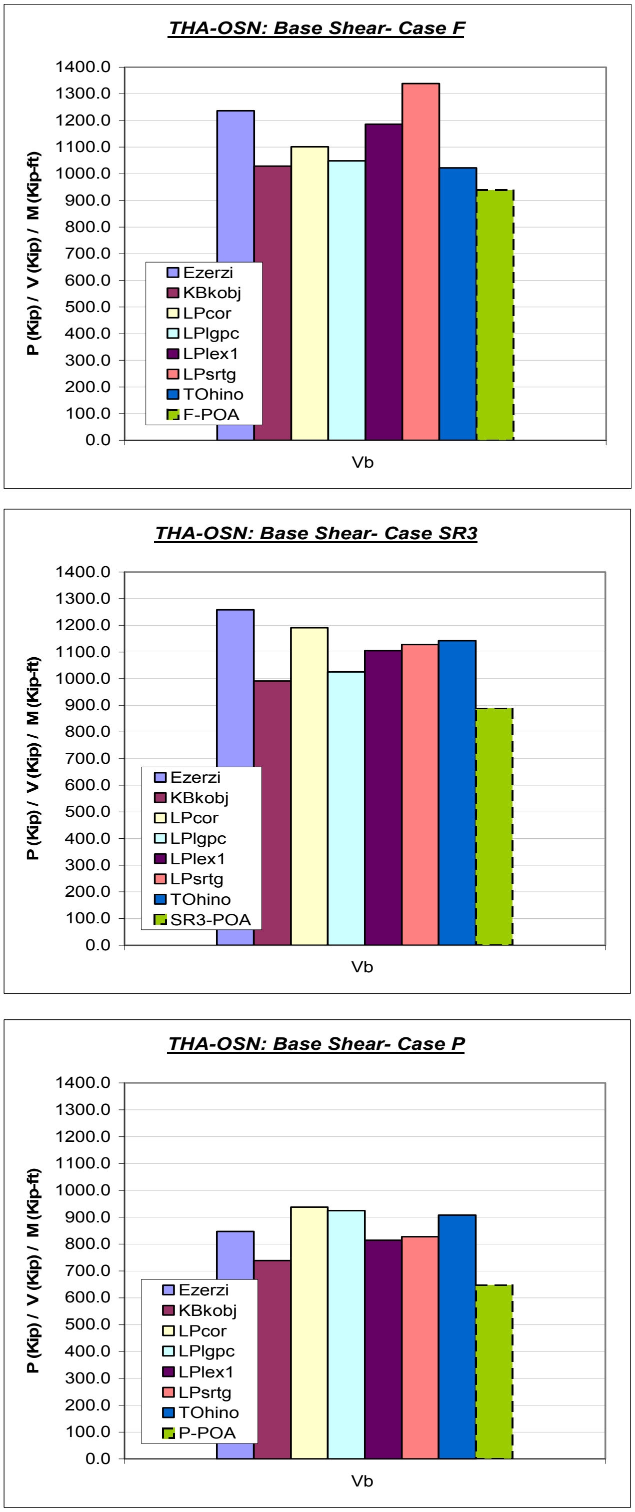

Fig. 3.10 Maximum base shear for the 7 ground motions used in time history analysis for models F, SR3, and P.

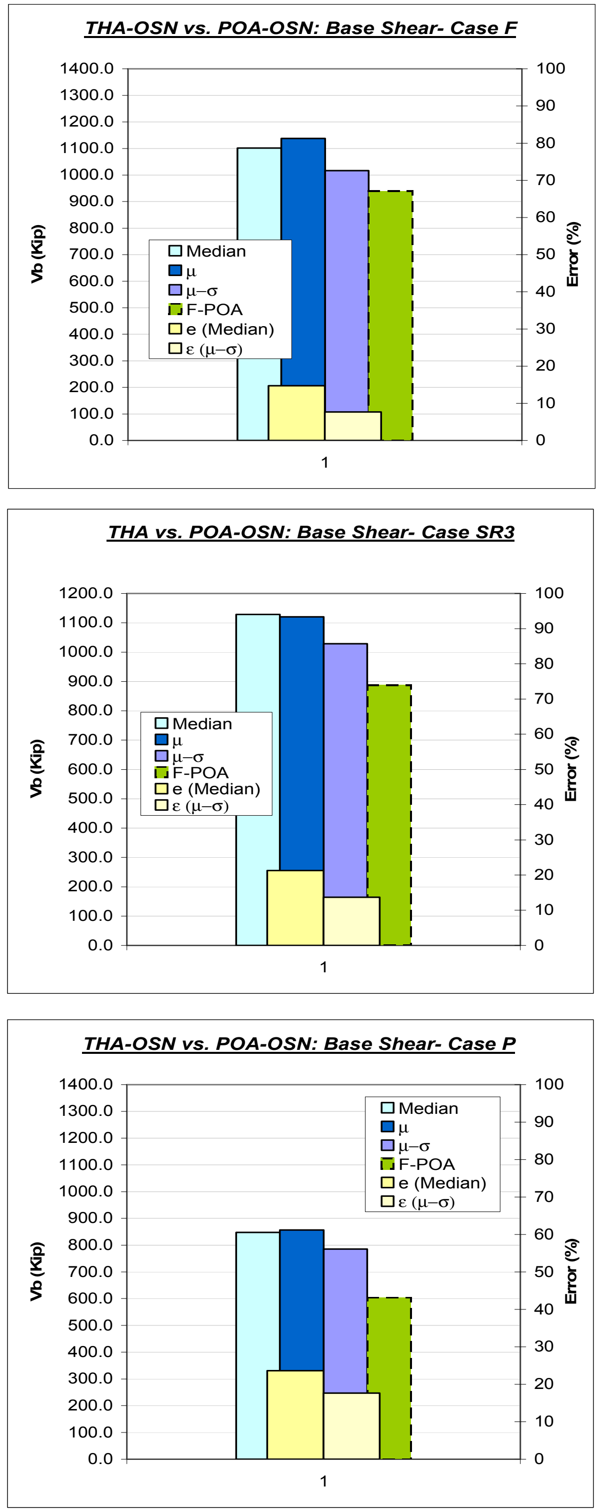

Fig. 3.11 Comparison between pushover analysis base shear and median, mean and mean minus one standard deviation values of time history analysis for models F, SR3, and P.

3.3.5 Joint Reactions

The results for axial force, shear, and bending moment for both interior and external first-story columns are presented for all frames and analysis types in Figure 3.12. The results for the pushover analyses obtained from SAP2000 Nonlinear and OpenSees Navigator differ by only 5, 4, and 9% for the F, SR3, and P frames, respectively.

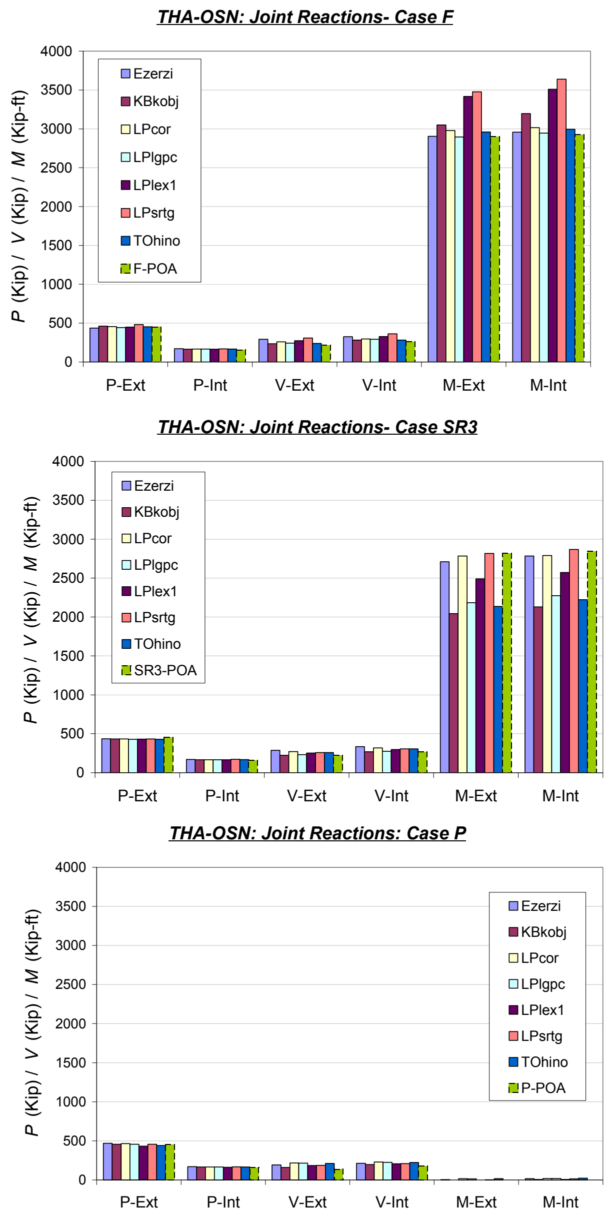

Fig. 3.12 Maximum external and internal column joint reactions for the 7 ground motion records used in time history analysis for models F, SR3, and P.

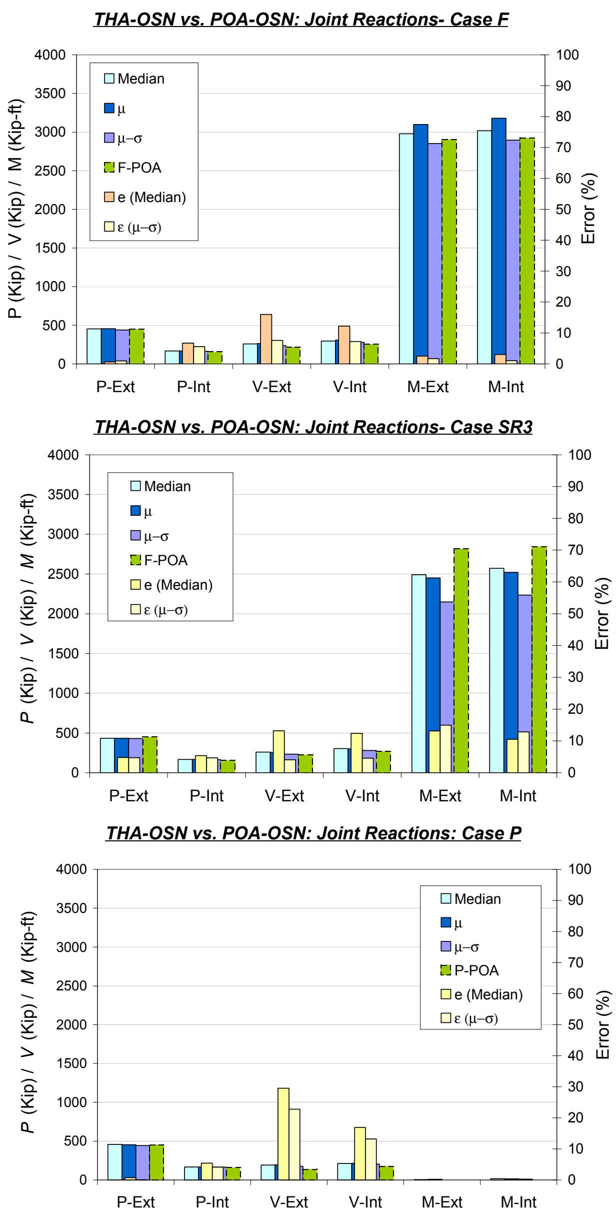

Fig. 3.13 Comparison between pushover analysis joint reactions and median, mean and mean minus one standard deviation values of time history analysis for models F, SR3, and P.

The axial forces in the columns are a function of the gravity loads that remain invariable throughout the analysis and the beam shears that are proportional to the beam's plastic moment capacity. Therefore, the axial demand on the columns is independent of base rigidity and remains close to constant for both the time history analysis and pushover analysis. The pushover results differ by only 7% from the median of the time history analysis values of axial joint reactions.

The maximum moment demand is very similar for the external and interior columns, since both have the same cross-section and plastic capacity. For the pinned case, no bending moment demand is generated in the column bases. The moment magnitude in the time history analysis varies according to the intensity of the ground motion records and the fundamental first period of the frames, which alters the seismic response of the fixed and semi-rigid models. Each ground motion causes a different strain rate and stress reversal cycles history, and therefore the increase in moment capacity after yielding of the column bases has a significant variation, as can be seen in Figure 3.12. The comparison in Figure 3.13 between the time history analysis and the pushover analysis shows that the pushover analysis underestimates the column moments by 13% and 15%, respectively, compared to the median and mean minus one standard deviation of the seven ground motions, respectively.

The column shears are obtained from the end moments of the columns. Because the column ends undergo different isotropic hardening increments after each yielding cycle, the variation of the first-story column shears is also dependent on the intensity and characteristics of the ground motion, as well as the frame type. The comparison between the time history analysis and pushover analysis shows that the pushover analysis column shears are 30 and 23% smaller than the median and mean of the seven ground motions, respectively. As stated previously for the base shear, the pushover analysis in OpenSees Navigator and SAP2000 Nonlinear models should be calibrated to account for isotropic hardening or yield strength increment during dynamic loading, to represent more realistically the behavior of the special moment-resisting steel frame.

4 Performance-Based Repair Cost Evaluation

4.1 GENERAL PURPOSE

The PEER Center performance-based earthquake engineering (PBEE) methodology (Yang 2005, 2006) was used to evaluate the effect of column base rotational stiffness on the post-earthquake repair cost of a typical low-rise special steel moment-resisting frame building. The ATC-58 example office building, located on the University of California at Berkeley campus, was analyzed using three frame column base models: the fixed column base (labeled “F,” with K_{norm}=18EI/L_{col}), the semi-rigid column base (“SR3,” with K_{norm}=1.4EI/L_{col}), and the pinned column base (“P,” with K_{norm}=0).

4.2 NONLINEAR TIME HISTORY ANALYSIS

The hazard levels considered in this PBEE analysis were the 2%, 5%, 10%, 50%, and 75% in 50 years probability of exceedance (PE), with a return period of 2475, 975, 475, 75, and 35 years, respectively. The interstory drifts and floor accelerations required for the PBEE analysis were computed for each moment-resisting frame and for these hazard levels using nonlinear time history analysis with the finite element software OpenSees Navigator, as described in Chapter 3.

The selection of the ground motions for the time history analysis of the building located on the UC Berkeley Main Campus was determined by spectral matching at the first-mode period of the structure. Seven ground motions were obtained accordingly for low and high hazard level groups, out of 10 possible records considered for the site with similar magnitude, distance, tectonic environment, and site classification. The fault-normal component was selected for each time history, accounting for forward directivity effects that can occur at the site. The selected ground motions and their main characteristics are listed in Tables 4.1 and 4.2.

Table 4.1 Ground motion time histories representing the 2%, 5%, and 10% in 50 yrs PE hazard levels.

Ground Motion	Earthquake	M_w	*Station*	*Distance to Epicenter (km)*
LPcorFN	Loma Prieta, USA 10/17/1989	7.0	Corralitos	3.4
LPlgpcFN	Loma Prieta, USA 10/17/1989	7.0	Los Gatos Presentation Center	3.5
LPsrtgFN	Loma Prieta, USA 10/17/1989	7.0	Saratoga Aloha Ave	8.3
LPlex1FN	Loma Prieta, USA 10/17/1989	7.0	Lexington Dam abutment	6.3
KBkobjFN	Kobe, Japan 01/17/1995	6.9	Kobe JMA	0.5
EzerziFN	Erzincan, Turkey 03/13/1992	6.7	Erzincan	1.8
TOhinoFN	Tottori, Japan 10/06/2000	6.6	Hino	1.0

Table 4.2 Ground motion time histories representing the 50% and 75% in 50 yrs PE hazard levels.

Ground Motion	Earthquake	M_w	*Station*	*Distance to Epicenter (km)*
CLgil6	Coyote Lake, USA 06/08/1979	5.7	Gilroy #6	1.2
PFcs05	Parkfield, USA 06/27/1966	6.0	Array #5	3.7
PFcs08	Parkfield, USA 06/27/1966	6.0	Array #8	8.0
PFtemb	Parkfield, USA 06/27/1966	6.0	Temblor	4.4
MHclyd	Morgan Hill, USA 04/24/1984	6.2	Coyote Lake Dam abutment	0.1
MHandd	Morgan Hill, USA 04/24/1984	6.2	Anderson Dam Downstream	4.5
MHall	Morgan Hill, USA 04/24/1984	6.2	Halls Valley	2.5

By scaling the ground motions to the spectral value at the first-mode period of each model (ranging from 0.75 to 1.10 sec, from the fixed to the pinned frame, respectively), the shape of the response spectra and particular characteristics of each ground motion were preserved. The corresponding scale factors (not exceeding 3) are presented in Appendix C. The unmodified response spectra used for low and high hazard level groups can be seen in Figures 3.1 and 4.1.

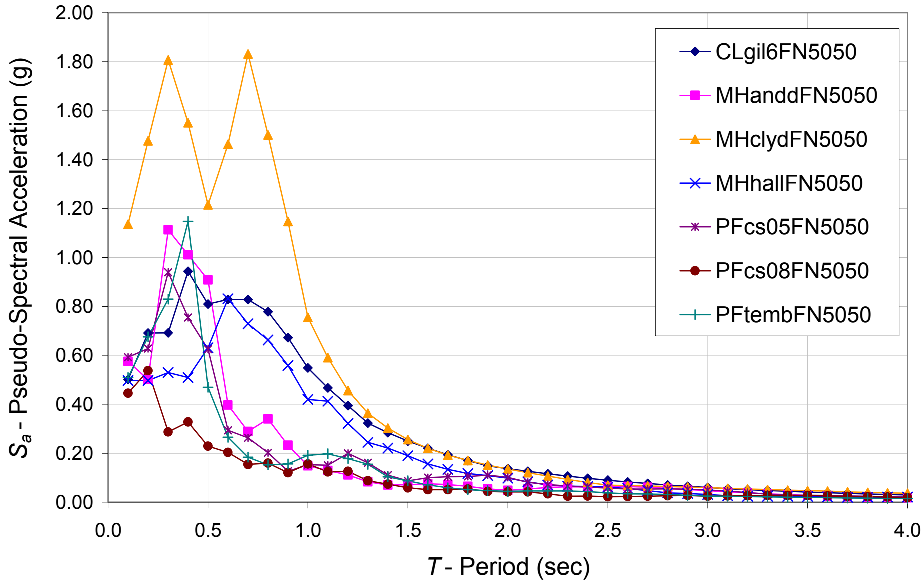

Fig. 4.1 Response spectra for selected ground motions (50% in 50 yrs PE), (ζ=5%).

4.3 HAZARD CURVES

For the PBEE analysis, the preferred ground motion intensity measure (IM) was the spectral acceleration at the estimated first natural period of the structure ($S_{a,T1}$ or PS_a/g at T_1). The values for the three models and for the five hazard levels considered in the analysis are presented in Table 4.3.

Table 4.3 Ground motion IM values at different hazard levels considered in the PBEE analysis.

Hazard Level PE in 50 yr	Return Period (yr)	1/R	Ps_a/g at T_1 F	SR3	P
2%	2475	0.00040	1.62	1.38	1.14
5%	975	0.00103	1.30	1.15	0.92
10%	475	0.00211	0.99	0.87	0.69
50%	75	0.01333	0.33	0.30	0.26
75%	36	0.02778	0.23	0.22	0.19

The following logarithmic relation was used in the PBEE analysis to approximate the site hazard curve:

$$H(s_a) = P[S_a \geq s_a] = k_o s_a^{-k} \tag{4.1}$$

The hazard level $H(S_a)$ is the inverse of the return period of a certain level of ground shaking. The coefficients for the logarithmic regression k and k_0 for the hazard curve are presented in Table 4.4 and the corresponding curves can be seen in Figure 4.2.

Table 4.4 Coefficients of regression analysis for hazard curves for models F, SR3, and P.

Regression Analysis: $f=1/R=k_oPS_{aT1}^{-k}$	F	SR3	P
$k=-\log(f_{,1}/f_{,2}))/\log(S_{aT1,1}/S_{aT1,2})=$	2.20	2.29	2.37
$k_o=f_{,1}/S_{aT1,1}^{-k}=$	1.17E-03	8.45E-04	5.51E-04

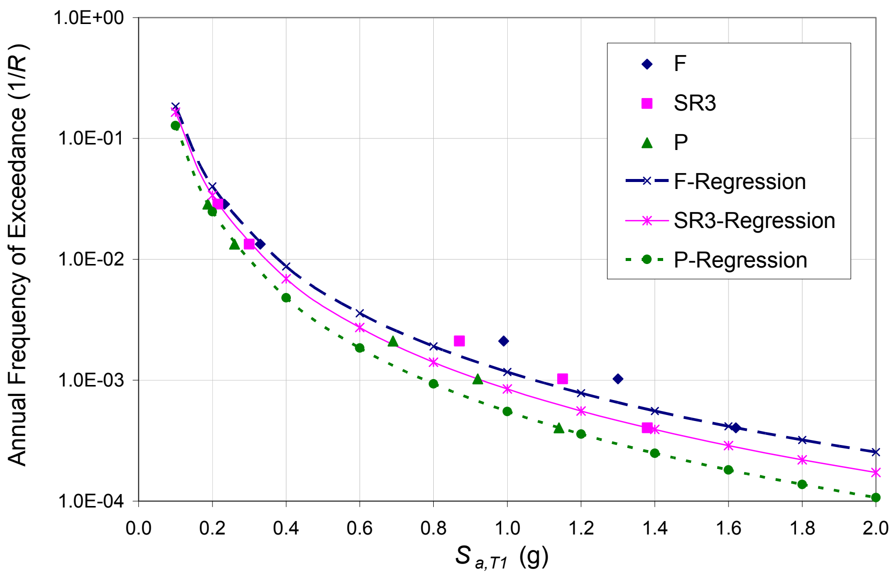

Fig. 4.2 Hazard curves for models F, SR3, and P.

The slope m of the hazard curve at a certain IM level (S_a value) is computed as the first derivative of the hazard curve:

$$m = d(H(s_a))/d(s_a) = -k \cdot k_o s_a^{-(k+1)} \tag{4.2}$$

The slopes of the hazard curves for the three frame models for all hazard levels are presented in Table 4.5. Note that the slopes of the hazard curves for low hazard levels are significantly larger than those for high hazard levels. This is the reason why frequent events with low levels of ground shaking may have a greater contribution to the mean annual total repair costs of the structure than extreme yet rare seismic events.

Table 4.5 Slope m of hazard curves for models F, SR3, and P.

Hazard Level	F	SR3	P
2%	-5.48E-04	-6.71E-04	-8.38E-04
5%	-1.11E-03	-1.22E-03	-1.73E-03
10%	-2.65E-03	-3.06E-03	-4.54E-03
50%	-8.88E-02	-1.02E-01	-1.21E-01
75%	-2.70E-01	-3.05E-01	-3.61E-01

4.4 REPAIR COSTS FRAGILITY CURVES

The EDPs for the three-story moment-resisting frame were the peak floor accelerations and interstory drifts. These six EDPs were computed for the three frame models and for seven representative ground motions at each hazard level considered (a total of 105 analyses). A correlation matrix representing the correlation structure among the six EDPs was computed for each hazard level. This correlation matrix with joint lognormal distribution, together with artificially generated standard normal random variables, were used to generate correlated EDP realizations for damage analysis by means of the Cholesky decomposition method. Instead of computing the peak response for additional time-consuming nonlinear dynamic analysis, the EDP matrix for all hazard levels and models can easily be extended to a very large number of ground motions.

The major structural and nonstructural components of the building susceptible to earthquake damage were organized into performance groups affected by a particular EDP, as presented in Table 4.6. The drift-sensitive performance groups include the structural lateral load-resisting system, the exterior façade, and the nonstructural interior partitions, while the acceleration-related performance groups include the interior nonstructural components, the contents, and the equipment. The notation used in Table 4.6 is Δu_i=interstory drift at the ith story, a_i= absolute total acceleration at the ith floor, μ= median value of EDP, and β=beta or slope of the fragility curve.

Table 4.6 Performance group summary and damage state fragility curves.

PG No.	Name	Location	EDP	Components	Fragilities	>= DS2	>= DS3	>= DS4
1	SH12	between levels 1 and 2	Δu_1	**Structural lateral:** lateral load resisting system; damage oriented fragility (direct loss calculations)	μ	1.5	2.5	3.5
					β	0.25	0.3	0.3
2	SH23	between levels 2 and 3	Δu_2		μ	1.5	2.5	3.5
					β	0.25	0.3	0.3
3	SH3R	between levels 3 and R	Δu_3		μ	1.5	2.5	3.5
					β	0.25	0.3	0.3
4	EXTD12	between levels 1 and 2	Δu_1	**Exterior enclosure:** panels, glass, etc.	μ	2.8	3.1	
					β	0.097	0.12	
5	EXTD23	between levels 2 and 3	Δu_2		μ	2.8	3.1	
					β	0.097	0.12	
6	EXTD3R	between levels 3 and R	Δu_3		μ	2.8	3.1	
					β	0.097	0.12	
7	INTD12	between levels 1 and 2	Δu_1	**Interior nonstructural drift sensitive:** partitions, doors, glazing,etc	μ	0.39	0.85	
					β	0.17	0.23	
8	INTD23	between levels 2 and 3	Δu_2		μ	0.39	0.85	
					β	0.17	0.23	
9	INTD3R	between levels 3 and R	Δu_3		μ	0.39	0.85	
					β	0.17	0.23	
10	INTA2	below level 2	a_2	**Interior nonstructural acceleration sensitive:** ceilings, lights, sprinkler heads, etc	μ	1	1.5	2
					β	0.15	0.2	0.2
11	INTA3	below level 3	a_3		μ	1	1.5	2
					β	0.15	0.2	0.2
12	INTAR	below level R	a_R		μ	1	1.5	2
					β	0.15	0.2	0.2
13	CONT1	at level 1	a_2	**Contents**: General office on first and second floor, computer center on third	μ	0.3	0.7	3.5
					β	0.2	0.22	0.25
14	CONT2	at level 2	a_3		μ	0.3	0.7	3.5
					β	0.2	0.22	0.25
15	CONT3	at level 3	a_R		μ	0.3	0.7	3.5
					β	0.2	0.22	0.25
16	EQUIPR	at level R	a_R	**Equipment on roof**	μ	1	2	
					β	0.15	0.2	

For each performance group, different damage states were defined in terms of fragility curves representing the probability of damage being equal to or greater than the threshold damage given a certain level of the associated EDP, P(EDP≥edp). The fragility curves are defined using a two-parameter lognormal conditional probability function. The parameters of this distribution are the value of the EDP corresponding to the damage median and the dispersion of the distribution (beta) corresponding to the slope of the fragility curve. The slope of the fragility curves [P(DS≤ds) vs. EDP] reflects the uncertainty associated with the damage state evaluation: the higher the slope, the higher the uncertainty (see Fig. 4.3).

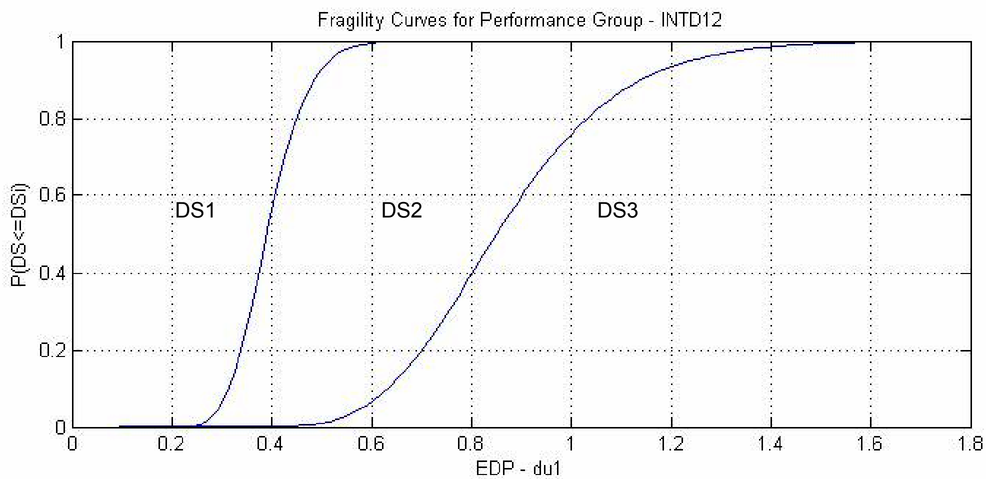

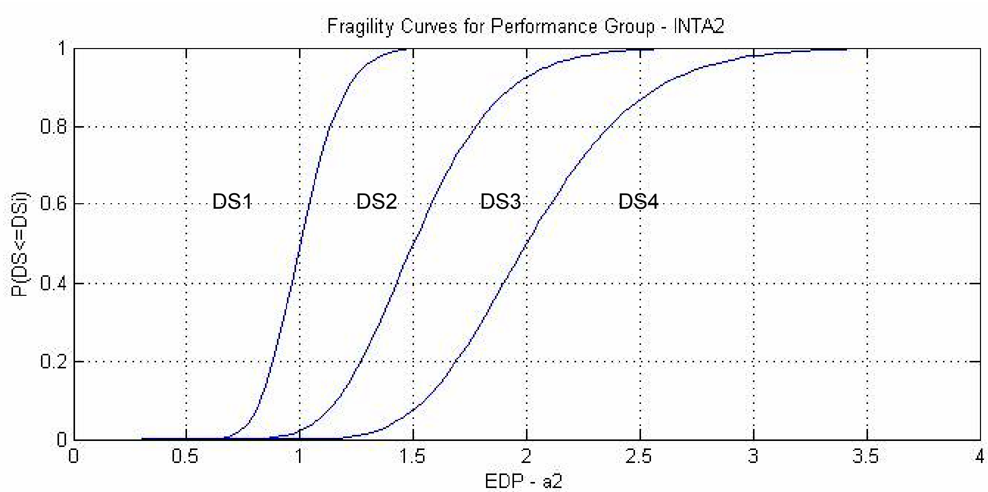

Fig. 4.3 Typical fragility curves.

The probability of the performance group being at a certain damage state, given an EDP value obtained using the correlated EDP generator for each hazard level, was computed using a uniformly distributed random number generator. The quantities of the material needed to repair each performance group in each damage state were defined in the ATC-58 project (see Appendix C). The amounts of materials needed to repair the entire building were computed for each correlated EDP value. Then, the cost of such repair was computed using a cost look-up table, accounting for the price uncertainty. The base unit cost was adjusted based on the tabulated beta factors of the fragility curves and a random number generator, before multiplying it by the total quantities associated with each repair measure. This Monte Carlo simulation procedure was used to generate a large number of cost realizations, making it possible to describe the conditional probability of repair costs exceeding threshold values, given a value of earthquake intensity measure. This procedure was repeated 500 times for each model at every hazard level. The number of simulations required to obtain a representative statistical probability measure was determined by the quality of the lognormal fit to the simulation data (Fig. 4.4). The fitted lognormal distribution of the building repair cost at a certain IM level is referred to as a cumulative distribution function or CDF.

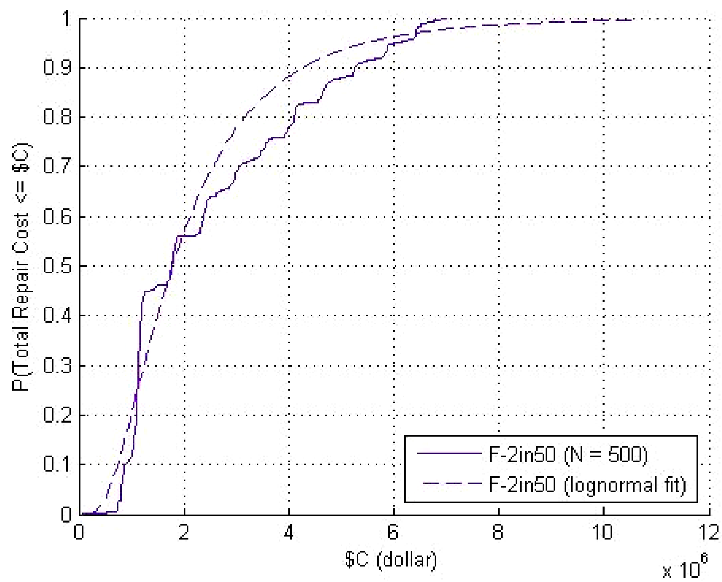

Fig. 4.4 Lognormal fit of the CDF curves for the cost realization simulations.

The CDF curves were generated for all three models for the five hazard levels considered. The threshold established for the repair cost estimation in this PBEE analysis is the 75% in 50 years PE hazard level. That is, it is assumed that low levels of ground shaking during very frequent earthquakes with a return period smaller than 35 years will not produce any damage in the building and the corresponding repair cost can be neglected. A minimum inspection and consulting fee of $1,000 dollars additional to the repair cost of the building and its content was assigned for all hazard levels to avoid a zero-cost realization outcome.

The damage in different performance groups in the same earthquake event was assumed to be statistically independent in this study. Thus, we can analyze their individual contributions to the total cost of repair. The disaggregation of the total repair cost among the different performance groups is provided in Appendix C or in Figure 4.5 for the fixed frame at the 2% in 50 years PE hazard level. As can be observed, the damage in the building corresponds to drift-related performance groups, primarily the interior nonstructural components and partitions group PG 1–9. The probability of damage to nonstructural components related to floor acceleration (PG 10–16) is almost negligible.

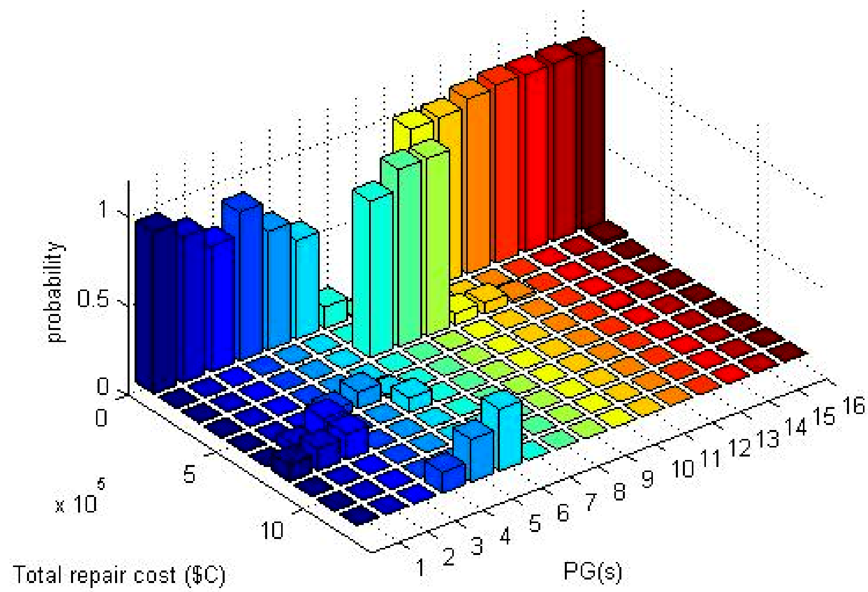

Fig. 4.5 Distribution of repair cost per performance groups, fixed-base frame at the 2% in 50 yrs PE hazard level.

The effects of different hazard levels can be observed clearly in Figure 4.6. For high levels of ground shaking, the increase in floor acceleration and interstory drift produces greater damage to the different performance groups, and hence the CDF curves for all frames shift towards higher repair cost values.

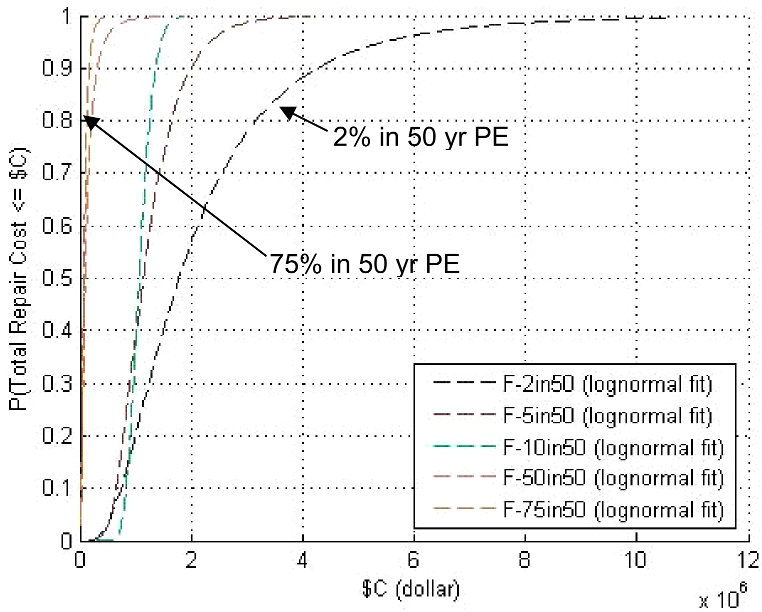

Fig. 4.6 Cumulative CDF curves for fixed moment-frame: effect of hazard level.

The complement of the CDF curves is presented as a surface in Figure 4.7a, with equal contributions from the different hazard levels. For each IM level the surface is multiplied by the slope of the hazard curves presented in Figure 4.3 at the corresponding IM (in this study the pseudo-acceleration S_a at T_1), thus obtaining the modified surfaces presented in Figure 4.7b. The integration of the complementary CDF with the hazard curve result in the annual rate of exceeding the total repair cost threshold. Linear interpolation was used to obtain complementary CDF values for hazard levels between the ones for which the computations were done.

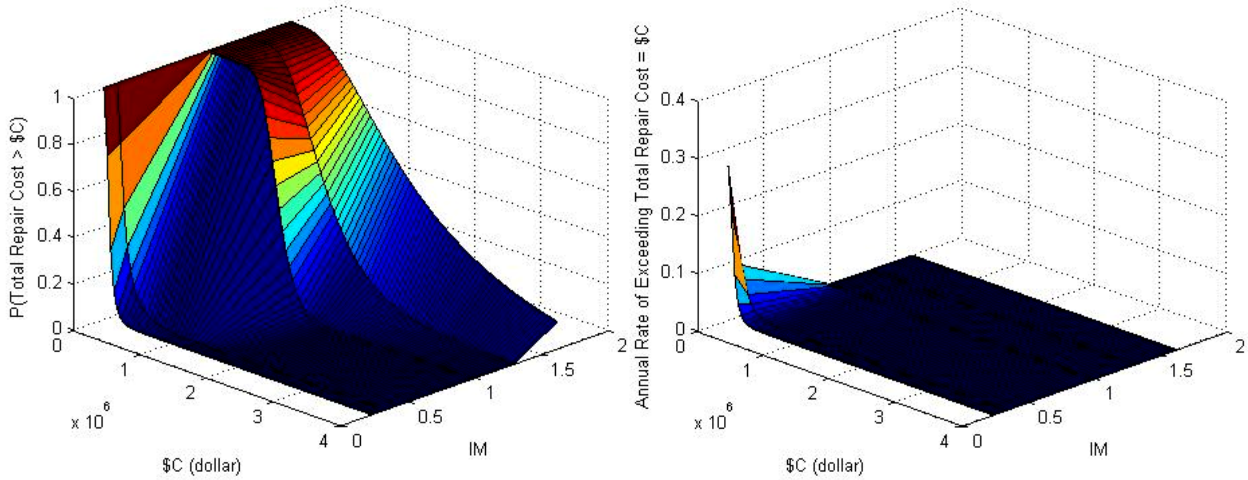

Fig. 4.7 Surfaces for fixed-base model: (a) CCDF curves at all IM levels representing probability of exceeding total repair cost threshold; (b) CCDF curves multiplied by slope of hazard curve at each IM level, representing annual rate of exceeding total repair cost threshold.

The resulting curve is integrated across the IM level, thus obtaining the loss curve, which is the annual rate of exceeding various values of total repair cost thresholds for all the IM levels (Fig. 4.8). The mean cumulative annual total repair cost is the area under the loss curve, obtained by integrating the curve over the range of repair cost thresholds.

Fig. 4.8 Loss curve for fixed-base model.

4.5 EFFECT OF COLUMN BASE BEHAVIOR

The effect of base fixity on the repair cost cumulative distribution functions (CDF) is shown in Appendix C, or in Figure 4.9 for the 2% in 50 years PE hazard level.

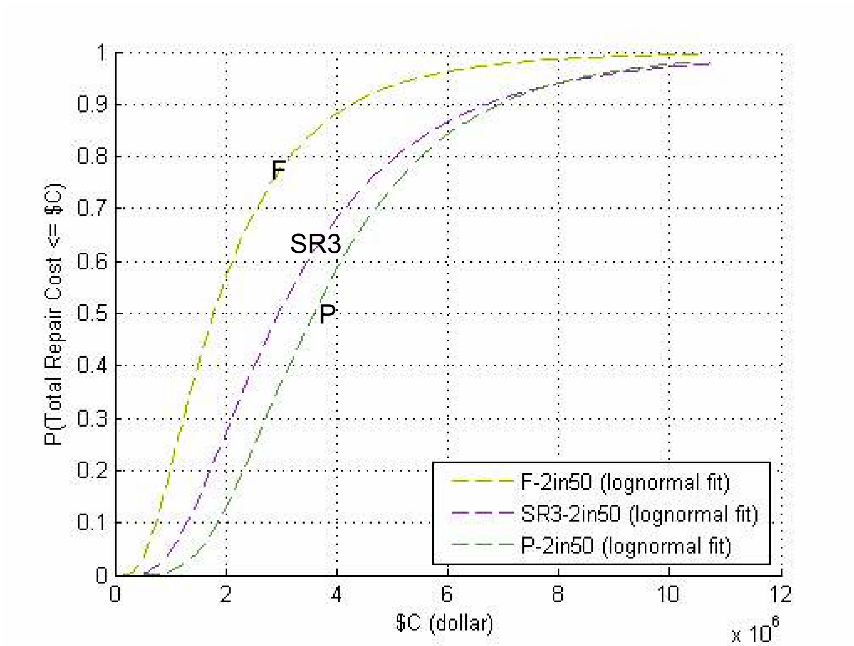

Fig. 4.9 CDF curves for the 2% in 50 yrs PE hazard level: effect of base fixity.

The probability of realizing a certain repair cost is the highest for the pinned model and the lowest for the fixed model. The repair cost probability for the semi-rigid base (SR3) frame is slightly higher than that for the fixed-base model. The same relation among the repair cost probabilities for different frame models occurs at other, lower, hazard levels, as seen in Appendix C.

The interstory drifts of the pinned and the semi-rigid frames exceed those of the stiffer fixed frame for all hazard levels by 17 and 41%, respectively, on average (Table 4.7). On the other hand, the average floor accelerations in the fixed and the semi-rigid frames exceed those of the pinned frame by 25 and 28%, respectively, on average (Table 4.8). However, since the lateral stiffness of the moment-resisting frame is relatively small for all three base fixity models, the resulting floor accelerations (equal to or smaller than 1.0g) do not produce significant damage and the associated repair costs do not contribute significantly to the mean annual total repair cost of the building. Since the repair cost is therefore dependent primarily on displacement-controlled performance groups, the fixed frame incurs the lower repair costs.

Table 4.7 Average peak interstory drift.

	Average Drift			Increase		
Hazard Level (PE in 50 yr)	F	SR3	P	F	SR3	P
2%	2.44	2.85	3.29	1	1.17	1.35
5%	1.85	2.14	2.41	1	1.15	1.30
10%	1.41	1.66	1.83	1	1.18	1.30
50%	0.58	0.68	0.90	1	1.16	1.54
75%	0.41	0.49	0.65	1	1.18	1.57
Average				1.00	1.17	1.41

Table 4.8 Average peak floor acceleration.

	Average Acceleration			Increase		
Hazard Level (PE in 50 yr)	F	SR3	P	F	SR3	P
2%	1.06	1.04	0.84	1.26	1.24	1
5%	0.93	0.87	0.68	1.37	1.28	1
10%	0.83	0.72	0.55	1.50	1.30	1
50%	0.52	0.55	0.45	1.15	1.21	1
75%	0.37	0.39	0.33	1.12	1.20	1
Average				1.28	1.25	1.00

Since the slope obtained from the regression of the hazard curve is higher for lower levels of ground shaking, the contribution to the mean cumulative annual total repair cost of the 50% and 75% in 50 years hazard levels is predominant, since those earthquakes are more frequent throughout the lifetime of the structure. Even though the repair cost of the building after rare earthquake events is high (on the order of millions of U.S. dollars for the mean probability of repair), the contribution from these events to the mean cumulative annual total repair cost is negligible and the average repair costs are on the order of tens of thousands of U.S. dollars.

For the elastic range of response, in the case of the 50% and 75% in 50 years PE hazard levels, the difference in the interstory drift and floor accelerations between the fixed and semi-rigid models is very small, thus producing similar damage at low levels of ground shaking. The corresponding cumulative distribution functions are therefore very similar. Since those hazard levels are controlling the mean cumulative annual total repair cost, the difference in this value between the fixed and semi-rigid models is only 0.4%. The loss curves for the fixed, semi-rigid, and pinned models are presented in Figure 4.10. Notice that the loss curve of the semi-rigid model is almost identical to that for the fixed case.

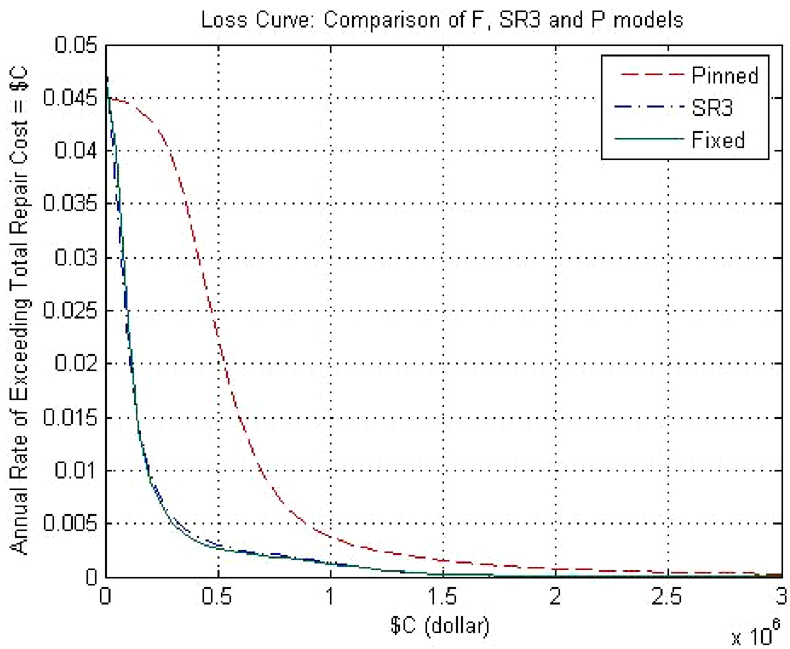

Fig. 4.10 Loss curves for models F, SR3, and P.

The area under the loss curve is the mean cumulative annual total repair cost. The pinned moment-resisting frame had the highest repair cost with an estimated $26,500 dollars associated primarily with drift-sensitive structural and nonstructural damage. That cost was about 3.25 times the cost of repair obtained for the fixed and semi-rigid frames, with a mean cumulative annual total repair cost of $8,150 and $8,180, respectively. Even though the response of the fixed frame in terms of drift control is superior and results in smaller damage and repair costs than the semi-rigid model for high levels of ground shaking, the contributions of those levels of damage to the mean annual total repair cost is negligible.

The ATC-58 example moment-resisting frame structure is a regular office building with a computer center located on the third floor. The repair cost of the building content performance group, which is acceleration-related, was computed separately to observe its contribution to the total repair cost. For the case of the fixed, semi-rigid, and pinned frames, the content repair cost was $1220, $1180, and $1120, respectively, representing 15, 14, and 4% of the total repair cost, respectively. However, even though the fixed and semi-rigid systems resulted in higher costs for the content repair, and their floor accelerations are 28 and 25% higher than in the pinned case, respectively, the increase in the repair cost was only on the order of 5 and 9%. In the case of special facilities with acceleration-sensitive equipment, the content repair cost represents a higher contribution of the total repair cost. The cost summary is presented in Table 4.9.

Table 4.9 Summary of repair cost of models F, SR3, and P.

Cost Comparison	F	SR3	P
Annual repair cost ($)	8150	8180	26500
Increase wrt' min (%)	0.0	0.4	225.2
Annual content repair cost ($)	1220	1180	1120
Increase wrt' min (%)	9	5	0
Content contribution (%)	15	14	4

The PBEE procedure implicitly assumes that the structure does not deteriorate and that it is immediately restored to its original state after each damaging earthquake. The non-ergodic or invariant behavior allocated to structural elements in the frame affect the accuracy in computing its maximum response measures. In the computation of probabilities of a performance measure or repair cost exceeding a specified threshold in the PBEE analysis, an error of as much as 30% can be expected for large probabilities and long time periods (Kiureghian 2005). This error, due to non-ergodic uncertainties, is found to be on the conservative side, that is, the damage and corresponding repair cost of the structure after the earthquake is overestimated. Also, since the object of this study is the comparison of the efficiency and behavior of moment-resisting frames with varying base rigidity, the main concern is the relative damage and repair cost of these systems, not the absolute values.

5 Reliability Analysis of Exposed Column Base Plate Connection

5.1 GENERAL PURPOSE

System reliability analysis is carried out for a typical moment-resisting base plate connection between a wide-flange column in a steel SMRF and its concrete foundation using an exposed steel base plate and anchor bolts. This evaluation assesses the safety of the structural system with respect to its diverse failure modes and the adequacy of the limit-state formulation. The relative importance of the different components of the connection and the sensitivity of the failure probability of the system to small variations in the parameters of the limit-state functions are determined as well. The computation of the reliability and sensitivity analysis is carried out using CalREL reliability software (Liu et al. 1989), which was developed at the University of California, Berkeley.

5.2 METHODOLOGY

5.2.1 Design of Base Plate Connection

A complete seismic design of a base plate connection is carried out following the AISC Design Guide No.1-2005 procedure for a typical low-rise moment-resisting frame subjected to seismic loading. The column base connection of an exterior column of the ATC-58 three-story, three-bay moment-resisting frame office building, located on the University of California at Berkeley campus (Yang et al. 2006), is used as an example (see Fig. 5.1).

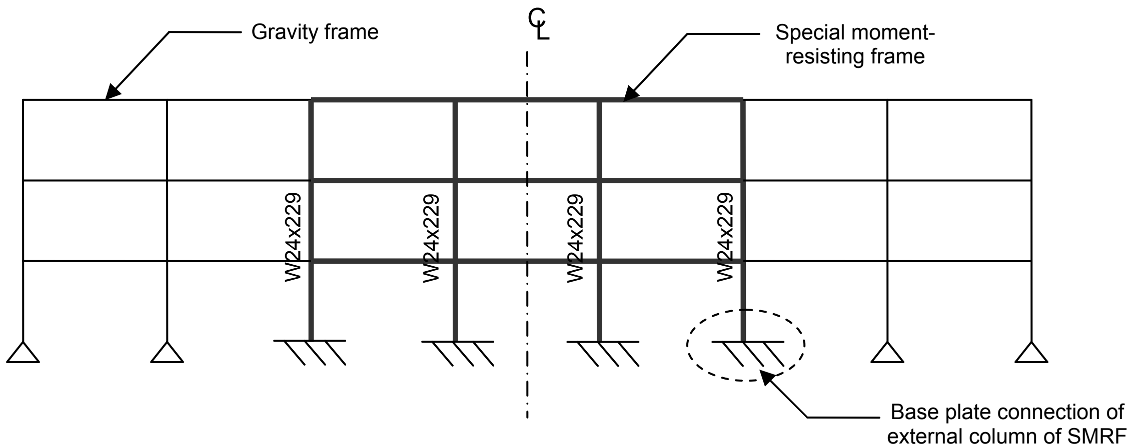

Fig. 5.1 Column base connection selected for reliability analysis.

The typical configuration of a connection between a wide-flange column and its foundation consists of an exposed steel base plate supported on a grout surface and anchored to the reinforced concrete foundation of the column through an array of anchor bolts and anchor plates (see Fig. 5.2). This assembly is designed to resist biaxial bending, shear, and axial loads developed in the column due to gravity and lateral forces. The theoretical behavior of a base plate connection is discussed in Section 1.2.

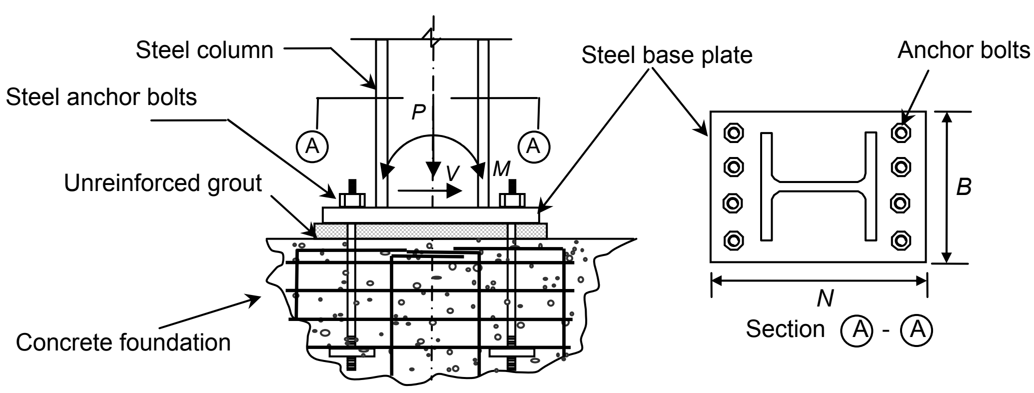

Fig. 5.2 Configuration of exposed base plate connection.

A wide-flange cross section (W24×229) was previously designed for both interior and external columns of the ATC-58 special moment-resisting frame. The critical combination of bending moment, and shear and axial forces is determined to occur for this specific frame at the external column.

The loads used for the design of the connection are obtained from a series of nonlinear time history analysis of the moment-resisting frame model with fixed column bases (model F). The median values of the joint reactions obtained from a suite of seven ground motions corresponding to the design earthquake hazard level (10% in 50 yrs PE), according to Bozorgnia and Bertero (2004), are used to design the connection. Several load combinations from each nonlinear time history analysis are considered to find the critical load combinations (see Table 5.1):

1. The maximum axial load in compression (P_{max}) and the corresponding shear force (V_p) and bending moment (M_p) occurring at the same time step. Uplift forces were developed at the external column; however, they were insignificant and therefore the minimum axial load combination did not represent a critical loading condition for the connection.
2. The maximum shear force (V_{max}) and the corresponding bending moment (M_v) and axial load (P_v) occurring at the same time step.
3. The maximum bending moment (M_{max}) and the corresponding shear (V_m) and axial (P_m) loads occurring at the same time step.

Table 5.1 Design loads for the connection corresponding to the median of 7 records used in the nonlinear time history analysis of the SMRF at 10% in 50 yrs PE hazard level.

	Median			c.o.v.		
Case	***P* (kip)**	***V* (kip)**	***M* (kip-in)**	***P***	***V***	***M***
P_{max}	430.3	195.2	31029.9	0.01	0.07	0.08
V_{max}	423.1	211.5	30668.8	0.03	0.11	0.09
M_{max}	429.6	209.2	31449.3	0.01	0.08	0.09

The mean values of the base plate dimensions, the anchor bolts, the concrete resistance, the shear lugs and the other components required to guarantee global equilibrium of the assembly are determined according to recent design guidelines (AISC Design Guide No.1-2005). The design is presented in Appendix D.

5.2.2 Limit-State Formulation

The limit-state for each failure mode of the base plate connection is formulated based on the AISC Design Guide No.1-2005 procedure. This guide assumes a rectangular stress distribution in the supporting concrete foundation, consistent with the LRFD method for design of reinforced concrete structures used in the U.S. According to the LRFD methodology, different components of the connection are considered to be at their plastic or ultimate capacities and their relative stiffnesses are disregarded for determination of internal forces. The flexibility of the base plate is neglected for calculating the bearing stress. The dimensions of the plate and the anchor bolts required to achieve the desired strength are obtained from global vertical and moment equilibrium equations. The yield-line theory is used to model the bending behavior of the base plate. The resulting base plate design is also checked for shear-friction resistance and anchor bolt shear. If the shear capacity is insufficient, bearing action to resist shear can be developed by adding shear lugs under the base plate. Shear checks are performed assuming no interaction between the shear and moment resistances.

The limit-state functions $g(x)$ for all failure modes used for the component and system reliability analyses are defined as the difference between the corresponding capacity and demand values: $g(x)$ = (Capacity – Demand) (see Section 5.3.1), where x denotes the set of random variables. Failure is defined as the event where demand exceeds capacity, i.e., $g(x) < 0$, and does not necessarily correspond to a physical collapse of the connection. For the ductile failure modes, a redistribution of forces among the components of the connection is expected to occur. Such behavior is disregarded in this formulation. Additionally, the stiffness of the column base can be reduced due to this failure mode, resulting in a lower force demand for the remaining resistance mechanisms. Therefore, the exceedance of a limit-state function corresponding to a ductile failure mode does not represent the complete failure of the connection. Conversely, the exceedance of one or more limit-state functions corresponding to a brittle failure will indicate the failure of the system (see Fig. 5.9).

5.2.3 Identification of Random Variables

Based on the typical configuration of a base plate connection required for global equilibrium of the system, the following components and parameters were defined as the random variables used for the reliability analysis of the assembly (see Fig. 5.3):

- Plan dimensions of rectangular base plate (N-length $\times$ B-width).
- Thickness of base plate (t_{PL}).
- Tension-yielding stress ($F_{y,pl}$) and ultimate tensile stress ($F_{u,PL}$) defined according to ASTM A-36 for steel plates.
- Dimensions of the concrete foundations (selected as $2B \times 2N \times h$, where h is the height of the pedestal).
- Anchor bolt diameter (d_b).
- Anchor bolt design strength (F_{yb}) defined according to ASTM F1554 for steel Grade 36, 55, or 105 ksi, and ultimate strength (F_{ub}).
- Anchor plate plan dimensions ($l_{ap} \times b_{ap}$) and embedment length (h_{ef}).
- Edge distance from bolt centerline (d_{edge}=1.5d_b) and spacing between anchor bolts (s=3d_b).
- Concrete compressive strength (f'_c).
- Grout thickness (t_g).
- Column depth (d_c) and flange width (b_f).
- Column plastic modulus (Z_{col}), which determines the plastic capacity of the section.
- Steel column tensile ($F_{u,col}$) and yielding stress ($F_{y,col}$) defined according to ASTM A992 or ASTM A572.
- Loads: bending moment (M), shear force (V), and axial load (P).
- Friction coefficient (μ) between the concrete surface and the steel plate.
- Shear lugs dimensions (l_{sl}-width, t_{sl}-thickness, b_{sl}-length). The material properties of a steel plate obtained from ASTM A36 are used and are the same as the base plate material.
- Weld dimension (b_w) and electrode strength (F_{EXX}) of shear lugs.

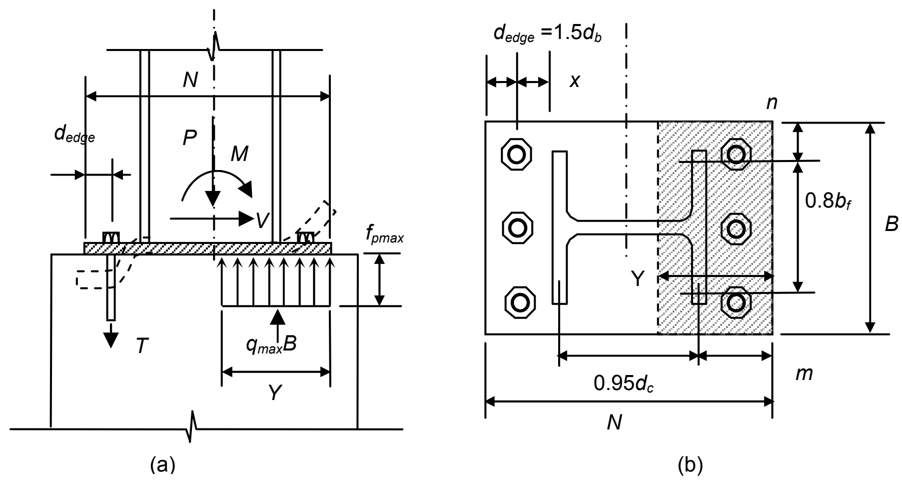

Fig. 5.3 (a) Force equilibrium and base plate bending; (b) dimensions of base plate connection.

The resulting vector of random variables $\underline{X}$ is then:

$$\underline{X} = \begin{bmatrix} N, B, t_{PL}, F_{y,pl}, F_{u,pl}, h, d_b, F_{yb}, F_{ub}, d_{edge}, f'_c, t_{grout}, Z_{col}, d_c, b_f, \\ F_{y,col}, F_{u,col}, M, V, P, l_{ap}, b_{ap}, h_{ef}, \mu, l_{sl}, t_{sl}, b_{sl}, b_w, F_{EXX} \end{bmatrix}^T$$

5.2.4 Failure Modes

The following are the main failure modes that can occur in a typical exposed base plate connection subjected to a combination of bending moment, and axial and shear loads, determined according to the AISC Design Guide No.1-2005.

5.2.4.1 Concrete Crushing

Concrete crushing is developed when the concrete bearing stresses produced due to the assumption of rigid body rotation of the base plate exceed the maximum stress of the concrete pedestal:

$$f_p = \frac{P}{A} + \frac{M}{S} \leq f_{p\max}$$

The maximum bearing stress is defined as $f_{p\max} = 0.85 f'_c\, k$, based on Whitney's equivalent stress block in concrete (ACI318-2005), where $k = \sqrt{A_2/A_1} \leq 2$ is the concrete confinement coefficient. The k factor can be taken as 2, assuming that the area of the supporting foundation is sufficiently large to provide adequate lateral confinement for the reinforced concrete pedestal ($A_2 \geq 4.0 A_1$) and adequate transverse reinforcement details are specified for the foundation element. Figure 5.4 illustrates this failure mode.

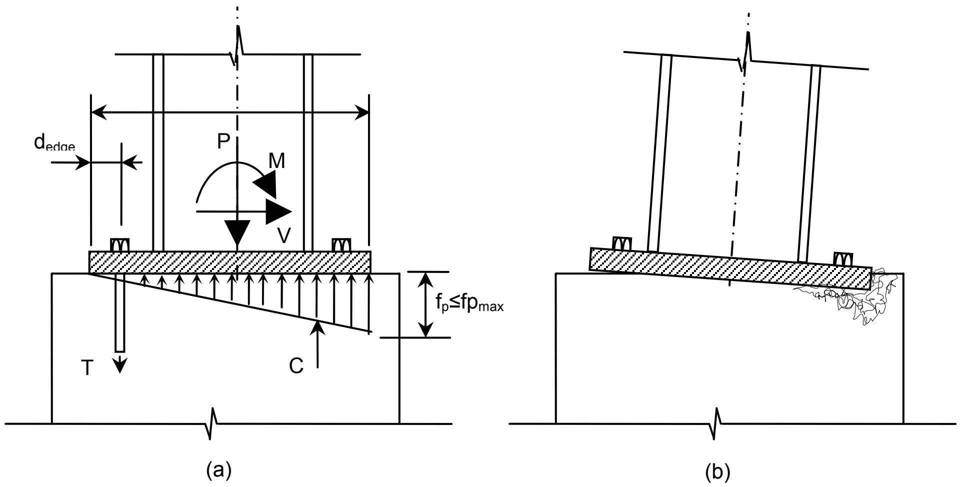

Fig. 5.4 (a) Bearing stress distribution assuming rigid body rotation and no uplift of base plate; (b) concrete crushing failure mode.

The resulting condition to avoid the concrete crushing failure mode is:

$$\frac{P}{NB} + \frac{M}{(1/6)BN^2} \leq 0.85kf'_c$$

The resulting limit-state function takes the following form:

$$f_1(\underline{X}) = 0.85kf'_c - \left(\frac{P}{NB} + \frac{M}{(1/6)BN^2} \right) \tag{5.1}$$

5.2.4.2 Yielding of Base Plate

The yielding of the base plate can occur on each side of the plate for bending of the column base with respect to the strong axis of the cross section (see Fig. 5.5).

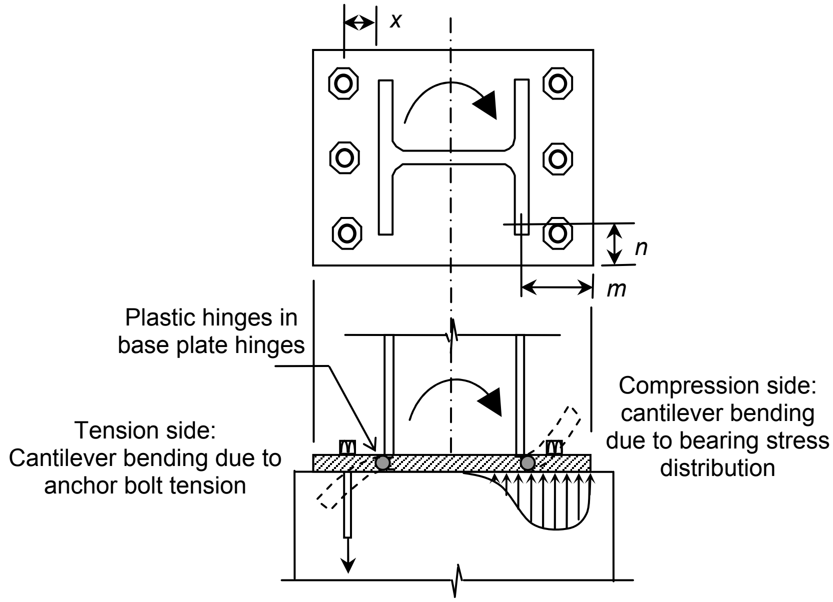

Fig. 5.5 Yielding of base plate.

(a) Cantilever bending of base plate due to bearing stress distribution on the compression side:

The largest cantilever span l of the base plate must be determined in order to obtain the critical bending section of the plate. This maximum span is determined as:

$$l = \max \begin{cases} m = \dfrac{N - 0.95 d_c}{2} \\ n = \dfrac{B - 0.8 b_f}{2} \\ \lambda n' = \lambda \dfrac{\sqrt{d_c b_f}}{4}, \lambda = 1 \end{cases}$$

The column cross-sectional dimensions are the flange width, b_f, and height, d_c. The AISC Design Guide No.1-2005 suggests the use of the cantilever in the direction of bending with respect to the strong axis as the dimension l, i.e., $l = m$. Since the dimension l as defined above is a nondifferentiable piece-wise function, the maximum length obtained from design can be taken instead. For the present design of the W24×229 section, the maximum cantilever is obtained as $l = n = (B - 0.8b_f)/2$, a formulation that will be used for this limit-state function. In order to avoid failure the following condition must be satisfied: $M_{n,pl} \geq M_{pl}$, where $M_{n,pl}$ is the plastic moment of the plate $M_{n,pl} = F_{yp} Z_p = F_{yp}(1)(t_p)^2/4$, and M_{pl} is the load corresponding to the bending of the largest cantilever bending due to the bearing stress distribution underneath the plate, which for large eccentricities will be the maximum concrete bearing stress $f_{p,max}$:

$$M_{pl} = f_{p,\max}\left(\frac{l^2}{2}\right) = 0.85kf'_c \cdot \left(\frac{l^2}{2}\right)$$

To avoid yielding of the base plate, the following conditions must be specified:

$$\frac{F_{y,pl}(t_p)^2}{4} \geq 0.85kf'_c \cdot \left(\frac{l^2}{2}\right)$$

Therefore, the resulting limit-state function for this failure mode is:

$$f_2(\underline{X}) = \frac{F_{y,pl}(t_p)^2}{4} - \left(\frac{P}{NB} + \frac{M}{(1/6)BN^2}\right) \cdot \left(\frac{l^2}{2}\right) \tag{5.2}$$

The dimension l is taken for simplicity as the largest cantilever obtained from design, in this case $l = (B - 0.8b_f)/2$.

(b) Cantilever bending between column tension flanges and anchor bolts:

The determination of the tensile forces in the anchor bolts is carried out as follows. The moment demand due to cantilever bending with a distance x between the anchor bolts and column tensile flanges is: $M_{pl} = Tx = T(N - d_c - 2d_{edge})/2$. The effective width of the plate-resisting bending should be determined at a 45° angle from the anchor bolts, ignoring base plate flexibility (see Fig. 5.6): $b_{eff} = \min(B, (n/2)(2x) = n(N - d_c - 2d_{edge})/2)$. Since b_{eff} is a nondifferentiable discontinuous piece-wise function, the minimum length obtained from design is used instead. The effective length determined for the design of the W24×229 column cross section is B.

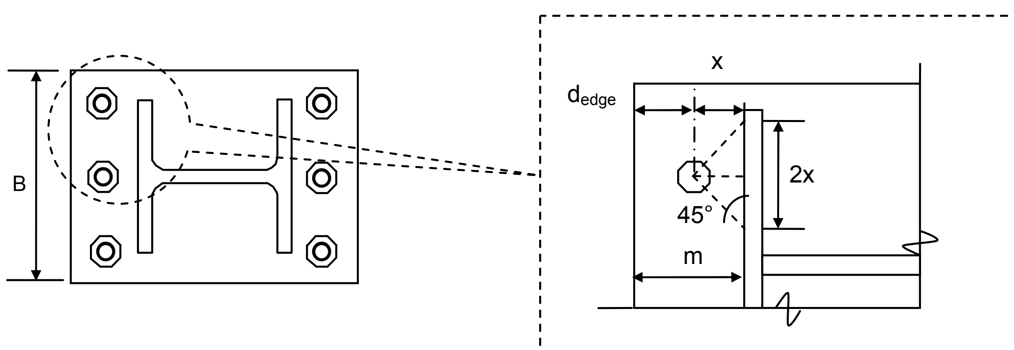

Fig. 5.6 Effective base plate width on the tension side.

To avoid failure the condition $M_{n,pl} \geq M_{pl}$ must be satisfied, which is equivalent to:

$$\frac{F_{y,pl} B(t_p)^2}{4} \geq T \cdot \frac{(N - d_c - 2d_{edge})}{2}$$

The resulting limit-state function for this failure mode is then:

$$f_3(\underline{X}) = \frac{F_{y,pl} be_{ff}(t_p)^2}{4} - (0.85kf'_c\, b_{eff} L - P)\frac{(N - d_c - 2d_{edge})}{2}$$
$$L = \left[(N - d_{edge}) - \sqrt{(N - d_{edge})^2 - 2\frac{P(M/P + N/2 - d_{edge})}{0.85kf'_c\, B}}\right] \tag{5.3}$$

The effective width, b_{eff} obtained in this design is the total width of the base plate, B.

5.2.4.3 Tension Yielding of Anchor Bolts

Tension fracture of the anchor bolts can be avoided by specifying an extruded cross section A_n greater or equal to the gross cross section A_g of the bolts, a recommended and well-adopted design practice. The breakout failure of individual or a group of anchor bolts (see Fig. 3.2.1 and 3.2.2 of AISC Design Guide No.1-2005) can be avoided by the use of sufficiently large anchor plates at the ends of the bolts, embedded in the concrete foundations. However, tension yielding of anchor bolts can be avoided only by adequately determining the number, the cross-sectional area, and the material strength of the anchor bolts. The tension in the anchor bolts is obtained by solving a quadratic equation that combines both vertical and moment equilibrium equations. The bearing stress f_p for large eccentricities is equal to the maximum values f_{pmax}.

- Vertical equilibrium: $\sum F_{vertical} = 0 : T = q_{\max} Y - P$, where $q_{\max} = f_{p\max} B = 0.85kf'_c\, B$, and Y is the bearing length in the supporting concrete.
- Moment equilibrium: $\sum M_{Anchor\_bolts} = 0 : q_{\max} Y(N/2 - Y/2 + f) - P_u(e + f)$, where the eccentricity $e = M/P$, and the distance $f = N/2 - d_{edge}$.

From the equilibrium conditions above we obtain a quadratic equation for the bearing length Y:

$$Y^2 - 2\left(\frac{N}{2} + f\right)Y + 2\frac{P(e + f)}{q_{\max}} = 0$$

The resulting solution to the equation can be written as:

$$Y = \left(f + \frac{N}{2} \right) - \sqrt{\left(f + \frac{N}{2} \right)^2 - 2\frac{P(e+f)}{q_{\max}}}$$

The capacity of the anchor bolts $T_n = (n/2)(0.75)F_{ub}A_b = (n/2)(0.75)F_{ub}\pi d_b^{\ 2}/4$, where $n/2$ is the number of bolts on one side of the plate-resisting tension, should be greater or equal to the applied load T, $T_n \geq T$ in order to avoid failure. This expression can also be expressed as:

$$\frac{n}{2}(0.75)F_{ub}\frac{\pi d_b^{\ 2}}{4} \geq 0.85kf'_c\, B\left[\left(\frac{N}{2} - d_{edge} + \frac{N}{2}\right) - \sqrt{\left(\frac{N}{2} - d_{edge} + \frac{N}{2}\right)^2 - 2\frac{P(M/P + N/2 - d_{edge})}{0.85kf'_c\, B}}\right] - P$$

The resulting limit-state function for this failure mode is:

$$\begin{aligned} f_4(\underline{X}) &= \frac{n}{2}(0.75)F_{ub}\frac{\pi d_b^{\ 2}}{4} - (0.85kf'_c\, BL - P) \\ L &= \left[(N - d_{edge}) - \sqrt{(N - d_{edge})^2 - 2\frac{P(M/P + N/2 - d_{edge})}{0.85kf'_c\, B}}\right] \end{aligned} \tag{5.4}$$

5.2.4.4 Shear Failure

The shear resistance is provided by a combination of three mechanisms.

(a) Friction along the contact area between the concrete surface and the steel base plate:

The shear strength V_n is calculated according to the ACI 318-2002 criteria: $V_{n,friction} = \mu P \leq 0.2 f'_c\, A_c$. The friction coefficient μ is defined as 0.55 for steel on grout, and 0.7 for steel on concrete. In the present case the mean value will be taken as the friction coefficient of steel against grout with a value of 0.80; however μ is also a random variable. To guarantee friction shear resistance $V_{n,friction} \geq V$, or $V \leq \min(\mu P, 0.2 f'_c\, A_c)$. Two limit-state functions will then define the shear failure as a series system, where either one of the following conditions (Eq. 5.5 or 5.6) will produce failure of the connection:

$$f_5(\underline{X}) = \mu P - V \tag{5.5}$$

$$f_6(\underline{X}) = 0.2 f'_c\, (NB) - V \tag{5.6}$$

The second limit-state function represents an upper bound for the shear resistance by friction. For the present design this limit-state function does not govern the behavior and is omitted from the system formulation.

(b) Bending and shear in the anchor bolts:

(b.1) Shear failure in anchor bolts (see Fig. 5.7): In this case, it is assumed as well that bending in the anchor bolts does not develop, since a relatively thin washer is specified and the anchor bolts are not long enough beyond the base plate to develop significant flexibility. For threaded or extruded (X) anchor bolts, the shear resistance per unit area F_{nv} is defined as $F_{nv} = 0.5F_{ub}$. The shear resistance of the anchor bolts is therefore simply: $V_n = F_{nv}A_b = 0.5F_{ub}\pi d_b^2/4$. The anchor bolts are assumed to be welded to the base plate through the washer. Conservatively, only half of the anchor bolts are assumed to be effective in resisting shear. To avoid shear failure in the anchor bolts $V_n \geq R_b$, or $0.5F_{ub}\pi d_b^2/4 \geq V/(n_b/2)$, where n_b is the total number of anchor bolts specified for the connection. The resulting limit-state function for this failure mode is:

$$f_7(\underline{X}) = 0.5F_{ub}\frac{\pi d_b^2}{4} - \frac{V}{(n_b/2)} \tag{5.7}$$

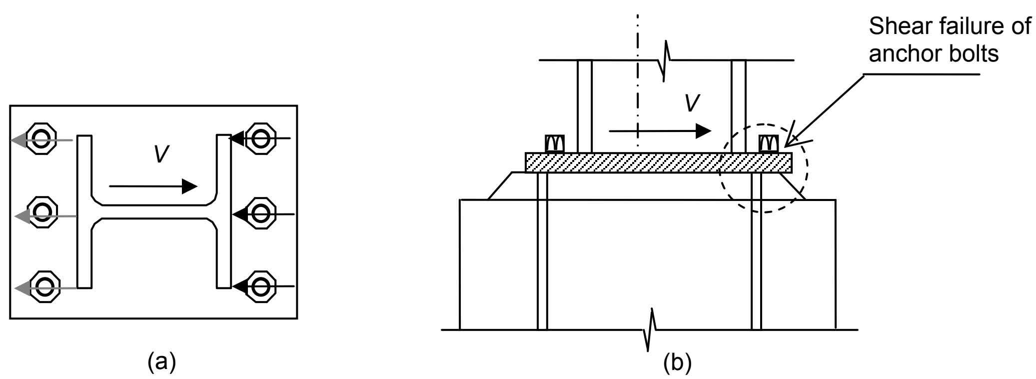

Fig. 5.7 (a) Shear resistance developed in anchor bolts; (b) shear failure of anchor bolts and sliding of base plate.

(b.2) Concrete edge breakout due to shear in the anchor bolts must be checked as well, even though sufficient concrete area and edge distances beyond the base plate dimensions are specified. If the concrete foundation is reinforced with conventional longitudinal bars and transverse hoops as in a typical concrete pedestal design, this breakout failure can be neglected. The concrete breakout resistance V_{cbg} is defined as $V_{cbg} = 10.4(A_v / A_{vo})\psi_6 \sqrt{d_b} \sqrt{f'_c} c_1^{1.5}$. The modification factor Ψ_6 is used to reduce the breakout capacity when the side cover limits the size of the breakout cone. This factor is taken as Ψ_6=1 for the present design. The term c_1 is the edge distance in the direction of load, determined as $c_1 = (2N - (N - 2d_{edge}))/2$. The term A_{vo} is the area of the full shear cone for a single anchor, $A_{vo} = 4.5 c_1^2$. The A_v term is the total breakout shear area for a single anchor or a group of anchors, $A_v = 4.5 c_1^2 + (n/2 - 1) sFc_1$, where F is a factor whose value is obtained from Figure 3.2.3 of the AISC Design Guide #1 as a function of $c_1/(N - 2d_{edge})$, and $s = 3d_b$ is the anchor bolt spacing in the transverse direction. To avoid edge breakout, the conditions $V_{cbg} \geq V$ must be satisfied, which can also be rewritten as:

$$10.4\left(\frac{4.5[(2N-(N-2d_{edge}))/2]^2 + (n/2-1)sF}{4.5[(2N-(N-2d_{edge}))/2]^2}\right)\sqrt{d_b}\sqrt{f'_c}\cdot[(2N-(N-2d_{edge}))/2]^{1.5} \geq V$$

The resulting limit-state function for this failure mode is:

$$f_8(\underline{X}) = 10.4\left(\frac{4.5[(2N-(N-2d_{edge}))/2]^2 + (n/2-1)sF}{4.5[(2N-(N-2d_{edge}))/2]^2}\right)\sqrt{d_b}\sqrt{f'_c}\cdot[(2N-(N-2d_{edge}))/2]^{1.5} - V \quad (5.8)$$

(c) Bearing of shear lugs installed underneath the base plate (see Fig. 5.8):

(c.1) Since the anchor rods are sized for only the required tensile forces to maintain moment equilibrium, the bearing capacity of the shear lugs against the concrete is defined as $P_{brg} = 0.8 f'_c A_l$, where A_l is the embedded area beneath the concrete pedestal of n_{sl} shear lugs spaced at a distance S_{sl}, $A_l = n_{sl} b_{sl} (l_{sl} - t_{grout})$. To avoid concrete bearing failure the condition $P_{brg} \geq V$ must be satisfied, also rewritten as $0.8 f'_c n_{sl} b_{sl} (l_{sl} - t_{grout}) \geq V$. The resulting limit-state function is:

$$f_9(\underline{X}) = 0.8 f'_c n_{sl} b_{sl} (l_{sl} - t_{grout}) - V \quad (5.9)$$

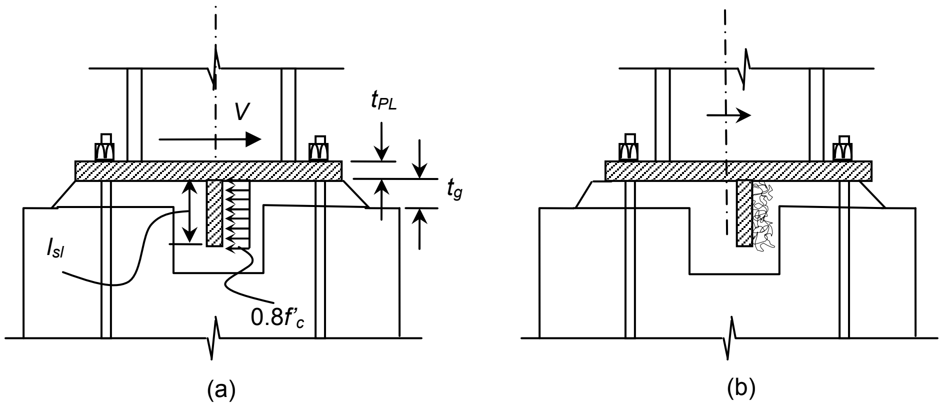

Fig. 5.8 (a) Bearing stress distribution in grout adjacent to shear lugs; (b) bearing failure of shear lugs.

(c.2) The concrete shear resistance required to prevent edge breakout must also be checked. Assuming a uniform tensile stress $4\sqrt{f'_c}$ in the projected area of the shear lugs A_v, at a 45° angle from the bearing edge of the shear lugs to the free surface, we have $A_v = 2Bh - b_{sl}\left(l_{sl} - t_{grout}\right)$. Figure 3.2.4 of AISC Design Guide No.1-2005 presents a scheme of this failure mode. The shear resistance is then $V_n = 4\sqrt{f'_c}A_v = 4\sqrt{f'_c}\left(2Bh - b_{sl}\left(l_{sl} - t_{grout}\right)\right) \geq V$. The limit-state function obtained for this failure mode is therefore:

$$f_{10}\left(\underline{X}\right) = 4\sqrt{f'_c}\left(2Bh - b_{sl}\left(l_{sl} - t_{grout}\right)\right) - V \tag{5.10}$$

(c.3) The capacity of the cantilevered shear lug in bending due to the bearing stress distribution in the surrounding grout can be defined as $M_n = Z_{sl}F_{y,pl} = F_{y,pl}b_{sl}\left(t_{sl}\right)^2/4$, where the thickness of the shear lug plate must not exceed that of the base plate. The bending moment in the shear lugs can be obtained as a function of the resultant of the bearing stress distribution, applied at mid-depth of the effective embedded length:

$$M_{cantilever} = \left(V/n_{sl}\right)\cdot\left(t_{grout} + h_{emb}/2\right) = \left(V/n_{sl}\right)\cdot\left(t_{grout} + \left(l_{sl} - t_{grout}\right)/2\right)$$

To avoid bending failure of the shear lug in bending: $M_n \geq M_{cantilever}$ or $F_{y,pl}b_{sl}\left(t_{sl}\right)^2/4 \geq \left(V/n_{sl}\right)\left(t_{grout} + \left(l_{sl} - t_{grout}\right)/2\right)$. The resulting limit-state function describing this failure is:

$$f_{11}(\underline{X}) = F_{y,pl}\frac{b_{sl}(t_{sl})^2}{4} - \left(\frac{V}{n_{sl}}\right)\cdot\left(t_{grout} + \frac{(l_{sl} - t_{grout})}{2}\right) \tag{5.11}$$

(c.4) The weld capacity of the shear lugs to the base plate is defined as $F_w = 0.60F_{EXX}t_w = 0.6F_{EXX}(0.707b_w)$. The contact area A_w of the fillet weld is $A_w = (t_{sl} + 2b_w)b_{sl}$, the compression stress in the weld is $f_c = M_{cantilver}/A_w$, and the shear stress in the weld is $f_v = V/NA_w$. The weld capacity must be greater or equal to the weld stress resultant to avoid failure: $F_w \geq f_r = \sqrt{f_c^{\ 2} + f_v^{\ 2}}$, which can also be expressed as:

$$0.6F_{EXX}(0.707b_w) \geq \sqrt{\left(\frac{M_{cantilever}}{(t_{sl} + 2b_w)b_{sl}}\right)^2 + \left(\frac{V}{N(t_{sl} + 2b_w)b_{sl}}\right)^2}$$

The limit-state function is therefore:

$$f_{12}(\underline{X}) = 0.6F_{EXX}(0.707b_w) - \sqrt{\left(\frac{(V/n_{sl})\cdot(t_{grout} + (l_{sl} - t_{grout})/2)}{(t_{sl} + 2b_w)b_{sl}}\right)^2 + \left(\frac{V}{N(t_{sl} + 2b_w)b_{sl}}\right)^2} \tag{5.12}$$

5.2.4.5 Pull-Out Failure of Anchor Bolts

The concrete breakout strength is defined as $N_{cbg} = (n/2)\psi_3 24\sqrt{f'_c}h_{ef}^{\ 1.5}(A_N/A_{No}),\ h_{ef} \leq 11"$, and $N_{cbg} = (n/2)\psi_3 16\sqrt{f'_c}h_{ef}^{\ 5/3}(A_N/A_{No}),\ h_{ef} > 11"$. The latter applies for the present case. The factor ψ_3 is taken as 1.25 for uncracked concrete and 1.0 for cracked concrete. A_N and A_{No} are the concrete breakout cone area for group and single anchor, respectively, obtained from the geometry of the anchor bolts layout and resulting in a value of 1.0 for the present design. To avoid pull-out failure, the condition $N_{cbg} \geq T$ must be satisfied. This condition can also be expressed as $(n/2)\psi_3 16\sqrt{f'_c}h_{ef}^{\ 5/3}(A_N/A_{No}) \geq T$, where T was defined for the tension-yielding failure mode. The resulting limit-state function is:

$$f_{13}(\underline{X}) = \left(\frac{n}{2}\right)\psi_3 16\sqrt{f'_c}h_{ef}^{\ 5/3}\left(\frac{A_N}{A_{No}}\right) - (0.85kf'_c\,BC - P)$$
$$C = \left[\left(N - \frac{M}{P} - d_{edge} + \frac{N}{2}\right) - \sqrt{\left(N - \frac{M}{P} - d_{edge} + \frac{N}{2}\right)^2 - 2\frac{P(N - d_{edge})}{0.85kf'_c\,B}}\right] \tag{5.13}$$

5.2.4.6 Bearing of Anchor Bolts against Base Plate

A bearing failure of the base plate or pull-through failure of the anchor bolts due to shear can occur, and the critical bearing length, L_c of the plate must be checked: $L_c = \min(d_{edge} = 1.5d_b, s - spacing = 3d_b)$. For standard bolt-hole sizes (d_{hole}=d_b+1/8″), the bearing resistance of the plate is defined by the Specification of Steel Construction LRFD as $R_n = 1.5L_c t_{pl} F_{u,pl} \leq 3.0 d_b t_{pl} F_{u,pl}$. A conservative assumption is that only half of the total number of bolts in the assembly are in bearing and resisting shear. Greater slip of the base plate and deformation would be required in order for all the anchor bolts to be considered effective in resisting shear. The shear demand R_b on each bolt is therefore $R_b = V/(n/2)$, where n is the total number of bolts (determined as 6 for the present design). To avoid bearing failure the conditions $R_n \geq R_b$ must be satisfied, rewritten as $(1.5L_c t_{pl} F_{u,pl} \leq 3.0 d_b t_{pl} F_{u,pl}) \geq V/(n/2)$. The behavior of this system consists of a series system of the following limit-state functions (Eqs. 5.14 and 5.15):

$$f_{14}(\underline{X}) = 1.5L_c t_{pl} F_{u,pl} - V/(n/2) \tag{5.14}$$

$$f_{15}(\underline{X}) = 3.0 d_b t_{pl} F_{u,pl} - V/(n/2) \tag{5.15}$$

5.2.4.7 Fracture of Welds

Due to geometrical constraints, the stress concentration in the welds is considered to be complex and its behavior unpredictable and extremely susceptible to flaws. Oversized weld thickness and electrode capacity has been specified in engineering practice to avoid this type of failure. Very few welding failures have been detected in properly welded base plate connections, and therefore this type of failure will not be considered in the analysis.

5.2.4.8 Plastic Hinge in the Column Base

The formation of a plastic hinge in the column base will not produce the failure of the connection, since the forces developed in the frame will be limited by the plastic capacity of the elements. Therefore, the condition $M_{n,col} \geq M$, where $M_{n,col}$ is the plastic moment of the column cross section at the base determined as $M_n = M_p = F_{ycol} Z_{col}$ will automatically be satisfied.

5.3 RELIABILITY ANALYSIS

5.3.1 System Definition

Selection of base plate dimensions and material strengths following the AISC Design Guide 1-2005 method resulted in some highly unlikely failure modes (i.e., these failure modes have high safety factors, see Appendix D). They are concrete edge breakout due to shear in the anchor bolts (limit-state function f_8) and due to bearing in the shear lugs (limit-state function f_{10}), anchor bolt pull-out failure (limit-state function f_{13}), bearing failure of the base plate (limit-state functions f_{14} and f_{15}), bending failure of the shear lugs (limit-state function f_{11}), and column-to-base-plate weld failure. These failure modes are therefore ignored in the reliability analysis for the following reasons. Concrete edge breakout can easily be prevented through sufficient concrete area and edge distances, as well as transverse reinforcement in the concrete foundation. Pull-out failure of the anchor bolts is prevented by longitudinal reinforcement of the concrete foundation. Since the SMRF is located in a high seismic hazard zone, it is assumed that the foundations of the building have adequate longitudinal and transverse reinforcement details. The bearing capacity of a steel plate resisting shear in the anchor bolts is generally very high, and for this particular design, this failure mode presents a high reliability index. The capacity of the shear lugs in bending is also very high in the current design of the connection, since two shear lugs with relatively thick plates are specified. Therefore, this failure mode is also disregarded from the system formulation.

A hierarchy of column base connection failure modes used in the reliability analysis is shown in Figure 5.9.

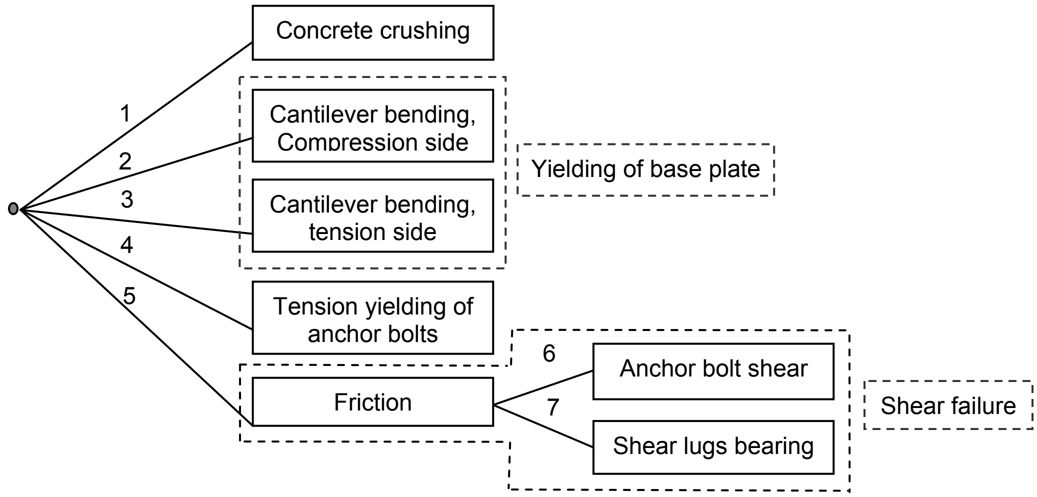

Fig. 5.9 System failure scheme for one load combination.

A typical base plate connection in a moment-resisting frame can be viewed as a general system combined of series and parallel subsystems. The failure of the concrete foundation, the steel base plate, the anchor bolts, or the shear resistance mechanisms will produce the global failure of the assembly. This system formulation consists of a series system of six possible failure modes (cut sets). The first four failure modes consist of one component each, described by one limit-state function. The final two failure modes corresponding to two types of shear failures are described as parallel subsystems. One subsystem is defined as friction-bolt shear failure, the other as friction-bearing failure.

The failure of the friction mechanism and the sliding of the base plate are necessary to develop shear resistance in the anchor bolts and bearing of shear lugs against the adjacent concrete and grout. However, the interaction between these shear resistance mechanisms is not included in the formulation of the system.

The limit-state functions used for the component and system reliability analysis are renumbered and defined as follows:

1. Concrete crushing (see Eq. 5.1):

$$g_1(\underline{X}) = 0.85kf'_c - \left(\frac{P}{NB} + \frac{M}{(1/6)BN^2}\right)$$

2. Yielding of the base plate due to cantilever bending on the compression side (see Eq. 5.2):

$$g_2(\underline{X}) = \frac{F_{y,pl}(t_p)^2}{4} - \left(\frac{P}{NB} + \frac{M}{(1/6)BN^2}\right) \cdot \frac{1}{2}\left(\frac{B - 0.80b_f}{2}\right)^2$$

3. Yielding of the base plate due to cantilever bending on the tension side (see Eq. 5.3):

$$g_3(\underline{X}) = \frac{F_{y,pl}B(t_p)^2}{4} - \left(0.85kf'_c\, B\left[(N - d_{edge}) - \sqrt{(N - d_{edge})^2 - 2\frac{P(M/P + N/2 - d_{edge})}{0.85kf'_c\, B}}\right] - P\right)\frac{(N - d_c - 2d_{edge})}{2}$$

4. Tension yielding of anchor bolts (see Eq. 5.4):

$$g_4(\underline{X}) = \frac{n}{2}(C_{ub1})F_{ub}\frac{\pi d_b^{\;2}}{4} - \left(0.85kf'_c\, B\left[(N - d_{edge}) - \sqrt{(N - d_{edge})^2 - 2\frac{P(M/P + N/2 - d_{edge})}{0.85kf'_c\, B}}\right] - P\right)$$

   The parameter C_{ub1}=0.75 is a coefficient for ultimate stress of the anchor bolts in tension. Only two bolts are assumed to be effective in resisting shear in the connection.

5. Friction failure or sliding of base plate (see Eq. 5.5): $g_5(\underline{X}) = \mu P - V$

6. Shear failure in the anchor bolts (see Eq. 5.7):

$$g_8(\underline{X}) = C_{ub2}F_{ub}\frac{\pi d_b^{\;2}}{4} - \frac{V}{2}$$

   The parameter C_{ub2}=0.50 is a coefficient for ultimate stress of the anchor bolts in shear.

7. Bearing failure of the shear lug against the adjacent concrete (see Eq. 5.9): $g_8(\underline{X}) = C_{brg}f'_c\, n_{sl}b_{sl}(l_{sl} - t_{grout}) - V$, where C_{brg}=0.80 is a concrete bearing coefficient.

The minimum cut-set formulation of the system is: C_{min}={(1)(2)(3)(4)(5,6)(5,7)}, i.e., the failure of the system can occur due to six failure modes. The component and system reliability analyses are carried out using the first-order reliability method (FORM) and the improved HL-RF algorithm, which is independent of the limit-state formulation and guarantees fast convergence of the reliability problem. A second-order approximation of the limit-state functions (SORM) through point-fitting is also performed for some components of the system, to verify the accuracy of the FORM approximation. Computations are carried out using the CalREL software (Der Kiureghian et al. 2006).

The system reliability analysis is carried out for four seismic hazard levels, including the low (50% in 50 yrs PE), moderate (10% in 50 yrs PE), and high (2 and 5% in 50 yrs PE). The total probability of failure of the connection is obtained as a function of the conditional failure probabilities for different hazard or intensity levels.

5.3.2 Summary of Random Variables and Parameters

The design of a base plate connection is carried out for an external column section W24×229 of the ATC-58 office building, consisting of a low-rise moment-resisting frame (three-story, three-bay frame) located in a high seismic zone in Berkeley, California, and designed according to the AISC Seismic Provisions (2005). Table 5.2 summarizes the random variables (RVs) used in the reliability analysis of this column base connection. These random variables and their distributions represent different column base components and parameters that influence the behavior of the selected column base connection at different hazard levels defined for this site. The mean values of dimensions and mechanical properties of the connection's components are established following the AISC Design Guide No.1-2005 procedure.

The standard deviations of the dimensions of steel components are established according to the tolerances specified by ASTM A6-05 for structural steel elements. The variability in anchor bolt diameter is defined according to the tolerances defined in ASTM F1554-04. The tolerances during the construction of the base plate connection, related to the distance between the edge of the base plate and the bolt centerline, as well as the thickness of the grout underneath the base plate is defined according to the Code of Standard Practice by AISC (2000). The variability for dimension variables with normal distribution is defined in this project by establishing the standard deviation as the tolerance of every steel or concrete component (σ_i=tol_i).

The normal distribution is assumed for dimension random variables with a relatively small coefficient of variation (c.o.v.<0.1), where negative dimension values are not likely to occur. The large amount of available statistical data of fundamental mechanical measures justifies the use of the normal distribution for the dimension random variables. Conversely, for dimension random variables with a relatively high coefficient of variation (c.o.v.>0.1), a beta distribution is assumed with upper and lower bounds defined as the mean value plus and minus the specified tolerance, respectively. The dimensions of the base plate, shear lugs, anchor bolts and grout thickness are considered to be statistically independent.

The variability of the material strengths for structural steel sections and plates are defined according to ASTM A992-04 and Liu (2005). The variability in the ultimate stress of the anchor bolts is defined by ASTM F1554-04, while the mean and dispersion in the concrete compressive strength is determined according to MacGregor (2005). The material strengths of different components in the system are also assumed to be statistically independent. A lognormal distribution is specified for the material strength random variables, since collected test data have indicated such a distribution.

The friction coefficient is taken to have a relatively high mean value of 0.80 as recommended by the AISC Design Guide No.1-2005 procedure. This value is used for this specific project, since net tension rarely occurs, even under severe ground motions corresponding to the highest seismic hazard level. For other moment-resisting frame with uplift forces and large eccentricities developing in the column base under severe seismic loading causing degradation of the contact surface between the concrete and the steel base plate, a friction coefficient of 0.4 is recommended (Fisher and Kloiber 2005).

The load values used in the reliability analysis are established as the joint reactions of the external column of the SMRF obtained from a suite of nonlinear time history analysis of the frame using seven records for each hazard level. Three critical loading cases corresponding to situations where the axial force, shear force, or bending moment take on maximum values (respectively described as P_{max}, V_{max}, and M_{max} cases) are considered, computing the remaining loads for each case at the corresponding time step of each record. The resulting mean load values and corresponding coefficients of variation computed for each hazard level are presented in Table 5.2. The load case corresponding to the maximum bending moment (M_{max}) and the corresponding shear (V_m) and axial (P_m) loads occurring at the same time instant is found to be the most critical for the connection, resulting in the highest failure probabilities. Additional load cases are also considered in the analysis but are not presented in this paper for brevity. The gravity load is included in the seismic axial load of the steel column transferred to the column base. The Nataf joint distribution model (Liu and Der Kiureghian 1986) is assumed for the loads. A Gumbel distribution (Type I largest value) is assumed for the critical load value, which can be justified as the appropriate distribution for extreme response values obtained from a complete time history record. The lognormal distribution is used for the remaining load random variables.

Table 5.2 Summary of random variables.

RV	X_i	Description	Distribution	Units	μ_i-Mean	c.o.v.$_i$	σ_i-St. dev.	Reference/Source
Dimensions								
d_c	X_1	Column depth	Normal	in	26.02	0.01	0.125	ASTM A6-05
b_f	X_2	Column flange width	Normal	in	13.11	0.01	0.1875	ASTM A6-05
N	X_3	Base plate length	Normal	in	38.0	0.025	1.0	ASTM A6-05
B	X_4	Base plate width	Normal	in	25.0	0.040	1.0	ASTM A6-05
t_{PL}	X_5	Base plate thickness	Normal	in	3.75	0.03	0.11	ASTM A6-05
l_{sl}	X_6	Shear lug depth	Beta	in	3.5	0.15	0.50	ASTM A6-05
b_{sl}	X_7	Shear lug length	Normal	in	25.0	0.025	0.75	ASTM A6-05
d_b	X_8	Anchor bolt diameter	Normal	in	2.0	0.05	0.10	ASTM F1554-04
d_{edge}	X_9	Edge distance from bolt centerline	Normal	in	3.0	0.085	0.25	AISC-Code Standard Practice (2000)
t_{grout}	X_{10}	Grout thickness	Beta	in	2.0	0.25	0.50	AISC-Code Standard Practice (2000)
Material Strength								
$F_{y,col}$	X_{11}	Column steel yield stress, Grade 50	Lognormal	ksi	60	0.05	3.0	ASTM A992-04, Liu (2003)
$F_{y,PL}$	X_{12}	Base plate steel yield stress, Grade 36	Lognormal	ksi	50	0.07	3.5	ASTM A992-04, Liu (2003)
F_{ub}	X_{13}	Anchor bolt ultimate stress, Grade 105	Lognormal	ksi	137.5	0.10	12.5	ASTM F1554-04
f'_c	X_{14}	Concrete compressive strength (4 ksi)	Lognormal	ksi	4.8	0.15	0.60	MacGregor (2005)
Coefficients								
μ	X_{15}	Friction coefficient	Beta	-	0.80	0.30	0.24	Fisher, Kloiber (2005)
Loads								
High hazard level -Collapse Prevention (2% in 50 yrs PE): Case V_{max}								
P_v	X_{16}	Seismic axial load	Lognormal	Kips	430.5	0.04	17.2	Appendix D
V_{max}	X_{17}	Seismic shear force	Gumbel	Kips	248.7	0.12	29.4	
M_v	X_{18}	Seismic bending moment	Lognormal	Kip-in	33871.6	0.12	4064.6	
High hazard level-Collapse Prevention (2% in 50 yrs PE): Case P_{max}								
P_{max}	X_{16}	Seismic axial load	Gumbel	Kips	453.8	0.03	13.6	Appendix D
V_p	X_{17}	Seismic shear force	Lognormal	Kips	208.1	0.15	31.2	
M_p	X_{18}	Seismic bending moment	Lognormal	Kip-in	33610.6	0.11	3697.2	
High hazard level-Collapse Prevention (2% in 50 yrs PE): Case M_{max}								
P_m	X_{16}	Seismic axial load	Lognormal	Kips	432.6	0.07	30.3	Appendix D
V_m	X_{17}	Seismic shear force	Lognormal	Kips	241.6	0.13	31.4	
M_{max}	X_{18}	Seismic bending moment	Gumbel	Kip-in	35664.2	0.08	2853.1	

Table 5.2—*Continued.*

RV	X_i	Description	Distribution	Units	μ_i-Mean	c.o.v.$_i$	σ_i-St. dev.	Reference/Source
High hazard level-Life Safety (5% in 50 yrs PE) : Case P_{max}								
P_{max}	X_{16}	Seismic axial load	Gumbel	Kips	432.2	0.01	4.3	Appendix D
V_p	X_{17}	Seismic shear force	Lognormal	Kips	198.6	0.08	15.9	
M_p	X_{18}	Seismic bending moment	Lognormal	Kip-in	31091.5	0.05	1554.6	
High hazard level-Life Safety (5% in 50 yrs PE) : Case V_{max}								
P_v	X_{16}	Seismic axial load	Lognormal	Kips	418.2	0.03	12.5	Appendix D
V_{max}	X_{17}	Seismic shear force	Gumbel	Kips	225.5	0.08	18.0	
M_v	X_{18}	Seismic bending moment	Lognormal	Kip-in	31234.9	0.08	2498.8	
High hazard level-Life Safety (5% in 50 yrs PE) : Case M_{max}								
P_m	X_{16}	Seismic axial load	Lognormal	Kips	430.6	0.01	4.31	Appendix D
V_m	X_{17}	Seismic shear force	Lognormal	Kips	218.4	0.09	19.7	
M_{max}	X_{18}	Seismic bending moment	Gumbel	Kip-in	32466.8	0.03	974.0	
Moderate hazard level- Immediate Occupancy (10% in 50 yrs PE): Case P_{max}								
P_{max}	X_{16}	Seismic axial load	Gumbel	Kips	429.8	0.01	4.3	Appendix D
V_p	X_{17}	Seismic shear force	Lognormal	Kips	197.9	0.07	13.9	
M_p	X_{18}	Seismic bending moment	Lognormal	Kip-in	30000.1	0.08	2400.0	
Moderate hazard level- Immediate Occupancy (10% in 50 yrs PE): Case V_{max}								
P_v	X_{16}	Seismic axial load	Lognormal	Kips	419.1	0.03	12.6	Appendix D
V_{max}	X_{17}	Seismic shear force	Gumbel	Kips	212.7	0.11	23.4	
M_v	X_{18}	Seismic bending moment	Lognormal	Kip-in	29909.9	0.09	2691.9	
Moderate hazard level- Immediate Occupancy (10% in 50 yrs PE): Case M_{max}								
P_m	X_{16}	Seismic axial load	Lognormal	Kips	428.8	0.01	4.3	Appendix D
V_m	X_{17}	Seismic shear force	Lognormal	Kips	206.5	0.08	16.5	
M_{max}	X_{18}	Seismic bending moment	Gumbel	Kip-in	30568.7	0.09	2751.2	
Low hazard level- Operational (50% in 50 yrs PE): Case P_{max}								
P_{max}	X_{16}	Seismic axial load	Gumbel	Kips	355.8	0.08	28.5	Appendix D
V_p	X_{17}	Seismic shear force	Lognormal	Kips	116.1	0.24	27.9	
M_p	X_{18}	Seismic bending moment	Lognormal	Kip-in	16424.4	0.23	3777.6	
Low hazard level-Operational (50% in 50 yrs PE): Case V_{max}								
P_v	X_{16}	Seismic axial load	Lognormal	Kips	351.7	0.09	31.7	Appendix D
V_{max}	X_{17}	Seismic shear force	Gumbel	Kips	121.6	0.22	26.8	
M_v	X_{18}	Seismic bending moment	Lognormal	Kip-in	16901.7	0.22	3718.4	
Low hazard level-Operational (50% in 50 yrs PE): Case M_{max}								
P_m	X_{16}	Seismic axial load	Lognormal	Kips	354.4	0.08	28.4	Appendix D
V_m	X_{17}	Seismic shear force	Lognormal	Kips	121.4	0.23	27.9	
M_{max}	X_{18}	Seismic bending moment	Gumbel	Kip-in	16997.3	0.21	3569.4	

The correlation between the seismic shear, the bending moment, and the axial loads is also determined based on seven records for each hazard level and critical load cases (P_{max}, V_{max}, and M_{max}). The correlation coefficients computed are presented in Table 5.3.

Table 5.3 Correlation coefficient between seismic loads on connection, computed for different hazard levels based on 7 records.

Hazard level	Case	$\rho_{P\text{-}V}$	$\rho_{P\text{-}M}$	$\rho_{M\text{-}V}$
2% in 50 yrs PE	P_{max}	0.65	0.80	0.96
	V_{max}	0.46	0.91	0.79
	M_{max}	-0.65	-0.12	0.81
5% in 50 yrs PE	P_{max}	0.65	0.77	0.75
	V_{max}	-0.17	0.57	0.59
	M_{max}	0.19	0.78	0.70
10% in 50 yrs PE	P_{max}	0.62	0.93	0.83
	V_{max}	-0.63	-0.16	0.85
	M_{max}	0.68	0.91	0.90
50% in 50 yrs PE	P_{max}	0.96	0.97	1.00
	V_{max}	0.78	0.86	0.99
	M_{max}	0.74	0.82	0.99

Since nonlinear behavior is developed in the steel frame for ground motion of moderate to high intensity, the relation between the axial, shear, and bending moment at the connection does not present a clear linear tendency (see Appendix D). Conversely, for the low hazard level (50% in 50 yrs PE), the correlation coefficients between the bending moment and the shear force are close to 1.0, indicating a nearly perfect linear relationship between these responses, as observed in Appendix D. For the other two cases ($\rho_{P\text{-}V}$, $\rho_{M\text{-}V}$), the correlation coefficients are high and approach a value of 1.0; however, some dispersion can be observed in the data and a perfect linear relation cannot be established for the axial load.

Several parameters are defined for the limit-state formulation corresponding to different coefficients used in the design procedure of the connection, defined according to AISC Design Guide No.1-2005 (see Table 5.4). A sensitivity analysis is carried out for these parameters to determine the effect of small variations in the values of the limit-state parameters on the failure probability and reliability index of the connection.

Table 5.4 Summary of limit-state parameters.

Parameter	θ_i	Description	Units	Value
k	θ_1	Concrete confinement coefficient for maximum stress	-	2.0
C_{ub1}	θ_2	Coefficient for tension in anchor bolts	-	0.75
C_{ub2}	θ_3	Coefficient for shear in anchor bolts	-	0.50
C_{brg}	θ_4	Coefficient for bearing of shear lugs	-	0.80

5.4 DISCUSSION OF RESULTS

5.4.1 Critical Load Case

The critical load case between P_{max}, V_{max}, or M_{max} is determined through a system reliability analysis using three different data sets of the demand loads in the base plate connection, for the high hazard level (2% in 50 yrs PE). The results of the reliability index and first-order failure probability for the system obtained for each load case are presented in Table 5.5.

Table 5.5 Reliability index and failure probability for the high hazard level (2% in 50 yrs PE) using three different load cases.

	Load case		
	P_{max}	V_{max}	M_{max}
Reliability index β	0.684	0.577	0.404
Failure probability P_{f1} (%)	24.7	28.2	34.3

Evidently, the M_{max} load case has the highest failure probability. However, the general orientation of the failure domain must be examined as well for the predominant failure modes of the connection, to justify the use of a single critical load case for the system reliability and sensitivity analysis.

Using the minimum cut-set formulation for the system, the reliability results of each failure mode are combined to obtain the connection's overall performance. The results for the reliability index and failure probability of each component and the system are presented in Table 5.6. As can be observed, the predominant failure modes include the yielding of the base plate on the compression side (ductile failure) and the concrete crushing (brittle failure). The shear failure consisting of friction failure and bearing failure of the shear lugs against the adjacent concrete also represent an important failure mode of the connection. Similar results are obtained for the other two load cases (V_{max}, P_{max}).

Table 5.6 System reliability index and failure probability for the high hazard level (2% in 50 yrs PE) and the M_{max} load case.

Failure Mode	Description	β	P_{f1}
1	Concrete crushing	1.570	5.818×10^{-2}
2	Yielding of base plate (compression side)	0.537	2.956×10^{-1}
3	Yielding of base plate (tension side)	3.261	5.554×10^{-4}
4	Tensile yielding of bolts	2.121	1.695×10^{-2}
5	Friction & bolt shear	6.579	2.370×10^{-11}
6	Friction & bearing of shear lugs	2.028	2.129×10^{-2}
System		**0.404**	**3.431×10^{-1}**

The alpha (α) vectors are unit vectors in the standard normal space directed toward the failure domain of each limit-state function. These are shown in Table 5.7 for limit states 1, 2, 5, and 7, which define the three most important failure modes as described above. The angle between these vectors obtained for different load cases (P_{max}, V_{max}, M_{max}) are presented for the predominant failure modes of the connection (see Table 5.8).

Table 5.7 α vectors for the connection's predominant failure modes, computed for each load case for the high hazard level (2% in 50 yrs PE).

Limit-state function		1			2			5			7		
No.	**RV**	P_{max}	V_{max}	M_{max}	P_{max}	V_{max}	M_{max}	P_{max}	V_{max}	M_{max}	P_{max}	V_{max}	M_{max}
1	d_c	0	0	0	0	0	0	0	0	0	0	0	0
2	b_f	0	0	0	-0.111	-0.1085	-0.1234	0	0	0	0	0	0
3	N	-0.2939	-0.2843	-0.3134	-0.2871	-0.2785	-0.3158	0	0	0	0	0	0
4	B	-0.2324	-0.2243	-0.247	0.5225	0.511	0.5814	0	0	0	0	0	0
5	t_{PL}	0	0	0	-0.3267	-0.3178	-0.3599	0	0	0	0	0	0
6	l_{sl}	0	0	0	0	0	0	0	0	0	-0.8451	-0.8387	-0.8373
7	b_{sl}	0	0	0	0	0	0	0	0	0	-0.0339	-0.0373	-0.0367
8	d_b	0	0	0	0	0	0	0	0	0	0	0	0
9	d_{edge}	0	0	0	0	0	0	0	0	0	0	0	0
10	t_{grout}	0	0	0	0	0	0	0	0	0	0.4822	0.4997	0.4953
11	$F_{y,col}$	0	0	0	0	0	0	0	0	0	0	0	0
12	$F_{y,PL}$	0	0	0	-0.3864	-0.3762	-0.4265	0	0	0	0	0	0
13	F_{ub}	0	0	0	0	0	0	0	0	0	0	0	0
14	f'_c	-0.7119	-0.688	-0.757	0	0	0	0	0	0	-0.1464	-0.1609	-0.1586
15	μ	0	0	0	0	0	0	-0.9908	-0.9924	-0.9742	0	0	0
16	P	0.4892	0.5639	-0.0361	0.4963	0.5619	-0.0782	0.0726	0.0157	-0.1908	0.1162	0.0663	-0.1080
17	V	0.3265	0.2677	0.5117	0.3507	0.292	0.4752	0.1142	0.1220	0.1205	0.1313	0.1236	0.1245
18	M	0.0823	0.0774	0.0678	0.0825	0.0774	0.0597	0	0	0	0	0	0

Table 5.8 Angles φ between α vectors for the connection's predominant failure modes, computed between each load case for the high hazard level (2% in 50 yrs PE).

	Limit-state function			
Load cases	**1**	**2**	**5**	**7**
(P_{max}-M_{max})	32.5^{o}	34.6^{o}	15.2^{o}	12.9^{o}
(V_{max}-M_{max})	38.1^{o}	39.4^{o}	11.9^{o}	10.0^{o}

Appendix D presents the results for the remaining failure modes and hazard levels. As observed, all angles between the α vectors obtained from different load cases for each failure mode are much smaller than 90o. As a result, a strong correlation between these load cases is obtained, computed as $\rho_{ij} = \alpha_i \bullet \alpha_j = \cos(\phi)$>0.5. This indicates that the α vectors have similar orientations and, therefore, the direction of the failure domain can be considered approximately independent of the load case and the reliability analysis can be performed for a single critical load case, Mmax, presenting the highest failure probabilities and lowest reliability indices for the individual components and the overall connection. Essentially, the failure domains for the other two load cases are subsets of the failure domain for the load case M_{max}. This is conceptually shown in Figure 5.10.

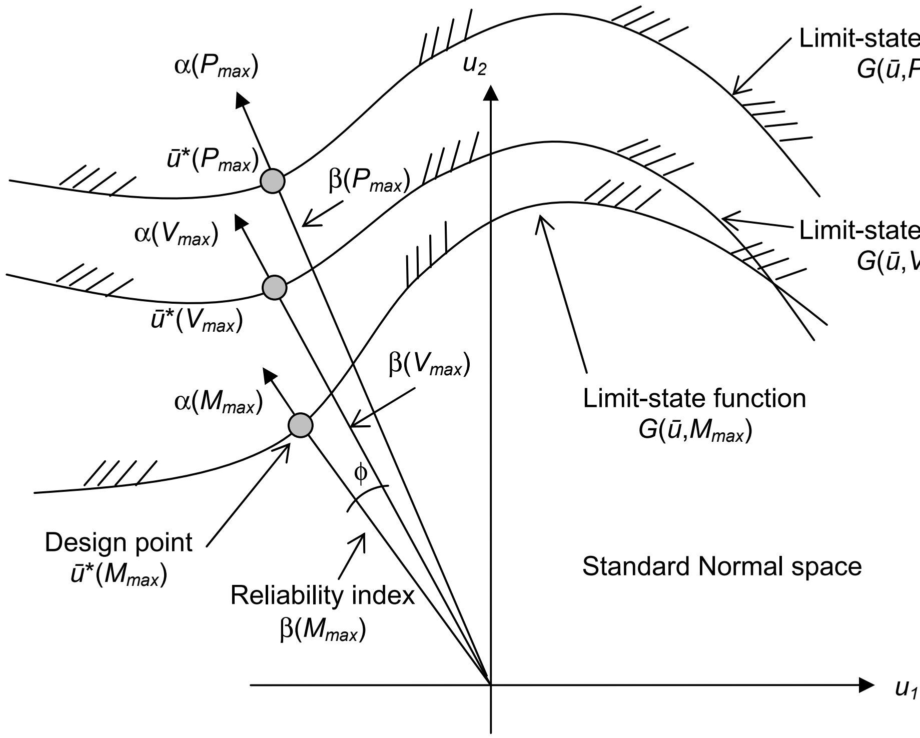

Fig. 5.10 Determination of critical load case.

For a more exact evaluation of the connection's failure in the case of exceptionally different directions of the failure domain obtained from different loading conditions (P_{max}, V_{max}, M_{max}), the system formulation must consist of a series system of the previous cut-set formulation (see Fig. 5.11), with the following minimum cut-set formulation: C_{min}={(1)(2)(3)(4)(5,6)(5,7)(8)(9)(10)(11)(12,13)(13,14)(15)(16)(17)(18)(19,20)(19,21)}.

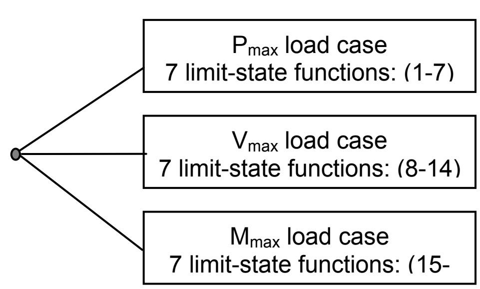

Fig. 5.11 System failure scheme for different load combinations.

The additional limit-state functions are identical to the first set of functions; however, the load demand values correspond to another critical load case. Even this extended cut-set formulation is a subset of the complete loading history and combinations that can occur in the assembly, and therefore it represents only a lower bound for the failure probability according to Turkstra's rule (Turkstra and Madsen 1986). The critical loading condition in the connection will not necessarily occur when one of the bending moments, or shear or axial forces are at their maximum value (M_{max}, V_{max} and P_{max} load cases, respectively); however, it is expected that it will be closely related to these maximum load cases.

5.4.2 FORM vs. SORM Approximation

The adequacy of the first-order reliability method (FORM) is verified through a comparison with the point-fitting second-order reliability method (SORM) (Der Kiureghian 2005a). The results of FORM and SORM component reliability analysis computed for the high hazard level corresponding to 2% in 50 yrs PE are presented in Table 5.9.

Table 5.9 FORM and SORM component reliability analysis results computed for the high hazard level (2% in 50 yrs PE).

Component	Description	β_{FORM}	β_{SORM}	$P_{f1,FORM}$ (%)	$P_{f2,SORM}$ (%)	ΔP_f (%)
1	Concrete crushing	1.570	1.501	5.81	6.66	12.7
2	Yielding of base plate, compression side	0.537	0.491	29.56	31.15	5.1
3	Yielding of base plate, tension side	3.261	3.268	0.055	0.054	2.6
4	Tension yielding of anchor bolts	2.121	2.086	1.70	1.85	8.4
5	Friction	0.939	0.915	17.40	18.00	3.3
6	Anchor bolt shear	6.608	6.596	0	0	0
7	Shear lugs bearing	0.127	0.309	44.94	38.27	17.4

On average, the difference between FORM and SORM component reliability analysis results is around 10%. Components 1 and 7 display higher differences between SORM and FORM, indicating higher nonlinearity in the limit-state function. The failure probabilities obtained through the first-order approximation are generally smaller than for the second-order results. The curvatures of the limit-state functions were not analyzed to verify the adequacy of the SORM approximation due to the high complexity in the limit-state formulation and the large number of random variables involved. Since an upper bound is not defined for the error in the approximation using any of the two methods and the results are relatively similar overall, the FORM reliability method is considered suitable for a general approximation of the connection reliability study. The system reliability analysis is therefore based on the FORM component reliability analysis.

5.4.3 Component Reliability Analysis

The component reliability analysis results computed for the high hazard level (2% in 50 yrs PE) are presented in Table 5.9. The results for the remaining hazard levels, presented in Appendix D, display a similar contribution of the different failure modes to the system failure. As discussed previously, the predominant failure modes in the connection are the yielding of the base plate and concrete crushing, both occurring on the compression side of the plate with individual failure probabilities of 29.56 and 5.82% (FORM approximation), respectively. The shear failure obtained due to base plate sliding and shear lug bearing failure is the third most likely failure mode, with a failure probability of 2.13%. Tension yielding of the anchor bolts resulted in a failure probability of 1.70%, while shear failure due to sliding of the base plate and anchor bolt shear failure had a zero failure probability, even for the high seismic hazard level.

5.4.3.1 Design Point

The yielding failure of the base plate cantilever due to the bearing stress distribution on the compression side of the plate, corresponding to component or limit-state function 2, is the predominant failure mode for all hazard levels (see Table 5.10).

Table 5.10 Reliability index and failure probability for the yielding of the base plate on the compression side, computed for all hazard levels considered.

Hazard level	β_{FORM}	$P_{f1,FORM}$ (%)
2% in 50 yrs PE	0.537	29.56
5% in 50 yrs PE	1.189	11.71
10% in 50 yrs PE	1.436	7.55
50% in 50 yrs PE	3.073	0.11

The limit state function $g_2(\underline{X}) = \frac{F_{y,pl}(t_p)^2}{4} - \left(\frac{P}{NB} + \frac{M}{(1/6)BN^2}\right) \cdot \frac{1}{2}\left(\frac{B - 0.80b_f}{2}\right)^2$ includes the following variables: $\underline{X} = [b_f, N, B, t_{PL}, F_{y,pl}, M, P]^T$. Therefore the results for the design point in the original and standard normal spaces, importance vectors, and sensitivity analysis ignore all other random variables and parameters. Using the improved HL-RF algorithm starting at the mean point, after 4 to 5 iterations the final reliability index and first-order approximation of the failure probability P_{f1} are computed. The design point in the original space and its relation to the mean are presented in Table 5.11.

Table 5.11 Design point in original space (x^*) obtained for base plate yielding on compression side for the high hazard level (2% in 50 yrs PE).

RV-Random Variable	μ- Mean	μ vs. *x**	*x**- Design point	RV classification
d_c	26.02	=	26.02	-
b_f	13.11	>	13.10	Capacity
N	38.0	>	37.83	Capacity
B	25.0	<	25.31	Demand
t_{PL}	3.75	>	3.729	Capacity
l_{sl}	3.5	=	3.50	-
b_{sl}	25.0	=	25.0	-
d_b	2.0	=	2.0	-
d_{edge}	3.0	=	3.0	-
t_{grout}	2.0	<	2.168	Demand
$F_{y,col}$	60	>	59.93	Capacity
$F_{y,PL}$	50	>	49.09	Capacity
F_{ub}	137.5	>	136.9	Capacity
f'_c	4.8	>	4.763	Capacity
μ	0.80	<	0.9063	Demand
P	432.6	>	430.3	-
V	241.6	<	246.5	-
M	35664.2	<	35890.0	-

In general, random variables corresponding to the capacity of the connection have a slightly lower value than the mean at the design point at failure, while the variables corresponding to demand loads or having a negative contribution to the connection's capacity have larger values than the mean. There may be some exceptions to this rule, especially when the variables are highly correlated. Random variables with a negligible contribution to the survival or failure of this specific resistance mechanism maintained the mean values for the design point. Since the largest cantilever length of the base plate is $\left(B-0.80b_f\right)/2$, the width of the plate is a demand random variable, while the flange width is a capacity variable. Namely, the larger the width of the base plate *B*, the higher the bending demand on the base plate and its probability of yielding. Conversely, a thicker base plate t_{PL} with higher the yield strength $F_{y,PL}$ and a longer column flange width b_f produce a more reliable connection. Also, a larger base plate length resulting in lower bearing stress values in the supporting concrete will also reduce the bending demand on the plate.

The bending moment (*M*), axial load (*P*), and shear force (*V*) in the connection are correlated with different positive and negative correlation coefficients computed for each hazard level. Therefore, it is difficult to determine the nature of these variables (as demand or capacity variables) based on a comparison of the design point with respect to its mean vector. Since the bending moment and axial load increase the bearing stress in the supporting concrete and the bending demand on the plate, both random variables are expected to represent demand variables. However, since the resulting eccentricity of the connection (bending moment divided by axial load) is reduced as well, the random variable corresponding to the axial load is contributing to the resistance of the connection, as observed in Table 5.11. On the other hand, the shear and bending moment are classified as demand variables according to the results in Table 5.11, increasing the failure probability of the plate. This might not be the case for other failure modes of the connection.

The failure mode of the connection due to concrete crushing (limit-state 1) presents similar results to the discussion above. The design point results for the bearing failure of the shear lugs against the adjacent concrete are presented in Table 5.12. The limit-state function for this failure mode $g_8\left(\underline{X}\right)=C_{brg}f'_c\, n_{sl}b_{sl}\left(l_{sl}-t_{grout}\right)-V$ involves the following random variables: $\underline{X}=\left[f'_c, b_{sl}, l_{sl}, t_g, V\right]^T$.

Table 5.12 Design point in original space (x^*) obtained for shear lugs bearing failure for the high hazard level (2% in 50 yrs PE).

RV- Random Variable	μ- Mean	μ vs. x^*	x^*- Design point	RV classification
d_c	26.02	=	26.02	-
b_f	13.11	=	13.11	-
N	38.0	=	38.0	-
B	25.0	=	25.0	-
t_{PL}	3.75	=	3.75	-
l_{sl}	3.5	>	3.414	Capacity
b_{sl}	25.0	=	25.0	-
d_b	2.0	=	2.0	-
d_{edge}	3.0	=	3.0	-
t_{grout}	2.0	<	2.199	Demand
$F_{y,col}$	60	>	59.93	Capacity
$F_{y,PL}$	50	>	49.88	Capacity
F_{ub}	137.5	>	136.9	Capacity
f'_c	4.8	>	4.751	Capacity
μ	0.80	<	0.9063	Demand
P	432.6	>	431.1	-
V	241.6	>	240.2	-
M	35664.2	>	35240.0	-

As expected, the compressive strength of the concrete foundation and dimensions of the shear lugs are the main capacity variables contributing to the resistance of the connection. A similar comparison can be carried out for the remaining components of the system, according to the results presented in Appendix D. As discussed above, since the random variables corresponding to the loads in the connection are correlated, their contribution to the connection's failure cannot be determined through a comparison of the design point with respect to its mean vector.

5.4.3.2 Importance Vectors

The importance vectors, α, γ, δ, η, are presented in Table 5.13 for the failure mode by plate yielding on the compression side. The importance vector α indicates the direction of the failure domain as well as the relative importance of the random variables in the Standard Normal space

U. From the importance vector γ, corresponding to the original space X, the order of importance of the random variables is presented, indicating that the increase of the base plate width B resulting in larger cantilever $(B-0.80b_f)/2$ and the bending moment demand on the column base M are the predominant causes in the connection's failure. The thickness of the steel base plate t_{PL} and its strength (expressed in terms of the yield stress $F_{y,PL}$) are the primary variables contributing to the connection's capacity. According to the γ vector, an increase in the length of the base plate N will also reduce the probability of failure of the connection, through a reduction in the value of the bearing stress distribution and the bending demand on the plate. The value of N is limited by the maximum cantilever of the plate, which will promote the connection's failure, i.e., the dimension $(N-0.95d_c)/2$ cannot exceed the cantilever length of the base obtained in the orthogonal direction, $(B-0.80b_f)/2$.

Table 5.13 Importance vectors base plate yielding on the compression side (high hazard level, 2% in 50 yrs PE).

RV	α (*U* space)	γ (*X* space)	δ	η	Classification	Order of importance
b_f	-0.1234	**-0.1249**	0.1234	-0.0082	Capacity	6
N	-0.3158	**-0.3198**	0.3158	-0.0536	Capacity	5
B	0.5814	**0.5888**	-0.5814	-0.1816	Demand	1
t_{PL}	-0.3599	**-0.3645**	0.3599	-0.0696	Capacity	4
$F_{y,PL}$	-0.4265	**-0.4319**	0.4359	-0.1272	Capacity	3
P	-0.0782	**0**	0	0	Capacity	8
V	0.4752	**0.0332**	-0.0325	-0.0030	Demand	7
M	0.0597	**0.4637**	-0.4648	-0.0375	Demand	2

The importance vector δ determines the effect on the reliability index β of statistically equivalent variations in the mean values, assuming fixed standard deviations of the random variables: $\delta = \nabla_{\mu}\beta \cdot \underline{D} = \{\partial\beta_i / \partial\mu_i \cdot \sigma_i\}$. For statistically independent random variables, the relative importance of the random variables in terms of their mean values is the same as the results obtained from the α vector. A positive sign in the entry δ_i corresponds to an increase in the reliability index, indicating that the random variable can be classified as a capacity variable. Conversely, a negative sign of δ_i corresponds to a demand variable, reducing the reliability index or equivalently increasing the failure probability.

The importance vector η determines the effect on the reliability index β of statistically equivalent variations in the standard deviation of the random variables, assuming fixed means: $\delta = \nabla_{\sigma}\beta \cdot \underline{D} = \{\partial\beta_i / \partial\sigma_i \cdot \sigma_i\}$. The η vector determines the relative importance of the random variables in terms of their dispersion, indicating reduction in the variability in the base plate width and strength will have the highest effect on the connection's reliability.

5.4.4 System Reliability Analysis

5.4.4.1 System Reliability at Different Hazard Levels

Using the minimum cut-set formulation for the column base connection system, component reliability analysis results are combined to obtain the conditional system failure probability of the connection for the four seismic hazard levels considered. The design of the connection remains unmodified throughout, i.e., the random variables such as dimensions, material strength, friction coefficients, and limit-state parameters are maintained constant for the reliability analysis at the hazard levels considered. The failure probabilities and reliability indices for each failure mode and for the system are presented in Tables 5.14–5.15.

Table 5.14 System reliability index computed for different hazard levels.

		β- Reliability index			
		Hazard level (PE in 50 yrs)			
Failure Mode	**Description**	**2%**	**5%**	**10%**	**50%**
1	Concrete crushing	1.570	2.301	2.345	3.621
2	Yielding of base plate (compression side)	0.537	1.189	1.436	3.073
3	Yielding of base plate (tension side)	3.261	4.672	5.500	5.740
4	Tensile yielding of bolts	2.121	4.193	4.411	4.825
5	Friction & bolt shear	6.579	6.654	6.667	6.731
6	Friction & bearing of shear lugs	2.028	2.223	2.309	2.558
System		**0.404**	**1.089**	**1.330**	**2.935**

Table 5.15 System failure probability computed for different hazard levels.

		P_{fT}- Failure probability			
		Hazard level (PE in 50 yrs)			
Failure Mode	**Description**	**2%**	**5%**	**10%**	**50%**
1	Concrete crushing	$5.818\text{x}10^{-2}$	$1.069\text{x}10^{-2}$	$9.524\text{x}10^{-3}$	$1.467\text{x}10^{-4}$
2	Yielding of base plate (compression side)	$2.956\text{x}10^{-1}$	$1.171\text{x}10^{-1}$	$7.551\text{x}10^{-2}$	$1.061\text{x}10^{-3}$
3	Yielding of base plate (tension side)	$5.554\text{x}10^{-4}$	$1.490\text{x}10^{-6}$	$1.898\text{x}10^{-8}$	$4.723\text{x}10^{-9}$
4	Tensile yielding of bolts	$1.695\text{x}10^{-2}$	$1.378\text{x}10^{-5}$	$5.155\text{x}10^{-6}$	$7.011\text{x}10^{-7}$
5	Friction & bolt shear	$2.370\text{x}10^{-11}$	$1.431\text{x}10^{-11}$	$1.307\text{x}10^{-11}$	$8.405\text{x}10^{-12}$
6	Friction & bearing of shear lugs	$2.129\text{x}10^{-2}$	$1.311\text{x}10^{-2}$	$1.046\text{x}10^{-2}$	$5.268\text{x}10^{-4}$
System		$\mathbf{3.431\text{x}10^{-1}}$	$\mathbf{1.381\text{x}10^{-1}}$	$\mathbf{9.170\text{x}10^{-2}}$	$\mathbf{1.700\text{x}10^{-3}}$

As can be observed, the largest contribution to the system failure is produced due to yielding of the base plate on the compression side, which is a ductile and desirable failure mode. The other predominant failure modes in the connection concrete are undesirable brittle failures including concrete crushing and shear failure due to sliding of the base plate and bearing failure of the shear lugs against the adjacent concrete. Tension yielding of the anchor bolts also has an important contribution; however, shear failure of the anchor bolts and yielding of the base plate on the tension side have negligible contribution to the system failure probability for this specific design of the connection.

5.4.4.2 Total System Failure Probability

The total failure probability for each failure mode and for the system are obtained by combining the corresponding conditional failure probabilities at each hazard level presented in Table 5.14, weighted by the corresponding probabilities of the hazard levels. This formulation can be expressed as:

$$P(failure) = \sum_{h} P(failure / H = h) \cdot P_H(h) \qquad (5.15)$$

where,

H: Random seismic hazard level

h: Four specific hazard levels considered in the analysis, including the high (2% and 5% in 50 yrs PE), moderate (10% in 50 yrs PE), and low (50% in 50 yrs PE)

$P(failure)$: Total failure probability of the base plate connection

$P(failure|H=h)$: Conditional probability of the base plate connection, given a hazard level h

$P_H(h)$: Marginal probability of the hazard level or level of intensity of the earthquake in the site, determined for a time period t

The marginal probabilities of the hazard levels are presented in Table 5.16, based on the hazard curves presented in Chapter 4. Table 5.17 presents the total failure probabilities for 1 year and for the expected 50 years lifespan of the structure. Also shown in Table 5.17 is the corresponding system reliability index.

Table 5.16 Marginal probabilities of hazard levels.

Performance Level	Hazard level *h*	$S_{a,T1}$ (g)	$P_H(h,t$=50 yrs)	$P_H(h,t$=1 yrs)
Collapse Prevention	High (2% in 50 yrs PE)	1.62	1.878×10^{-2}	3.597×10^{-4}
Life Safety	High (5% in 50 yrs PE)	1.30	3.564×10^{-2}	5.089×10^{-4}
Immediate Occupancy	Moderate (10% in 50 yrs PE)	0.99	8.757×10^{-2}	2.050×10^{-3}
Operational	Low (50% in 50 yrs PE)	0.33	8.580×10^{-1}	9.971×10^{-1}

Table 5.17 System failure probability P_{f1} and reliability index β.

Failure Mode	Description	$P_{f1,t=50\ yrs}$ (%)	$P_{f1,t=1\ yrs}$ (%)
1	Concrete crushing	3.234×10^{-3}	1.993×10^{-4}
2	Yielding of base plate (compression side)	2.026×10^{-2}	1.405×10^{-3}
3	Yielding of base plate (tension side)	1.983×10^{-5}	2.879×10^{-7}
4	Tensile yielding of bolts	6.054×10^{-4}	9.340×10^{-6}
5	Friction & bolt shear	9.469×10^{-12}	8.425×10^{-12}
6	Friction & bearing of shear lugs	2.373×10^{-3}	5.623×10^{-4}
System- P_{f1}		**2.431×10^{-2}**	**2.107×10^{-3}**
System- β		**1.972**	**2.862**

The contribution of the different failure modes considered in the analysis can be observed from Table 5.17. The largest contribution to the system failure probability is due to yielding of the base plate on the compression side, which is a ductile and desirable failure mode. The other dominant failure modes are undesirable brittle failures including concrete crushing and shear failure due to sliding of the base plate and bearing failure of the shear lugs against the adjacent concrete. Tension yielding of the anchor bolts also has an important contribution. The remaining failure modes have negligible contribution to system failure for this connection design.

The resulting system reliability index β of 1.972 and failure probability P_{f1} of 2.43% computed for the expected 50 years lifespan of the structure may be considered relatively low and high, respectively. The design, carried out for the 10% in 50 years PE hazard level, also results in relatively high conditional failure probability of 9.17% for an earthquake of relatively moderate intensity. For the highest seismic hazard level of 2% in 50 years PE, the failure probability of 34.31% is also relatively high.

The failure probability estimates presented above, which employ the well-known PEER formula based on total probability theorem, entail an error due to the presence of non-ergodic (aleatory or epistemic) variables (Der Kiureghian 2005b). The original PEER formula was intended to compute the mean annual rate of a performance measure exceeding a specified threshold. Approximation of the exceedance probability using this formula may result in as much as 20% error for probabilities around 0.05 and 30% error for probabilities around 0.10. For failure probabilities less than 0.01, the approximation has a negligible error. In the present project the total failure probability of the connection computed for one year is less than 0.01. Therefore, this approximation of the failure probability has a negligible error. For the lifespan of the structure of 50 years, the error in the failure probability of 2.43% may be as much as 20%. However, since the error is on the conservative side (Der Kiureghian 2005b), this approximation of the connection reliability is found to be acceptable.

Based on the results of this reliability analysis, the AISC Design Guide No. 1-2005 column base plate connection design procedure should be modified by reducing resistance factors and increasing demand amplification factors to increase the reliability of the connection. It is also important for the design procedure to promote the occurrence of ductile failure modes over brittle failure modes. A capacity design approach could guarantee the desired behavior of the connection, following a predetermined sequence of failure modes of the different components of the connection. The desired reliability of the connection can also be adjusted for a given set of design loads by specifying larger dimensions and material strengths of its components.

5.4.4.3 Fragility Curves

Fragility curves are obtained by relating the conditional failure probabilities of the occurrence of each failure mode and the occurrence of system failure to an earthquake intensity measure (IM) or hazard level H. In this study, IM is the spectral acceleration at the first-mode period ($S_{a,T1}$ or $PS_{a,T1}$) of the moment-resisting frame (see Tables 4.3 and 5.16). This measure was computed at each hazard level using the hazard data for a location in Berkeley, California.

Fragility curves are obtained through a lognormal fit to the data presented in Table 5.16 and a least-square approximation of the error. The mean (μ) and standard deviation (σ) of the lognormal distribution are obtained for the system and the different failure modes, as presented in Table 5.18.

Table 5.18 Parameters of lognormal fit: system reliability analysis results.

Failure Mode	Description	μ- Mean (g)	σ- St. Dev. (g)
1	Concrete crushing	1.01	0.34
2	Yielding of base plate (compression side)	0.74	0.45
3	Yielding of base plate (tension side)	0.61	0.04
4	Tensile yielding of bolts	0.58	0.04
5	Friction & bolt shear	60.68	9.12
6	Friction & bearing of shear lugs	3.63	1.55
System		0.67	0.44

The fitted curves for all failure modes using the lognormal distribution parameters of Table 5.18 are displayed in Appendix D. The lognormal fit to the system failure probability P_{f1} in terms of the intensity measure (S_a=$PS_{a,T1}$) is presented in Figure 5.12.

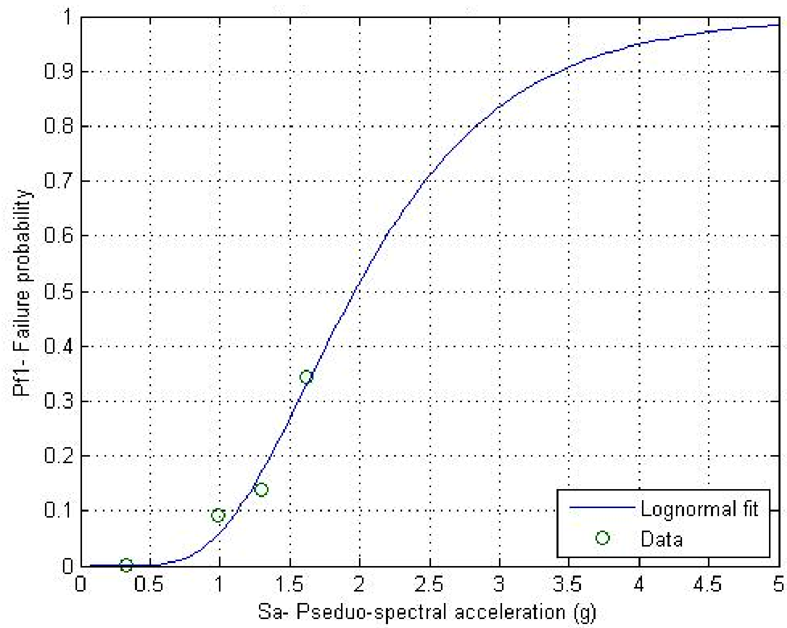

Fig. 5.12 Lognormal fit to failure probabilities of base plate connection.

As discussed before, the failure probabilities obtained for the high seismic hazard levels present extremely high values for a structural system (highest data point). The total failure probability of the connection can also be obtained by integrating the fragility curves over the entire range of intensity, considering the marginal probability of the intensity level. Since the contribution of failure probabilities at higher intensity or higher hazard level is relatively small (due to the small probability of occurrence of the hazard), the approach of Section 5.4.4.2 is considered suitable for a general estimation of the system overall reliability. Using values at 4 discrete points of the entire intensity range, the resulting failure probability of the connection in 50 years is 2.43%.

The fragility curves for the system and the predominant failure modes discussed in Section 5.4.1 are presented in Figure 5.13. Clearly, the yielding of the base plate (mode 2) has the largest contribution to the system failure for any seismic hazard or intensity level. This failure mode is followed by the concrete crushing of the foundation (mode 1). The third most important failure mode is the shear failure (mode 6), corresponding to base plate sliding and shear lugs bearing failure. As discussed previously, a desired design procedure of a base plate connection would be controlled by ductile failure modes. The failure sequence of the connection would therefore consist of failure modes 2, 3, and 4 (ductile), followed by failure modes 1, 5, and 6 (brittle).

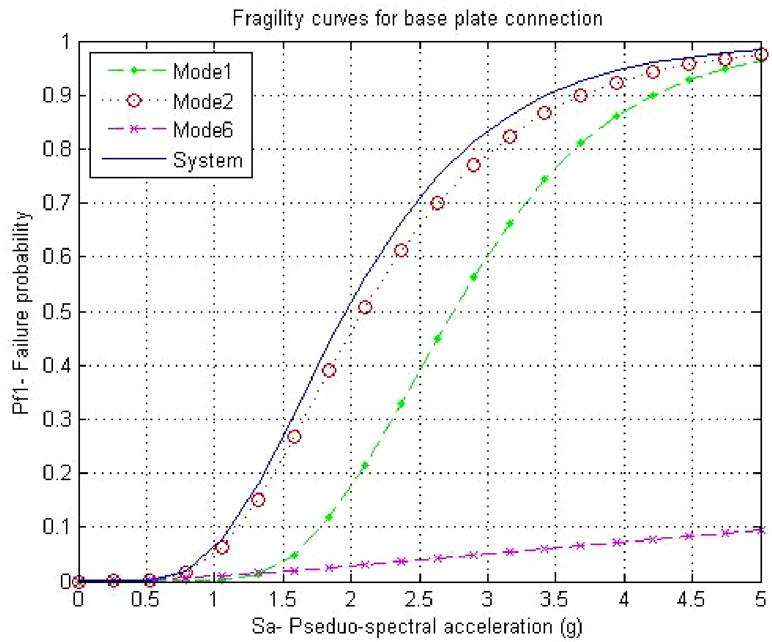

Fig. 5.13 Fragility curves for the system and predominant failure modes of base plate connection.

5.4.5 Relative Importance of Random Variables

Determining the order of importance of random variables for column base connection behavior is performed by perturbing the mean values of these variables (on the order of 10%), determining the resulting variations in connection reliability, and computing the importance value $\delta=(\partial\beta/\partial\mu)\sigma$ for each variable. This computation is carried out for one of the hazard levels (2% in 50 yrs PE) and is presented in Appendix D. The characterization as a capacity or demand variable is established for each random variable according to the sign of the corresponding element in vector δ. The results computed for the 2% in 50 years PE hazard level are summarized in Table 5.19.

Table 5.19 Importance vector δ obtained from system reliability analysis.

RV	$\delta_i=(\Delta\beta/\Delta\mu_i)\sigma_i$	Order of Importance	Classification
d_c	$2.40\text{x}10^{-5}$	17	Capacity
b_f	$8.65\text{x}10^{-2}$	7	Capacity
N	$2.72\text{x}10^{-1}$	4	Capacity
B	$-5.23\text{x}10^{-1}$	1	Demand
t_{PL}	$2.20\text{x}10^{-1}$	5	Capacity
l_{sl}	$2.86\text{x}10^{-3}$	14	Capacity
b_{sl}	$3.46\text{x}10^{-3}$	12	Capacity
d_b	$3.00\text{x}10^{-3}$	13	Capacity
d_{edge}	$-4.17\text{x}10^{-4}$	16	Demand
t_{grout}	$-7.25\text{x}10^{-2}$	9	Demand
$F_{y,col}$	$0.00\text{x}10^{0}$	18	-
$F_{y,PL}$	$3.20\text{x}10^{-1}$	3	Capacity
F_{ub}	$4.09\text{x}10^{-3}$	11	Capacity
f'_c	$1.02\text{x}10^{-1}$	6	Capacity
μ	$7.80\text{x}10^{-2}$	8	Capacity
P	$-2.80\text{x}10^{-3}$	15	Demand
V	$-5.72\text{x}10^{-2}$	10	Demand
M	$-4.90\text{x}10^{-1}$	2	Demand

On the demand side, the base plate dimension directly affecting the cantilever length and bending moment of the column base plate has the highest influence on the failure of the connection. On the capacity side, the base plate thickness and base plate steel strength represent important components of the system resistance. The strength of the concrete foundation and the friction coefficient between the base plate and grout are the next important aspects affecting the reliability of the column base connection. Since the strength of the steel column ($F_{y,col}$) is not used in any of the limit-state functions, it has neither positive nor negative contribution to the system failure and can be eliminated from the formulation.

These results are similar to the ones obtained for the component analysis corresponding to bending failure of the plate on the compression side (limit-state function 2), which has the largest contribution to the connection failure. The other failure modes are less significant, thus their random variables and parameters have smaller importance in the reliability of the system.

5.4.6 Sensitivity Analysis of Limit-State Parameters

The sensitivity of the failure probability P_{f1} of the system with respect to the limit-state parameters, denoted θ_g, are obtained through a small perturbation in the parameter values (on the order of 5%) and the computation of the resulting variations in P_{f1}. The results for the 2% in 50 years PE hazard level are presented in Table 5.20.

Table 5.20 Sensitivities of β and P_{f1} of the system to variation in limit-state parameters θ_g.

Parameter	θ_{gi}	$\Delta\theta_{gi}$	$\nabla_{\theta_g}\beta \cdot \theta_g$	$\nabla_{\theta_g}P_{f1} \cdot \theta_g$	$\nabla_{\theta_g}P_{f1} \cdot \left(\frac{\theta_g}{P_{f1}}\right)$
k	2.0	-0.10	-0.850	0.307	0.89
C_{ub1}	0.75	-0.0375	-0.090	0.033	0.10
C_{ub2}	0.50	-0.025	0.000	0.000	0.00
C_{brg}	0.80	-0.04	-0.130	0.048	0.14

The confinement coefficient k, which for the present design is equal to 2.0 based on the assumption of adequate transverse reinforcement and large cross section of the concrete pedestal, has a sensitivity $\nabla_{\theta g}P_f\,(\theta_g/P_f)$ of 0.89. For example, this corresponds to an increase of 0.089 (or 8.9%) in the system failure probability P_{f1} for the 2% in 50 years hazard level if the value of parameter k is reduced by 10% due to inadequate confinement. The remaining limit-state parameters have small to negligible effect on the failure probabilities of the connection, even for the highest hazard level. Values of 0.0010, 0.0, and 0.0014 increase in the system failure probability are obtained with a reduction of 1% in the values of parameters C_{ub1}, C_{ub2}, and C_{brg}, respectively.

The effect on the system failure probability due to larger variations in the limit-state parameters cannot be computed using the above estimations, which are obtained through finite difference approximations. Instead, the analysis should be repeated using a different set of values of the limit-state parameters.

This analysis is repeated for the confinement coefficient k for the remaining hazard levels, where the results are presented in Table 5.21. The total effect of confinement on the failure probability of the connection is computed as follows:

$$\nabla_{\theta_g}P_{f1} = \frac{\partial P(failure)}{\partial \theta_g} = \sum_h \frac{\partial P(failure/H=h)}{\partial \theta_g} \cdot P_H(h) \qquad (5.16)$$

The term $\partial P(failure)/\partial\theta_g$ is the partial derivative or the gradient of the failure probability with respect to a limit-state parameter, in this case the confinement coefficient ($\theta_g = k$).

Table 5.21 Sensitivities of β and P_{f1} of the system to variation in limit-state parameter θ_g=k, corresponding to confinement coefficient.

Hazard level (h)	$\nabla_{\theta_g} P(failure/H=h)\cdot(\theta_g / P_{f1})$	$P_H(h,t{=}50)$	$P_H(h,t{=}1)$
2% in 50 yrs PE	0.89	3.564x10^{-2}	5.089x10^{-4}
5% in 50 yrs PE	0.80	1.878x10^{-2}	3.597x10^{-4}
10% in 50 yrs PE	0.84	8.757x10^{-2}	2.050x10^{-3}
50% in 50 yrs PE	0.56	8.580x10^{-1}	9.971x10^{-1}
Total effect $\nabla_{\theta_g} P_{f1}(\theta_g / P_{f1})$		**0.600**	**0.561**

A sensitivity $\nabla_{\theta_g} P_{f1}(\theta_g / P_{f1})$ of 0.60 is computed for the life span of 50 years of the connection. For example, this corresponds to an increase of 0.060 (or 6.0%) in the failure probability of the connection in 50 yrs due to a reduction of 10% in the coefficient *k* due to inadequate confinement. If confinement cannot be guaranteed in the foundation, the system reliability analysis must be repeated using a minimum coefficient *k* of 1.0 (instead of 2.0), resulting in higher failure probabilities. The importance of adequate confinement details specified for concrete foundations in seismic regions is illustrated through this sensitivity value.

5.4.7 Effect of Friction Resistance

The AISC Design Guide No.1-2005 procedure establishes the following shear resistance mechanisms: (1) friction along the contact area between the concrete surface and the steel base plate, which should be taken as the effective bearing area resisting compressive loads; (2) bending and shear in the anchor bolts; and (3) bearing of shear lugs installed underneath the base plate (or the side of the base plate if it is embedded) against the adjacent concrete or grout.

In the present design, the effective area was assumed to be the entire width times the bearing depth for the friction capacity. The anchor bolts are contributing only with shear resistance, since no washers are specified between the base plate, thus ignoring bending of the rods. Bearing resistance is considered only for the shear lugs installed under the plate, which is completely exposed and does not bear against the adjacent unreinforced grout.

The combination of these three mechanisms in a parallel system as defined through the cut-set formulation of the system provides the overall shear resistance and horizontal equilibrium of the column base connection. However, when uplift forces are produced in the base plate under seismic loading, the ability of the reduced compression zone to resist horizontal shear due to friction is reduced. This estimation is not appropriately addressed in the design procedure, which does not clearly indicate the conditions to develop each of the resistance mechanisms.

Since the failure modes related to shear resistance contribute no more than about 10% to the total failure probability of the connection (see Section 5.4.4), a reduction in the friction resistance and bearing of shear lugs would not significantly alter the system behavior. However, the proper evaluation and interaction of these resistance mechanisms must be further examined.

6 Conclusions

The following chapter summarizes the findings obtained for each of the four main sections of this report. The primary aspects and considerations of the analysis procedures performed for this project are restated, including the different seismic response evaluations of the SMRFs with different degrees of restraint of column bases, as well as the column base connection reliability and sensitivity analyses.

6.1 PUSHOVER ANALYSIS OF SMRF

A parametric study of the effect of column base stiffness and strength on the seismic demand and behavior of a typical low-rise steel moment-resisting frame was carried out using a three-story, three-bay frame in the building designed for the ATC-58 PEER project, located in Berkeley, California. The modal and pushover analyses were carried out using the software program SAP2000 Nonlinear, modeling the column base plate connection as a rotational spring with varying stiffness from pinned to fixed (K_{norm}=18.0, 9.1, 3.6, 1.4, 0.6, 0.2, 0 of EI/L_{col}).

The rotational stiffness of the column bases significantly affects the lateral stiffness of a low-rise steel moment-resisting frame. The principal finding of this study is that a reduction in base fixity resulted in an increase of the displacement demand and a change of the first vibration mode shape such that deformations concentrated in the first story of the frame. Such increase in interstory drifts and rotational demand on the plastic hinges in the first-story girders and column bases will not only result in concentrated structural and nonstructural damage in this region of the frame, but could also develop an undesired soft-story mechanism in the first floor.

Frames with stiffer column base connections are a more efficient lateral force-resisting system because such frames can develop a complete collapse mechanism at the end of the pushover analysis and resist higher base shear. Frames with soft (pin-like) column bases do not form mechanisms that include plastic hinges at the bottoms of the columns: thus, the amount of plastic work done by such flexible-base frames is smaller than that done by stiff-base frames. The base shear capacity of the frames with column base connections stiff and strong enough to induce formation of column plastic hinges right above the column base connection asymptotically approach that of a frame with fixed column bases. The second principal finding of this study is that the seismic response of low-rise steel moment-resisting frames with semi-rigid column base connections with normalized rotational stiffness K_{norm}>4EI/L_{col} approaches that of the identical frames with fixed column bases, assuming that column bases are strong enough to develop the plastic moment strength of the column.

The hierarchy in the formation of plastic hinges varied with different column base stiffness and strength. There is an exponential increase in the rotational demand on the plastic hinges of the girders when column bases are flexible, with normalized stiffness in the range between 0 and 2 EI/L_{col}. Furthermore, a small variation in the stiffness will result in pronounced variation in the frame response. For the stiff column base connections (K_{norm}>4EI/L_{col}), the variation of girder rotation demand is reduced, which is desirable, as it allows for demand re-distribution to more frame elements and connections and increases the degree of redundancy in the lateral force-resisting system. The joint beam and column-moment demand ratios in moment-resisting frames with base rigidity exceeding 4EI/L_{col} are practically constant, making it possible to consistently achieve strong column–weak girder behavior.

The seismic demands in terms of total base shear, overturning moment, and joint reactions in low-rise steel moment-resisting frames with stiffer column base connections are very similar to those modeled with a completely fixed column base. The axial force and moment demand on column bases remained practically constant regardless of column base stiffness, since these forces are dependent primarily on beam and column plastic capacity, respectively. The shear demand was largest for stiff column base connections where plastic hinges had just formed at the base of the column, decreasing slightly with increasing stiffness of the column base and approaching asymptotically the fixed-base frame value. The shear force for interior column bases is slightly larger than that for the exterior column bases due to the larger stiffness of the interior beam-column subassemblies.

In order to observe the effect of column base fixity in computer models of low-rise steel moment-resisting frames, it is essential to account for the actual strength and stiffness of the partially restrained column base connection. Convenient fully restrained (fixed) or free-to-rotate (pinned) column base connection models can be achieved in practice only with special design and detailing of the connections that is very different from conventional steel column base details. Furthermore, column base connection stiffness and strength can be reduced due to inadequate detailing, poor construction quality, long-term deformations, deterioration of foundation's concrete, or cumulative effects of past earthquakes. The semi-rigid models of column bases developed using nonlinear zero-length rotation springs, presented in this report, may be used.

Relatively stiff column bases are needed to control the displacements and interstory drifts and to comply with the acceptance criteria established in current U.S. design codes. The pushover analyses conducted in this study indicate that low-rise steel moment-resisting frames with flexible column base connections (K_{norm} between 0 and $0.2EI/L_{col}$) may develop drifts exceeding FEMA 356 Collapse Prevention performance level, may develop a soft-story mechanism, and may become instable due to P-Delta effects. In such cases, the size of the first-story columns should be increased to reduce the risk of forming a soft-story mechanism.

6.2 TIME HISTORY ANALYSIS OF SMRF

Nonlinear time history analysis was performed on the three low-rise moment-resisting frame models with fixed (F, K_{norm}=18EI/L_{col})), semi-rigid (SR3, K_{norm}=1.4EI/L_{col}), and pinned (P, K_{norm}=0) column bases. The OpenSees Navigator finite element analysis software package, built using the OpenSees finite element analysis framework, was used to determine the response of the frames under a representative set of seven ground motions scaled to the 2% in 50 years PE hazard level, corresponding to the Collapse Prevention level for the assumed location of the frames on the UC Berkeley campus. The nonlinear time history analyses results were compared to nonlinear static analysis (pushover) results computed using the OpenSees Navigator and the SAP2000 Nonlinear software packages. This comparison was carried out using the median and the appropriate fractals of the statistical distribution of the response quantities obtained from the seven time histories analyses assuming a normal distribution of the data.

The pushover analyses were conducted using a load pattern proportional to the deformations of the first vibration mode of each frame model and a roof displacement target obtained using the FEMA 356 coefficient method. The OpenSees Navigator and the SAP2000 Nonlinear models of the frames utilized different finite elements to model the frame elements, but had the same mass magnitude and distribution, and were calibrated to have similar initial stiffness (and thus similar first-mode vibration periods), and similar yield and ultimate strength. The hazard levels considered in this PBEE analysis were the 2%, 5%, 10%, 50%, and 75% in 50 years probability of exceedance (PE), with a return period of 2475, 975, 475, 75, and 35 years, respectively. The pushover analysis results obtained from the two software packages were similar: the base shear capacities differed by less than 7%, the joint reactions by less than 9%, the fundamental periods by less than 9%, and the interstory drifts by less than 1%. The two programs are therefore comparable and both can be used to conduct nonlinear static analyses of low-rise steel moment-resisting frames.

The time history analyses were conducted using the same frame models developed for the pushover analyses. The analyses conducted by SAP2000 Nonlinear using the direct integration method did not converge, while those conducted using the modal superposition method, which ignores material and geometric nonlinearities, produced unrealistic outcomes with predominantly symmetric response of the frames and no residual deformation for the very intense ground motion excitations used in this study. Therefore, only the OpenSees Navigator time history analyses were used in this study.

The deformation mechanism and displacement time history of the moment-resisting frames vary with the column base fixity of each model. The maximum displacements decrease with increasing base rigidity. The displacement demand obtained using the FEMA356 coefficient method of FEMA 356 was larger than the mean plus one standard deviation (μ+σ) values of the maximum displacements and interstory drifts of the F, SR3, and P model, by only 7, 6, and 11%, respectively. Therefore, the coefficient method is adequate for estimating the maximum deformation of low-rise steel moment-resisting frames. While the first vibration mode shape dominated the deformed shape of the frames observed during the time history analyses, the effect of higher modes was evident in somewhat reduced maximum displacements and interstory drifts of the frames.

The values of the residual displacements observed at the end of the applied earthquake ground motions varied significantly among the analyzed models and did not follow a particular pattern.

The maximum values of frame base shear varied according to the intensity of the records and the fundamental vibration period of each model. The median of the maximum base shear values obtained from the seven ground motions exceeded by 15, 21, and 24% the results obtained from the pushover analysis for the F, SR3, and P frames, respectively. However, the difference was reduced to 8, 14, and 18% when comparing the pushover analysis results with the mean minus one standard deviation (μ-σ) values of the time history analyses. The axial forces in the columns are a function of beam plastic moment capacity and do not vary as much: the pushover column axial forces differ by 7% from the median of the time history values.

The maximum joint shear and moment values due to the seven ground motions exceed those computed from the pushover analyses for the three frame types due to significant kinematic strain hardening. This hardening model is sensitive to the number of strain reversals and, for the utilized intense ground motions, produces an increase in post-yield stress values larger than the 3% of the initial stiffness value used in the pushover models. The frame element demands obtained from the time history analyses are, therefore, more conservative.

6.3 PERFORMANCE-BASED EARTHQUAKE ENGINEERING: REPAIR COST EVALUATION OF SMRF

The PEER Center performance-based earthquake engineering (PBEE) methodology was used to evaluate the effect of column base rotational stiffness and strength on the post-earthquake repair cost of a typical low-rise special steel moment-resisting frame building. The ATC-58 example office building, located on the University of California at Berkeley campus, was analyzed using three F, SR3, and P frame models. The seismic hazard was evaluated using the Seismic Guidelines for UC Berkeley Campus. The hazard levels considered in this PBEE analysis were the 2%, 5%, 10%, 50%, and 75% in 50 years probability of exceedance. Two groups of ground motions with characteristics expected for a building site at UC Berkeley main campus were selected for the low and high hazard levels. The interstory drifts and floor accelerations required for the PBEE analysis were computed for each frame and each hazard level using nonlinear time history analysis in OpenSees Navigator. The structural and nonstructural elements of the building were grouped into performance groups such that their damage states are governed by the same demand parameter. The damage state and the subsequent repair cost for each performance group were computed using the ATC-58 Project fragility curves and repair cost data. An implementation of PEER PBEE methodology based on an EDP correlation matrix and Monte Carlo simulation of the damage and repair cost states was used to integrate the total probability integral and compute the resulting repair cost fragilities and annual probabilities of exceedance.

The time history analysis results showed an increase in the displacements, interstory drifts, and plastic rotation demand on the first-story girders, columns, and connections due to a reduction of column base stiffness and strength. In a typical office building (without acceleration-sensitive equipment), the damage and associated repair costs are controlled primarily by interstory drift: therefore, reduction in column base stiffness and strength results in higher repair costs. In the case of the analyzed ATC-58 building, the mean annual total repair cost of the pinned-base moment-resisting frame was over three times greater than that for the fixed-base model. The response and therefore the repair costs associated with the semi-rigid column base frame approached that of the fixed-base frame. The mean annual repair costs were on the order of $10,000 for the analyzed ATC-58 building.

The third principal finding of this study is that the accumulation of repair costs induced by frequent small and moderate earthquakes dominate the computed estimates of the main annual total repair cost, even though a single strong, but rare, earthquake may cause repairs costing two to three orders of magnitude more than the mean annual repair cost. This happens because frequent events have a high probability of occurring several times during the building service life. Therefore, in order to reduce repair costs, it is important to design the column base connections to be relatively stiff and strong, and to maintain these mechanical characteristics throughout the expected service life of the structure despite long-term deterioration and several small to moderate earthquakes. This design requirement is in addition to the collapse-prevention-related design requirement for ductile detailing of all frame elements and connections.

In the case of structures housing acceleration-sensitive equipment, the content repair cost may have a significant contribution to the total repair cost of the building. An increase in column base fixity, desirable to control repair cost of drift-sensitive building components, will result in higher seismic forces and floor accelerations, causing more damage to the acceleration-sensitive components and thus increasing the total repair cost. An accurate evaluation of column base rotational stiffness and strength is therefore essential for an accurate performance-based evaluation of damage, repair cost, and overall economic feasibility of structures housing acceleration-sensitive content.

6.4 RELIABILITY ANALYSIS OF BASE PLATE CONNECTION IN SMRF

The reliability of an exposed column base designed according to the AISC Design guide No. 1-2005 provisions was evaluated. A sample exposed column base plate was designed for the external column of the moment-resisting frame of the ATC-58 building located in a high seismic zone. The design of loads for the connection were obtained from the median response values of a suite of nonlinear time history analysis results of the SMRF joint reactions, defined for the 10% in 50 years PE hazard level. Random variables describing this design were characterized using ASTM and AISC design code data. The demands on the column base for the reliability analysis were also characterized using data from suites of nonlinear time history earthquake response analyses of the ATC-58 building frame conducted at four different seismic hazard levels (2, 5, 10, and 50% in 50 yrs probabilities of exceedance). A hierarchy of column base connection failure modes was established. Reliability analysis was carried out using the FORM and SORM approximation to compute the reliability index of the connection. Fragility curves for each failure mode and the system were developed using a lognormal fit.

The most likely failure modes of the analyzed column base connection were yielding of the base plate on the compression side (ductile), concrete compression crushing (brittle), and shear failure due to base plate sliding and bearing failure of shear lugs (brittle). The fourth principal finding of this study is that, in order to promote ductile failure modes and a desirable failure mode sequence of the column base connection, the resistance factors in AISC Design Guide No. 1-2005 should be decreased and a capacity design approach should be rigorously adhered to. Although a relatively high failure probability (34.3%) was computed for the column base connection at the high seismic hazard level (2% probability of exceedance in 50 yrs), the combined total probability of failure in a 50-years period equals 2.43% (corresponding to a reliability index β=1.97). Nevertheless, this combined total failure probability is relatively high for a critical structural connection such as the column base connection. The column base connection design procedure proposed in AISC Design Guide No.1-2005 can therefore be considered to be unconservative.

A sensitivity analysis was carried out to evaluate the importance of the random variables, as well as the sensitivity of the failure probabilities to variations in the limit-state function parameters. On the demand side, the largest cantilever length of the base plate has the highest importance for the connection’s failure. This dimension should be minimized during the design process to reduce the bending demand on the plate. The overall dimensions of the base plate should not be excessively reduced, since that could lead to an increase in the concrete bearing stress and the probability of concrete crushing. The thickness of the plate and its yield strength are also important variables controlling failure. Base plate flexibility alters its yielding pattern, the degree of semi-rigidity of the connection, and the corresponding demand loads on all other components of the connection. Therefore, the effect of base plate flexibility should be incorporated into the design equations and included in the system reliability analysis. Finally, a reduction in the confinement of the foundation can lead to an important increase of the failure probability of the connection due to crushing of concrete. Steel frame and foundation designers should interact to ensure adequate confinement of the foundation, particularly for column bases of perimeter columns. Additional failure modes such as pull-out failure of the anchor bolts, bearing failure of the base plate due to anchor bolt shear, foundation edge breakout, or welding failure in the case uplift-forces, had large safety factors for this particular column base connection design and were therefore omitted from the reliability analysis.

7 Future Work

Many important aspects related to the behavior of column base connections are not addressed sufficiently in current design procedures. A capacity design approach is required in order to guarantee the desired sequence of failure modes in the different components of the column base plate connection. A new capacity design procedure of the connection should be developed based on the findings and recommendations of the reliability analysis presented in this report (see Chapter 5). Finite element modeling and experimental work of the base plate connection with different configurations and loading conditions are recommended for the elaboration of the new design criteria. Additionally, the design of economic moment-resisting frames with stable behavior (see Chapters 2–4) should be based on adequate modeling considerations of the degree of semi-rigidity of column bases. An additional reliability and sensitivity analysis of the base plate connection and moment frame system is recommended for such assessment.

Future investigations of the seismic behavior and design of typical column base connections and moment-resisting frames, commonly used in U.S. practice, should address the following pending issues:

Base plate mechanics: The effects of plate flexibility, yielding line patterns, as well as anchor bolt dimensions and spacing should be considered when analyzing the normal stresses in the base plate of exposed column base connections. Instead of assuming that the base plate is rigid, local bending of the base plate about both horizontal axes should be accounted for when computing the effective widths of the base plate sections that resist bending. A minimum thickness of the base plate is required to avoid high local stress concentration in the proximity of the anchor bolts that could result in undesirable prying failure on the tension side. On the compression side, bending of the base plate also depends on the distribution of the bearing stresses, making it difficult to determine if the tension or the compression side bending will govern the design.

Finally, the through thickness plate shear stresses should be incorporated to evaluate if stress interaction reduces the resistance of the base plate.

Bearing stress distribution: The general design assumption is that the base plate is thick or rigid enough to produce a uniform pressure over the supporting concrete surface on the compression side. However, the base plate is not rigid, the underlying ground is not monolithic, and the bond between the anchor bolts and the concrete foundation is often weakened during an earthquake. More research is needed to determine the distribution and intensity of the compression stress bulb under the base plate, and to propose a design procedure that accounts for the actual compression stress distribution by using equivalent uniform stress blocks applied over an effective bearing area that depends on the base plate configuration, plate flexibility, and relative strength of the base plate connection components.

Anchor bolt design: The number of anchor bolts and their arrangement affect the deformed shape and the yielding pattern of the base plate on the tension side and the bearing stress distribution on the compression side, a fact that has been overlooked in current design methods. The anchor bolt forces, in turn, depend on the base plate stiffness and are usually not uniform, as assumed by most design procedures. Finally, the stiffness of the anchor bolts should be considered in the design as well.

Shear resistance mechanism: It is necessary to investigate the conditions required to develop different shear resistance mechanisms in the column base plate connection and the interaction between these mechanisms. Shear resistance is especially important for column bases with high axial and shear load, such as those found in braced frames. The friction resistance developed between the steel base plate and supporting concrete in the compression zone cannot be developed when uplift forces are produced in the base plate under seismic loading and slip occurs, a fact which is ignored in some design procedures. Further investigation of other shear resistance mechanisms, such as bearing through shear lugs or shear and bending resistance in the anchor bolts, and resistance by bearing on shallowly embedded column is needed.

Degree of column base semi-rigidity: Exposed column base connections, typical for U.S. construction of steel moment-resisting frames, have the initial stiffness and strength such that they can be classified as semi-rigid under cyclic loading. Such partial fixity condition is due to the flexibility of the base plate, flexibility of anchor bolts, and gaps between the bearing surface and plate caused by concrete crushing during reversed cyclic. A further unintended reduction in the connection stiffness can result from poor workmanship, long-term deformation and deterioration of the concrete foundation, or cumulative effects of previous earthquakes. It is essential to correctly estimate the rotational stiffness and the actual moment and shear capacity of the column base connection, since these mechanical properties significantly affect the seismic demand and structural behavior of the frame, as well as the post-earthquake repair costs of the building and feasibility of the project.

The findings of this study are that low-rise steel moment-resisting frames column base connections with a normalized rotation stiffness $K_{norm}>4EI/L_{col}$ and strength sufficient to develop the plastic moment capacity of the column perform in a manner that is, within engineering precision, the same as the performance of identical frames with fixed column bases. It is therefore imperative to determine experimentally the stiffness and strength characteristics of typical U.S. exposed column base connections, both in their initial condition and after they have sustained deformations consistent with small to moderate frequent earthquakes. These experimental investigations should be extended to failure to determine the failure mechanism sequence for typical U.S. column base connections and to establish their rotation capacity. Such investigations may be extended to account for soil-structure interaction. A higher degree of base fixity can be achieved by embedding the columns into the concrete foundation; however, there are no codified procedures of design of such connections in the U.S. today.

Capacity design approach: A new design procedure for exposed column base connections should be developed using a capacity design approach. This approach should be used to promote the desired ductile behavior and to ensure a desirable hierarchy of the failure modes of the different components of the column base assembly. Since the column base behavior differs significantly with base plate thickness, the hierarchy of failure modes for thick and thin base plate connections will be different. One possible hierarchy is shown in Figure 7.1 (Astaneh, Bergsma, and Shen 1992).

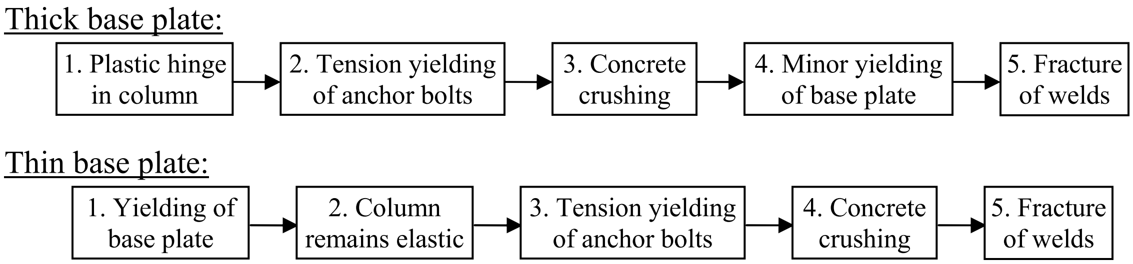

Fig. 7.1 Desired sequence of failure modes for thick and thin base plates.

In order to develop a capacity design procedure, further experimental investigations are needed to determine the actual force flow throughout the column base connection. The dimensions of the connection components are determined by the commercial availability of sizes, while the actual strength of the component is affected by the strain-hardening behavior of steel and concrete. These parameters modify the relative strength and stiffness of the different components of the connection, and affect the force flow. The outcome of these investigations should be a new set of strength reduction (or safety) factors for the new design procedure to promote the desired performance while achieving a sufficiently low probability of collapse.

Modeling of column base connections: Base plate connections have been modeled using solid-element finite element models with some success. However, such models are too complex for practical design and frame analysis. Designers would benefit most from simple and practical column base connection models ready for use in frame analysis software. Such models should reflect the principal characteristics of the seismic response of column bases: the semi-rigid nature of the response, the rate of strain hardening after yielding under different excitations, the rate of degradation of unloading stiffness, and the energy dissipated by inelastic deformation during cyclic loading. Further investigations are needed to develop such models, either as macro-models representing the entire column base connection or component models representing the components of column base connections and their interaction.

Connection reliability analysis: The reliability and sensitivity analysis presented in this report was performed for a single configuration of an exposed column base connection. The same procedure should be repeated for different connection designs and configurations to determine the reliability of such connections, the likely failure mode sequences, the sensitivity of connection performance to connection design parameters, and to establish the reliability coefficients for the connections.

Performance evaluation of structural systems: The reliability, sensitivity, and performance analyses can be extended to all structural components and the entire structural system. Such analyses would provide insight into the effect of different code design provisions, such as those related to ensuring a strong column–weak beam behavior, or connection types and configurations on the safety and performance of the structure. Such analyses can be extended to evaluate the life-cycle costs and economic feasibility of structures.

REFERENCES

American Institute of Steel Construction (2002). *Seismic Provisions for Structural Steel Buildings*. AISC, Chicago, Illinois, S6.2.

ACI 318 (2005). *Building Code Requirements for Structural Concrete (ACI318-05) and Commentary (ACI318R-05).* ACI Committee 318. American Concrete Institute, Detroit Michigan.

AISC-LRFD (2001). *Specification for Structural Steel Buildings, Manual of Steel Construction*. 3rd Edition. American Institute of Steel Construction, Inc., Chicago, Illinois.

American Institute of Steel Construction (2000). *Code of Standard Practice for Steel Buildings and Bridges*. American Institute of Steel Construction, Inc., Chicago, Illinois.

American Institute of Steel Construction (1999). *Load and Resistance Factor Design Specification for Structural Steel Buildings*. American Institute of Steel Construction, Inc., Chicago, Illinois.

American Institute of Steel Construction (2005). Seismic Provisions for Structural Steel Buildings. American Institute of Steel Construction, Inc., Chicago, Illinois.

ATC-58 (in progress). Development of Next-Generation Performance-Based Seismic Design Procedures for New and Existing Buildings, Applied Technology Council, Committee 58, http://www.atcouncil.org/atc-58.html.

Aslani, H. and Miranda, E. (2005). Probability-Based Seismic Response Analysis. *Engineering Structures* 27 (2005) 1151–1163.

Astaneh-Asl, A., Bergsma, G., and Shen, J. H. (1992). Behavior and Design of Base Plates for Gravity, Wind and Seismic Loads. *Proceedings of the National Steel Construction Conference*, Las Vegas, Nevada.

ASTM A572 (2004). *Standard Specification for High-Strength Low-Alloy Columbium-Vanadium Structural Steel*. American Standards for Testing and Materials, ASTM International, West Conshohocken, Pennsylvania.

ASTM A992 (2004). *Standard Specification for Structural Steel Shapes*. American Standards for Testing and Materials, ASTM International, West Conshohocken, Pennsylvania.

ASTM A6 (2005). *Standard Specification for General Requirements for Rolled Structural Steel Bars, Plates, Shapes, and Sheet Piling*. American Standards for Testing and Materials, ASTM International, West Conshohocken, Pennsylvania.

ASTM F1554 (2004). *Standard Specification for Anchor Bolts, Steel, 36, 55, and 105-ksi Yield Strength*. American Standard for Testing and Materials, ASTM International, West Conshohocken, Pennsylvania.

Aviram, A., Mackie, K. and Stojadinovic, B. (2008). *Guidelines for Nonlinear Analysis of Bridge Structures in California*. Technical Report 2008. Pacific Earthquake Engineering Research Center, University of California, Berkeley.

Aviram, A. and Stojadinovic, B. (2006). Evaluation of Design Methods for Column-Base Plate Connections in Gravity and Moment Resisting Frame. *Proceeding of the 8th National Conference on Earthquake Engineering*, Earthquake Engineering Research Institute, San Francisco, California.

Aviramtraubita A., Stojadinovic, B. (2006). Effect of Column Base Rigidity on Post-Earthquake Repair Cost of Steel Moment-Resisting Frame Structures. *Proceedings of the 1st European Conference on Earthquake Engineering and Seismology*, Geneva, Switzerland.

Baker, J.W., Cornell, C.A. (2005). A Vector-Valued Ground Motion Intensity Measure Consisting of Spectral Acceleration and Epsilon. Department of Civil and Environmental Engineering, Stanford University, California.

Bertero V.V., Anderson J.C., and Krawinkler, H. (1994). *Performance of Steel Building Structures during the Northridge Earthquake*. Report No. UCB/EERC-94/09. Earthquake Engineering Research Center, University of California at Berkeley.

Bozorgnia, Y. and Bertero, V.V. (2004). *Earthquake Engineering: from Engineering Seismology to Performance-Based Engineering*. CRC Press, Boca Raton, Florida.

Burda, J. J. and Itani, A.M. (1999). *Studies of Seismic Behavior of Steel Base Plate*", Report No. CCEER 99-7, Center for Civil Engineering Earthquake Research, Department of Civil Engineering. University of Nevada, Reno, Nevada.

Cabrero, J.M., Bayo, E. (2005). Development of Practical Design Methods for Steel Structures with Semi-Rigid Connections. *Engineering Structures* 27 (2005) 1125–1137.

Carballo, J.E, Cornell, C.A. (2000). *Probabilistic Seismic Demand Analysis: Spectrum Matching and Design*. Reliability of Marine Structures Report No. RMS-41. Dept. of Civil and Envir. Engineering, Stanford University, California.

Chopra, A.K. (2006). *Dynamics of Structures: Theory and Applications to Earthquake Engineering.* 3rd edition. Prentice Hall, New Jersey.

Chopra, A.K. and Goel, R.K. (2001). *A Modal Pushover Analysis Procedure to Estimate Seismic Demands for Buildings*. Report No. 2001/03. Pacific Earthquake Engineering Research Center, University of California, Berkeley.

CSI (2005). *CSI Analysis Reference Manual for SAP2000, ETABS, and SAFE.* Computers and Structures, Inc. Berkeley, California.

CSI (2007). *Technical Papers and Support*. Computers and Structures. Web site: http://www.csiberkeley.com/support_technical_papers.html.

CSI (2005). *SAP2000-Linear and Nonlinear Static and Dynamic Analysis and Design of Three-Dimensional Structures: Basic Analysis Reference Manual*. Computers and Structures, Inc. Berkeley, California.

Der Kiureghian, A. (2005). *CEE 229-Structural System Reliability*. Class Notes for Spring Semester, 2005, University of California at Berkeley, California.

Der Kiureghian, A. (2005). Non-ergodicity and PEER's Framework Formula. *Earthquake Engineering and Structural Dynamics* 34:1643-1652.

Der Kiureghian, A., Haukaas, T. and Fujimura, K. (2006). Structural reliability software at the University of California, Berkeley. *Structural Safety*, 28(1-2):44-67.

DeWolf, J.T. and Bicker, D.T. (1990). *Design Guide No.1-Column Base Plates*. American Institute of Steel Construction.

Drake, R.M. and Elkin, S.J. (1999). *Beam-Column Base Plate Design: LRFD Method*, Engineering Journal, AISC, Vol.36, No.1, First Quarter, pp 29-38.

Fahmy, M., Stojadinovic, B., Goel, S.C., and Sokol, Z. (1998). Load Path and Deformation Mechanism of Moment Resisting Steel Column Bases. *Proceedings of the 6th US National Conference on Earthquake Engineering*, Earthquake Engineering Research Institute, Oakland, California.

Fahmy, M., Goel S.C., Stojadinovic, B. (1999). Analytical and Experimental Studies on the Seismic Response of Steel Column Bases. *Proceeding of the 8th Canadian Conference of Earthquake Engineering*, Canadian Association for Earthquake Engineering, Vancouver, British Columbia, Canada.

FEMA-273. (1996). *NEHRP Guidelines for the Seismic Rehabilitation of Buildings*. Report No. FEMA-273. Federal Emergency Management Agency, Washington D.C.

FEMA-302. (1997). *NEHRP Recommended Provisions for Seismic Regulations for New Buildings and Other Structures*. Report No. FEMA-302. Federal Emergency Management Agency, Washington D.C.

FEMA-350. (July 2000b). *Recommended Seismic Design Criteria for New Steel Moment-Frame Buildings*. Report No. FEMA-350. Federal Emergency Management Agency, Washington D.C.

FEMA-356. (2000a). *Prestandard and Commentary for the Seismic Rehabilitation of Buildings*. Report No. FEMA-356. Federal Emergency Management Agency, Washington D.C.

Fisher, J.M. and Kloiber, L.A., 2005. *AISC Design Guide No. 1-Column Base Plates*, American Institute of Steel Construction.

Grauvilardell, J.E., Lee, D., Hajjar, J.F., and Dexter, R.J. (2004). *Synthesis of Design, Testing and Analysis Research on Steel Column Base Plate Connections in High-Seismic Zones*. Structural Engineering Report No. ST-04-02. Department of Civil Engineering, University of Minnesota, Minneapolis, Minnesota.

Hilber, H. M., Hughes, T. J. R., and Taylor, R. L. (1977). Improved Numerical Dissipation for Time Integration Algorithms in Structural Dynamics. *Earthquake Engineering and Structural Dynamics*, 5:283-292.

Honeck, W.C. and Westphal, D. (1999). *Practical Design and Detailing of Steel Column Base Plates*. Steel Tips, Structural Steel Educational Council, July 1999.

International Code Council (2000). International Building Code. *International Code Council*, Washington, DC.

Jalayer, F. (2003). *Direct Probabilistic Seismic Analysis: Implementing Non-Linear Dynamic Assessments*. PhD Dissertation, Department of Civil and Environmental Engineering, Stanford University, California.

Kent, D.C., and Park, R. (1971). Flexural Members with Confined Concrete. *Journal of Structural Engineering*, 97(ST7): 1969-1990.

Kramer, S.L. (1996). *Geotechnical Earthquake Engineering*. Prentice Hall.

Krawinkler, H., Anderson, J., and Bertero, V. (1996). Steel Buildings. *Earthquake Spectra* volume 12-s1-1996, pp 25-47.

Lee, D., Goel, Stojadinovic, B. (2002). Relative Strength Effects on Seismic Behavior of Column-Base Plate Connections Under Weak Axis Bending. *Proceeding of 7th US National Conference of Earthquake Engineering*, Earthquake Engineering Research Institute, Oakland, California.

Lee, D., Goel, S.C., and Stojadinovic, B. (2000). Boundary Effects in Steel Moment Connections. *Proceedings of the 12th World Conference on Earthquake Engineering*, Auckland, New Zealand.

Lee, K. and Foutch, D. A. (2001). Performance Evaluation of New Steel Frame Building for Seismic Loads. *Earthquake Engineering and Structural Dynamics*; 31:653-670.

Li, T., Sakai, J., and Matsui, C. (2000). Seismic Behavior of Steel-Concrete Composite Column Bases. *Proceedings of the 12th World Conference on Earthquake Engineering*, Auckland, New Zealand, Paper 1072.

Liu, J. (2003). *Examination of Expected Yield and Tensile Strength Ratio*. Report for the American Institute of Steel Construction. Purdue University, Wet Lafayette, Indiana.

Liu, P-L., and A. Der Kiureghian (1986). Multivariate distribution models with prescribed marginals and covariances. *Probabilistic Engineering Mechanics*, 1: 105-112.

MacGregor, J. G. and Wight, J. K. (2005). *Reinforced Concrete: Mechanics and Design*. 4th Edition, Prentice Hall, Upper Saddle River, New Jersey.

Mackie, K. R., and Stojadinovic, B. (2006). Fourway: a Graphical Tool for Performance-based Earthquake Engineering. *Journal of Structural Engineering*, 132(8): 1274-1283.

Mander, J.B., Priestley, M.J.N., and Park, R. (1988). Theoretical Stress-Strain Model for Confined Concrete. *Journal of the Structural Engineering*, 114(ST8): 1804-1826.

Marino, E.M., Nakashima M., Mosalam, K.M. (2005). Comparison of European and Japanese seismic design of steel building structures. *Engineering Structures* 27 (2005) 827–840.

McKenna, F., and Fenves, G.L. (2000). An Object-Oriented Software Design for Parallel Structural Analysis. *Proceedings of the 2000 Structures Congress & Exposition: Advanced Technology in Structural Engineering*, May 8-10, 2000, Philadelphia, Pennsylvania.

Mckenna, F., Fenves, G.L., Scott, M.H., and Jeremic, B. (2000). *Open System for Earthquake Engineering Simulation*. http://OpenSees.berkeley.edu.

Medina, R., Krawinkler, H., and Alavi, B. (2001). Seismic Drift and Ductility Demands and their Dependence on Ground Motions. *Proceedings of the US-Japan Seminar on Advanced Stability and Seismicity Concepts for Performance-Based Design of Steel and Composite Structures*, July 23-27, 2001, Kyoto, Japan.

Moehle, J., and Deierlein, G.G. (2004). A Framework Methodology for Performance-Based Earthquake Engineering. *Proceedings of 13th World Conference on Earthquake Engineering*, Vancouver, Canada, August 1-6, 2004, CD, paper No. 679.

PEER Strong Motion Catalog. http://peer.berkeley.edu/smcat. Web page.

Scott, M.H., and Fenves, G.L. (2006). Plastic Hinge Integration Methods for Force-Based Beam-Column Elements. *Journal of Structural Engineering*, 132(2):244-252.

Shome, N., Cornell, C.A., Bazzurro, P., and Carballo, J.E. (1998). Earthquakes, Records, and Nonlinear Responses. *Earthquake Spectra*, 14(3): 467-500.

Shome, N., and Cornell, C.A. (1999). *Probabilistic Seismic Demand Analysis of Nonlinear Structures*. Reliability of Marine Structures Report No. RMS-35, Dept. of Civil and Envir. Engineering, Stanford University, California.

Stojadinovic, B., Spacone, E., Goel, S.C., and Kwon, M. (1998). Influence of Semi-Rigid Column Base Models on the Response of Steel MRF Buildings. *Proceedings of the 6th US National Conference on Earthquake Engineering*, Earthquake Engineering Research Institute, Oakland, California.

Timoshenko, S. P., and Goodier, J. N. (1969). *Theory of Elasticity*. 3rd edition. McGraw-Hill, New York.

Turkstra, C.J., and Madsen, H.O. (1986). Load combinations in codified structural design. *Journal of Structural Division ASCE* 106:2527-2543.

UCB (1997). Open System for Earthquake Engineering Simulation Framework. *Pacific Earthquake Engineering Research Center*, University of California, Berkeley, http://OpenSees.berkeley.edu/.

USGS. National Seismic Hazard Mapping Project Zip Code Look-up for Ground Motion Values. http://eqint.cr.usgs.gov/eq/html/zipcode.shtml. Web page.

UCB (2003). *U.C. Berkeley Seismic Guideline.* University of California, Berkeley.

Wald, F. (2000). *Column Base Modeling. Semi-Rigid Connections in Structural Steelwork*. CISM (International Center for Mechanical Sciences), Courses and Lectures No. 419, Editorial Springer Wien, New York.

Wilson, E.L. (1998). *Three Dimensional Static and Dynamic Analysis: A physical Approach with emphasis on Earthquake Engineering*. 2nd edition. Computer and Structures, Inc. Berkeley, California.

Yang, T.Y., Moehle, J., Stojadinovic, B. and Der Kiureghian, A. (2006). An Application of PEER Performance-Based Earthquake Engineering Methodology. *Proceedings of 8th US National Conference on Earthquake Engineering*, San Francisco, California, USA, April 18-22, 2006, CD, paper No.1271.

Yang, T.Y., Moehle, J., and Stojadinovic, B. (2005). Performance-Based Earthquake Engineering Assessment Toolbox. *Pacific Earthquake Engineering Research Center*, University of California, Berkeley, California, USA.

http://peer.berkeley.edu/~yang/ATC58website/.

Youssef, N.F.G., Bonowitz, D., and Gross, J.L. (1995). *A Survey of Steel Moment-Resisting Frame Buildings Affected by the 1994 Northridge Earthquake*. NISTIR 5625. National Institute of Standard and Technology, Gaithersburg, Maryland.

Appendix A: SAP2000 Modal and Pushover Analyses Results of SMRF

This appendix presents additional results obtained from the modal and pushover analysis of the SMRF for varying column base rotational stiffness, including story displacements, joint reactions, base shear and overturning moment, as well as the joint equilibrium results at the beam-column connections.

Modal Analysis Results

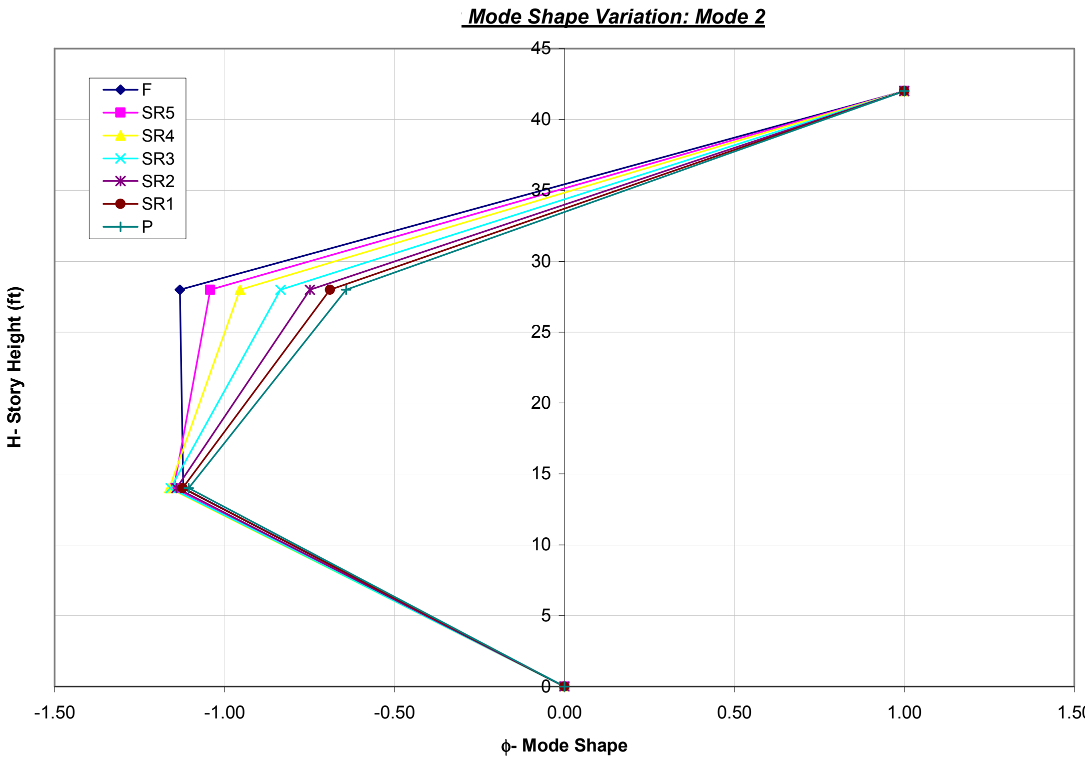

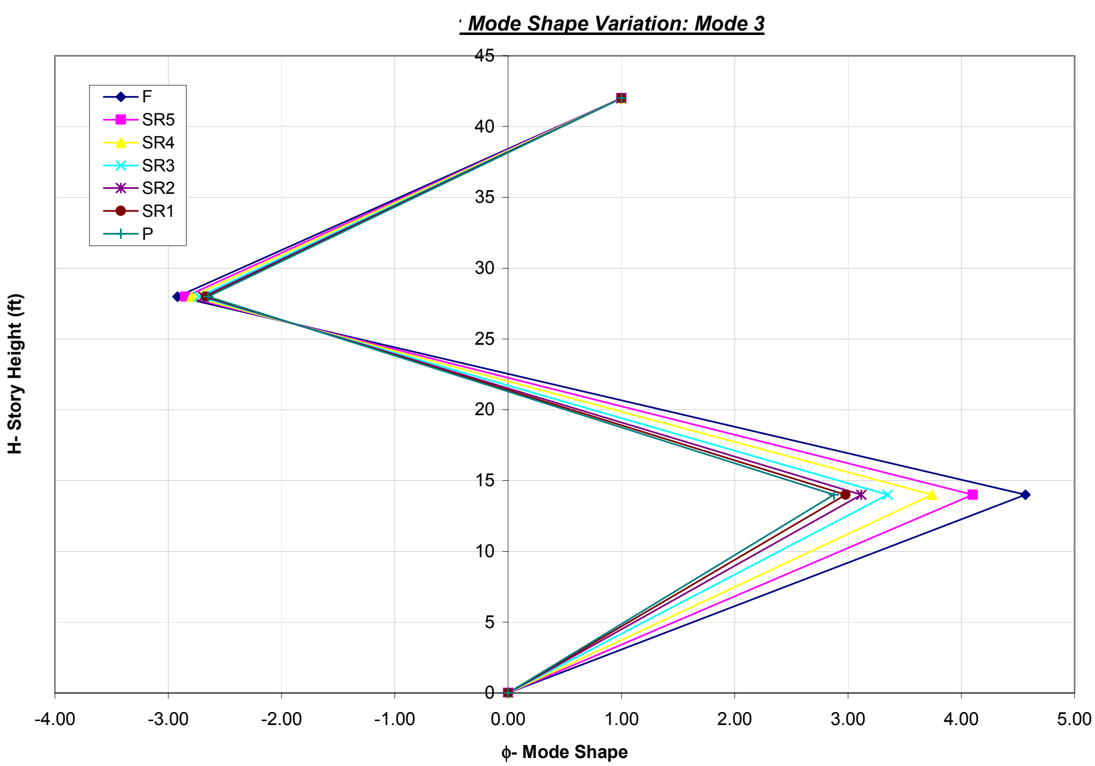

Joint Reactions

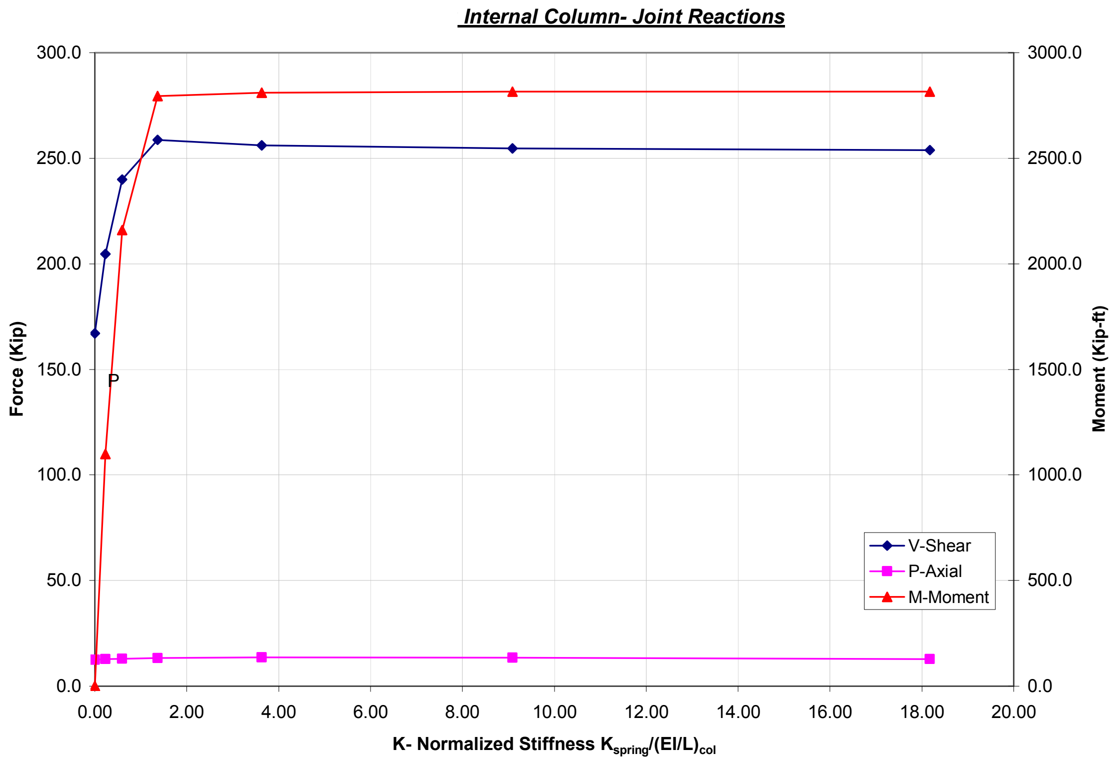

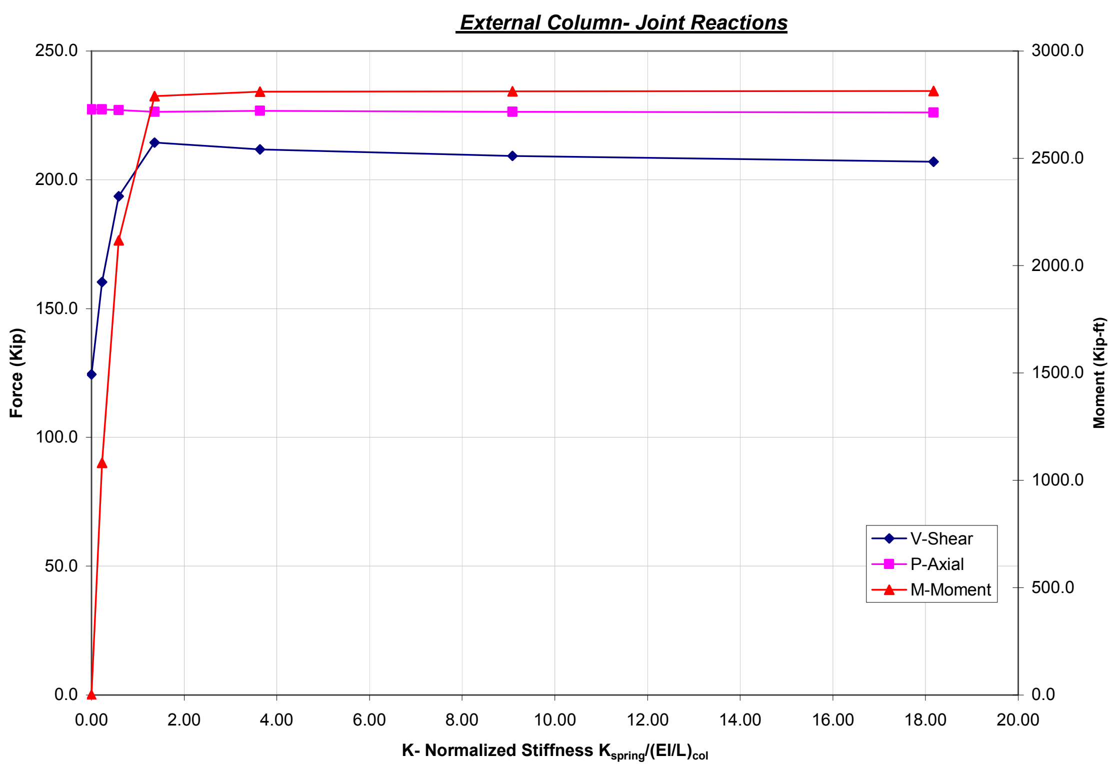

TABLE 2.10: Joint Reactions							
Element	**Case**	**V** Kip	**P** Kip	**M** K-ft	**V/V_p**	**P/N_p**	**M/M_p**
Ext. Col	F	207.0	226.1	2814.0	0.166	0.067	1.001
	SR5	209.3	226.4	2812.1	0.168	0.067	1.000
	SR4	211.8	226.7	2811.0	0.170	0.067	0.999
	SR3	214.4	226.4	2790.1	0.172	0.067	0.992
	SR2	193.6	227.0	2118.4	0.155	0.068	0.753
	SR1	160.4	227.3	1081.2	0.128	0.068	0.384
	P	124.4	227.3	0.0	0.100	0.068	0.000
Int. Col	F	253.9	12.8	2815.7	0.203	0.004	1.001
	SR5	254.7	13.4	2814.7	0.204	0.004	1.001
	SR4	256.2	13.6	2810.7	0.205	0.004	0.999
	SR3	258.7	13.2	2793.7	0.207	0.004	0.993
	SR2	240.0	13.0	2159.6	0.192	0.004	0.768
	SR1	204.6	12.7	1098.8	0.164	0.004	0.391
	P	167.1	12.5	0.0	0.134	0.004	0.000

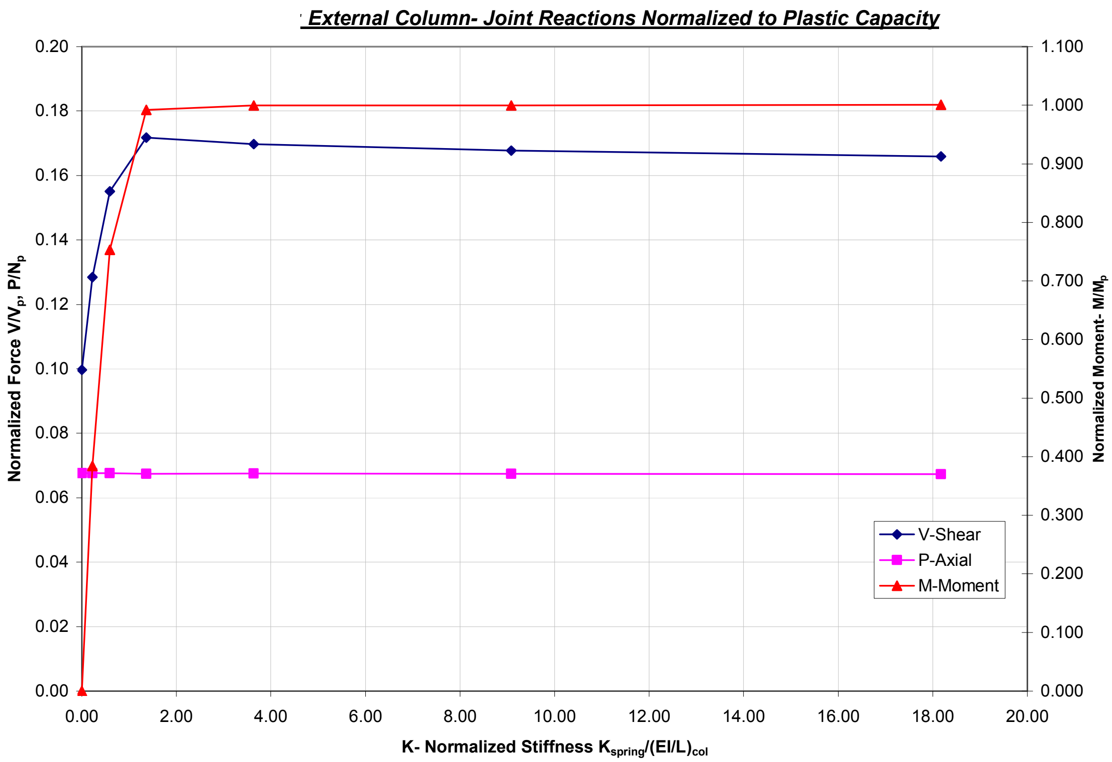

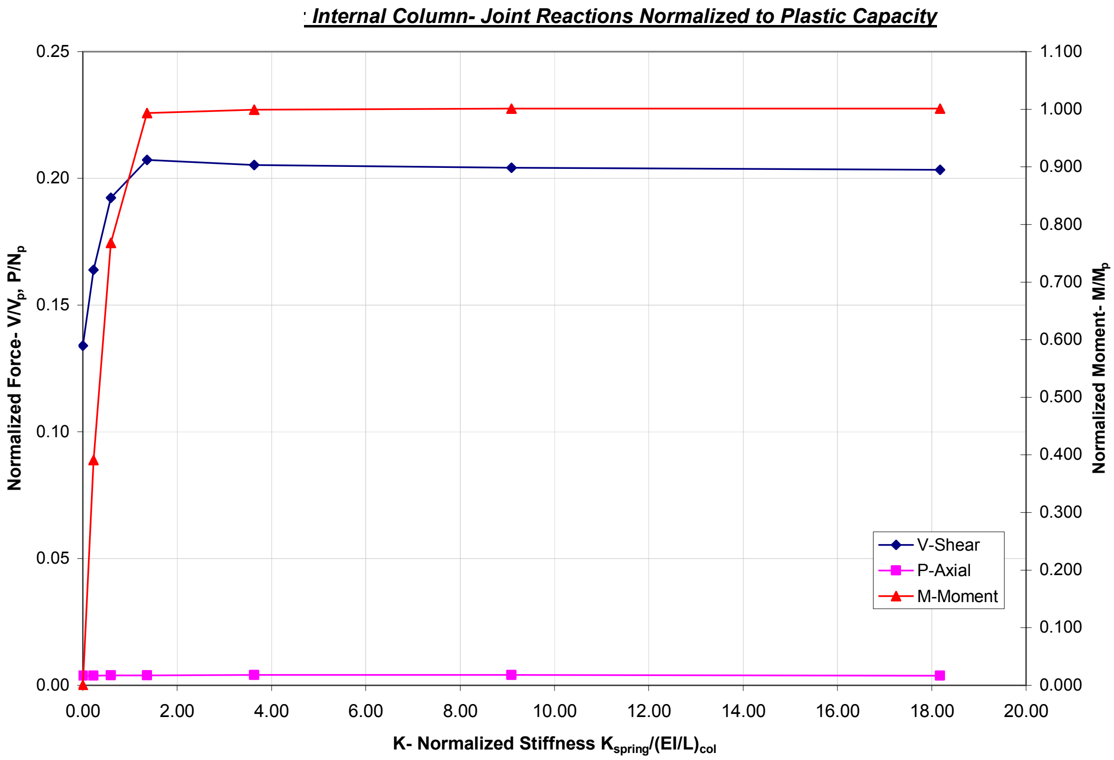

Base Shear and Overturning Moment

TABLE 2.11: Base Shear and Moment		
Case	V_b	M_b
	(Kip)	(Kip-ft)
F	1240.7	30244.9
SR5	903.3	30267.6
SR4	913.8	30288.1
SR3	926.2	30203.7
SR2	858.7	27636.3
SR1	735.8	23448.0
P	603.7	19079.6

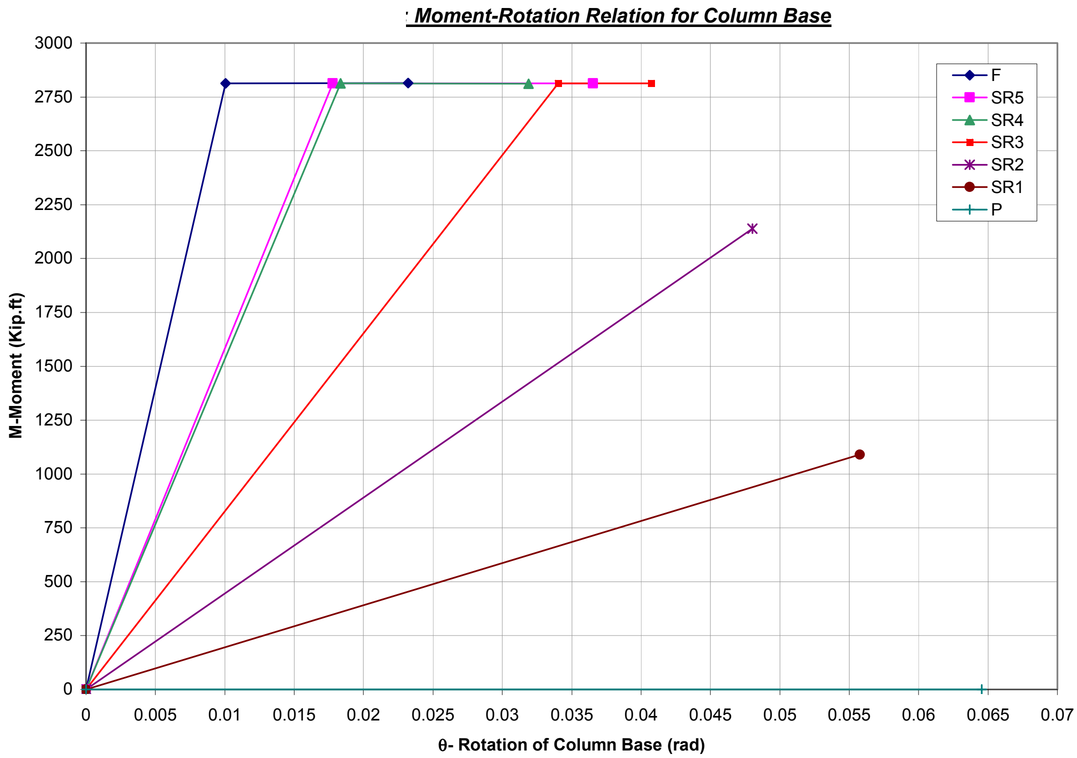

Moment-Rotation Relation for Column Base
M-Moment (Kip.ft)
θ- Rotation of Column Base (rad)
F
SR5
SR4
SR3
SR2
SR1
P

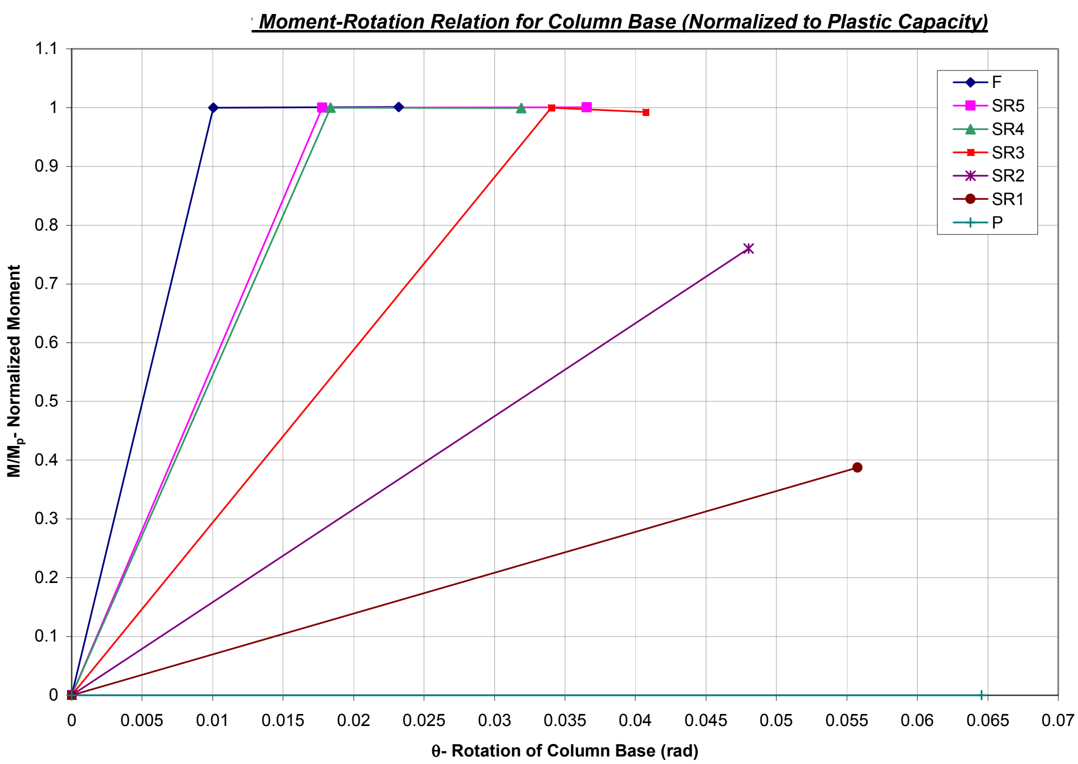

Moment-Rotation Relation for Column Base (Normalized to Plastic Capacity)
M/Mp- Normalized Moment
θ- Rotation of Column Base (rad)
F
SR5
SR4
SR3
SR2
SR1
P

Joint Equilibrium

TABLE 2.13: Joint Equilibrium ($\Sigma M_c/\Sigma M_g$)							
Node	**F**	**SR5**	**SR4**	**SR3**	**SR2**	**SR1**	**SR1**
10	1.17	1.25	1.33	1.46	1.38	1.17	1.38
11	1.09	1.09	1.13	1.19	1.16	1.17	1.24
12	1.00	1.00	1.00	1.00	1.00	1.00	1.00
14	1.06	1.11	1.16	1.23	1.19	1.08	1.11
15	1.03	1.04	1.06	1.09	1.08	1.04	1.06
16	1.00	1.00	1.00	1.00	1.00	1.00	1.00

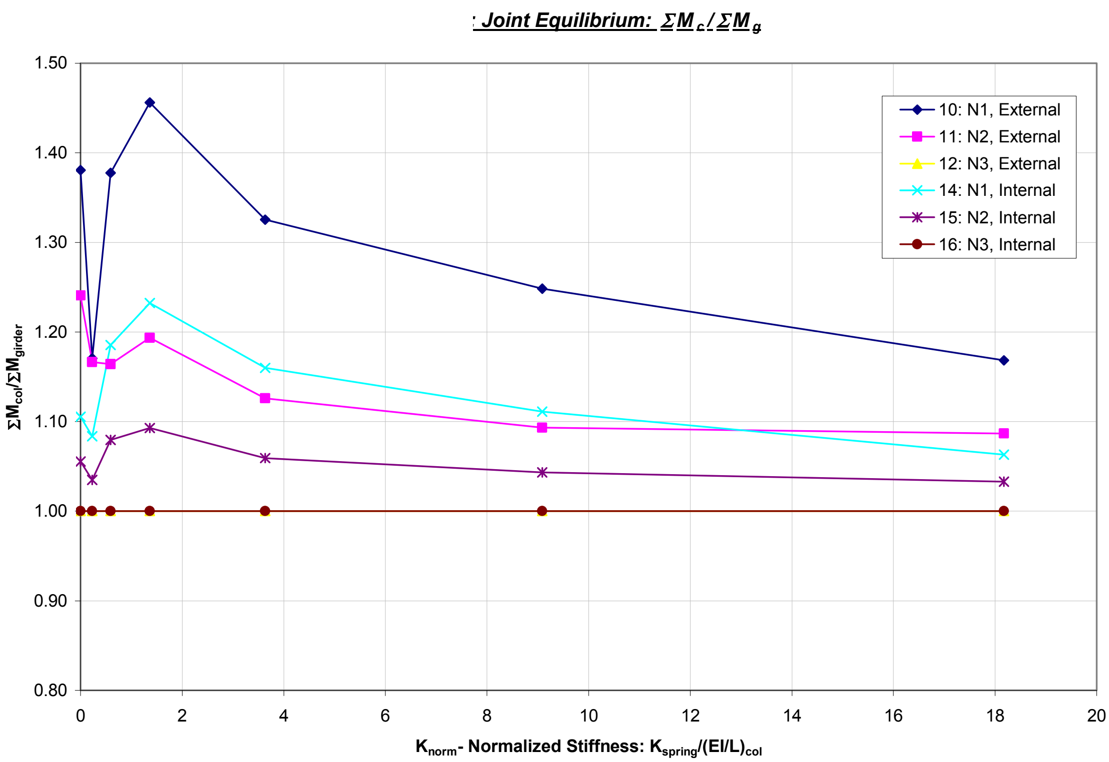

Appendix B: OpenSEES Time History Analysis Results of SMRF

This appendix presents the time history results for the fixed (model F), semi-rigid (model SR3), and pinned (model P) SMRFs, obtained for the 2% in 50 years PE hazard level using the OpenSEES structural analysis program. Among these results are the displacement time history for the seven records selected for the analysis, the joint reactions, and the base shear of the frame.

Time history analysis-OpenSees Navigator (2% and 5% Rayleigh damping) vs. time history analysis-SAP: Case F

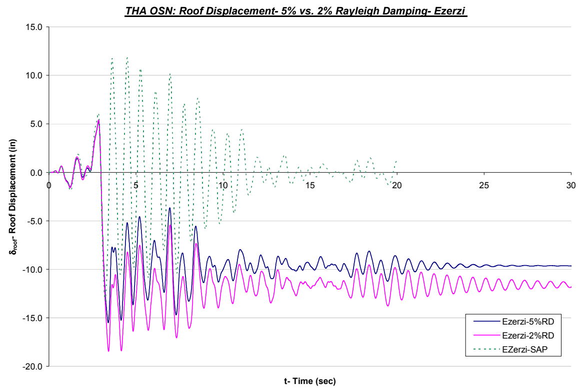

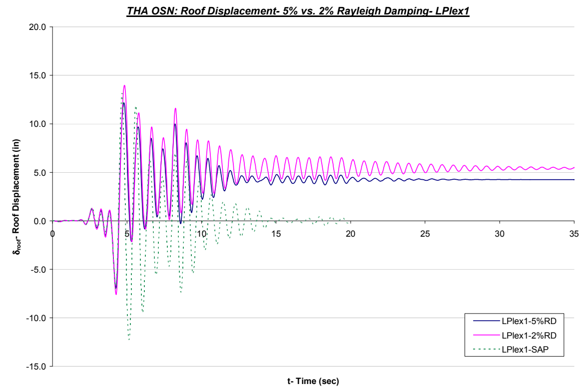

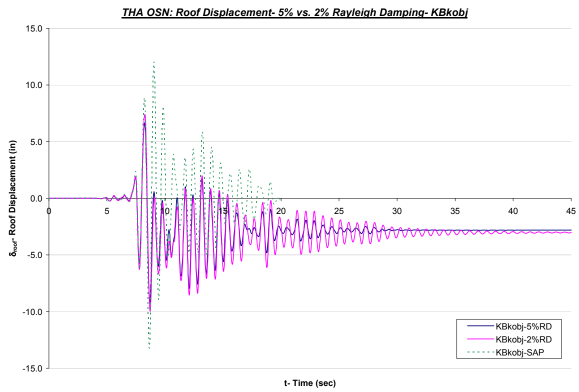

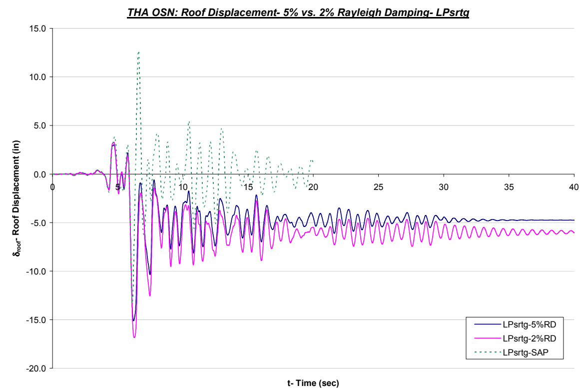

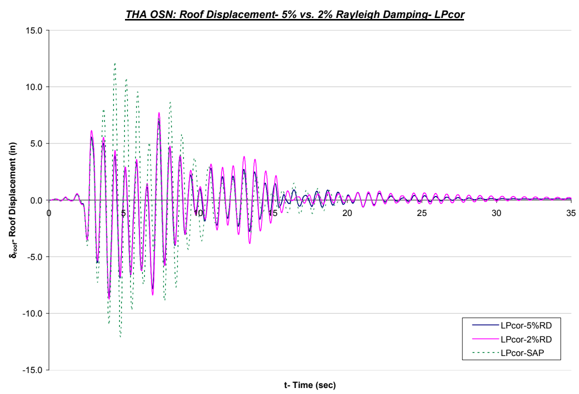

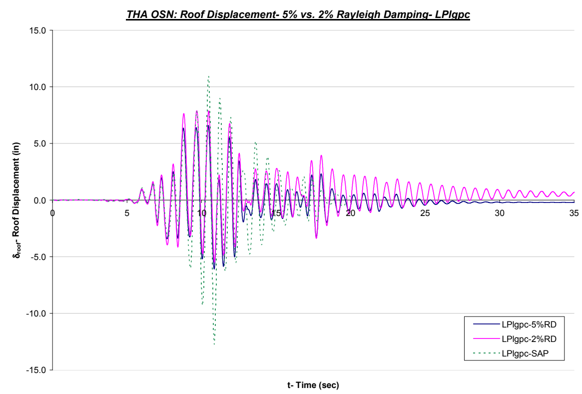

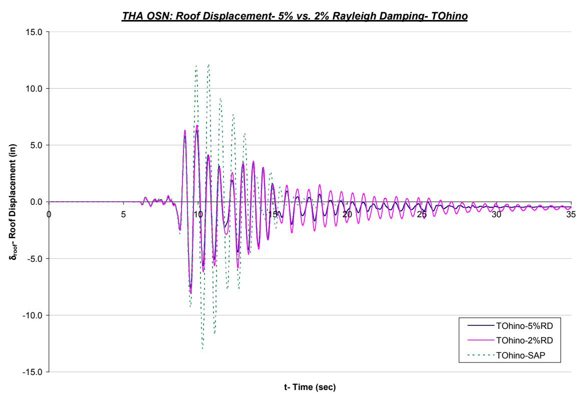

Time history analysis-OpenSees Navigator (2% and 5% Rayleigh damping) vs. time history analysis-SAP: Case SR3

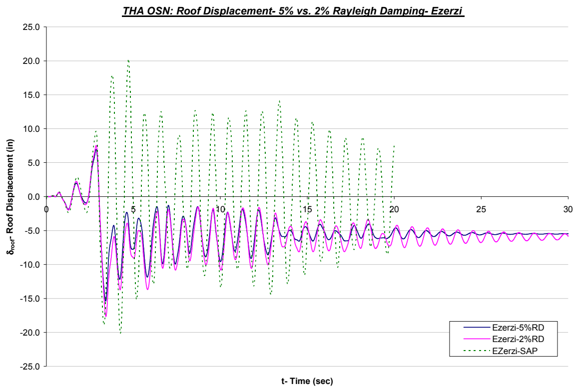

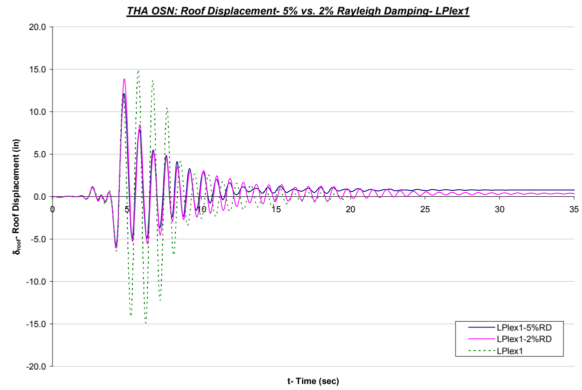

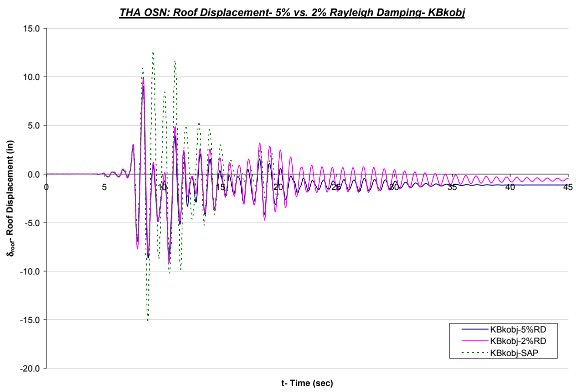

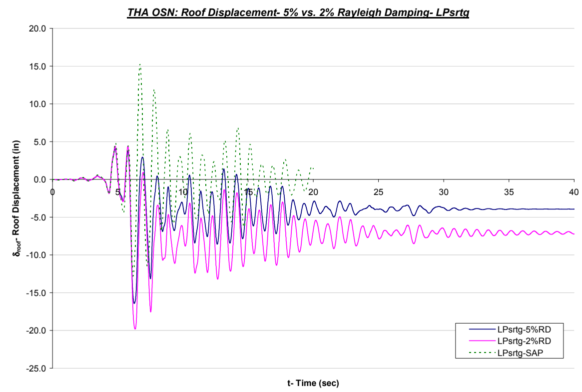

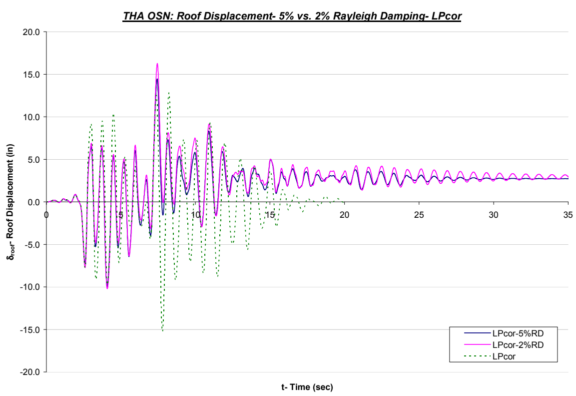

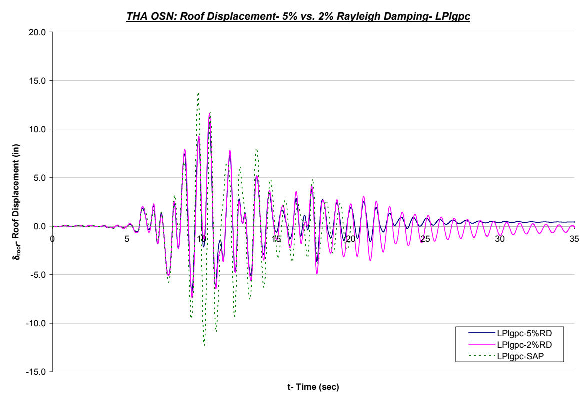

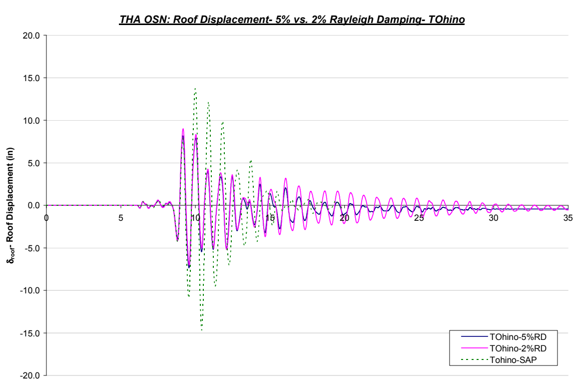

Time history analysis-OpenSees Navigator (2% and 5% Rayleigh damping) vs. time history analysis-SAP: Case P

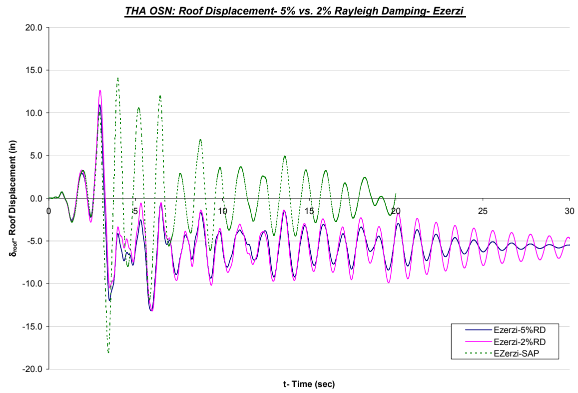

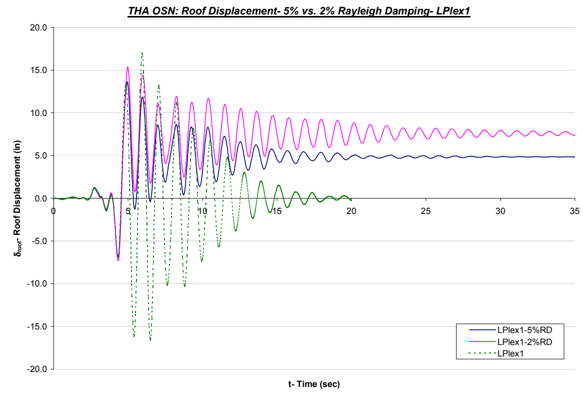

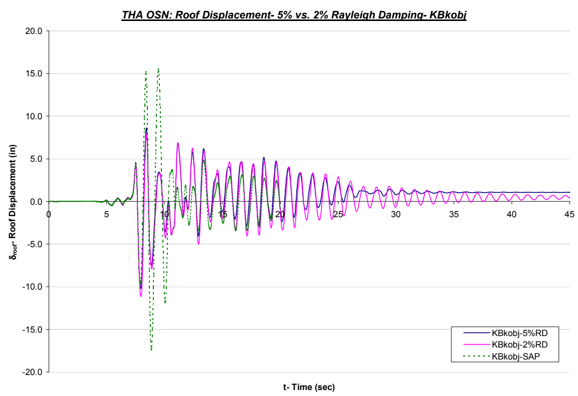

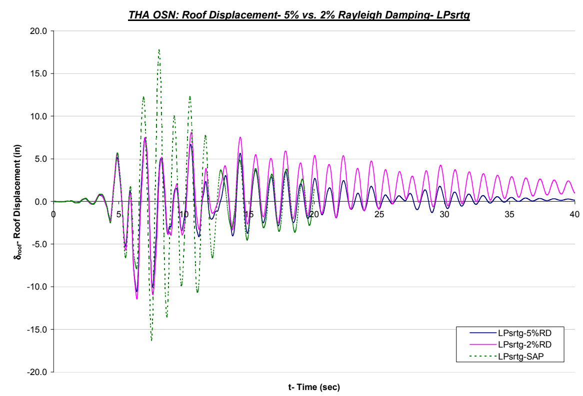

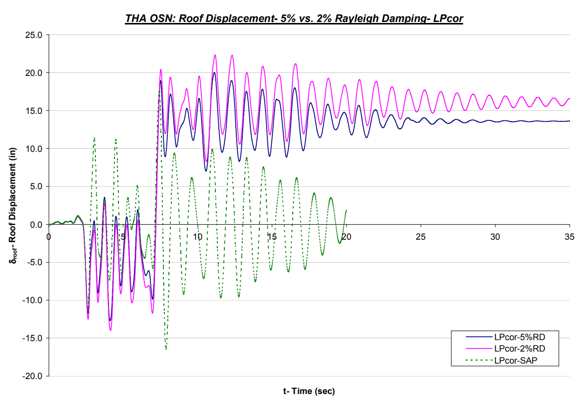

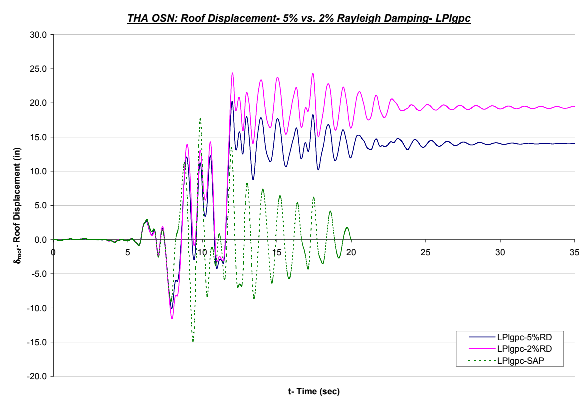

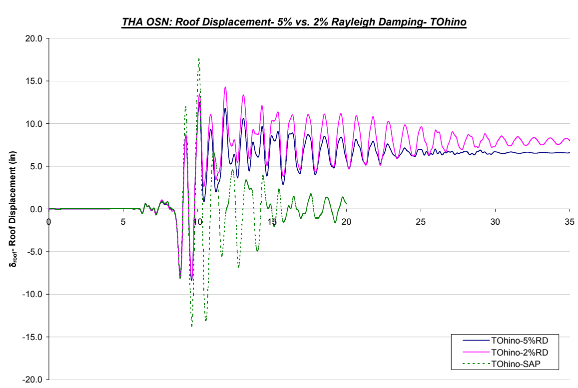

Time history analysis: story displacements and drifts, Case F

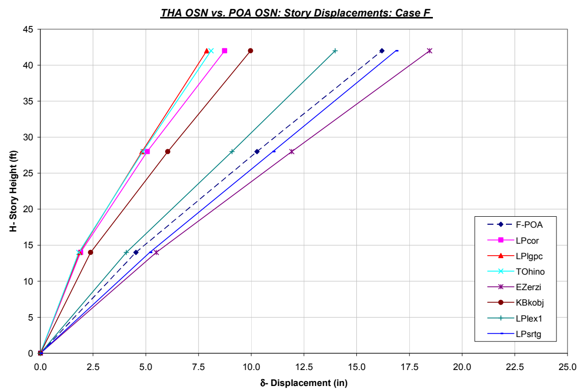

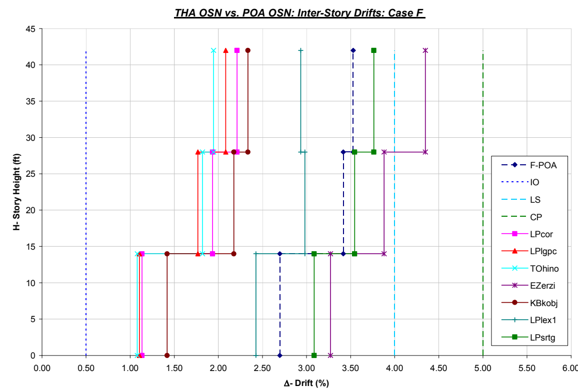

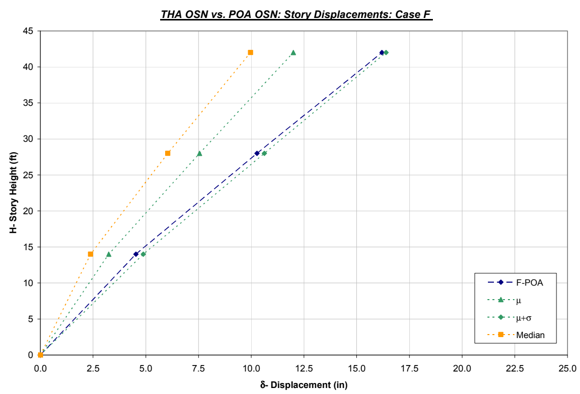

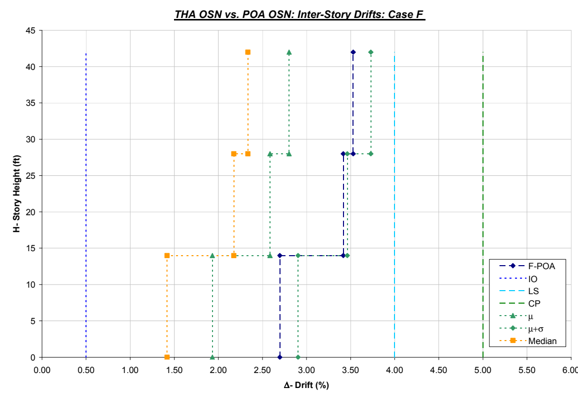

F- Displacements (in)				
Height (ft)	0	14	28	42
LPcor	0.00	1.91	5.07	8.73
LPsrtg	0.00	5.18	11.03	16.85
LPlgpc	0.00	1.86	4.82	7.89
LPlex1	0.00	4.07	9.09	13.98
KBkobj	0.00	2.39	6.04	9.96
EZerzi	0.00	5.50	11.93	18.46
TOhino	0.00	1.82	4.86	8.10
μ THA	0.00	3.25	7.55	12.00
(μ+σ)THA	0.00	4.88	10.62	16.40
Median-THA	0.00	2.39	6.04	9.96
POA-SAP	0.00	4.58	10.34	16.25
POA-OSN	0.00	4.53	10.27	16.20
ε POA OSN-SAP (%)	0	1	1	0
ε POA-Median THA (%)	**0**	**90**	**70**	**63**
ε POA-(μ+σ)THA (%)	**0**	**-7**	**-3**	**-1**

F- Inter-Story Drifts (%)						
Height (ft)	0	14	14	28	28	42
LPcor	1.14	1.14	1.93	1.93	2.21	2.21
LPsrtg	3.09	3.09	3.55	3.55	3.76	3.76
LPlgpc	1.11	1.11	1.77	1.77	2.08	2.08
LPlex1	2.43	2.43	2.98	2.98	2.93	2.93
KBkobj	1.42	1.42	2.18	2.18	2.34	2.34
EZerzi	3.27	3.27	3.88	3.88	4.35	4.35
TOhino	1.08	1.08	1.82	1.82	1.95	1.95
μ THA	1.93	1.93	2.59	2.59	2.80	2.80
(μ+σ)THA	2.90	2.90	3.46	3.46	3.73	3.73
Median-THA	1.42	1.42	2.18	2.18	2.34	2.34
POA-SAP	2.73	2.73	3.43	3.43	3.52	3.52
POA-OSN	2.70	2.70	3.42	3.42	3.53	3.53
ε POA OSN-SAP (%)	1	1	0	0	0	0
ε POA-Median THA (%)	**90**	**90**	**57**	**57**	**51**	**51**
ε POA-(μ+σ)THA (%)	**-7**	**-7**	**-1**	**-1**	**-5**	**-5**

Time history analysis: story displacements and drifts, Case SR3

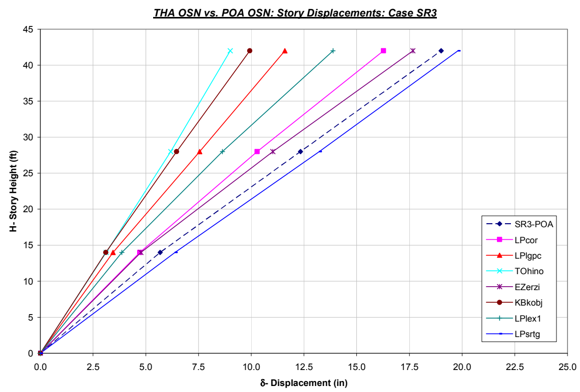

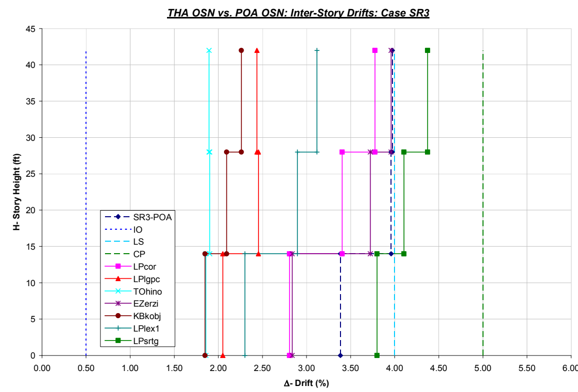

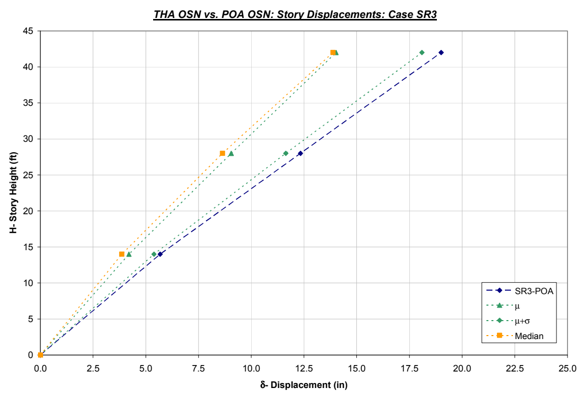

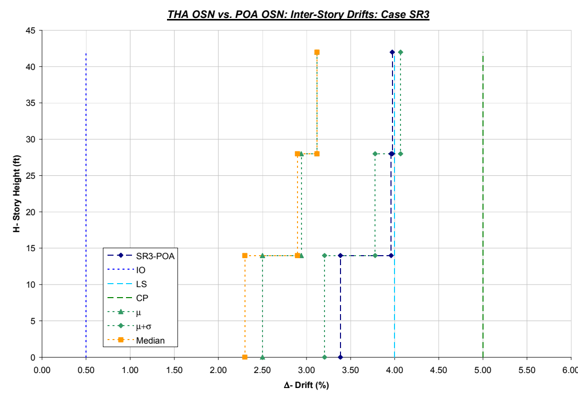

SR3- Displacements (in)				
Height (ft)	0	14	28	42
LPcor	0.00	4.72	10.28	16.27
LPsrtg	0.00	6.38	13.23	19.81
LPlgpc	0.00	3.45	7.55	11.60
LPlex1	0.00	3.87	8.64	13.88
KBkobj	0.00	3.11	6.46	9.93
EZerzi	0.00	4.77	11.02	17.67
TOhino	0.00	3.12	6.18	9.01
μ THA	0.00	4.20	9.05	14.02
(μ+σ)THA	0.00	5.38	11.64	18.10
Median-THA	0.00	3.87	8.64	13.88
POA-SAP	0.00	5.66	12.32	19.01
POA-OSN	0.00	5.68	12.34	19.01
ε POA OSN-SAP (%)	0	0	0	0
ε POA-Median THA (%)	**0**	**47**	**43**	**37**
ε POA-(μ+σ)THA (%)	**0**	**6**	**6**	**5**

SR3- Inter-Story Drifts (%)						
Height (ft)	0	14	14	28	28	42
LPcor	2.81	2.81	3.40	3.40	3.78	3.78
LPsrtg	3.80	3.80	4.10	4.10	4.37	4.37
LPlgpc	2.05	2.05	2.45	2.45	2.44	2.44
LPlex1	2.30	2.30	2.90	2.90	3.12	3.12
KBkobj	1.85	1.85	2.09	2.09	2.26	2.26
EZerzi	2.84	2.84	3.72	3.72	3.96	3.96
TOhino	1.86	1.86	1.90	1.90	1.90	1.90
μ THA	2.50	2.50	2.94	2.94	3.12	3.12
(μ+σ)THA	3.20	3.20	3.78	3.78	4.07	4.07
Median-THA	2.30	2.30	2.90	2.90	3.12	3.12
POA-SAP	3.37	3.37	3.97	3.97	3.98	3.98
POA-OSN	3.38	3.38	3.96	3.96	3.97	3.97
ε POA OSN-SAP (%)	0	0	0	0	0	0
ε POA-Median THA (%)	**47**	**47**	**37**	**37**	**27**	**27**
ε POA-(μ+σ)THA (%)	**6**	**6**	**5**	**5**	**-2**	**-2**

Time history analysis: story displacements and drifts, Case P

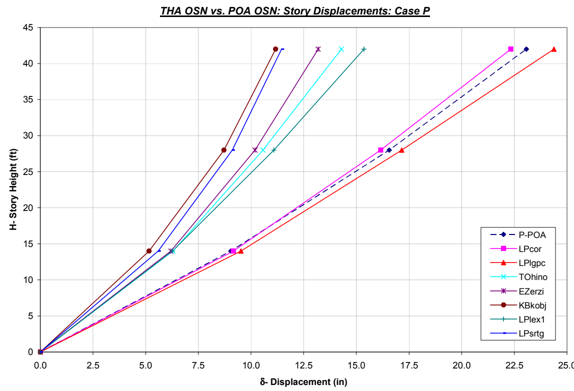

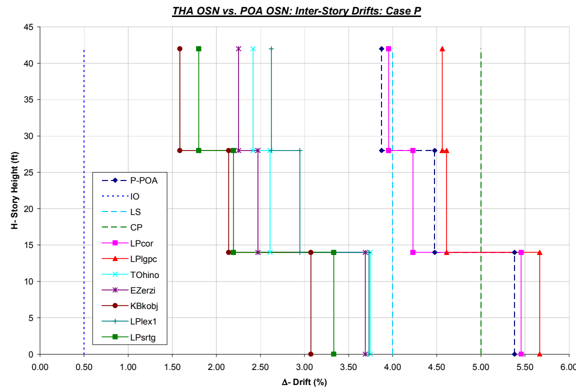

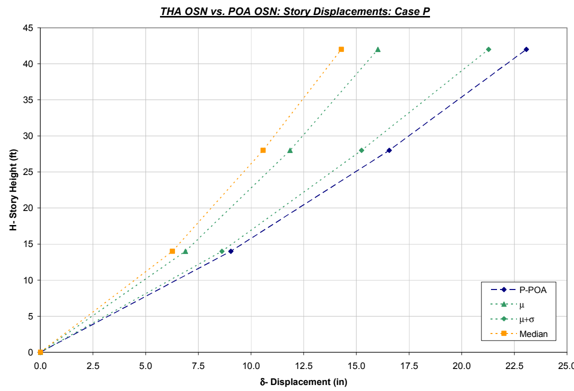

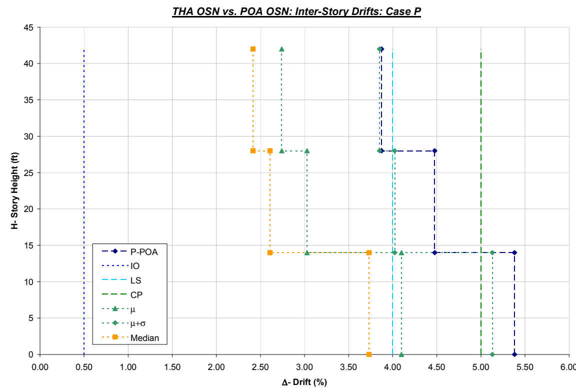

P- Displacements (in)				
Height (ft)	0	14	28	42
LPcor	0.00	9.17	16.16	22.33
LPsrtg	0.00	5.60	9.11	11.45
LPlgpc	0.00	9.52	17.15	24.38
LPlex1	0.00	6.27	11.09	15.36
KBkobj	0.00	5.16	8.71	11.17
EZerzi	0.00	6.20	10.19	13.19
TOhino	0.00	6.29	10.57	14.29
μ THA	0.00	6.89	11.86	16.02
(μ+σ)THA	0.00	8.62	15.25	21.28
Median-THA	0.00	6.27	10.57	14.29
POA-SAP	0.00	8.94	16.49	23.07
POA-OSN	0.00	9.04	16.56	23.07
ε POA OSN-SAP (%)	0	1	0	0
ε POA-Median THA (%)	**0**	**44**	**57**	**61**
ε POA-(μ+σ)THA (%)	**0**	**5**	**9**	**8**

P- Inter-Story Drifts (%)						
Height (ft)	0	14	14	28	28	42
LPcor	5.46	5.46	4.23	4.23	3.95	3.95
LPsrtg	3.33	3.33	2.19	2.19	1.80	1.80
LPlgpc	5.67	5.67	4.61	4.61	4.56	4.56
LPlex1	3.73	3.73	2.95	2.95	2.62	2.62
KBkobj	3.07	3.07	2.14	2.14	1.59	1.59
EZerzi	3.69	3.69	2.47	2.47	2.25	2.25
TOhino	3.75	3.75	2.61	2.61	2.42	2.42
μ THA	4.10	4.10	3.03	3.03	2.74	2.74
(μ+σ)THA	5.13	5.13	4.02	4.02	3.85	3.85
Median-THA	3.73	3.73	2.61	2.61	2.42	2.42
POA-SAP	5.32	5.32	4.49	4.49	3.92	3.92
POA-OSN	5.38	5.38	4.48	4.48	3.87	3.87
ε POA OSN-SAP (%)	1	1	0	0	1	1
ε POA-Median THA (%)	**44**	**44**	**71**	**71**	**60**	**60**
ε POA-(μ+σ)THA (%)	**5**	**5**	**11**	**11**	**1**	**1**

Time history analysis-OpenSees Navigator vs. pushover analysis-OpenSees Navigator: joint reactions and base shear, Case F

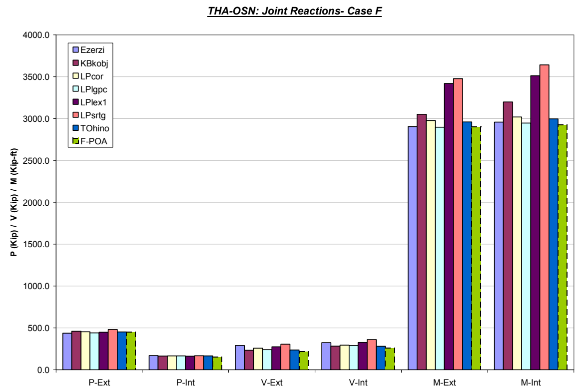

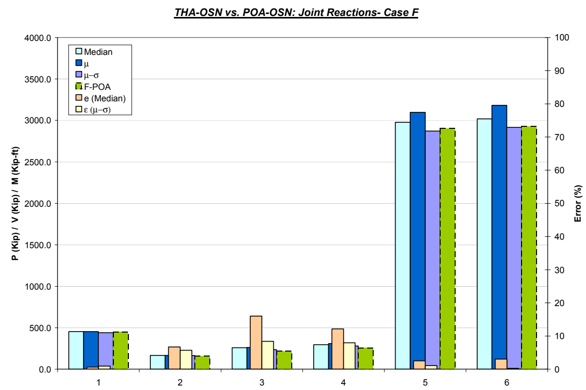

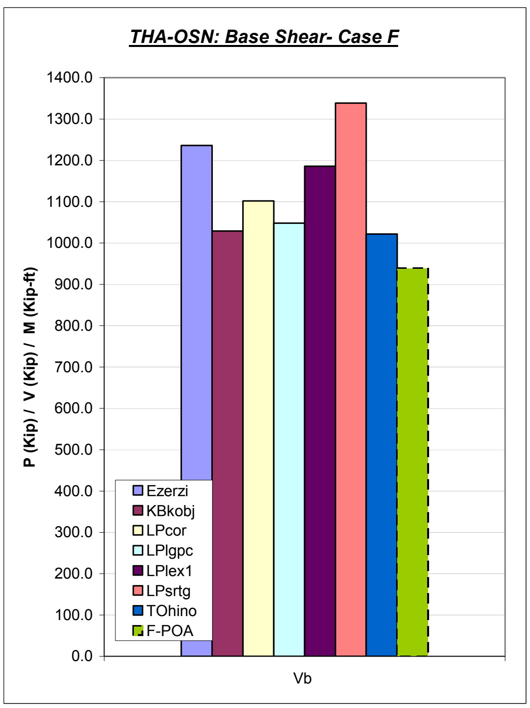

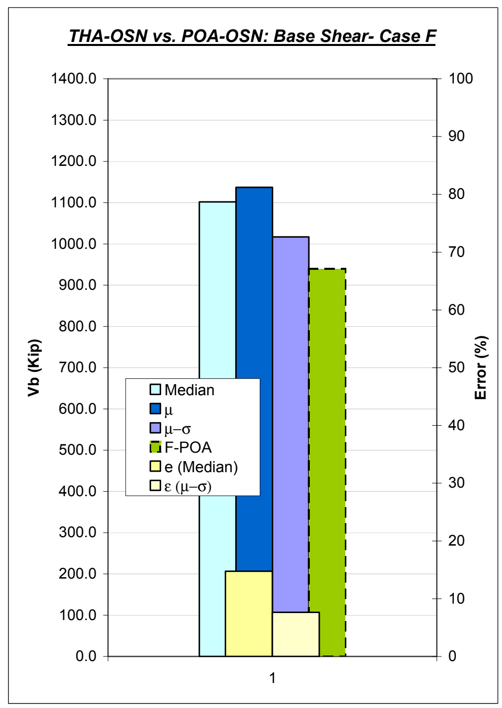

Joint Reactions- F						
Case	P-Ext	P-Int	V-Ext	V-Int	M-Ext	M-Int
	Kip	Kip	Kip	Kip	K-ft	K-ft
EZerzi	436.5	170.3	291.4	324.5	2905.5	2957.4
KBkobj	461.3	165.0	233.7	282.7	3051.8	3198.3
LPcor	454.9	166.2	258.6	294.5	2977.6	3017.6
LPlgpc	441.9	166.2	241.7	290.6	2896.2	2945.9
LPlex1	448.2	163.4	274.7	326.2	3419.1	3509.9
LPsrtg	481.5	168.6	307.1	361.8	3477.4	3641.1
TOhino	452.4	166.2	237.5	280.8	2960.7	2996.4
μ–THA	453.8	166.6	263.5	308.7	3098.3	3180.9
(μ-σ) THA	440.2	164.5	237.2	281.1	2871.4	2917.4
Median	452.4	166.2	258.6	294.5	2977.6	3017.6
F-POA-SAP	448.1	160.8	207.0	253.9	2814.0	2815.7
F-POA-OSN	449.5	155.1	217.2	258.7	2902.1	2925.3
ε POA OSN-SAP (%)	0	4	5	2	3	4
ε POA- Median THA (%)	1	7	16	12	3	3
ε POA- (μ-σ) THA (%)	1	6	8	8	1	0

Base Shear	
Case	V_b
	(Kip)
EZerzi	1236.3
KBkobj	1029.2
LPcor	1101.6
LPlgpc	1048.3
LPlex1	1186.1
LPsrtg	1338.5
TOhino	1021.9
μ–THA	1137.4
(μ-σ) THA	1017.1
Median	1101.6
F-POA-SAP	893.3
F-POA-OSN	939.1
ε POA OSN-SAP (%)	5
ε POA- Median THA (%)	15
ε POA- (μ-σ) THA (%)	8

Time history analysis-OpenSees Navigator vs. pushover analysis-OpenSees Navigator: joint reactions and base shear, Case SR3

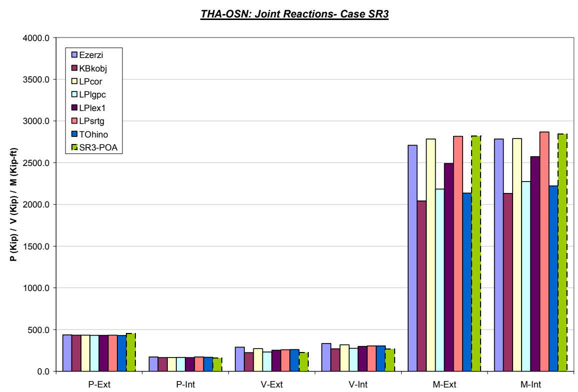

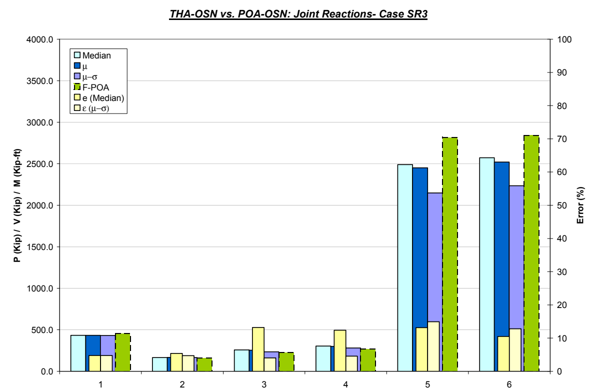

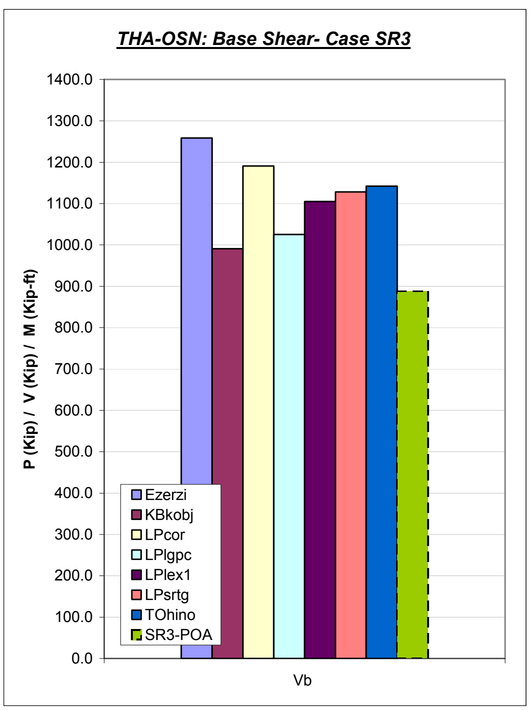

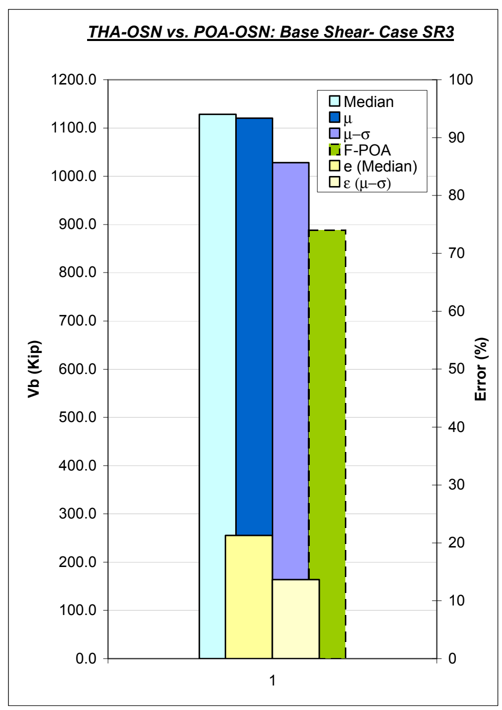

Joint Reactions- SR3						
Case	P-Ext	P-Int	V-Ext	V-Int	M-Ext	M-Int
	Kip	Kip	Kip	Kip	K-ft	K-ft
EZerzi	435.6	171.1	288.6	334.1	2709.5	2783.8
KBkobj	432.2	165.2	222.8	269.0	2042.5	2131.0
LPcor	433.6	165.5	271.1	317.5	2783.2	2790.2
LPlgpc	430.3	165.8	230.9	274.8	2184.7	2273.4
LPlex1	430.8	164.7	252.0	298.5	2490.5	2572.7
LPsrtg	433.4	172.2	258.6	304.2	2816.5	2868.4
TOhino	429.9	167.5	259.6	305.3	2135.4	2222.7
μ–THA	432.3	167.4	254.8	300.5	2451.8	2520.3
(μ-σ)THA	430.3	164.6	233.9	279.4	2147.1	2235.6
Median	432.2	165.8	258.6	304.2	2490.5	2572.7
SR3-POA-SAP	448.4	161.2	214.4	258.7	2790.1	2793.7
SR3-POA-OSN	452.7	156.9	224.5	266.7	2817.5	2843.3
ε POA OSN-SAP (%)	1	3	4	3	1	2
ε POA- Median THA (%)	5	5	13	12	13	11
ε POA- (μ-σ) THA (%)	5	5	4	5	15	13

Base Shear	
Case	V_b
	(Kip)
EZerzi	1258.4
KBkobj	990.9
LPcor	1191.0
LPlgpc	1025.2
LPlex1	1105.1
LPsrtg	1128.2
TOhino	1142.1
μ–THA	1120.1
(μ-σ)THA	1028.3
Median	1128.2
SR3-POA-SAP	926.2
SR3-POA-OSN	888.0
ε POA OSN-SAP (%)	4
ε POA- Median THA (%)	21
ε POA- (μ-σ) THA (%)	14

Time history analysis-OpenSees Navigator vs. pushover analysis-OpenSees Navigator: joint reactions and base shear, Case P

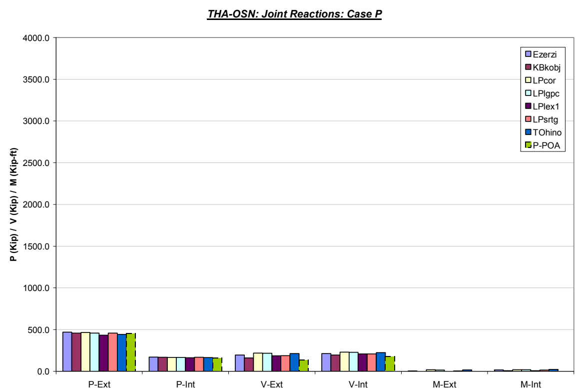

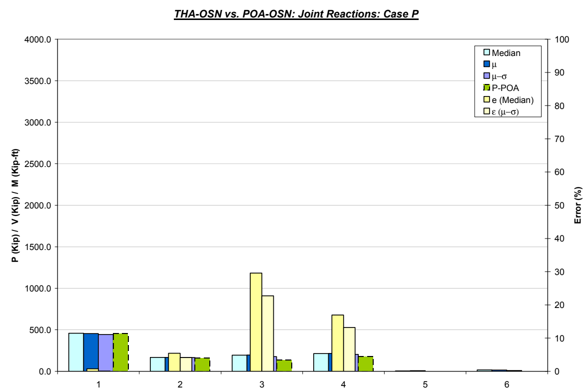

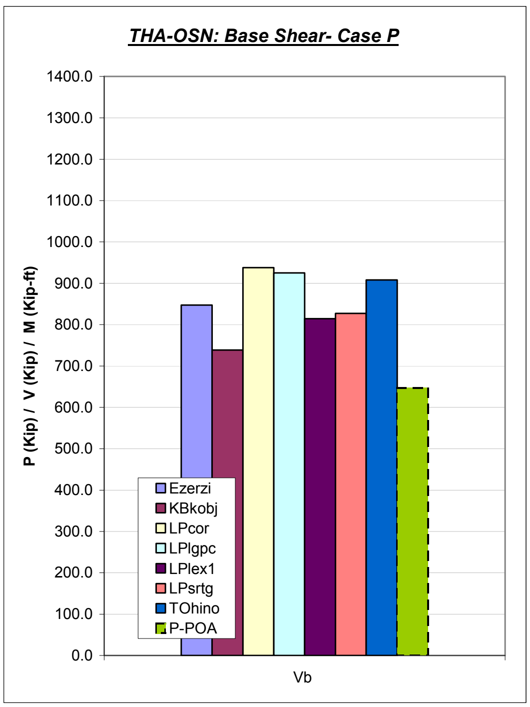

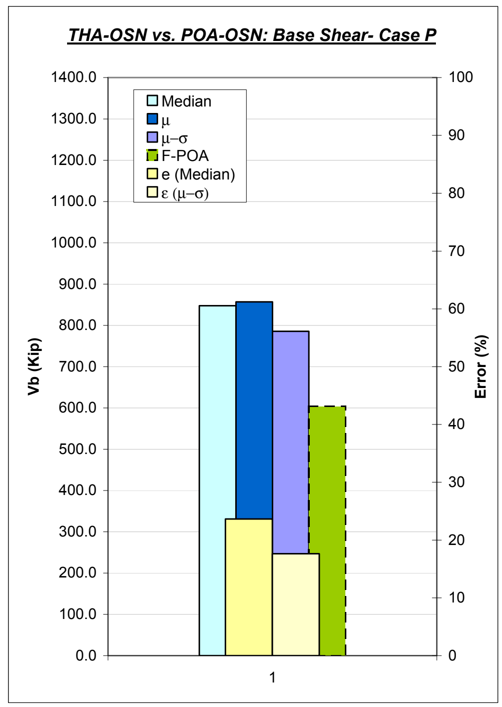

Joint Reactions- P						
Case	P-Ext	P-Int	V-Ext	V-Int	M-Ext	M-Int
	Kip	Kip	Kip	Kip	K-ft	K-ft
EZerzi	468.3	169.7	193.3	212.6	3.5	16.2
KBkobj	456.8	167.2	159.6	195.5	0.1	7.3
LPcor	466.1	166.4	217.6	229.6	17.0	19.2
LPlgpc	457.5	166.7	214.9	226.7	14.1	19.2
LPlex1	432.0	162.6	185.3	207.4	0.4	6.5
LPsrtg	457.9	168.5	186.9	208.7	2.4	14.4
TOhino	441.4	165.1	211.0	222.8	16.3	22.1
μ–THA	454.3	166.6	195.5	214.8	7.7	15.0
(μ-σ)THA	442.2	164.5	176.3	203.4	0.5	9.4
Median	457.5	166.7	193.3	212.6	3.5	16.2
P-POA-SAP	449.3	160.5	124.4	167.1	0.0	0.0
P-POA-OSN	454.2	157.7	136.2	176.6	0.0	0.0
ε POA OSN-SAP (%)	1	2	9	5	0	0
ε POA- Median THA (%)	1	5	30	17	0	0
ε POA- (μ-σ) THA (%)	0	4	23	13	0	0

Base Shear	
Case	V_b
	(Kip)
EZerzi	847.5
KBkobj	738.6
LPcor	938.0
LPlgpc	925.0
LPlex1	814.4
LPsrtg	827.5
TOhino	907.9
μ–THA	857.0
(μ-σ)THA	785.6
Median	847.5
P-POA-SAP	603.7
P-POA-OSN	647.0
ε POA OSN-SAP (%)	7
ε POA- Median THA (%)	24
ε POA- (μ-σ) THA (%)	18

Appendix C: PBEE Results for SMRF

Appendix C presents the PBEE results for the fixed (model F), semi-rigid (model SR3), and pinned (model P) frames, including the cumulative cost distribution functions for all hazard levels considered (2, 5, 10, and 50% in 50 yrs PE), as well as the distribution of costs according to the performance groups obtained for all frame models and all hazard levels analyzed in this study.

Cumulative Cost Distribution Functions: Effect of Base Fixidity

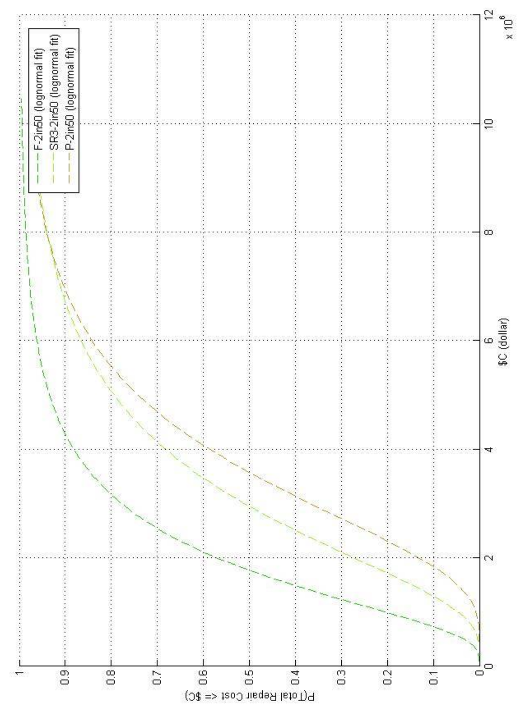

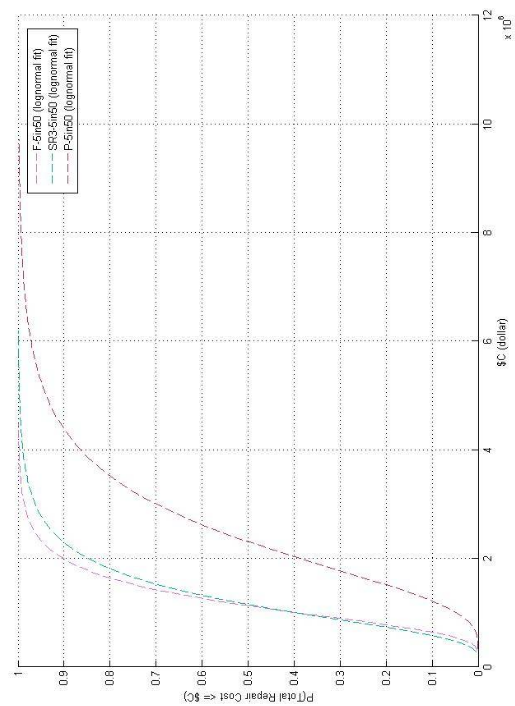

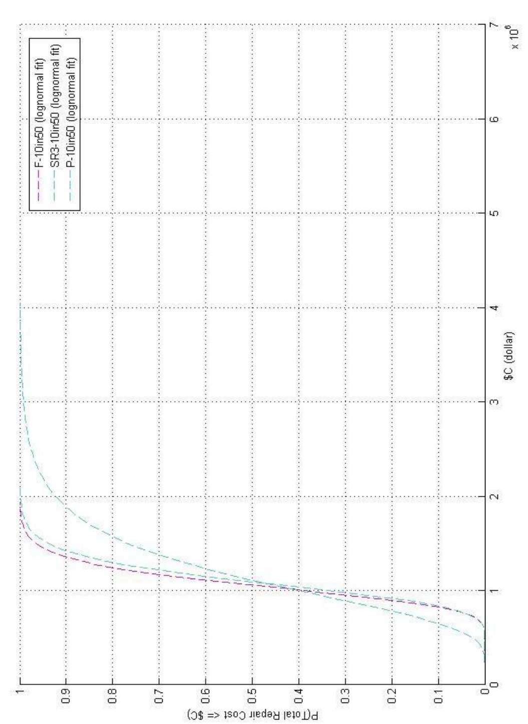

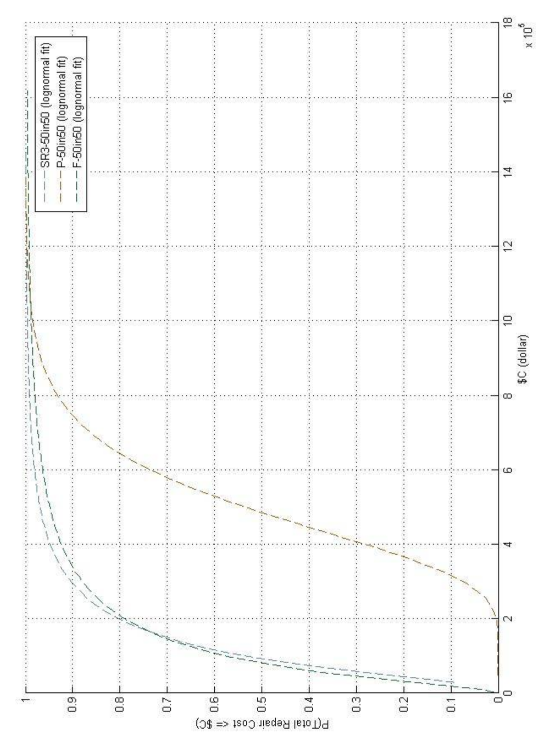

Cumulative Cost Distribution Functions: Effect of Hazard Level

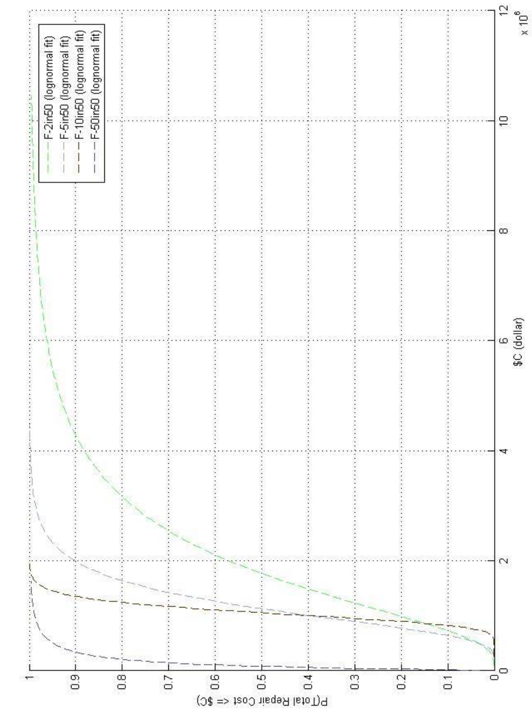

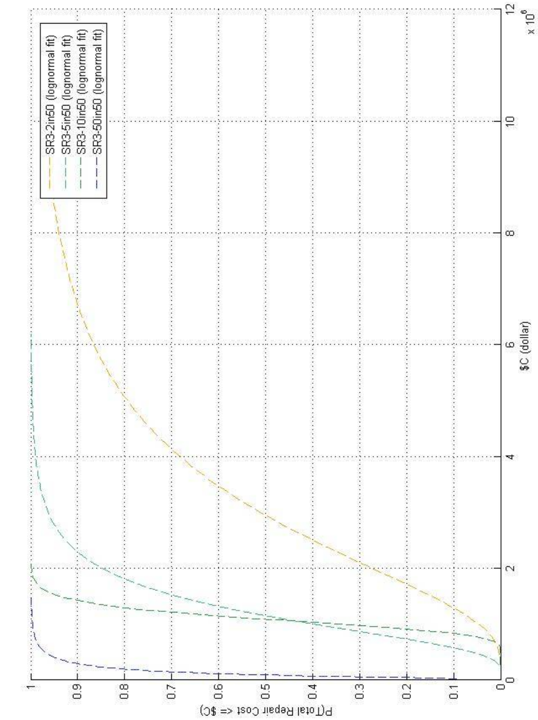

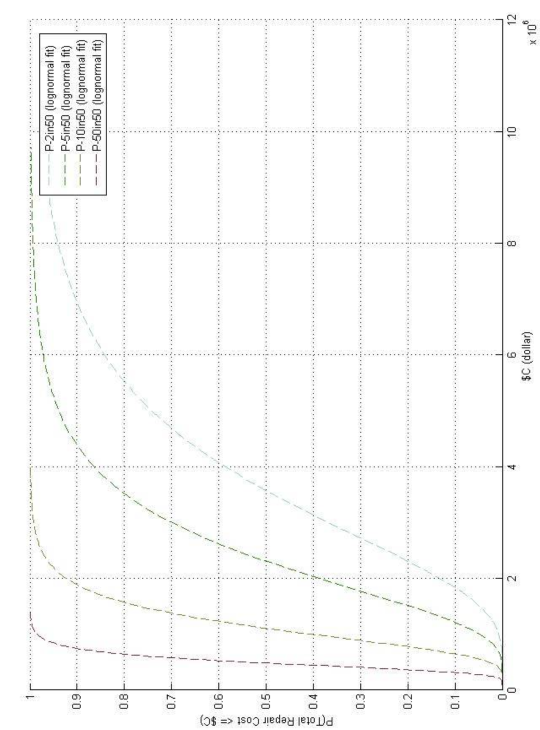

Distribution of Cost According to Performance Group: Effect of Base Fixidity and Hazard Level

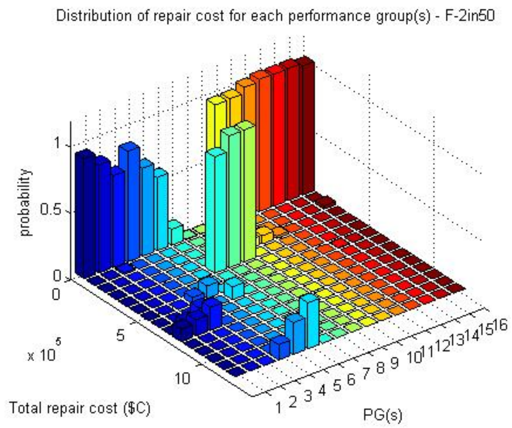

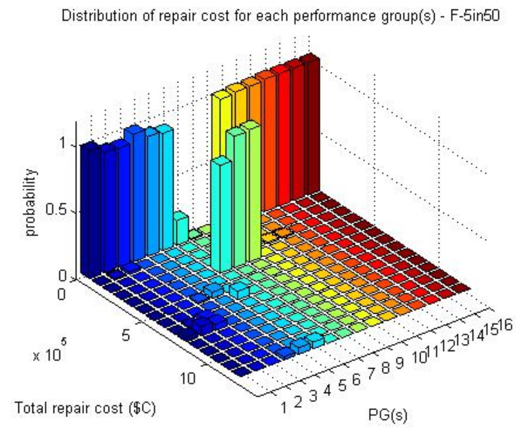

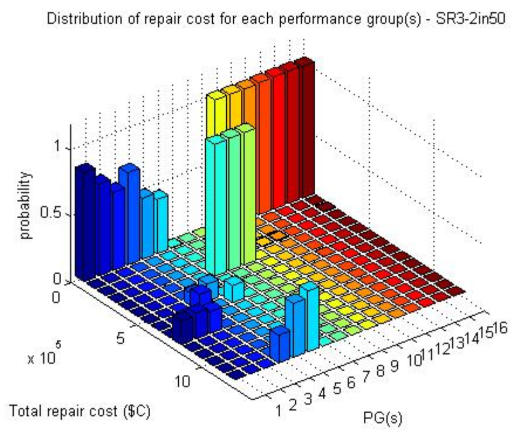

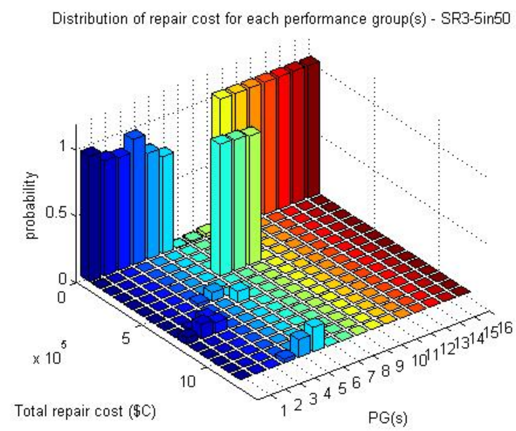

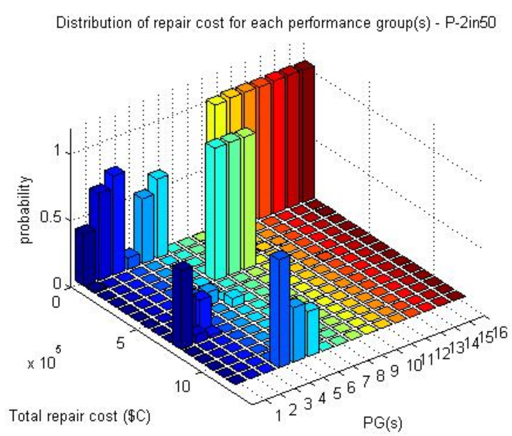

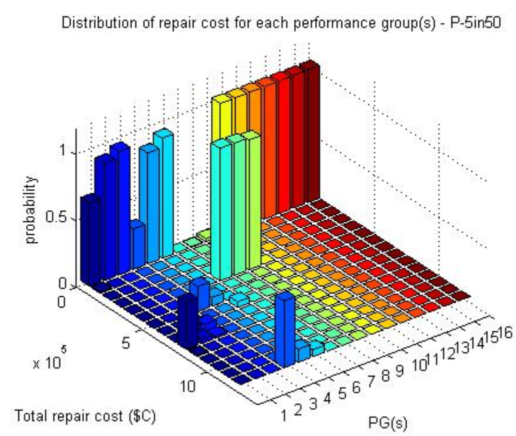

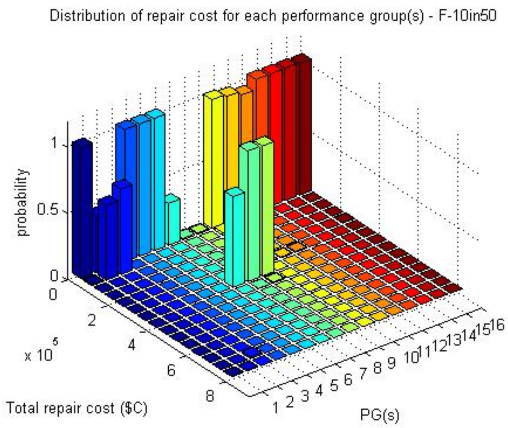
Distribution of repair cost for each performance group(s) - F-10in50
probability
Total repair cost ($C)
x 10^5
PG(s)

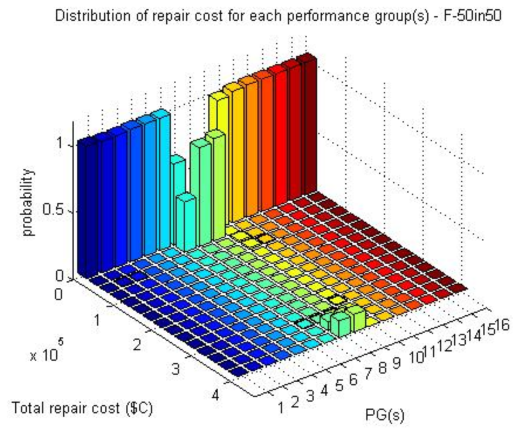
Distribution of repair cost for each performance group(s) - F-50in50
probability
Total repair cost ($C)
x 10^5
PG(s)

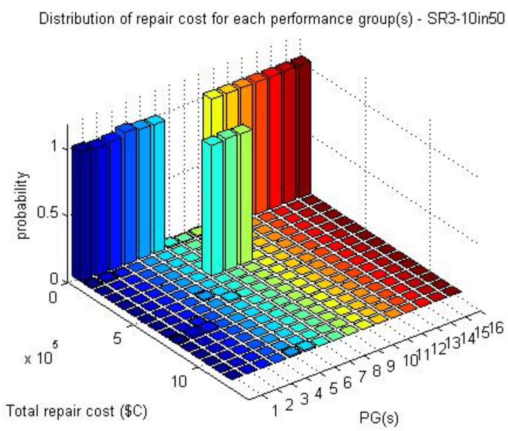
Distribution of repair cost for each performance group(s) - SR3-10in50
probability
Total repair cost ($C)
x 10^5
PG(s)

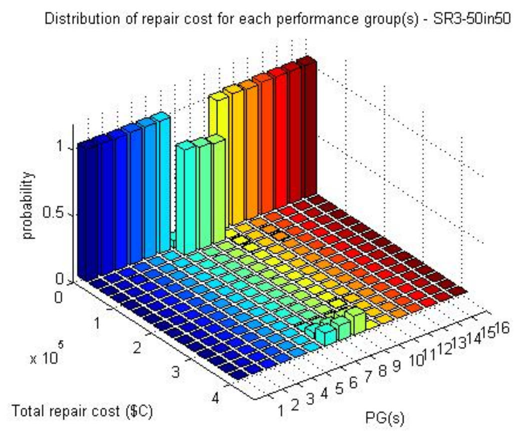
Distribution of repair cost for each performance group(s) - SR3-50in50
probability
Total repair cost ($C)
x 10^5
PG(s)

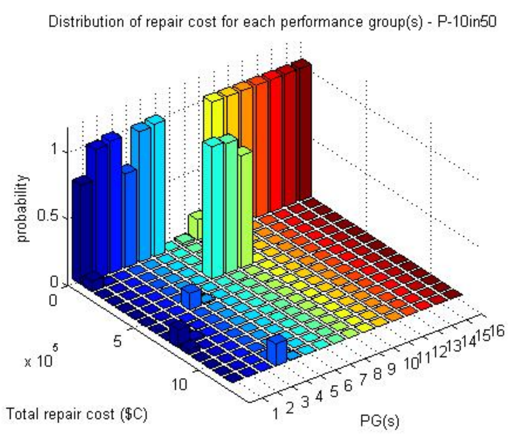
Distribution of repair cost for each performance group(s) - P-10in50
probability
Total repair cost ($C)
x 10^5
PG(s)

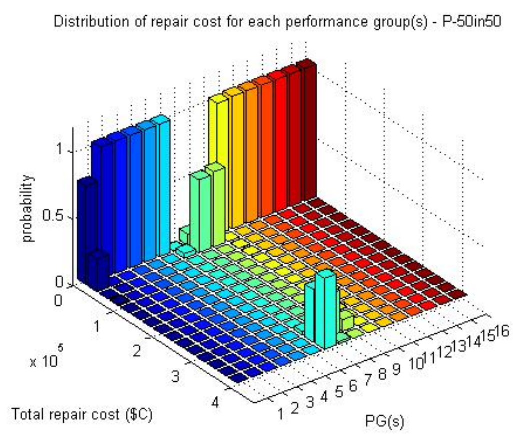
Distribution of repair cost for each performance group(s) - P-50in50
probability
Total repair cost ($C)
x 10^5
PG(s)

Appendix D: Results of Reliability Analysis of Base Plate Connection in SMRF

Appendix D presents the reliability analysis results of the base plate connection designed according to the AISC Design Guide #1 (2005), using the demand loads determined for the external column of the ATC-58 SMRF, assuming a fixed base (model F). The component and system reliability analysis results for different hazard levels are presented, including sensitivity analysis results for the limit-state parameters and importance vectors of the random variables. The complete output file for the high hazard level (2% in 50 yrs PE) for the M_{max} load case is included at the end of the appendix.

Joint reactions for external column of SMRF obtained for 7 records at different hazard levels

Hazard level: 2% in 50 yr PE

Joint Reactions- F: Ext	Pmax			Pmin			Vmax			Vmin			Mmax			Mmin		
Case	**P (K)**	**V (K)**	**M (Kip-in)**	P (K)	V (K)	M (Kip-in)	P (K)	V (K)	M (Kip-in)	**P (K)**	**V (K)**	**M (Kip-in)**	P (K)	V (K)	M (Kip-in)	**P (K)**	**V (K)**	**M (Kip-in)**
EZerzi	436.5	-207.9	-32281.4	13.7	227.1	32019.0	139.1	291.4	30131.6	426.8	-272.7	-34587.5	14.7	245.7	33242.3	369.7	-266.2	-34865.7
KBkobj	461.3	-230.5	-36621.2	-9.9	225.4	34996.8	-1.0	232.4	33995.3	439.6	-233.7	-34799.9	-6.5	227.7	35020.0	461.3	-230.5	-36621.2
LPcor	454.9	-195.2	-33117.9	-15.4	215.3	35713.7	56.6	258.6	31441.2	400.9	-231.2	-28392.5	-15.1	216.6	35731.3	451.5	-216.7	-34758.7
LPlgpc	441.9	-148.6	-26675.3	-9.0	215.5	34248.8	0.3	241.7	34667.8	410.6	-229.2	-29591.4	-2.2	239.4	34754.7	434.3	-222.4	-32361.7
LPlex1	448.2	-223.0	-33899.6	-47.4	262.6	40857.6	-42.3	274.7	40963.6	443.5	-236.3	-34625.7	-44.2	272.4	41028.9	446.1	-234.1	-34731.7
LPsrtg	481.5	-244.4	-38650.6	13.0	255.8	35354.0	14.0	258.2	35490.7	451.2	-307.1	-40853.5	26.6	255.5	35935.7	417.3	-299.3	-41728.2
TOhino	452.4	-206.9	-34028.0	-8.1	225.2	34967.3	0.2	237.5	35523.8	440.7	-230.8	-34250.4	-1.6	237.4	35528.0	448.2	-222.2	-34582.0
Mean	**453.8**	**-208.1**	**-33610.6**	-9.0	232.4	35451.0	23.8	256.4	34602.0	**430.5**	**-248.7**	**-33871.6**	-4.0	242.1	35891.6	**432.6**	**-241.6**	**-35664.2**
Median	**452.4**	**-207.9**	**-33899.6**	-9.0	225.4	34996.8	0.3	258.2	34667.8	**439.6**	**-233.7**	**-34587.5**	-2.2	239.4	35528.0	**446.1**	**-230.5**	**-34758.7**
c.o.v.=σ/abs(μ)	**0.03**	**0.15**	**0.11**	2.27	0.08	0.08	2.46	0.08	0.10	**0.04**	**0.12**	**0.12**	5.57	0.08	0.07	**0.07**	**0.13**	**0.08**

	Pmax	Pmin	Vmax	Vmin	Mmax	Mmin
$\rho_{P\text{-}V}$=	**-0.65**	-0.28	0.57	**-0.46**	-0.18	**0.65**
$\rho_{P\text{-}M}$=	**-0.80**	-0.88	-0.87	**-0.91**	-0.77	**0.12**
$\rho_{M\text{-}V}$=	**0.96**	0.66	-0.11	**0.79**	0.63	**0.81**

Correlation Matrix

	P_{max}	V_p	M_p	P_v	V_{max}	M_v	P_m	V_m	M_{max}
P_{max}	1.00	-0.65	-0.80	0.50	-0.53	-0.64	0.28	-0.51	-0.90
V_p	-0.65	1.00	0.96	-0.78	0.54	0.81	0.01	0.57	0.80
M_p	-0.80	0.96	1.00	-0.71	0.52	0.76	-0.12	0.53	0.86
P_v	0.50	-0.78	-0.71	1.00	-0.46	-0.91	-0.02	-0.54	-0.63
V_{max}	-0.53	0.54	0.52	**-0.46**	1.00	0.79	0.65	0.99	0.82
M_v	-0.64	0.81	0.76	**-0.91**	**0.79**	1.00	0.29	0.84	0.84
P_m	0.28	0.01	-0.12	-0.02	0.65	0.29	1.00	0.65	0.12
V_m	-0.51	0.57	0.53	-0.54	0.99	0.84	0.65	1.00	0.81
M_{max}	-0.90	0.80	0.86	-0.63	0.82	0.84	0.12	0.81	1.00

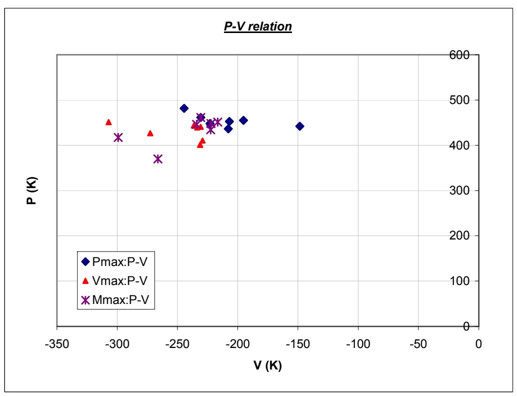

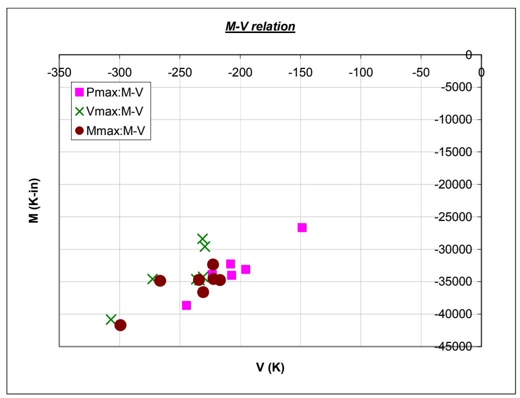

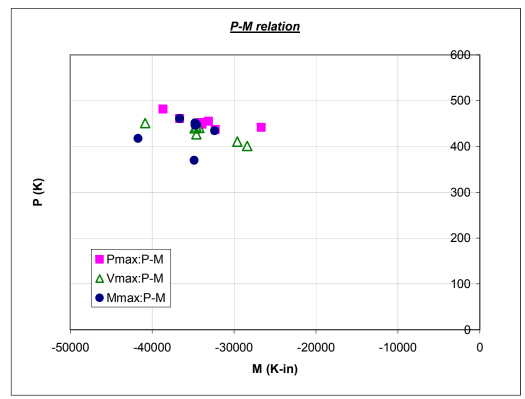

Hazard level: 5% in 50 yr PE

Joint Reactions- F: Ext	**Pmax**			Pmin			Vmax			**Vmin**			Mmax			**Mmin**		
Case	**P** (K)	**V** (K)	**M** (Kip-in)	P (K)	V (K)	M (Kip-in)	P (K)	V (K)	M (Kip-in)	**P** (K)	**V** (K)	**M** (Kip-in)	P (K)	V (K)	M (Kip-in)	**P** (K)	**V** (K)	**M** (Kip-in)
EZerzi	435.3	-228.6	-33048.8	24.7	165.0	26041.6	101.1	263.0	31165.9	407.5	-256.6	-33527.5	101.1	263.0	31165.9	432.3	-250.8	-33958.2
KBkobj	432.6	-198.2	-32934.8	7.0	211.6	33217.0	11.3	223.7	32673.2	427.7	-216.5	-32679.3	7.5	214.3	33238.7	432.5	-200.6	-32941.3
LPcor	431.9	-202.2	-31662.7	10.8	178.4	29510.4	33.3	229.7	28444.4	396.0	-217.1	-27886.9	11.7	211.7	31874.9	431.1	-209.9	-32306.6
LPlgpc	430.1	-180.2	-28737.5	11.9	193.5	29463.4	22.5	226.2	30256.3	413.8	-212.8	-27587.2	12.8	220.1	31719.9	427.8	-206.4	-30693.9
LPlex1	429.2	-198.3	-29701.4	0.7	234.8	34441.5	4.0	236.0	33978.5	426.2	-218.7	-31324.2	0.7	234.8	34441.5	428.5	-213.0	-31614.8
LPsrtg	433.3	-192.1	-30467.1	15.7	230.9	32349.6	50.6	258.1	33124.5	426.2	-245.8	-33339.2	51.4	257.4	33144.7	430.1	-239.3	-33391.1
TOhino	433.0	-190.8	-31088.4	10.1	189.9	31236.2	12.9	205.3	31066.3	430.1	-211.2	-32300.1	18.8	203.9	31897.9	431.9	-208.6	-32361.8
Mean	**432.2**	**-198.6**	**-31091.5**	11.6	200.6	30894.2	33.7	234.6	31529.9	**418.2**	**-225.5**	**-31234.9**	29.2	229.3	32497.6	**430.6**	**-218.4**	**-32466.8**
Median	**432.6**	**-198.2**	**-31088.4**	10.8	193.5	31236.2	22.5	229.7	31165.9	**426.2**	**-217.1**	**-32300.1**	12.8	220.1	31897.9	**431.1**	**-209.9**	**-32361.8**
c.o.v.=σ/abs(μ)	**0.00**	**0.08**	**0.05**	0.64	0.13	0.09	1.00	0.09	0.06	**0.03**	**0.08**	**0.08**	1.22	0.10	0.04	**0.00**	**0.09**	**0.03**

	Pmax	Pmin	Vmax	Vmin	Mmax	Mmin
$\rho_{P\text{-}V}$=	**-0.65**	-0.62	0.79	**0.17**	0.79	**-0.19**
$\rho_{P\text{-}M}$=	**-0.77**	-0.85	-0.19	**-0.57**	-0.50	**-0.78**
$\rho_{M\text{-}V}$=	**0.75**	0.90	0.25	**0.59**	0.04	**0.70**

Correlation Matrix

	P_{max}	V_p	M_p	P_v	V_{max}	M_v	P_m	V_m	M_{max}
P_{max}	1.00	-0.65	-0.77	-0.12	-0.70	-0.63	0.81	-0.66	-0.90
V_p	-0.65	1.00	0.75	0.41	0.69	0.45	-0.58	0.65	0.73
M_p	-0.77	0.75	1.00	0.18	0.38	0.52	-0.94	0.27	0.80
P_v	-0.12	0.41	0.18	1.00	0.17	-0.57	-0.03	0.19	0.01
V_{max}	-0.70	0.69	0.38	**0.17**	1.00	0.59	-0.26	0.98	0.78
M_v	-0.63	0.45	0.52	**-0.57**	**0.59**	1.00	-0.55	0.54	0.78
P_m	0.81	-0.58	-0.94	-0.03	-0.26	-0.55	1.00	-0.19	-0.78
V_m	-0.66	0.65	0.27	0.19	0.98	0.54	-0.19	1.00	0.70
M_{max}	-0.90	0.73	0.80	0.01	0.78	0.78	-0.78	0.70	1.00

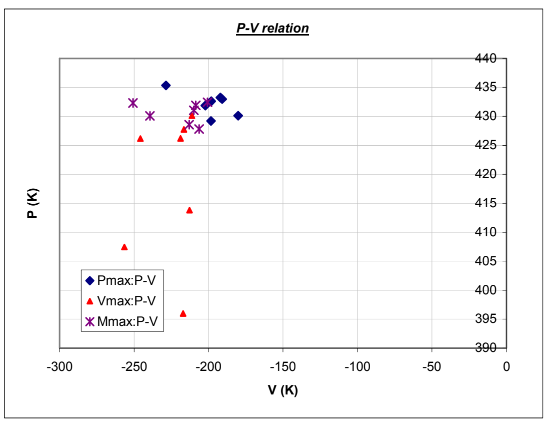

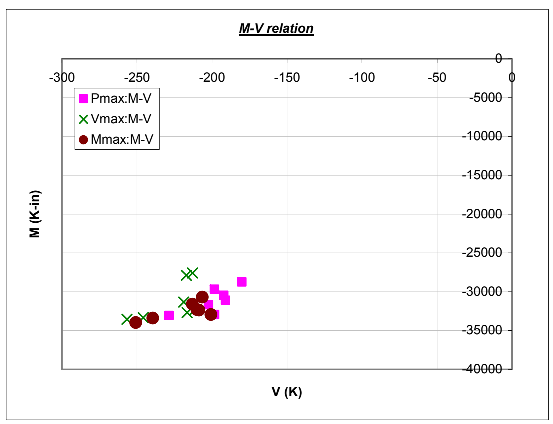

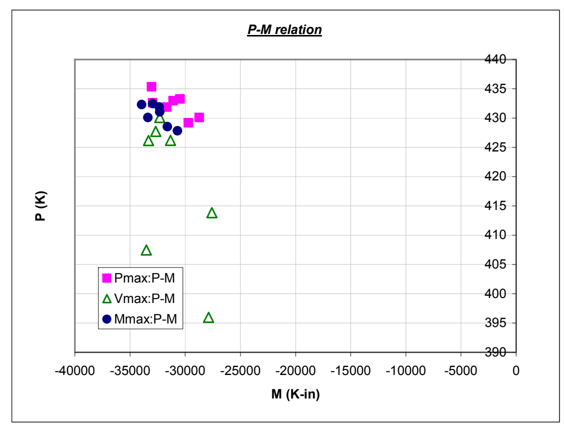

Hazard level: 10% in 50 yr PE

Joint Reactions- F: Ext	Pmax			Pmin			Vmax			Vmin			Mmax			Mmin		
Case	**P** (K)	**V** (K)	**M** (Kip-in)	P (K)	V (K)	M (Kip-in)	P (K)	V (K)	M (Kip-in)	**P** (K)	**V** (K)	**M** (Kip-in)	P (K)	V (K)	M (Kip-in)	**P** (K)	**V** (K)	**M** (Kip-in)
EZerzi	432.9	-224.1	-32873.8	27.2	154.8	23470.7	90.1	241.2	30485.9	392.7	-253.8	-32441.3	39.4	228.0	31028.3	432.3	-227.0	-33043.7
KBkobj	433.0	-195.2	-31746.4	9.6	216.2	32290.6	10.0	216.9	32310.0	427.9	-215.2	-32316.7	10.0	216.9	32310.0	431.4	-211.5	-32543.6
LPcor	430.3	-203.6	-31042.0	12.0	184.0	28904.8	35.8	222.6	27875.5	423.1	-211.5	-30668.8	22.9	222.0	30974.4	429.1	-209.2	-31449.3
LPlgpc	429.3	-183.1	-28395.2	13.2	202.5	30144.2	15.7	212.2	30534.2	418.0	-198.9	-27322.4	14.0	211.3	30773.5	428.4	-192.1	-29125.6
LPlex1	421.2	-184.0	-25691.9	4.8	219.6	33830.2	5.5	228.6	33783.7	420.2	-187.3	-25821.1	6.2	220.8	33831.2	420.2	-187.3	-25821.1
LPsrtg	431.9	-205.5	-31029.9	27.9	175.6	24071.0	104.4	217.7	27054.0	427.1	-229.4	-32614.9	32.1	202.7	27628.6	430.4	-227.5	-32701.0
TOhino	429.8	-190.1	-29221.2	10.0	187.6	30072.7	11.4	203.1	31014.5	424.6	-192.5	-28184.2	10.8	202.6	31126.3	429.6	-190.9	-29296.4
Mean	**429.8**	**-197.9**	**-30000.1**	15.0	191.5	28969.2	39.0	220.3	30436.8	**419.1**	**-212.7**	**-29909.9**	19.3	214.9	31096.0	**428.8**	**-206.5**	**-30568.7**
Median	**430.3**	**-195.2**	**-31029.9**	12.0	187.6	30072.7	15.7	217.7	30534.2	**423.1**	**-211.5**	**-30668.8**	14.0	216.9	31028.3	**429.6**	**-209.2**	**-31449.3**
c.o.v.=σ/abs(μ)	**0.01**	**0.07**	**0.08**	0.60	0.12	0.13	1.06	0.06	0.08	**0.03**	**0.11**	**0.09**	0.65	0.05	0.06	**0.01**	**0.08**	**0.09**
																		-2708.62

	Pmax	Pmin	Vmax	Vmin	Mmax	Mmin
$\rho_{P\text{-}V}$=	**-0.62**	-0.84	0.46	**0.63**	0.22	**-0.68**
$\rho_{P\text{-}M}$=	**-0.93**	-0.97	-0.68	**0.16**	-0.65	**-0.91**
$\rho_{M\text{-}V}$=	**0.83**	0.94	0.09	**0.85**	0.54	**0.90**

Correlation Matrix

	P_{max}	V_p	M_p	P_v	V_{max}	M_v	P_m	V_m	M_{max}
P_{max}	1.00	-0.62	-0.93	-0.15	-0.70	-0.86	0.99	-0.72	-0.94
V_p	-0.62	1.00	0.83	0.64	0.95	0.80	-0.62	0.89	0.78
M_p	-0.93	0.83	1.00	0.31	0.85	0.94	-0.92	0.86	0.98
P_v	-0.15	0.64	0.31	1.00	0.63	0.16	-0.21	0.33	0.20
V_{max}	-0.70	0.95	0.85	**0.63**	1.00	0.85	-0.69	0.94	0.84
M_v	-0.86	0.80	0.94	**0.16**	**0.85**	1.00	-0.81	0.94	0.97
P_m	0.99	-0.62	-0.92	-0.21	-0.69	-0.81	1.00	-0.68	-0.91
V_m	-0.72	0.89	0.86	0.33	0.94	0.94	-0.68	1.00	0.90
M_{max}	-0.94	0.78	0.98	0.20	0.84	0.97	-0.91	0.90	1.00

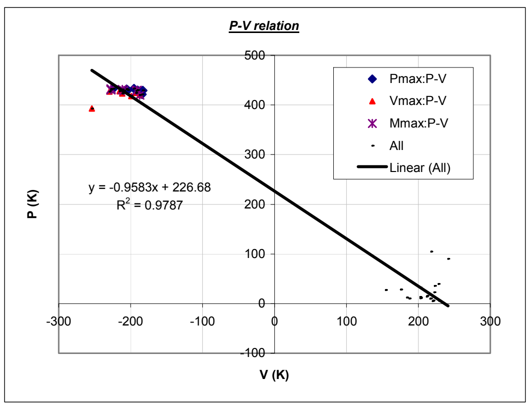

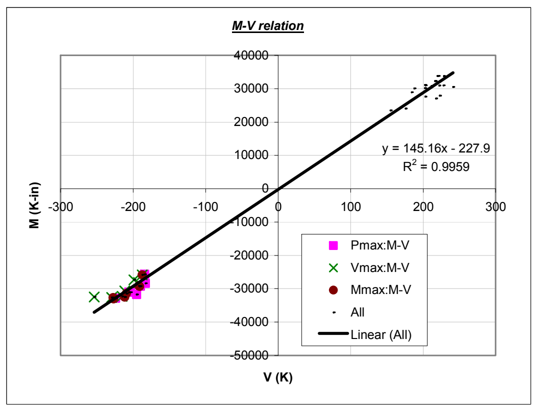

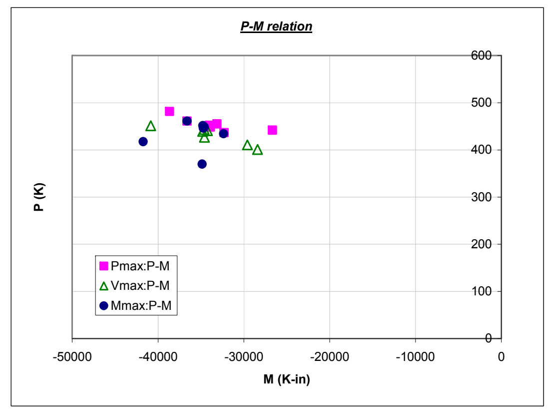

Hazard level: 50% in 50 yr PE

Joint Reactions- F: Ext	**Pmax**			Pmin			Vmax			**Vmin**			Mmax			**Mmin**		
Case	**P** (K)	**V** (K)	**M** (Kip-in)	P (K)	V (K)	M (Kip-in)	P (K)	V (K)	M (Kip-in)	**P** (K)	**V** (K)	**M** (Kip-in)	P (K)	V (K)	M (Kip-in)	**P** (K)	**V** (K)	**M** (Kip-in)
CLgil6	339.6	-90.5	-13124.8	119.0	99.7	13718.5	121.2	104.1	14158.5	339.6	-90.5	-13124.8	121.2	104.1	14158.5	339.6	-90.5	-13124.8
MHhandd	374.0	-133.9	-18790.4	57.4	142.4	20120.8	60.0	146.7	20469.9	372.5	-136.2	-19083.0	60.0	146.7	20469.9	371.5	-136.2	-19086.5
MHclyd	353.4	-109.8	-15699.6	97.6	110.3	15436.6	101.6	112.1	15539.1	348.2	-112.1	-15764.3	100.6	111.9	15553.7	351.9	-111.6	-15840.7
MHhall	323.2	-82.0	-11809.0	123.2	81.3	11609.0	129.8	84.6	11776.9	306.3	-83.0	-11402.1	126.1	84.2	11835.7	322.6	-82.5	-11849.6
PFcs05	388.5	-142.4	-20205.9	66.3	140.1	19593.2	67.2	140.4	19595.8	388.2	-142.5	-20204.5	67.2	140.4	19595.8	388.5	-142.4	-20205.9
PFcs08	387.5	-155.2	-21549.3	36.5	157.1	22331.7	51.3	163.6	22473.6	386.8	-155.6	-21569.6	37.2	158.8	22490.5	386.8	-155.6	-21569.6
PFtemb	324.4	-98.7	-13791.8	119.2	81.0	11944.5	129.9	139.7	17710.2	320.2	-131.2	-17163.8	129.9	139.7	17710.2	320.2	-131.2	-17163.8
Mean	**355.8**	**-116.1**	**-16424.4**	88.4	116.0	16393.5	94.5	127.3	17389.1	**351.7**	**-121.6**	**-16901.7**	91.8	126.6	17402.0	**354.4**	**-121.4**	**-16977.3**
Median	**353.4**	**-109.8**	**-15699.6**	97.6	110.3	15436.6	101.6	139.7	17710.2	**348.2**	**-131.2**	**-17163.8**	100.6	139.7	17710.2	**351.9**	**-131.2**	**-17163.8**
c.o.v.=σ/abs(μ)	**0.08**	**0.24**	**0.23**	0.40	0.27	0.26	0.36	0.22	0.22	**0.09**	**0.22**	**0.22**	0.40	0.21	0.22	**0.08**	**0.23**	**0.21**

	Pmax		Pmin		Vmax		Vmin		Mmax		Mmin	
	ρ_{P-V}=	**-0.96**	ρ_{P-V}=	-0.98	ρ_{P-V}=	-0.77	**ρ_{P-V}=**	**-0.78**	ρ_{P-V}=	-0.75	**ρ_{P-V}=**	**-0.74**
	ρ_{P-M}=	**-0.97**	ρ_{P-M}=	-0.99	ρ_{P-M}=	-0.86	**ρ_{P-M}=**	**-0.86**	ρ_{P-M}=	-0.86	**ρ_{P-M}=**	**-0.82**
	ρ_{M-V}=	**1.00**	ρ_{M-V}=	1.00	ρ_{M-V}=	0.99	**ρ_{M-V}=**	**0.99**	ρ_{M-V}=	0.98	**ρ_{M-V}=**	**0.99**

Correlation Matrix

	P_{max}	V_p	M_p	P_v	V_{max}	M_v	P_m	V_m	M_{max}
P_{max}	1.00	-0.96	-0.97	0.99	-0.77	-0.85	1.00	-0.77	-0.85
V_p	-0.96	1.00	1.00	-0.95	0.91	0.95	-0.95	0.91	0.95
M_p	-0.97	1.00	1.00	-0.96	0.89	0.94	-0.96	0.89	0.94
P_v	0.99	-0.95	-0.96	1.00	-0.78	-0.86	0.99	-0.78	-0.86
V_{max}	-0.77	0.91	0.89	**-0.78**	1.00	0.99	-0.74	1.00	0.99
M_v	-0.85	0.95	0.94	**-0.86**	**0.99**	1.00	-0.82	0.99	1.00
P_m	1.00	-0.95	-0.96	0.99	-0.74	-0.82	1.00	-0.74	-0.82
V_m	-0.77	0.91	0.89	-0.78	1.00	0.99	-0.74	1.00	0.99
M_{max}	-0.85	0.95	0.94	-0.86	0.99	1.00	-0.82	0.99	1.00

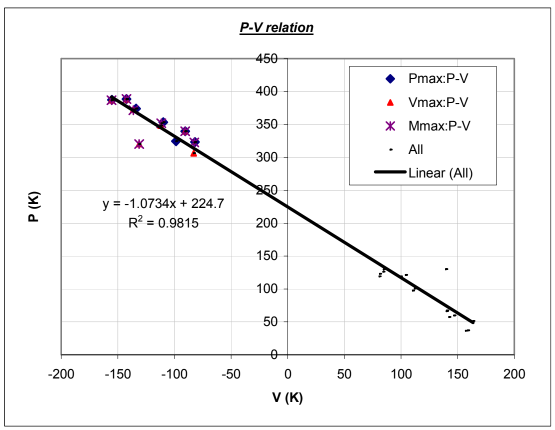

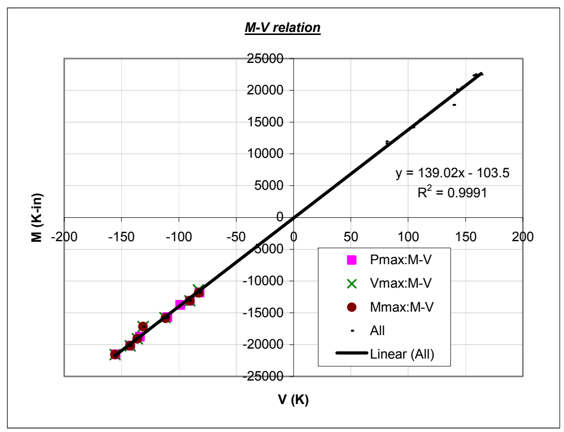

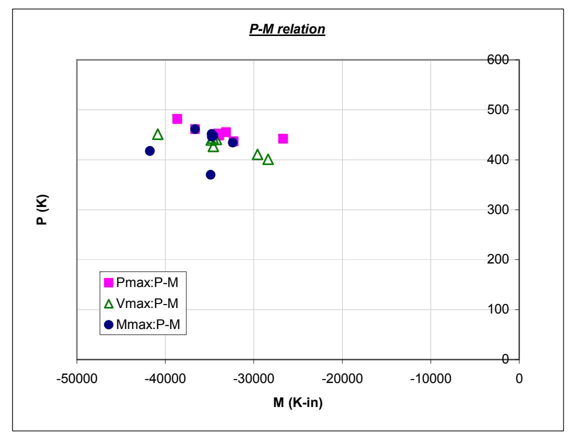

Spreadsheet for the design of the base plate connection (AISC Design Guide #1)

AISC DESIGN GUIDE #1: 2005

Column:	
Section=	**W24x229**
d_c (in)=	**26.02**
b_f (in)=	**13.11**
N_{min}=d+2(1.5d_b)=	32.02
B_{min}=b_f+2(1.5d_b)=	19.11

Input
Calcs
Output

Loads:	**A-P_{max}**	**B-V_{max}**	**C-M_{max}**	
M_u (Kips-ft)=	**2585.8**	**2555.7**	**2620.8**	**2620.8**
P_u (Kips)=	**430.3**	**423.1**	**429.6**	**429.6**
V_u (K)=	**195.2**	**211.5**	**209.2**	**209.2**

Foundations:		
f'$_c$ (ksi)=	**4**	
A_1- Base plate (in^2)=	950	
Pedestal: N* (in)=	**76**	
B* (in)=	**50**	
h (in)=	**52**	2d_c
A_2=N*B* (in^2)=	3800	
$(A_2/A_1)^{1/2}$<2.0=	2.0	
ϕ_c=	0.60	*
$f_{p(max)}=\phi_c(0.85f'_c)(A_2/A_1)^{1/2}$ (ksi)=	4.08	
$q_{max}=f_{p(max)}B$ (kips/in)=	102.00	
$Y_{min}=P_u/q_{max}$ (in)=	4.21	

Eccentricity:	**Large**
$e=M_u/P_u$ (in)=	73
$e_{crit}=N/2-Y_{min}/2$=	16.9
$a_1=(f+N/2)^2$=	1225.0
$a_2=2P_u(e+f)/q_{max}$=	751.4
$(f+N/2)^2>2P_u(e+f)/q_{max}$=	**O.K.**

Bearing Length:		
Small e: Y=N-2e, $f_p=P_u/BY$		*
Large e: $Y=(a_1)^{1/2}$+-$(a_1-a_2)^{1/2}$, $f_p=f_{p(max)}$		
Y (in)=	13.24	
$q=P_u/Y$ (kips/in)=	-	
$q<q_{max}$=	-	
f_p (ksi)=	4.08	

Base Plate:	
F_y (ksi)=	**36**
F_u (ksi)=	**58**
ϕ_b=	0.90
Compression:	
Y>m: $t_{p\ req}=1.49m(f_{p(max)}/F_y)^{1/2}$ (in)=	3.64
Y<m: $t_{p\ req}=2.11(f_{p(max)}Y(m-Y/2)/F_y)^{1/2}$ (in)=	-
$t_{p\ req}$ (in)=	3.64
Tension:	
$T_u=qY-P_u$ (kips)=	920.71
$t_{p\ req}=2.11(T_ux/BF_y)^{1/2}$ (in)=	**3.69**
t_p (in)=	**3.75**

Dimensions (in):

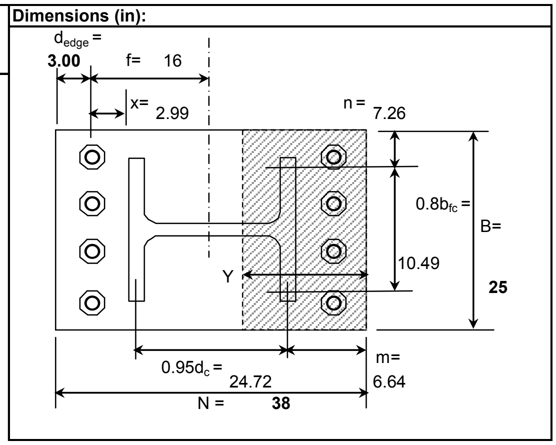

Figure: Force Equilibrium:

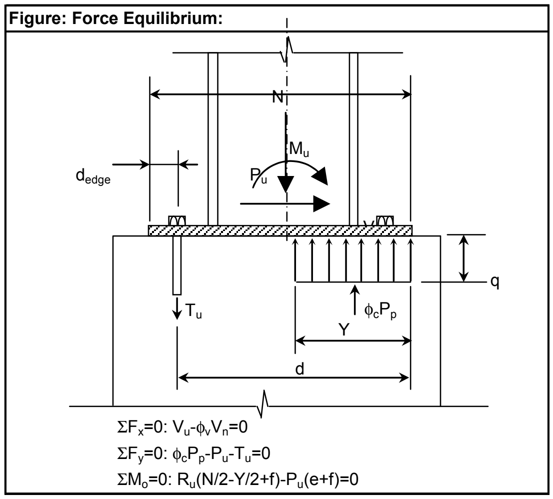

Figure: Base Plate Bending

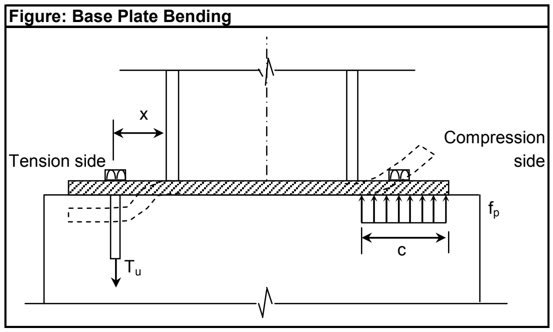

Bolts: Data	n_b-Number=	8
T_u (kips)=		920.71
$T_{ub}=T_u/(n_b/2)$ (kips)=		230.18
$V_{ub}=V_u/(n_b/2)$ (K)=		52.3
Bolt type=		**F1554-Gr.105**
Threads (N/X)=		**X**
F_{yb} (ksi)=		**105**
F_{ub} (ksi)=		**125**
d_b (in)=		**2.00**
A_b (in^2)=		3.14
S- spacing (in)=		6.0
$d_{edge(min)}=1.5d_b$ (in)=		3.00
$d_{edge}>d_{min}$=		**O.K.**

Anchor Bolt Embedment Length:	
ϕ=	0.70
ψ_3 (un/cracked:1.25/1.0)=	**1.25**
h_{ef} (in)=	**30.0**
c_1- edge distance- N direction (in)=	**19.0**
c_2- edge distance- B direction (in)=	**12.5**
Anchor plate (Y/N)=	**Y**
Continuous (Y/N)=	**Y**
b_{PL}- N direction (in)=	**8.0**
L_{PL}- B direction (in)=	**30.0**
A_{No}- Single anchor bolt (in^2)=	6300.0
A_N- Group (in^2)=	6300.0
ϕN_{cbg} (kips)=	256.5
ϕ_c- Concrete strength=	0.75
$\phi_c\phi N_{cbg}$ (kips)=	192.35
$\phi_c\phi N_{cbg}>T_u$=	**O.K.**

Bearing Base Plate:	
t_{washer} (in)=	**0.00**
ϕ=	0.75
$L_c=\min(s,d_{edge})$ (in)=	3.00
$\phi R_n=\phi 1.5L_ctF_u<\phi 3.0d_btF_u$ (K)=	734.1
$\phi R_n>V_{ub}$=	**O.K.**

Bolts: Tensile Strength		
ϕ=		0.75
$d=(t_p+t_{washer}/2)/2$=		1.88
$M=V_{ub}d$ (kips.in)=		98.1
$Z=(2d)^3/6$ (in^3)=		8.79
Bending: $f_{tb}=M/Z$ (ksi)=		0.0
Axial: $f_{ta}=T_{ub}/A_b$ (ksi)=		73.3
$f_t=f_{tb}+f_{ta}$ (ksi)=		73.3
$F_{nt}=0.75F_u$ (ksi)=		93.75
$F_{nt}'=1.3F_{nt}-(F_{nt}/\phi F_{nv})f_v<F_{nt}$ (ksi)=		93.8
$\phi T_n=\phi F_{nt}'A_b$ (kips)=		220.9
$\phi T_n>T_{ub}$=	(within 10%)	**O.K.**

Bolts: Shear	Bolts resist shear (Y/N)=	Y
ϕ=		0.90
$f_v=V_u/(nA_b)$ (ksi)=		16.65
$F_{nv}=0.5F_u$ (X)/$0.4F_u$ (N) (ksi)=		62.5
$\phi V_n=\phi F_{nv}A_b$ (kips)=		176.7
$\phi V_n>V_{ub}$=		**O.K.**

Shear Lug: Shear (Confinement components ignored)	
N- number of shear lug=	**2**
S- Spacing (in)=	**10**
h-Total height (in)=	**3.5**
t_{grout} (in)=	**2.0**
h_{emb}- Concrete embedded height (in)=	1.5
L (in)=	25.0
$A_l=Nh_{emb}L$ (in^2)=	75.0
a- Free edge in B direction (in)=	12.5
b- Free edge in N direction (in)=	32.375
$h=\min(h_{concrete},b+h_{emb})$ (in)=	33.9
A_V (in^2)=	1656.3
Concrete bearing: $\phi R_n=0.8f'_cA_l$ (kips)=	240
Concrete shear: $\phi R_n=4\phi f'_c{}^{1/2}A_V$ (ksi)=	314.3
$\phi R_n>V_u$=	**O.K.**

Shear Lug: Bending	
t_{PL}- shear lug (in)=	**1.25**
F_y (ksi)=	**36**
ϕ_b=	0.90
Cantilever: $M_l=V_u/N(t_{grout}+h_{emb}/2)$ (Kip.ft)=	24.0
$t_{req}=(4M_l/(\phi F_yL))^{1/2}$ (in)=	**1.19**
$t_{PL}>t_{req}$=	**O.K.**

Shear Lug: Welds	
b_w (in)=	**0.375**
F_{EXX} (ksi)=	**60**
$t_w=0.707b_w$ (in)=	0.27
$s=t_{PL}+2b_w$ (in)=	2
$f_c=M_l/(sL)$ (kip/in)=	5.75
$f_v=V_u/(2NL)$ (kip/in)=	2.09
$f_r=(f_c^2+f_v^2)^{1/2}$ (kip/in)=	6.12
ϕ=	0.75
$\phi F_w=\phi 0.60F_{EXX}t_w$ (kip/in)=	7.2
$\phi F_w>f_r$=	**O.K.**

Limit-state function definition in CalREL (user.for)

```
      subroutine ugfun(g,x,tp,ig)
      implicit real*8 (a-h,l-z)
      dimension x(1),tp(1)
      go to (1,2,3,4,5,6,7) ig
1     g = x(16)/(x(4)*x(3))+x(18)/((1./6.)*x(4)*x(3)**2.)
      g = 0.85*tp(1)*x(14)-g
      return
2     g = x(17)/(x(3)*x(4))+x(18)/((1./6.)*x(4)*x(3)**2.)
      g = g*(((x(4)-0.80*x(2))/2.)**2.)/2.
      g = (x(12)*x(5)**2.)/4.-g
      return
3     g = 2.*x(17)*(x(18)/x(16)+x(3)/2.-x(9))
      g = g/(0.85*tp(1)*x(14)*x(4))
      g = (x(3)-x(9))**2.-g
      g = (x(3)-x(9))-g**0.5
      g = 0.85*tp(1)*x(14)*x(4)*g
      g = (x(3)-x(1)-2.0*x(9))/2.*(g-x(16))
      g = (x(12)*x(4)*x(5)**2.)/4.-g
      return
4     g = 2.*x(17)*(x(18)/x(16)+x(3)/2.-x(9))
      g = g/(0.85*tp(1)*x(14)*x(4))
      g = (x(3)-x(9))**2.-g
      g = (x(3)-x(9))-g**0.5
      g = 0.85*tp(1)*x(14)*x(4)*g
      g = 8./2.*tp(2)*x(13)*(3.14*x(8)**2.)/4.-g
      return
5     g = x(15)*x(16)-x(17)
      return
6     g = tp(3)*x(13)*(3.14*x(8)**2.)/4.-x(17)/(8./2.)
      return
7     g = tp(4)*x(14)*2.*x(7)*(x(6)-x(10))-x(17)
      return
      end

      subroutine udgx(dgx,x,tp,ig)
      implicit real*8 (a-h,l-z)
      dimension x(1),dgx(1),tp(1)
      return
      end

      subroutine udd(x,par,sg,ids,cdf,pdf,bnd,ib)
      implicit real*8 (a-h,l-z)
      dimension x(1),par(4),bnd(2)
      return
      end

      subroutine usize
      common /blkrel/ mtot,np,ia(100000)
      mtot=100000
      return
      end
```

Input file in CalREL (In_2in50yr_Mmax.txt) defining random variables, reliability analysis procedures, and parameters

```
CALRel ngf=7 nig=2 nrx=18 ntp=4
DATA
TITL nline title
1
Reliability of base plate connection as a general system
FLAG icl, igr
3 0
OPTI iop,ni1,ni2,tol,op1,op2,op3
5,-1000,-50,0.001
STAT igt(i),nge,ngm nv,ids,ex,sg,p3,p4,x0
1 15
dc    1,  1,  26.02,  0.125,  0.,  0.,  26.02
bf    2,  1,  13.11,  0.1875, 0.,  0.,  13.11
n     3,  1,  38.,    1.,     0.,  0.,  38.
b     4,  1,  25.,    1.,     0.,  0.,  25.
tp    5,  1,  3.75,   0.11,   0.,  0.,  3.75
lsl   6,  7,  3.5,    0.5,    2.75,4.25,3.5
bsl   7,  1,  25.,    0.75,   0.,  0.,  25.
db    8,  1,  2.,     0.10,   0.,  0.,  2.
de    9,  1,  3.      0.25,   0.,  0.,  3.
tg    10, 7,  2.,     0.5,    0.,  2.5, 2.
fyc   11, 2,  60.,    3.,     0.,  0.,  60.
fyp   12, 2,  50.,    3.5,    0.,  0.,  50.
fub   13, 2,  137.5,  12.5,   0.,  0.,  137.5
fc    14, 2,  4.8,    0.60,   0.,  0.,  4.8
mu    15, 7,  0.80,   0.24,   0.,  1.,  0.80
2 3
pm    16, 2,  432.6,  30.3,   0.,  0.,  432.6
vm    17, 2,  241.6,  31.4,   0.,  0.,  241.6
mmax  18, 11, 35664.2,2853.1, 0.,  0.,  35664.2
-0.65
-0.12 0.81
PARA
2., 0.75, 0.50, 0.80
CUTS
6 8
1 0 2 0 3 0 4 0 5 6 0 5 7 0
END
FORM ini=0 ist=0 npr=1
SORM
SCIS nsm=100000 npr=10000 cov=0.001 stp=98766587 ind=0
SENS
exit
```

Component and system reliability analysis results for all hazard levels considered

Component and System Relibaility Results

											Weighted results	
2% in 50 yr PE hazard level							Component	Pf1	PH(h,t=50)	PH(h,t=1)	t=50	t=1
	5.82E-02	2.61E-02	2.33E-04	5.06E-03	2.76E-11	1.52E-03	1	5.82E-02	0.02	4.04E-04	0.001164	2.35E-05
	2.61E-02	2.96E-01	4.44E-04	1.16E-02	4.33E-11	7.83E-03	2	2.96E-01	0.02	4.04E-04	0.005912	1.19E-04
	2.33E-04	4.44E-04	5.55E-04	4.91E-04	3.97E-11	5.72E-05	3	5.55E-04	0.02	4.04E-04	1.11E-05	2.24E-07
	5.06E-03	1.16E-02	4.91E-04	1.70E-02	4.84E-11	1.10E-03	4	1.70E-02	0.02	4.04E-04	0.000339	6.85E-06
	2.76E-11	4.33E-11	3.97E-11	4.84E-11	2.37E-11	1.47E-11	5	2.37E-11	0.02	4.04E-04	4.74E-13	9.58E-15
	1.52E-03	7.83E-03	5.72E-05	1.10E-03	1.47E-11	2.13E-02	6	2.13E-02	0.02	4.04E-04	0.000426	8.60E-06
Pf1		3.40E-01	3.47E-01				System-P_{f1}	3.43E-01	0.02	4.04E-04	0.006861	1.39E-04
Beta		0.395	0.413				System-β	4.04E-01	0.02	4.04E-04	0.00808	1.63E-04
5% in 50 yr PE hazard level							Component	Pf1	PH(h,t=50)	PH(h,t=1)	t=50	t=1
	1.07E-02	1.21E-03	2.15E-12	1.09E-06	7.25E-13	1.12E-04	1	1.07E-02	0.05	1.03E-03	0.000535	1.10E-05
	1.21E-03	1.17E-01	1.49E-11	4.48E-06	5.57E-12	1.64E-03	2	1.17E-01	0.05	1.03E-03	0.005855	1.20E-04
	2.15E-12	1.49E-11	0.00E+00	2.66E-12	1.03E-16	5.01E-12	3	0.00E+00	0.05	1.03E-03	0	0.00E+00
	1.09E-06	4.48E-06	2.66E-12	1.38E-05	2.21E-11	4.03E-07	4	1.38E-05	0.05	1.03E-03	6.89E-07	1.41E-08
	7.25E-13	5.57E-12	1.03E-16	2.21E-11	1.43E-11	3.21E-12	5	1.43E-11	0.05	1.03E-03	7.16E-13	1.47E-14
	1.12E-04	1.64E-03	5.01E-12	4.03E-07	3.21E-12	1.31E-02	6	1.31E-02	0.05	1.03E-03	0.000656	1.34E-05
Pf1		1.38E-01	1.38E-01				System-P_{f1}	1.38E-01	0.05	1.03E-03	0.006903	1.42E-04
Beta		1.089	1.089				System-β	1.09E+00	0.05	1.03E-03	0.05445	1.12E-03
10% in 50 yr PE hazard level							Component	Pf1	PH(h,t=50)	PH(h,t=1)	t=50	t=1
	9.52E-03	2.71E-03	1.67E-08	2.70E-05	3.91E-12	1.10E-04	1	9.52E-03	0.10	2.11E-03	0.000952	2.01E-05
	2.71E-03	7.55E-02	1.84E-08	4.03E-05	9.38E-12	9.92E-04	2	7.55E-02	0.10	2.11E-03	0.007551	1.59E-04
	1.67E-08	1.84E-08	1.90E-08	1.41E-08	1.12E-14	5.99E-10	3	1.90E-08	0.10	2.11E-03	1.9E-09	4.00E-11
	2.70E-05	4.03E-05	1.41E-08	5.16E-05	1.79E-11	1.17E-06	4	5.16E-05	0.10	2.11E-03	5.16E-06	1.09E-07
	3.91E-12	9.38E-12	1.12E-14	1.79E-11	1.31E-11	2.07E-12	5	1.31E-11	0.10	2.11E-03	1.31E-12	2.75E-14
	1.10E-04	9.92E-04	5.99E-10	1.17E-06	2.07E-12	1.05E-02	6	1.05E-02	0.10	2.11E-03	0.001046	2.20E-05
Pf1		9.17E-02	9.18E-02				System-P_{f1}	9.17E-02	0.10	2.11E-03	0.009174	1.93E-04
Beta		1.33	1.33				System-β	1.33E+00	0.10	2.11E-03	0.133	2.80E-03
50% in 50 yr PE hazard level							Component	Pf1	PH(h,t=50)	PH(h,t=1)	t=50	t=1
	1.47E-04	6.24E-05	4.46E-08	4.39E-06	2.11E-11	4.83E-07	1	1.47E-04	0.50	1.33E-02	7.34E-05	1.96E-06
	6.24E-05	1.06E-03	4.71E-08	6.25E-06	2.31E-11	4.11E-06	2	1.06E-03	0.50	1.33E-02	0.000531	1.41E-05
	4.46E-08	4.71E-08	4.72E-08	4.33E-08	8.07E-12	8.87E-10	3	4.72E-08	0.50	1.33E-02	2.36E-08	6.30E-10
	4.39E-06	6.25E-06	4.33E-08	7.01E-06	2.35E-11	7.52E-08	4	7.01E-06	0.50	1.33E-02	3.51E-06	9.35E-08
	2.11E-11	2.31E-11	8.07E-12	2.35E-11	8.41E-12	1.70E-12	5	8.41E-12	0.50	1.33E-02	4.2E-12	1.12E-13
	4.83E-07	4.11E-06	8.87E-10	7.52E-08	1.70E-12	5.27E-04	6	5.27E-04	0.50	1.33E-02	0.000263	7.02E-06
Pf1		1.67E-03	1.67E-03				System-P_{f1}	1.67E-03	0.50	1.33E-02	0.000834	2.22E-05
Beta		2.935	2.935				System-β	2.94E+00	0.50	1.33E-02	1.4675	3.91E-02

Sensitivity analysis for limit-state parameter: system reliability analysis for different hazard levels.

Sensitivity Analysis: Limit-state parameters θ_g

Perturbation			β-Reliability Index					P_{f1}-Failure Probability (FORM)				
Parameter	θ_{gi}	$\Delta\theta_{gi}$	β_{min}	β_{max}	β_{ave}	$\Delta_{\theta g}\beta\theta_g$	$\Delta_{\theta g}\beta(\theta_g/\beta)$	$P_{f\text{- }min}$	$P_{f\text{- }max}$	$P_{f\text{-}ave}$	$\Delta_{\theta g}P_f\theta_g$	$\Delta_{\theta g}P_f\ (\theta_g/P_f)$
Original	-	-	0.395	0.413	0.404	-	-	3.40E-01	3.47E-01	0.3431	-	-
k	2.0	0.1	0.439	0.454	0.447	0.850	**2.10**	3.25E-01	3.30E-01	0.3278	-0.307	**-0.89**
C_{ub1}	0.75	-0.0375	0.386	0.413	0.400	0.090	**0.22**	3.40E-01	3.50E-01	0.3448	-0.033	**-0.10**
C_{ub2}	0.5	-0.025	0.395	0.413	0.404	0.000	**0.00**	3.40E-01	3.47E-01	0.3431	0.000	**0.00**
C_{brg}	0.8	-0.04	0.388	0.407	0.398	0.130	**0.32**	3.42E-01	3.49E-01	0.3456	-0.048	**-0.14**

Sensitivity Analysis: Limit-state parameter θ_g=k

Perturbation			β-Reliability Index					P_{f1}-Failure Probability (FORM)				
Parameter	θ_{gi}	$\Delta\theta_{gi}$	β_{min}	β_{max}	β_{ave}	$\Delta_{\theta g}\beta\theta_g$	$\Delta_{\theta g}\beta(\theta_g/\beta)$	$P_{f\text{- }min}$	$P_{f\text{- }max}$	$P_{f\text{-}ave}$	$\Delta_{\theta g}P_f\theta_g$	$\Delta_{\theta g}P_f\ (\theta_g/P_f)$
Original-2%	-	-	0.395	0.413	0.404	-	-	3.40E-01	3.47E-01	0.3431	-	-
2% in 50 yr	2.0	0.1	0.439	0.454	0.447	0.850	**2.10**	3.25E-01	3.30E-01	0.3278	-0.307	**-0.89**
Original-5%	-	-	1.089	1.089	1.089	-	-	1.38E-01	1.38E-01	0.1381	-	-
5% in 50 yr	2.0	0.1	1.116	1.116	1.116	0.540	**0.50**	1.32E-01	1.32E-01	0.1323	-0.116	**-0.84**
Original-10%	-	-	1.33	1.33	1.330	-	-	9.17E-02	9.18E-02	0.0917	-	-
10% in 50 yr	2.0	0.1	1.353	1.353	1.353	0.460	**0.35**	8.80E-02	8.80E-02	0.0880	-0.073	**-0.80**
Original-50%	-	-	2.935	2.935	2.935	-	-	1.67E-03	1.67E-03	0.0017	-	-
50% in 50 yr	2.0	0.1	2.944	2.944	2.944	0.180	**0.06**	1.62E-03	1.62E-03	0.0016	-0.001	**-0.56**

Computation of δ vector for relative importance of random variables: System reliability analysis at 2% in 50 yrs PE hazard level

No.	RV_i	μ_i	σ_i	$\Delta\mu$	β_{min}	β_{max}	β_{ave}	$\delta=(\Delta\beta/\Delta\mu)_i\sigma_i$	Order	Classification
Original	-	–	–	–	0.395	0.413	0.404	-	-	-
1	d_c	26.02	0.125	2.60	0.395	0.414	0.4045	2.40E-05	17	Capacity
2	b_f	13.11	0.1875	1.31	0.993	1.025	1.009	8.65E-02	7	Capacity
3	N	38	1	3.80	1.425	1.451	1.438	2.72E-01	4	Capacity
4	B	25	1	2.50	-0.905	-0.9	-0.9025	-5.23E-01	1	Demand
5	t_{PL}	3.75	0.11	0.38	1.136	1.171	1.1535	2.20E-01	5	Capacity
6	l_{sl}	3.5	0.5	0.35	0.397	0.415	0.406	2.86E-03	14	Capacity
7	b_{sl}	26	0.75	2.60	0.406	0.426	0.416	3.46E-03	12	Capacity
8	d_b	2	0.1	0.20	0.407	0.413	0.41	3.00E-03	13	Capacity
9	d_{edge}	3	0.25	0.30	0.394	0.413	0.4035	-4.17E-04	16	Demand
10	t_{grout}	2	0.5	0.20	0.364	0.386	0.375	-7.25E-02	9	Demand
11	$F_{y,col}$	60	3	6.00	0.395	0.413	0.404	0.00E+00	18	-
12	$F_{y,PL}$	50	3.5	5.00	0.847	0.875	0.861	3.20E-01	3	Capacity
13	F_{ub}	137.5	12.5	13.75	0.404	0.413	0.4085	4.09E-03	11	Capacity
14	f'_c	4.8	0.6	0.48	0.481	0.49	0.4855	1.02E-01	6	Capacity
15	μ	0.8	0.24	-0.08	0.367	0.389	0.378	7.80E-02	8	Capacity
16	P	432.6	30.3	43.26	0.395	0.405	0.4	-2.80E-03	15	Demand
17	V	241.6	31.4	24.16	0.343	0.377	0.36	-5.72E-02	10	Demand
18	M	35664.2	2853.1	3566.42	-0.224	-0.193	-0.2085	-4.90E-01	2	Demand

Fragility curves obtained for different failure modes of the connection using lognormal fit

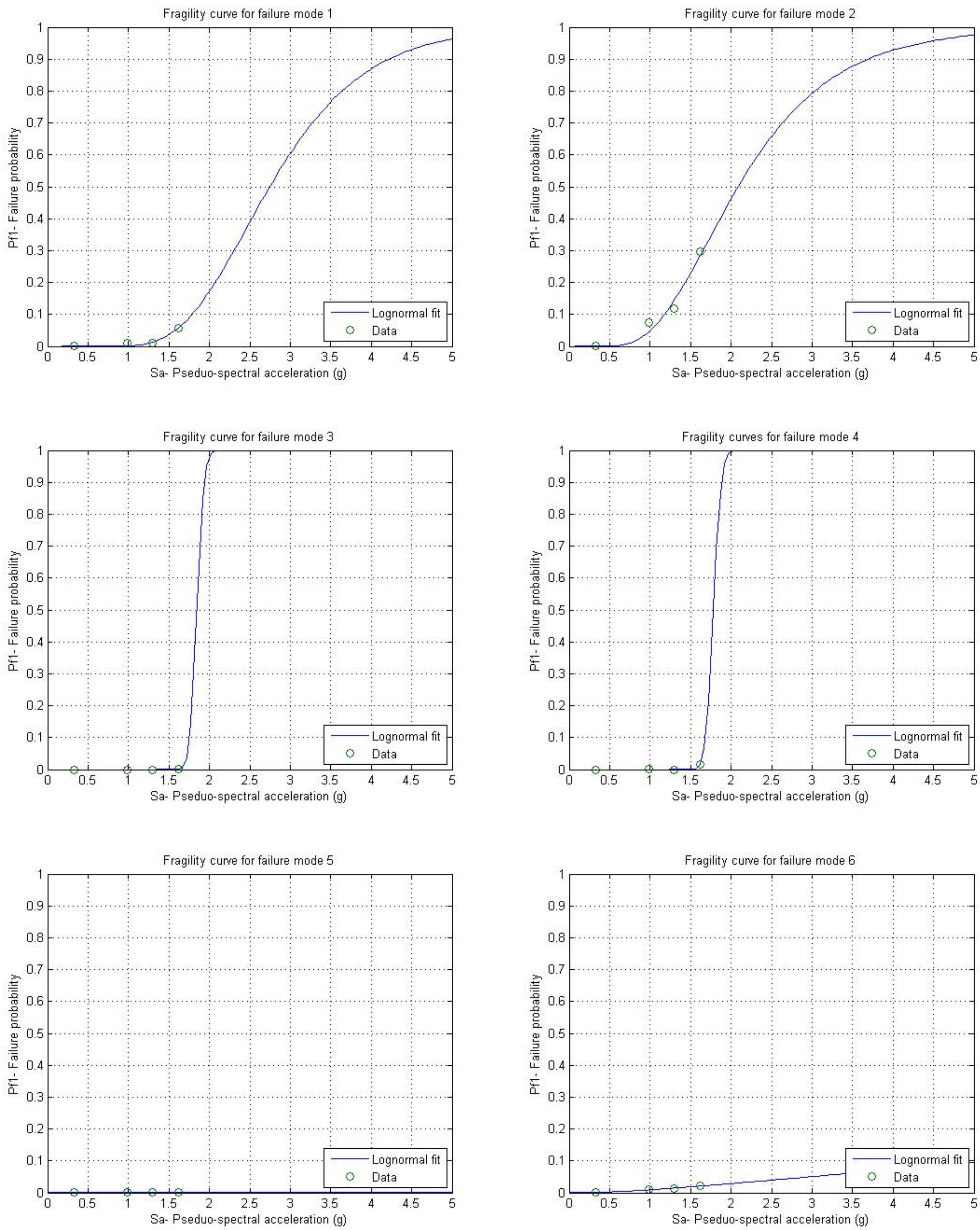

PEER REPORTS

PEER reports are available individually or by yearly subscription. PEER reports can be ordered at http://peer.berkeley.edu/publications/peer_reports.html or by contacting the Pacific Earthquake Engineering Research Center, 1301 South 46th Street, Richmond, CA 94804-4698. Tel.: (510) 665-3448; Fax: (510) 665-3456; Email: peer_editor@berkeley.edu

PEER 2010/03 *Shear Wave Velocity as a Statistical Function of Standard Penetration Test Resistance and Vertical Effective Stress at Caltrans Bridge Sites.* Scott J. Brandenberg, Naresh Bellana, and Thomas Shantz. June 2010.

PEER 2010/02 *Stochastic Modeling and Simulation of Ground Motions for Performance-Based Earthquake Engineering.* Sanaz Rezaeian and Armen Der Kiureghian. June 2010.

PEER 2010/01 *Structural Response and Cost Characterization of Bridge Construction Using Seismic Performance Enhancement Strategies.* Ady Aviram, Božidar Stojadinović, Gustavo J. Parra-Montesinos, and Kevin R. Mackie. March 2010.

PEER 2009/03 *The Integration of Experimental and Simulation Data in the Study of Reinforced Concrete Bridge Systems Including Soil-Foundation-Structure Interaction.* Matthew Dryden and Gregory L. Fenves. November 2009.

PEER 2009/02 *Improving Earthquake Mitigation through Innovations and Applications in Seismic Science, Engineering, Communication, and Response. Proceedings of a U.S.-Iran Seismic Workshop.* October 2009.

PEER 2009/01 *Evaluation of Ground Motion Selection and Modification Methods: Predicting Median Interstory Drift Response of Buildings.* Curt B. Haselton, Ed. June 2009.

PEER 2008/10 *Technical Manual for Strata.* Albert R. Kottke and Ellen M. Rathje. February 2009.

PEER 2008/09 *NGA Model for Average Horizontal Component of Peak Ground Motion and Response Spectra.* Brian S.-J. Chiou and Robert R. Youngs. November 2008.

PEER 2008/08 *Toward Earthquake-Resistant Design of Concentrically Braced Steel Structures.* Patxi Uriz and Stephen A. Mahin. November 2008.

PEER 2008/07 *Using OpenSees for Performance-Based Evaluation of Bridges on Liquefiable Soils.* Stephen L. Kramer, Pedro Arduino, and HyungSuk Shin. November 2008.

PEER 2008/06 *Shaking Table Tests and Numerical Investigation of Self-Centering Reinforced Concrete Bridge Columns.* Hyung IL Jeong, Junichi Sakai, and Stephen A. Mahin. September 2008.

PEER 2008/05 *Performance-Based Earthquake Engineering Design Evaluation Procedure for Bridge Foundations Undergoing Liquefaction-Induced Lateral Ground Displacement.* Christian A. Ledezma and Jonathan D. Bray. August 2008.

PEER 2008/04 *Benchmarking of Nonlinear Geotechnical Ground Response Analysis Procedures.* Jonathan P. Stewart, Annie On-Lei Kwok, Yousseff M. A. Hashash, Neven Matasovic, Robert Pyke, Zhiliang Wang, and Zhaohui Yang. August 2008.

PEER 2008/03 *Guidelines for Nonlinear Analysis of Bridge Structures in California.* Ady Aviram, Kevin R. Mackie, and Božidar Stojadinović. August 2008.

PEER 2008/02 *Treatment of Uncertainties in Seismic-Risk Analysis of Transportation Systems.* Evangelos Stergiou and Anne S. Kiremidjian. July 2008.

PEER 2008/01 *Seismic Performance Objectives for Tall Buildings.* William T. Holmes, Charles Kircher, William Petak, and Nabih Youssef. August 2008.

PEER 2007/12 *An Assessment to Benchmark the Seismic Performance of a Code-Conforming Reinforced Concrete Moment-Frame Building.* Curt Haselton, Christine A. Goulet, Judith Mitrani-Reiser, James L. Beck, Gregory G. Deierlein, Keith A. Porter, Jonathan P. Stewart, and Ertugrul Taciroglu. August 2008.

PEER 2007/11 *Bar Buckling in Reinforced Concrete Bridge Columns.* Wayne A. Brown, Dawn E. Lehman, and John F. Stanton. February 2008.

PEER 2007/10 *Computational Modeling of Progressive Collapse in Reinforced Concrete Frame Structures.* Mohamed M. Talaat and Khalid M. Mosalam. May 2008.

PEER 2007/09 *Integrated Probabilistic Performance-Based Evaluation of Benchmark Reinforced Concrete Bridges.* Kevin R. Mackie, John-Michael Wong, and Božidar Stojadinović. January 2008.

PEER 2007/08 *Assessing Seismic Collapse Safety of Modern Reinforced Concrete Moment-Frame Buildings.* Curt B. Haselton and Gregory G. Deierlein. February 2008.

PEER 2007/07 *Performance Modeling Strategies for Modern Reinforced Concrete Bridge Columns.* Michael P. Berry and Marc O. Eberhard. April 2008.

PEER 2007/06 *Development of Improved Procedures for Seismic Design of Buried and Partially Buried Structures.* Linda Al Atik and Nicholas Sitar. June 2007.

PEER 2007/05 *Uncertainty and Correlation in Seismic Risk Assessment of Transportation Systems.* Renee G. Lee and Anne S. Kiremidjian. July 2007.

PEER 2007/04 *Numerical Models for Analysis and Performance-Based Design of Shallow Foundations Subjected to Seismic Loading.* Sivapalan Gajan, Tara C. Hutchinson, Bruce L. Kutter, Prishati Raychowdhury, José A. Ugalde, and Jonathan P. Stewart. May 2008.

PEER 2007/03 *Beam-Column Element Model Calibrated for Predicting Flexural Response Leading to Global Collapse of RC Frame Buildings.* Curt B. Haselton, Abbie B. Liel, Sarah Taylor Lange, and Gregory G. Deierlein. May 2008.

PEER 2007/02 *Campbell-Bozorgnia NGA Ground Motion Relations for the Geometric Mean Horizontal Component of Peak and Spectral Ground Motion Parameters.* Kenneth W. Campbell and Yousef Bozorgnia. May 2007.

PEER 2007/01 *Boore-Atkinson NGA Ground Motion Relations for the Geometric Mean Horizontal Component of Peak and Spectral Ground Motion Parameters.* David M. Boore and Gail M. Atkinson. May. May 2007.

PEER 2006/12 *Societal Implications of Performance-Based Earthquake Engineering.* Peter J. May. May 2007.

PEER 2006/11 *Probabilistic Seismic Demand Analysis Using Advanced Ground Motion Intensity Measures, Attenuation Relationships, and Near-Fault Effects.* Polsak Tothong and C. Allin Cornell. March 2007.

PEER 2006/10 *Application of the PEER PBEE Methodology to the I-880 Viaduct.* Sashi Kunnath. February 2007.

PEER 2006/09 *Quantifying Economic Losses from Travel Forgone Following a Large Metropolitan Earthquake.* James Moore, Sungbin Cho, Yue Yue Fan, and Stuart Werner. November 2006.

PEER 2006/08 *Vector-Valued Ground Motion Intensity Measures for Probabilistic Seismic Demand Analysis*. Jack W. Baker and C. Allin Cornell. October 2006.

PEER 2006/07 *Analytical Modeling of Reinforced Concrete Walls for Predicting Flexural and Coupled–Shear-Flexural Responses.* Kutay Orakcal, Leonardo M. Massone, and John W. Wallace. October 2006.

PEER 2006/06 *Nonlinear Analysis of a Soil-Drilled Pier System under Static and Dynamic Axial Loading.* Gang Wang and Nicholas Sitar. November 2006.

PEER 2006/05 *Advanced Seismic Assessment Guidelines.* Paolo Bazzurro, C. Allin Cornell, Charles Menun, Maziar Motahari, and Nicolas Luco. September 2006.

PEER 2006/04 *Probabilistic Seismic Evaluation of Reinforced Concrete Structural Components and Systems.* Tae Hyung Lee and Khalid M. Mosalam. August 2006.

PEER 2006/03 *Performance of Lifelines Subjected to Lateral Spreading.* Scott A. Ashford and Teerawut Juirnarongrit. July 2006.

PEER 2006/02 *Pacific Earthquake Engineering Research Center Highway Demonstration Project.* Anne Kiremidjian, James Moore, Yue Yue Fan, Nesrin Basoz, Ozgur Yazali, and Meredith Williams. April 2006.

PEER 2006/01 *Bracing Berkeley. A Guide to Seismic Safety on the UC Berkeley Campus.* Mary C. Comerio, Stephen Tobriner, and Ariane Fehrenkamp. January 2006.

PEER 2005/16 *Seismic Response and Reliability of Electrical Substation Equipment and Systems.* Junho Song, Armen Der Kiureghian, and Jerome L. Sackman. April 2006.

PEER 2005/15 *CPT-Based Probabilistic Assessment of Seismic Soil Liquefaction Initiation.* R. E. S. Moss, R. B. Seed, R. E. Kayen, J. P. Stewart, and A. Der Kiureghian. April 2006.

PEER 2005/14 *Workshop on Modeling of Nonlinear Cyclic Load-Deformation Behavior of Shallow Foundations.* Bruce L. Kutter, Geoffrey Martin, Tara Hutchinson, Chad Harden, Sivapalan Gajan, and Justin Phalen. March 2006.

PEER 2005/13 *Stochastic Characterization and Decision Bases under Time-Dependent Aftershock Risk in Performance-Based Earthquake Engineering.* Gee Liek Yeo and C. Allin Cornell. July 2005.

PEER 2005/12 *PEER Testbed Study on a Laboratory Building: Exercising Seismic Performance Assessment.* Mary C. Comerio, editor. November 2005.

PEER 2005/11 *Van Nuys Hotel Building Testbed Report: Exercising Seismic Performance Assessment.* Helmut Krawinkler, editor. October 2005.

PEER 2005/10 *First NEES/E-Defense Workshop on Collapse Simulation of Reinforced Concrete Building Structures.* September 2005.

PEER 2005/09 *Test Applications of Advanced Seismic Assessment Guidelines.* Joe Maffei, Karl Telleen, Danya Mohr, William Holmes, and Yuki Nakayama. August 2006.

PEER 2005/08 *Damage Accumulation in Lightly Confined Reinforced Concrete Bridge Columns.* R. Tyler Ranf, Jared M. Nelson, Zach Price, Marc O. Eberhard, and John F. Stanton. April 2006.

PEER 2005/07 *Experimental and Analytical Studies on the Seismic Response of Freestanding and Anchored Laboratory Equipment.* Dimitrios Konstantinidis and Nicos Makris. January 2005.

PEER 2005/06 *Global Collapse of Frame Structures under Seismic Excitations*. Luis F. Ibarra and Helmut Krawinkler. September 2005.

PEER 2005//05 *Performance Characterization of Bench- and Shelf-Mounted Equipment.* Samit Ray Chaudhuri and Tara C. Hutchinson. May 2006.

PEER 2005/04 *Numerical Modeling of the Nonlinear Cyclic Response of Shallow Foundations.* Chad Harden, Tara Hutchinson, Geoffrey R. Martin, and Bruce L. Kutter. August 2005.

PEER 2005/03 *A Taxonomy of Building Components for Performance-Based Earthquake Engineering.* Keith A. Porter. September 2005.

PEER 2005/02 *Fragility Basis for California Highway Overpass Bridge Seismic Decision Making*. Kevin R. Mackie and Božidar Stojadinović. June 2005.

PEER 2005/01 *Empirical Characterization of Site Conditions on Strong Ground Motion.* Jonathan P. Stewart, Yoojoong Choi, and Robert W. Graves. June 2005.

PEER 2004/09 *Electrical Substation Equipment Interaction: Experimental Rigid Conductor Studies.* Christopher Stearns and André Filiatrault. February 2005.

PEER 2004/08 *Seismic Qualification and Fragility Testing of Line Break 550-kV Disconnect Switches.* Shakhzod M. Takhirov, Gregory L. Fenves, and Eric Fujisaki. January 2005.

PEER 2004/07 *Ground Motions for Earthquake Simulator Qualification of Electrical Substation Equipment.* Shakhzod M. Takhirov, Gregory L. Fenves, Eric Fujisaki, and Don Clyde. January 2005.

PEER 2004/06 *Performance-Based Regulation and Regulatory Regimes.* Peter J. May and Chris Koski. September 2004.

PEER 2004/05 *Performance-Based Seismic Design Concepts and Implementation: Proceedings of an International Workshop.* Peter Fajfar and Helmut Krawinkler, editors. September 2004.

PEER 2004/04 *Seismic Performance of an Instrumented Tilt-up Wall Building.* James C. Anderson and Vitelmo V. Bertero. July 2004.

PEER 2004/03 *Evaluation and Application of Concrete Tilt-up Assessment Methodologies.* Timothy Graf and James O. Malley. October 2004.

PEER 2004/02 *Analytical Investigations of New Methods for Reducing Residual Displacements of Reinforced Concrete Bridge Columns.* Junichi Sakai and Stephen A. Mahin. August 2004.

PEER 2004/01 *Seismic Performance of Masonry Buildings and Design Implications.* Kerri Anne Taeko Tokoro, James C. Anderson, and Vitelmo V. Bertero. February 2004.

PEER 2003/18 *Performance Models for Flexural Damage in Reinforced Concrete Columns.* Michael Berry and Marc Eberhard. August 2003.

PEER 2003/17 *Predicting Earthquake Damage in Older Reinforced Concrete Beam-Column Joints.* Catherine Pagni and Laura Lowes. October 2004.

PEER 2003/16 *Seismic Demands for Performance-Based Design of Bridges.* Kevin Mackie and Božidar Stojadinović. August 2003.

PEER 2003/15 *Seismic Demands for Nondeteriorating Frame Structures and Their Dependence on Ground Motions.* Ricardo Antonio Medina and Helmut Krawinkler. May 2004.

PEER 2003/14 *Finite Element Reliability and Sensitivity Methods for Performance-Based Earthquake Engineering.* Terje Haukaas and Armen Der Kiureghian. April 2004.

PEER 2003/13 *Effects of Connection Hysteretic Degradation on the Seismic Behavior of Steel Moment-Resisting Frames.* Janise E. Rodgers and Stephen A. Mahin. March 2004.

PEER 2003/12 *Implementation Manual for the Seismic Protection of Laboratory Contents: Format and Case Studies.* William T. Holmes and Mary C. Comerio. October 2003.

PEER 2003/11 *Fifth U.S.-Japan Workshop on Performance-Based Earthquake Engineering Methodology for Reinforced Concrete Building Structures.* February 2004.

PEER 2003/10 *A Beam-Column Joint Model for Simulating the Earthquake Response of Reinforced Concrete Frames.* Laura N. Lowes, Nilanjan Mitra, and Arash Altoontash. February 2004.

PEER 2003/09 *Sequencing Repairs after an Earthquake: An Economic Approach.* Marco Casari and Simon J. Wilkie. April 2004.

PEER 2003/08 *A Technical Framework for Probability-Based Demand and Capacity Factor Design (DCFD) Seismic Formats.* Fatemeh Jalayer and C. Allin Cornell. November 2003.

PEER 2003/07 *Uncertainty Specification and Propagation for Loss Estimation Using FOSM Methods.* Jack W. Baker and C. Allin Cornell. September 2003.

PEER 2003/06 *Performance of Circular Reinforced Concrete Bridge Columns under Bidirectional Earthquake Loading*. Mahmoud M. Hachem, Stephen A. Mahin, and Jack P. Moehle. February 2003.

PEER 2003/05 *Response Assessment for Building-Specific Loss Estimation.* Eduardo Miranda and Shahram Taghavi. September 2003.

PEER 2003/04 *Experimental Assessment of Columns with Short Lap Splices Subjected to Cyclic Loads*. Murat Melek, John W. Wallace, and Joel Conte. April 2003.

PEER 2003/03 *Probabilistic Response Assessment for Building-Specific Loss Estimation.* Eduardo Miranda and Hesameddin Aslani. September 2003.

PEER 2003/02 *Software Framework for Collaborative Development of Nonlinear Dynamic Analysis Program.* Jun Peng and Kincho H. Law. September 2003.

PEER 2003/01 *Shake Table Tests and Analytical Studies on the Gravity Load Collapse of Reinforced Concrete Frames.* Kenneth John Elwood and Jack P. Moehle. November 2003.

PEER 2002/24 *Performance of Beam to Column Bridge Joints Subjected to a Large Velocity Pulse.* Natalie Gibson, André Filiatrault, and Scott A. Ashford. April 2002.

PEER 2002/23 *Effects of Large Velocity Pulses on Reinforced Concrete Bridge Columns.* Greg L. Orozco and Scott A. Ashford. April 2002.

PEER 2002/22 *Characterization of Large Velocity Pulses for Laboratory Testing.* Kenneth E. Cox and Scott A. Ashford. April 2002.

PEER 2002/21 *Fourth U.S.-Japan Workshop on Performance-Based Earthquake Engineering Methodology for Reinforced Concrete Building Structures*. December 2002.

PEER 2002/20 *Barriers to Adoption and Implementation of PBEE Innovations.* Peter J. May. August 2002.

PEER 2002/19 *Economic-Engineered Integrated Models for Earthquakes: Socioeconomic Impacts.* Peter Gordon, James E. Moore II, and Harry W. Richardson. July 2002.

PEER 2002/18 *Assessment of Reinforced Concrete Building Exterior Joints with Substandard Details.* Chris P. Pantelides, Jon Hansen, Justin Nadauld, and Lawrence D. Reaveley. May 2002.

PEER 2002/17 *Structural Characterization and Seismic Response Analysis of a Highway Overcrossing Equipped with Elastomeric Bearings and Fluid Dampers: A Case Study.* Nicos Makris and Jian Zhang. November 2002.

PEER 2002/16 *Estimation of Uncertainty in Geotechnical Properties for Performance-Based Earthquake Engineering.* Allen L. Jones, Steven L. Kramer, and Pedro Arduino. December 2002.

PEER 2002/15 *Seismic Behavior of Bridge Columns Subjected to Various Loading Patterns.* Asadollah Esmaeily-Gh. and Yan Xiao. December 2002.

PEER 2002/14 *Inelastic Seismic Response of Extended Pile Shaft Supported Bridge Structures.* T.C. Hutchinson, R.W. Boulanger, Y.H. Chai, and I.M. Idriss. December 2002.

PEER 2002/13 *Probabilistic Models and Fragility Estimates for Bridge Components and Systems.* Paolo Gardoni, Armen Der Kiureghian, and Khalid M. Mosalam. June 2002.

PEER 2002/12 *Effects of Fault Dip and Slip Rake on Near-Source Ground Motions: Why Chi-Chi Was a Relatively Mild M7.6 Earthquake.* Brad T. Aagaard, John F. Hall, and Thomas H. Heaton. December 2002.

PEER 2002/11 *Analytical and Experimental Study of Fiber-Reinforced Strip Isolators*. James M. Kelly and Shakhzod M. Takhirov. September 2002.

PEER 2002/10 *Centrifuge Modeling of Settlement and Lateral Spreading with Comparisons to Numerical Analyses***.** Sivapalan Gajan and Bruce L. Kutter. January 2003.

PEER 2002/09 *Documentation and Analysis of Field Case Histories of Seismic Compression during the 1994 Northridge, California, Earthquake.* Jonathan P. Stewart, Patrick M. Smith, Daniel H. Whang, and Jonathan D. Bray. October 2002.

PEER 2002/08 *Component Testing, Stability Analysis and Characterization of Buckling-Restrained Unbonded Braces™.* Cameron Black, Nicos Makris, and Ian Aiken. September 2002.

PEER 2002/07 *Seismic Performance of Pile-Wharf Connections.* Charles W. Roeder, Robert Graff, Jennifer Soderstrom, and Jun Han Yoo. December 2001.

PEER 2002/06 *The Use of Benefit-Cost Analysis for Evaluation of Performance-Based Earthquake Engineering Decisions.* Richard O. Zerbe and Anthony Falit-Baiamonte. September 2001.

PEER 2002/05 *Guidelines, Specifications, and Seismic Performance Characterization of Nonstructural Building Components and Equipment.* André Filiatrault, Constantin Christopoulos, and Christopher Stearns. September 2001.

PEER 2002/04 *Consortium of Organizations for Strong-Motion Observation Systems and the Pacific Earthquake Engineering Research Center Lifelines Program: Invited Workshop on Archiving and Web Dissemination of Geotechnical Data, 4–5 October 2001.* September 2002.

PEER 2002/03 *Investigation of Sensitivity of Building Loss Estimates to Major Uncertain Variables for the Van Nuys Testbed.* Keith A. Porter, James L. Beck, and Rustem V. Shaikhutdinov. August 2002.

PEER 2002/02 *The Third U.S.-Japan Workshop on Performance-Based Earthquake Engineering Methodology for Reinforced Concrete Building Structures.* July 2002.

PEER 2002/01 *Nonstructural Loss Estimation: The UC Berkeley Case Study.* Mary C. Comerio and John C. Stallmeyer. December 2001.

PEER 2001/16 *Statistics of SDF-System Estimate of Roof Displacement for Pushover Analysis of Buildings.* Anil K. Chopra, Rakesh K. Goel, and Chatpan Chintanapakdee. December 2001.

PEER 2001/15 *Damage to Bridges during the 2001 Nisqually Earthquake.* R. Tyler Ranf, Marc O. Eberhard, and Michael P. Berry. November 2001.

PEER 2001/14 *Rocking Response of Equipment Anchored to a Base Foundation.* Nicos Makris and Cameron J. Black. September 2001.

PEER 2001/13 *Modeling Soil Liquefaction Hazards for Performance-Based Earthquake Engineering.* Steven L. Kramer and Ahmed-W. Elgamal. February 2001.

PEER 2001/12 *Development of Geotechnical Capabilities in OpenSees.* Boris Jeremi . September 2001.

PEER 2001/11 *Analytical and Experimental Study of Fiber-Reinforced Elastomeric Isolators.* James M. Kelly and Shakhzod M. Takhirov. September 2001.

PEER 2001/10 *Amplification Factors for Spectral Acceleration in Active Regions.* Jonathan P. Stewart, Andrew H. Liu, Yoojoong Choi, and Mehmet B. Baturay. December 2001.

PEER 2001/09 *Ground Motion Evaluation Procedures for Performance-Based Design.* Jonathan P. Stewart, Shyh-Jeng Chiou, Jonathan D. Bray, Robert W. Graves, Paul G. Somerville, and Norman A. Abrahamson. September 2001.

PEER 2001/08 *Experimental and Computational Evaluation of Reinforced Concrete Bridge Beam-Column Connections for Seismic Performance.* Clay J. Naito, Jack P. Moehle, and Khalid M. Mosalam. November 2001.

PEER 2001/07 *The Rocking Spectrum and the Shortcomings of Design Guidelines.* Nicos Makris and Dimitrios Konstantinidis. August 2001.

PEER 2001/06 *Development of an Electrical Substation Equipment Performance Database for Evaluation of Equipment Fragilities.* Thalia Agnanos. April 1999.

PEER 2001/05 *Stiffness Analysis of Fiber-Reinforced Elastomeric Isolators.* Hsiang-Chuan Tsai and James M. Kelly. May 2001.

PEER 2001/04 *Organizational and Societal Considerations for Performance-Based Earthquake Engineering.* Peter J. May. April 2001.

PEER 2001/03 *A Modal Pushover Analysis Procedure to Estimate Seismic Demands for Buildings: Theory and Preliminary Evaluation.* Anil K. Chopra and Rakesh K. Goel. January 2001.

PEER 2001/02 *Seismic Response Analysis of Highway Overcrossings Including Soil-Structure Interaction.* Jian Zhang and Nicos Makris. March 2001.

PEER 2001/01 *Experimental Study of Large Seismic Steel Beam-to-Column Connections.* Egor P. Popov and Shakhzod M. Takhirov. November 2000.

PEER 2000/10 *The Second U.S.-Japan Workshop on Performance-Based Earthquake Engineering Methodology for Reinforced Concrete Building Structures.* March 2000.

PEER 2000/09 *Structural Engineering Reconnaissance of the August 17, 1999 Earthquake: Kocaeli (Izmit), Turkey.* Halil Sezen, Kenneth J. Elwood, Andrew S. Whittaker, Khalid Mosalam, John J. Wallace, and John F. Stanton. December 2000.

PEER 2000/08 *Behavior of Reinforced Concrete Bridge Columns Having Varying Aspect Ratios and Varying Lengths of Confinement.* Anthony J. Calderone, Dawn E. Lehman, and Jack P. Moehle. January 2001.

PEER 2000/07 *Cover-Plate and Flange-Plate Reinforced Steel Moment-Resisting Connections.* Taejin Kim, Andrew S. Whittaker, Amir S. Gilani, Vitelmo V. Bertero, and Shakhzod M. Takhirov. September 2000.

PEER 2000/06 *Seismic Evaluation and Analysis of 230-kV Disconnect Switches.* Amir S. J. Gilani, Andrew S. Whittaker, Gregory L. Fenves, Chun-Hao Chen, Henry Ho, and Eric Fujisaki. July 2000.

PEER 2000/05 *Performance-Based Evaluation of Exterior Reinforced Concrete Building Joints for Seismic Excitation.* Chandra Clyde, Chris P. Pantelides, and Lawrence D. Reaveley. July 2000.

PEER 2000/04 *An Evaluation of Seismic Energy Demand: An Attenuation Approach.* Chung-Che Chou and Chia-Ming Uang. July 1999.

PEER 2000/03 *Framing Earthquake Retrofitting Decisions: The Case of Hillside Homes in Los Angeles.* Detlof von Winterfeldt, Nels Roselund, and Alicia Kitsuse. March 2000.

PEER 2000/02 *U.S.-Japan Workshop on the Effects of Near-Field Earthquake Shaking.* Andrew Whittaker, ed. July 2000.

PEER 2000/01 *Further Studies on Seismic Interaction in Interconnected Electrical Substation Equipment.* Armen Der Kiureghian, Kee-Jeung Hong, and Jerome L. Sackman. November 1999.

PEER 1999/14 *Seismic Evaluation and Retrofit of 230-kV Porcelain Transformer Bushings*. Amir S. Gilani, Andrew S. Whittaker, Gregory L. Fenves, and Eric Fujisaki. December 1999.

PEER 1999/13 *Building Vulnerability Studies: Modeling and Evaluation of Tilt-up and Steel Reinforced Concrete Buildings.* John W. Wallace, Jonathan P. Stewart, and Andrew S. Whittaker, editors. December 1999.

PEER 1999/12 *Rehabilitation of Nonductile RC Frame Building Using Encasement Plates and Energy-Dissipating Devices.* Mehrdad Sasani, Vitelmo V. Bertero, James C. Anderson. December 1999.

PEER 1999/11 *Performance Evaluation Database for Concrete Bridge Components and Systems under Simulated Seismic Loads.* Yael D. Hose and Frieder Seible. November 1999.

PEER 1999/10 *U.S.-Japan Workshop on Performance-Based Earthquake Engineering Methodology for Reinforced Concrete Building Structures.* December 1999.

PEER 1999/09 *Performance Improvement of Long Period Building Structures Subjected to Severe Pulse-Type Ground Motions*. James C. Anderson, Vitelmo V. Bertero, and Raul Bertero. October 1999.

PEER 1999/08 *Envelopes for Seismic Response Vectors.* Charles Menun and Armen Der Kiureghian. July 1999.

PEER 1999/07 *Documentation of Strengths and Weaknesses of Current Computer Analysis Methods for Seismic Performance of Reinforced Concrete Members.* William F. Cofer. November 1999.

PEER 1999/06 *Rocking Response and Overturning of Anchored Equipment under Seismic Excitations.* Nicos Makris and Jian Zhang. November 1999.

PEER 1999/05 *Seismic Evaluation of 550 kV Porcelain Transformer Bushings.* Amir S. Gilani, Andrew S. Whittaker, Gregory L. Fenves, and Eric Fujisaki. October 1999.

PEER 1999/04 *Adoption and Enforcement of Earthquake Risk-Reduction Measures.* Peter J. May, Raymond J. Burby, T. Jens Feeley, and Robert Wood.

PEER 1999/03 *Task 3 Characterization of Site Response General Site Categories*. Adrian Rodriguez-Marek, Jonathan D. Bray, and Norman Abrahamson. February 1999.

PEER 1999/02 *Capacity-Demand-Diagram Methods for Estimating Seismic Deformation of Inelastic Structures: SDF Systems*. Anil K. Chopra and Rakesh Goel. April 1999.

PEER 1999/01 *Interaction in Interconnected Electrical Substation Equipment Subjected to Earthquake Ground Motions.* Armen Der Kiureghian, Jerome L. Sackman, and Kee-Jeung Hong. February 1999.

PEER 1998/08 *Behavior and Failure Analysis of a Multiple-Frame Highway Bridge in the 1994 Northridge Earthquake.* Gregory L. Fenves and Michael Ellery. December 1998.

PEER 1998/07 *Empirical Evaluation of Inertial Soil-Structure Interaction Effects.* Jonathan P. Stewart, Raymond B. Seed, and Gregory L. Fenves. November 1998.

PEER 1998/06 *Effect of Damping Mechanisms on the Response of Seismic Isolated Structures.* Nicos Makris and Shih-Po Chang. November 1998.

PEER 1998/05 *Rocking Response and Overturning of Equipment under Horizontal Pulse-Type Motions.* Nicos Makris and Yiannis Roussos. October 1998.

PEER 1998/04 *Pacific Earthquake Engineering Research Invitational Workshop Proceedings, May 14–15, 1998: Defining the Links between Planning, Policy Analysis, Economics and Earthquake Engineering.* Mary Comerio and Peter Gordon. September 1998.

PEER 1998/03 *Repair/Upgrade Procedures for Welded Beam to Column Connections.* James C. Anderson and Xiaojing Duan. May 1998.

PEER 1998/02 *Seismic Evaluation of 196 kV Porcelain Transformer Bushings.* Amir S. Gilani, Juan W. Chavez, Gregory L. Fenves, and Andrew S. Whittaker. May 1998.

PEER 1998/01 *Seismic Performance of Well-Confined Concrete Bridge Columns.* Dawn E. Lehman and Jack P. Moehle. December 2000.

ONLINE REPORTS

The following PEER reports are available by Internet only at http://peer.berkeley.edu/publications/peer_reports.html

PEER 2010/109 *Report of the Seventh Joint Planning Meeting of NEES/E-Defense Collaboration on Earthquake Engineering. Held at the E-Defense, Miki, and Shin-Kobe, Japan, September 18–19, 2009.* August 2010.

PEER 2010/107 *Performance and Reliability of Exposed Column Base Plate Connections for Steel Moment-Resisting Frames.* Ady Aviram, Božidar Stojadinovic, and Armen Der Kiureghian. August 2010.

PEER 2010/106 *Verification of Probabilistic Seismic Hazard Analysis Computer Programs.* Patricia Thomas, Ivan Wong, and Norman Abrahamson. May 2010.

PEER 2010/105 *Structural Engineering Reconnaissance of the April 6, 2009, Abruzzo, Italy, Earthquake, and Lessons Learned.* M. Selim Günay and Khalid M. Mosalam. April 2010.

PEER 2010/104 *Simulating the Inelastic Seismic Behavior of Steel Braced Frames, Including the Effects of Low-Cycle Fatigue.* Yuli Huang and Stephen A. Mahin. April 2010.

PEER 2010/103 *Post-Earthquake Traffic Capacity of Modern Bridges in California.* Vesna Terzic and Božidar Stojadinović. March 2010.

PEER 2010/102 *Analysis of Cumulative Absolute Velocity (CAV) and JMA Instrumental Seismic Intensity (I_{JMA}) Using the PEER–NGA Strong Motion Database.* Kenneth W. Campbell and Yousef Bozorgnia. February 2010.

PEER 2010/101 *Rocking Response of Bridges on Shallow Foundations.* Jose A. Ugalde, Bruce L. Kutter, Boris Jeremic

PEER 2009/109 *Simulation and Performance-Based Earthquake Engineering Assessment of Self-Centering Post-Tensioned Concrete Bridge Systems.* Won K. Lee and Sarah L. Billington. December 2009.

PEER 2009/108 *PEER Lifelines Geotechnical Virtual Data Center.* J. Carl Stepp, Daniel J. Ponti, Loren L. Turner, Jennifer N. Swift, Sean Devlin, Yang Zhu, Jean Benoit, and John Bobbitt. September 2009.

PEER 2009/107 *Experimental and Computational Evaluation of Current and Innovative In-Span Hinge Details in Reinforced Concrete Box-Girder Bridges: Part 2: Post-Test Analysis and Design Recommendations.* Matias A. Hube and Khalid M. Mosalam. December 2009.

PEER 2009/106 *Shear Strength Models of Exterior Beam-Column Joints without Transverse Reinforcement.* Sangjoon Park and Khalid M. Mosalam. November 2009.

PEER 2009/105 *Reduced Uncertainty of Ground Motion Prediction Equations through Bayesian Variance Analysis.* Robb Eric S. Moss. November 2009.

PEER 2009/104 *Advanced Implementation of Hybrid Simulation.* Andreas H. Schellenberg, Stephen A. Mahin, Gregory L. Fenves. November 2009.

PEER 2009/103 *Performance Evaluation of Innovative Steel Braced Frames.* T. Y. Yang, Jack P. Moehle, and Božidar Stojadinovic. August 2009.

PEER 2009/102 *Reinvestigation of Liquefaction and Nonliquefaction Case Histories from the 1976 Tangshan Earthquake.* Robb Eric Moss, Robert E. Kayen, Liyuan Tong, Songyu Liu, Guojun Cai, and Jiaer Wu. August 2009.

PEER 2009/101 *Report of the First Joint Planning Meeting for the Second Phase of NEES/E-Defense Collaborative Research on Earthquake Engineering.* Stephen A. Mahin et al. July 2009.

PEER 2008/104 *Experimental and Analytical Study of the Seismic Performance of Retaining Structures.* Linda Al Atik and Nicholas Sitar. January 2009.

PEER 2008/103 *Experimental and Computational Evaluation of Current and Innovative In-Span Hinge Details in Reinforced Concrete Box-Girder Bridges. Part 1: Experimental Findings and Pre-Test Analysis.* Matias A. Hube and Khalid M. Mosalam. January 2009.

PEER 2008/102 *Modeling of Unreinforced Masonry Infill Walls Considering In-Plane and Out-of-Plane Interaction.* Stephen Kadysiewski and Khalid M. Mosalam. January 2009.

PEER 2008/101 *Seismic Performance Objectives for Tall Buildings.* William T. Holmes, Charles Kircher, William Petak, and Nabih Youssef. August 2008.

PEER 2007/101 *Generalized Hybrid Simulation Framework for Structural Systems Subjected to Seismic Loading.* Tarek Elkhoraibi and Khalid M. Mosalam. July 2007.

PEER 2007/100 *Seismic Evaluation of Reinforced Concrete Buildings Including Effects of Masonry Infill Walls.* Alidad Hashemi and Khalid M. Mosalam. July 2007.